



The University of
Nottingham

UNITED KINGDOM • CHINA • MALAYSIA

**Development of Integrated Chemical Kinetic Mechanism
Reduction Scheme for Diesel and Biodiesel Fuel
Surrogates for Multi-Dimensional CFD Applications**

Hiew Mun Poon, B.Eng. (Hons)

*Thesis Submitted to the University of Nottingham Malaysia Campus
for the Degree of Doctor of Philosophy*

March 2016

ABSTRACT

This thesis describes the research undertaken to formulate a systematic chemical kinetic mechanism reduction scheme to generate compact yet comprehensive chemical kinetic models for diesel and biodiesel fuels, for multi-dimensional Computational Fluid Dynamics (CFD) applications. The integrated mechanism reduction scheme was formulated based on the appraisal of various existing mechanism reduction techniques. It consists of five stages including Directed Relation Graph (DRG) with Error Propagation method using Dijkstra's algorithm, isomer lumping, reaction path analysis, DRG method and adjustment of reaction rate constants. Consequently, a single-component diesel surrogate fuel model with only 79 species (i.e. n-hexadecane (HXNv2)) and a multi-component biodiesel surrogate fuel model (i.e. methyl decanoate/methyl-9-decenoate/n-heptane (MCBSv2)) with only 80 species were successfully derived from their respective detailed mechanisms, which contain thousands of species and elementary reactions. Here, both auto-ignition and jet-stirred reactor (JSR) conditions were applied as the data source for mechanism reduction. An overall 97 % reduction in mechanism size in terms of total number of species as well as an average 97 % reduction in computational runtime in zero-dimensional (0-D) chemical kinetic simulations was achieved. Both HXNv2 and MCBSv2 were also comprehensively validated in 0-D simulations in terms of ignition delay (ID) timings and species concentration profiles. Good agreement between the predictions and measurements was obtained throughout the test conditions.

Subsequently, HXNv2 and MCBSv2 were integrated into the OpenFOAM-2.0.x solver to simulate spray combustion in a constant volume combustion chamber. The simulation results were validated against the experimental data of no.2 Diesel Fuel (D2) for diesel combustion and Soy Methyl Ester for biodiesel combustion. It was found that MCBSv2 was able to capture the combustion and soot formation events reasonably well. However, further refinement on HXNv2 was essential to improve the complex soot formation predictions. Fuel blending was then suggested to match the diesel fuel kinetics and compositions. As a result, two different versions of multi-component diesel surrogate fuel models were produced

in the form of MCDS1 (HXNv2 + 2,2,4,4,6,8,8-heptamethylnonane (HMN)) and MCDS2 (HXNv2 + HMN + toluene + cyclohexane). All the fuel constituent reduced mechanisms and the integrated mechanisms were extensively validated in 0-D simulations under a wide range of shock tube and JSR conditions. Successively, the fidelity of the multi-component diesel surrogate fuel models was evaluated in two-dimensional spray combustion simulations. The computations were compared with the experimental data of D2 fuel. MCDS1 was found to be useful for simulations with less aromatic chemistry effects. In contrast, MCDS2 was a more appropriate surrogate model for fuels with aromatics and cyclo-paraffinic contents. Following that, fidelity of MCDS2 and MCBSv2 was further assessed in three-dimensional internal combustion engine simulations. The performance of the surrogate models was compared under the same operating conditions in a light-duty, direct injection diesel engine. The computed peak pressure and heat-release rate for biodiesel combustion were lower than diesel owing to the advanced ignition timing. The soot formation of biodiesel was also found to be 1.4 times lower than diesel due to oxygenated effects. Overall, the integrated reduction scheme proves to be an attractive approach for large-scale mechanism reduction to reduce the computational time-cost as well as to expedite multi-dimensional CFD computations.

LIST OF PUBLICATIONS

Journal/Technical Papers:

- ❖ Poon, H.M., Pang, K.M., Ng, H.K., Gan, S., Schramm, J. Development of Multi-Component Diesel Surrogate Fuel Models – Part II: Validation of the Integrated Mechanisms in 0-D Kinetic and 2-D CFD Spray Combustion Simulations. *Fuel* 181: 120 – 130, 2016. DOI: 10.1016/j.fuel.2016.04.114.
- ❖ Poon, H.M., Pang, K.M., Ng, H.K., Gan, S., Schramm, J. Development of Multi-Component Diesel Surrogate Fuel Models – Part I: Validation of Reduced Mechanisms of Diesel Fuel Constituents in 0-D Kinetic Simulations. *Fuel* 180: 433 – 441, 2016. DOI: 10.1016/j.fuel.2016.04.043.
- ❖ Pang, K.M., Poon, H.M., Ng, H.K., Gan, S., Schramm, J. Soot Formation Modelling of n-dodecane and Diesel Sprays under Engine-Like Conditions. *SAE Technical Paper 2015-24-2468*, 2015. DOI: 10.4271/2015-24-2468.
- ❖ Poon, H.M., Ng, H.K., Gan, S., Pang, K.M., Schramm, J. Chemical Kinetic Mechanism Reduction Scheme for Diesel Fuel Surrogate. *Applied Mechanics and Materials* 541 – 542: 1006 – 1010, 2014. DOI: 10.4028/www.scientific.net/AMM.541-542.1006.
- ❖ Poon, H.M., Ng, H.K., Gan, S., Pang, K.M., Schramm, J. Development and Validation of Chemical Kinetic Mechanism Reduction Scheme for Large-Scale Mechanisms. *SAE International Journal of Fuels and Lubricants* 7(3): 653 – 662, 2014. DOI: 10.4271/2014-01-2576.
- ❖ Poon, H.M., Ng, H.K., Gan, S., Pang, K.M., Schramm, J. Evaluation and Development of Chemical Kinetic Mechanism Reduction Scheme for Biodiesel and Diesel Fuel Surrogates. *SAE International Journal of Fuels and Lubricants* 6(3): 729 – 744, 2013. DOI: 10.4271/2013-01-2630.

- ❖ Poon, H.M., Ng, H.K., Gan, S. Application of Integrated Chemical Kinetic Mechanism Reduction Scheme on Small-Scale Mechanism – Ethylene. (Submitted to Proceedings of the Institution of Mechanical Engineers, Part C: Journal of Mechanical Engineering Science).

- ❖ Poon, H.M., Ng, H.K., Gan, S., Pang, K.M., Schramm, J. Implementation of a Revised Biodiesel Surrogate Fuel Model for Multi-Dimensional CFD Simulations. (in preparation).

TABLE OF CONTENTS

ABSTRACT.....	i
LIST OF PUBLICATIONS	iii
TABLE OF CONTENTS.....	v
ABBREVIATIONS	xi
NOMENCLATURE	xiv
LIST OF FIGURES	xviii
LIST OF TABLES	xxv
ACKNOWLEDGEMENTS.....	xxix
CHAPTER 1 INTRODUCTION	1
1.1 Background	1
1.1.1 Coupling of Chemical Kinetics with CFD Modelling.....	1
1.1.2 Development of Diesel Surrogate Fuel Model	2
1.1.3 Development of Biodiesel Surrogate Fuel Model	5
1.1.4 In-cylinder Soot Formation	7
1.2 Aim and Objectives	8
1.3 Layout of the Thesis	11
CHAPTER 2 LITERATURE REVIEW	13
2.1 Introduction	13
2.2 Chemical Kinetic Mechanisms.....	13
2.2.1 Diesel Surrogate Fuel Mechanisms	13
2.2.2 Biodiesel Surrogate Fuel Mechanisms	20
2.2.3 Single-Component Diesel Surrogate Fuel Model – Detailed HXN Mechanism.....	24
2.2.4 Biodiesel Surrogate Fuel Model – Detailed MD/MD9D/nHep Mechanism.....	27

2.3 Chemical Kinetic Mechanism Reduction Techniques	28
2.3.1 Conventional Mechanism Reduction Techniques	29
2.3.2 Recent Developments of Mechanism Reduction Techniques	32
2.4 Concluding Remarks	36
CHAPTER 3 GOVERNING EQUATIONS.....	38
3.1 Introduction	38
3.2 Chemical Kinetics	38
3.2.1 0-D Closed Homogeneous Batch Reactor	39
3.2.2 PSR	39
3.2.3 Chemistry Set	40
3.2.4 Gas-Phase Chemical Kinetic Rates	41
3.3 CFD Sub-Models.....	42
3.3.1 Spray Breakup Model – Reitz-Diwakar Model	42
3.3.2 Turbulence Model.....	44
3.3.2.1 Standard k- ϵ model	44
3.3.2.2 RNG k- ϵ model	45
3.3.3 Soot Model – Multistep Model.....	47
3.4 Concluding Remarks	49
CHAPTER 4 APPRAISAL OF CHEMICAL KINETIC MECHANISM REDUCTION TECHNIQUES	50
4.1 Introduction	50
4.2 Theoretical Backgrounds.....	50
4.2.1 DRG.....	50
4.2.2 DRGASA.....	52
4.2.3 DRGEP	54
4.2.4 DRGEP SA	55
4.3 Descriptions of the Base Mechanisms for Mechanism Reduction.....	56

4.4 Validations in 0-D Chemical Kinetic Simulations	58
4.4.1 DRG	59
4.4.2 DRGASA	64
4.4.3 DRGEP	66
4.4.4 DRGEP SA	67
4.5 Performance Benchmarking	69
4.6 Concluding Remarks	71
CHAPTER 5 DEVELOPMENT AND VALIDATION OF CHEMICAL KINETIC MECHANISM REDUCTION SCHEME.....	73
5.1 Introduction	73
5.2 Formulation of Chemical Kinetic Mechanism Reduction Scheme	73
5.3 Implementation of Chemical Kinetic Mechanism Reduction Scheme on Large-Scale Mechanism Reduction - Diesel and Biodiesel Surrogate Fuel Models	76
5.3.1 Derivation of Reduced Models	76
5.3.2 Model Validations in 0-D Chemical Kinetic Simulations	85
5.4 Implementation of Chemical Kinetic Mechanism Reduction Scheme on Small-Scale Mechanism Reduction - Ethylene	96
5.4.1 Derivation of Reduced Model	96
5.4.2 Further Validations in 0-D Chemical Kinetic Simulations	98
5.5 Concluding Remarks	105
CHAPTER 6 VALIDATIONS OF THE DIESEL AND BIODIESEL SURROGATE FUEL MODELS IN 2-D SPRAY COMBUSTION SIMULATIONS	106
6.1 Introduction	106
6.2 Numerical Formulations and Setups	106
6.2.1 Parametric Study I: Grid Independence Test.....	110
6.2.2 Parametric Study II: Time Step	114

6.2.3 Parametric Study III: Turbulence Model	115
6.2.4 Parametric Study IV: Droplet Breakup Model	118
6.2.5 Parametric Study V: Number of Parcels.....	119
6.2.6 Best-Fit Numerical Setups.....	120
6.3 Non- Reacting and Reacting Diesel/Biodiesel Sprays	121
6.3.1 Diesel Fuel Spray Combustion	121
6.3.2 Biodiesel Fuel Spray Combustion	126
6.4 Concluding Remarks	131
CHAPTER 7 DEVELOPMENT OF MULTI-COMPONENT DIESEL SURROGATE FUEL MODELS	133
7.1 Introduction	133
7.2 Descriptions of the Diesel Fuel Constituents	133
7.3 Derivation of Reduced Models for Fuel Constituents.....	135
7.4 Derivation of Multi-Component Diesel Surrogate Fuel Models.....	142
7.5 0-D Chemical Kinetic Simulations	146
7.5.1 Validation of Individual Diesel Surrogate Fuel Component	147
7.5.2 Validation of Multi-Component Diesel Surrogate Fuel Models	157
7.6 2-D Spray Combustion Simulations Using the Derived Multi-Component Diesel Surrogate Fuel Models	170
7.6.1 Sensitivity Test of the MCDS1 Surrogate Model on CN Variations	172
7.6.2 Validation using D2 experimental data	173
7.7 Concluding Remarks	180
CHAPTER 8 VALIDATIONS OF THE MULTI-COMPONENT DIESEL AND BIODIESEL SURROGATE FUEL MODELS IN 3-D INTERNAL COMBUSTION ENGINE SIMULATIONS	182
8.1 Introduction	182

8.2 Numerical Formulations and Setups	182
8.2.1 Parametric Study I: Grid Independence Test.....	185
8.2.2 Parametric Study II: CFD Time Step	187
8.2.3 Parametric Study III: Droplet Breakup Model	188
8.2.4 Parametric Study IV: Turbulence Model.....	189
8.2.5 Best-Fit Numerical Setups.....	190
8.3 3-D Internal Combustion Simulations.....	191
8.3.1 In-Cylinder Combustion Event.....	192
8.3.2 In-Cylinder Soot Formation Event	193
8.4 Concluding Remarks	196
CHAPTER 9 CONCLUSIONS AND FUTURE WORK.....	198
9.1 Conclusions	198
9.1.1 Appraisal of Various DRG-Based Mechanism Reduction Techniques	198
9.1.2 Development and Validations of a Systematic Chemical Kinetic Mechanism Reduction Scheme for Small- and Large-Scale Mechanisms	200
9.1.3 Validations of the Single-Component Diesel and Multi-Component Biodiesel Surrogate Fuel Models in 2-D Spray Combustion Simulations	201
9.1.4 Development and Validations of Multi-Component Diesel Surrogate Fuel Models	202
9.1.5 Further Validations of the Multi-Component Diesel and Biodiesel Surrogate Fuel Models in 3-D Internal Combustion Engine Simulations	203
9.2 Suggestions for Future Work	204
REFERENCES	206
APPENDICES	228
A. MATLAB CODES FOR DRG MECHANISM REDUCTION TECHNIQUE	229

B. MATLAB CODES FOR DRGEP MECHANISM REDUCTION TECHNIQUE	233
C. CHEMICAL KINETIC MECHANISMS	236

ABBREVIATIONS

0-D	Zero-Dimensional
1-D	One-Dimensional
2-D	Two-Dimensional
3-D	Three-Dimensional
AC	Adaptive Chemistry
ASI	After Start of Injection
ATDC	After Top Dead Centre
Avg	Average
BFS	Breadth First Search
C:H:O	Carbon:Hydrogen:Oxygen
C/H	Carbon/Hydrogen
C ₂ H ₂	Acetylene
C ₂ H ₄	Ethylene
C ₆ H ₆	Benzene
CAD	Crank Angle Degree
CFD	Computational Fluid Dynamics
CHX	Cyclohexane
CN	Cetane Number
CO	Carbon Monoxide
CO ₂	Carbon Dioxide
CSP	Computational Singular Perturbation
D2	No. 2 Diesel Fuel
DAC	Dynamic Adaptive Chemistry
DERE	Direct Elementary Reaction Error
DFS	Depth First Search
DI	Direct Injection
DIC	Direct Interaction Coefficient
DOS	Diesel Oil Surrogate
DPRF	Diesel Primary Reference Fuel
DRG	Directed Relation Graph

DRGASA	Directed Relation Graph aided Sensitivity Analysis
DRGEP	Directed Relation Graph with Error Propagation
DRGEPSA	Directed Relation Graph with Error Propagation and Sensitivity Analysis
ECN	Engine Combustion Network
EVO	Exhaust Valve Open
FAME	Fatty Acid Methyl Esters
FSN	Filter Smoke Numbers
H/C	Hydrogen/Carbon
H	Hydrogen Atom
H ₂	Hydrogen Molecule
H ₂ O	Hydrogen Oxide
H ₂ O ₂	Hydrogen Peroxide
HCCI	Homogeneous Combustion Compression Ignition
HCO	Formyl
HMN	2,2,4,4,6,8,8-Heptamethylnonane
HO ₂	Hydroperoxyl
HRR	Heat Release Rate
HXN	n-Hexadecane
ID	Ignition Delay
IDEA	Integrated Diesel European Action
ILDm	Intrinsic Low Dimensional Manifold
IVC	Intake Valve Closure
JSR	Jet Stirred Reactor
LII	Laser-Induced Incandescence
LLNL	Lawrence Livermore National Laboratory
LOL	Lift-Off Length
LPL	Liquid Penetration Length
MB	Methyl Butanoate
MB2D	Methyl(E)-2-Butenoate
MCDS1	Multi-Component Diesel Surrogate No. 1
MCDS2	Multi-Component Diesel Surrogate No. 2

MD	Methyl Decanoate
MD5D	Methyl-5-Decenoate
MD9D	Methyl-9-Decenoate
MHep	Methyl Heptanoate
MHex	Methyl Hexanoate
min	Minute
MOct	Methyl Octanoate
N ₂	Nitrogen
nHep	n-Heptane
NTC	Negative Temperature Coefficient
O ₂	Oxygen
OH	Hydroxyl
PAH	Polycyclic Aromatic Hydrocarbon
PCA	Principle Component Analysis
PMC	Premixed Combustion
ppm	Parts Per Million
PRF	Primary Reference Fuels
PSR	Perfectly-Stirred Reactor
ratio _{SVF}	Ratio of increment in maximum soot volume fraction from ambient temperature of 900 K to 1000 K
Ref	Reference
RME	Rapeseed Methyl Ester
RNG	Re-Normalisation Group
s	Second
SEM-CM	Simulation Error Minimisation Connectivity Method
SME	Soy Methyl Ester
SOC	Start of Combustion
SOI	Start of Injection
SVF	Soot Volume Fraction
TDC	Top Dead Centre
TRF-PAH	Toluene Reference Fuel/Polycyclic Aromatic Hydrocarbon
VPL	Vapour Penetration Length

NOMENCLATURE

'	Forward Stoichiometric Coefficients [-]
"	Reverse Stoichiometric Coefficients [-]
$[X_i]$	Molar Concentration of the i^{th} Species [mol/m^3]
Δ	Conversion from Reactants to Products [-]
a_n	Polynomial Fitted Coefficient [-]
A	Pre-Exponential Factor [Vary depending on the order of reaction]
$C_{1\varepsilon}$	Model Constants in Standard/RNG k - ε Model [-]
$C_{2\varepsilon}$	Model Constants in Standard/RNG k - ε Model [-]
$C_{3\varepsilon}$	Model Constants in Standard/RNG k - ε Model [-]
C_p	Specific Heats [$\text{J}/\text{kg}\cdot\text{K}$]
C_v	Model Constants in RNG k - ε Model [-]
C_x	Overall Consumption Rate of Species x [$\text{mol}/\text{m}^3\cdot\text{s}$]
C_α	Model Constant for Soot Inception Rate [$1/\text{s}$]
C_β	Model Constant for Coagulation Rate [-]
C_γ	Surface Growth Rate Scaling Factor [$\text{kg}/\text{mol}^{0.5}\cdot\text{kmol}\cdot\text{s}$]
C_μ	Model Constants in Standard/RNG k - ε Model [-]
$C_{\omega,1}$	Model Constant for Soot Oxidation due to OH [$\text{kg}\cdot\text{m}/\text{kmol}\cdot\text{K}^{0.5}\cdot\text{s}$]
$C_{\omega,2}$	Model Constant for Soot Oxidation due to O_2 [$\text{kg}\cdot\text{m}/\text{kmol}\cdot\text{K}^{0.5}\cdot\text{s}$]
d	Droplet Diameter [m]
D_1	Model Constant for Bag Breakup [-]
D_2	Model Constant for Stripping Breakup [-]
dM/dt	Net Soot Production Rate [$\text{kg}/\text{m}^3\cdot\text{s}$]
dN/dt	Instantaneous Production Rate of Soot Particles [$\text{particles}/\text{m}^3\cdot\text{s}$]
E_a	Activation Energy [J/mol]
E_t	Threshold Value [-]
F	Mass Fraction [-]
F_i	Input Molar Flow Rate of Species i [mol/s]
F_i^0	Output Molar Flow Rate of Species i [mol/s]
G_b	Generation of Turbulence Kinetic Energy caused by Buoyancy [m^2/s^2]

G_k	Generation of Turbulence Kinetic Energy caused by Mean Velocity Gradients [m^2/s^2]
H	Enthalpies [J]
J	Total Number of Reactions [-]
k	Turbulence Kinetic Energy [m^2/s^2]
K_{Cj}	Equilibrium Constant of j^{th} Reaction [Units vary]
k_f	Forward Rate Constant [Units vary]
K_{pj}	Equilibrium Constant of j^{th} Reaction [Units vary]
k_r	Reverse Rate Constant [Units vary]
l	Turbulence Length Scale [m]
M	Soot Mass Concentration [kg/m^3]
M_p	Mass of an Initial Soot Particle [lg/kmol]
N	Soot Particle Number Density [particles/ m^3]
N_A	Avogadro Number [1/ kmol]
N_R	Total Number of Elementary Reactions [-]
N_S	Total Number of Species [-]
P_x	Overall Production Rate of Species x [$\text{mol}/\text{m}^3\text{-s}$]
R	Universal Gas Constant [Units vary]
r	Droplet Radius [m]
Re	Reynolds Number [-]
R_{xy}	Overall Interaction Coefficient [-]
r_{xy}	Normalised Contribution of Species y to the Production Rate of Species x [-]
R_ε	Rate-of-Strain [1/s]
S	Entropies [J/K]
S_k	User-defined source term for k in Standard/RNG k - ε Model [-]
S_ε	User-defined source term for ε in Standard/RNG k - ε Model [-]
s	Placeholder for the Intermediate Species which starts at Species x and ends at Species y [-]
Sc_t	Turbulent Schmidt Number [-]
T	Temperature [K]
t	Time [Units vary]

t_1	Lifetimes of Unstable Droplets for Bag Breakup [s]
t_2	Lifetimes of Unstable Droplets for Stripping Breakup [s]
T_C	Computational Runtime [min, s]
T_α	Activation Temperature of Soot Inception [K]
T_γ	Activation Temperature of Surface Growth [K]
$T_{\omega,2}$	Activation Temperature due to O ₂ [K]
u_{rel}	Relative Velocity between Liquid Droplet and Ambient Gas [m/s]
u_{rms}	Root Mean Square Velocity [m/s]
V	Volume of the Reactor [m ³]
$V_{AL,MAX}$	Maximum Allowable Induced Error [%]
$V_{ID,MAX}$	Maximum Errors induced on Ignition Timings [%]
ν_i	Species Stoichiometric Coefficient for i^{th} species [-]
$\nu_{x,j}$	Stoichiometric Coefficient of Species x [-]
We	Weber Number [-]
ω	Reaction Rate [Units vary]
ω_j	Net Production Rate of j^{th} elementary reaction [mol/s]
$\dot{\omega}_i$	Production Rate of i^{th} Species [mol/m ³ -s]
X_{O_2}	Mole Fraction for O ₂ [-]
X_{OH}	Mole Fraction for OH [-]
X_{prec}	Mole Fraction of the Soot Precursor [-]
X_{sgs}	Mole Fraction of the Participating Surface Growth Species [-]
Y_M	Contribution of the Fluctuating Dilatation in Compressible Turbulence to the Overall Dissipation Rate [-]
Y_{soot}	Soot Mass Fraction [-]
α_{ij}	Third Body Coefficient [-]
α_k	Inverse Effective Prandtl Numbers for Turbulent Kinetic Energy [-]
α_ϵ	Inverse Effective Prandtl Numbers for Dissipation [-]
β	Temperature Exponent [-]
δ_{yj}	Participation of Species y in i^{th} Elementary Reaction [-]
ϵ	Dissipation Rate [m ² /s ³]
ϵ_{EP}	Threshold Value during Error Propagation Phase [-]
η_{coll}	Collision Efficiency Parameter [-]

μ_{eff}	Effective Viscosity [kg/m-s]
μ_t	Turbulent Viscosity [kg/m-s]
\vec{v}	Fluid Velocity [m/s]
ν_g	Kinematic Viscosity of the Gas [m ² /s]
ρ_g	Gas Density [kg/m ³]
ρ_{soot}	Soot Mass Density [kg/m ³]
σ	Surface Tension [N/m]
σ_k	Turbulent Prandtl Numbers for Turbulent Kinetic Energy [-]
σ_ϵ	Turbulent Prandtl Numbers for Dissipation [-]
ϕ_N	Particle Number Density [1/m ³]
Φ	Equivalence Ratio [-]

LIST OF FIGURES

Figure 1-1: Average Compositions of RME.....	6
Figure 1-2: Structure of the methyl ester components in RME.....	6
Figure 1-3: Schematic diagram of soot formation process [25].	8
Figure 4-1: Adapted reduction procedure of DRGASA methodology [118].	53
Figure 4-2: Adapted reduction procedure of DRGEP SA methodology [40].....	56
Figure 4-3: Dependency of N_S in the reduced mechanism of (a) HXN and (b) MDBIO on E_t for single-stage, two-stage and multi-stage DRG reduction to truncate weak relations of the species.....	60
Figure 4-4: Comparisons of IDs computed by the detailed mechanisms (lines) with the predictions by the reduced (a) HXN and (b) MDBIO mechanisms generated from single-stage (\square), two-stage (Δ) and multi-stage (x) DRG for initial pressure of 60 bar and Φ of 0.5 (green), 1.0 (black), 2 (red).....	62
Figure 4-5: Average T_C for the detailed and reduced mechanisms of (a) HXN and (b) MDBIO mechanisms.....	64
Figure 4-6: Comparisons of IDs computed by the detailed mechanisms (lines) with the predictions by the reduced (a) HXN and (b) MDBIO mechanisms (Δ) generated from DRGASA reductions for initial pressure of 60 bar and Φ of 0.5 (green), 1.0 (black), 2 (red).....	65
Figure 4-7: Comparisons of IDs computed by the detailed mechanisms (lines) with the predictions by the reduced (a) HXN and (b) MDBIO mechanisms (Δ) generated from DRGEP reductions for initial pressure of 60 bar and Φ of 0.5 (green), 1.0 (black), 2 (red).....	67
Figure 4-8: Comparisons of IDs computed by the detailed mechanisms (lines) with the predictions by the reduced (a) HXN and (b) MDBIO mechanisms (Δ)	

generated from DRGEPSA reductions for pressure of 60 bar and Φ of 0.5 (green), 1.0 (black), 2 (red).	68
Figure 5-1: Flow chart of the novel integrated chemical kinetic mechanism reduction scheme.	74
Figure 5-2: Main reaction pathways of (a) HXN and (b) MD/MD9D/nHep oxidations for initial pressure of 60 bar, initial temperature of 950 K and Φ of 1.81	
Figure 5-3: Normalised temperature A -factor sensitivity for (a) HXNv2 and (b) MCBSv2 for initial pressure of 60 bar, initial temperature of 950 K and Φ of 1. [**Only results for HXNv2 and MCBSv2 are demonstrated here for clearer description of the reaction rate optimisation procedure.]	84
Figure 5-4: Comparisons of ID calculated by the detailed (line) and reduced (a) HXNv1 (Δ) / HXNv2 (\square) diesel surrogate fuel models and (b) MCBSv1 (Δ) / MCBSv2 (\square) biodiesel surrogate fuel models for initial pressure of 60 bar and Φ of 0.5 (green), 1.0 (black), 2.0 (red).	86
Figure 5-5: Comparison of the predicted species mole fractions between the reduced and detailed mechanisms under auto-ignition condition for initial pressure of 60 bar, initial temperature of 950 K and Φ of 1.0.	88
Figure 5-6: Comparison of species profiles predicted by the reduced (a) diesel and (b) biodiesel surrogate fuel mechanisms with the respective detailed mechanisms under JSR condition as a function of temperature, with initial pressure of 60 bar and Φ of 1.	91
Figure 5-7: Computed and experimental species mole fractions obtained from the oxidation of (a) 0.03 % HXN and (b) 0.05 % of RME in a JSR. [Note: The associated operating conditions are depicted in Table 5-1.]	94
Figure 5-8: Main reaction pathways during ethylene combustion.....	97
Figure 5-9: Comparison of the flame temperature profiles generated by the reduced (\blacktriangleright) and detailed (—) ethylene mechanisms.	98

Figure 5-10: Comparisons of the respective ID timing predictions with the detailed mechanisms (lines) using the reduced ethylene mechanism (○) generated from the integrated reduction scheme for initial pressure of (a) 13.5 bar and (b) 41 bar and Φ of 0.5 (green), 1.0 (black), 2 (red). 100

Figure 5-11: Comparison of species profiles of the reduced (—) and detailed (○) ethylene mechanisms under auto-ignition condition as a function of temperature, with initial pressure of 41 bar, initial temperature of 1050 K and Φ of 1. 101

Figure 5-12: Comparison of species profiles of the reduced (—) and detailed (○) ethylene mechanisms under JSR condition as a function of temperature, with initial pressure of 41 bar and Φ of 1. 102

Figure 5-13: Computed and experimental species mole fraction obtained from the oxidation of 0.15 % C_2H_4 in a JSR at pressure of 5 atm and Φ of 2. 104

Figure 6-1: Schematic cross-section of the constant volume combustion chamber [162]. 107

Figure 6-2: Comparison of the predicted (a) LPL and (b) VPL with the measurements using different grid sizes. 111

Figure 6-3: Comparison of the predicted (a) LPL and (b) VPL with the measurements using different mesh gradings. 113

Figure 6-4: Comparison of the predicted (a) LPL and (b) VPL with the measurements using different time steps. 114

Figure 6-5: Comparison of the predicted (a) LPL and (b) VPL with the measurements using different turbulence models. 116

Figure 6-6: Comparison of the predicted (a) LPL and (b) VPL with the measurements using different $C_{1\epsilon}$ values of standard $k-\epsilon$ model. 117

Figure 6-7: Comparison of the predicted (a) LPL and (b) VPL with the measurements using different C_s values of Reitz and Diwakar breakup model. . 118

Figure 6-8: Comparison of the predicted (a) LPL and (b) VPL with the measurements using different number of parcels injected..... 119

Figure 6-9: Wedge mesh of the constant volume combustion chamber applied in the 2-D simulations..... 121

Figure 6-10: Comparison of the computations (—) of (a) LPL and (b) VPL with the measurements (--) using the diesel surrogate fuel fuels..... 122

Figure 6-11: Comparison of the IDs and LOLs predicted by the HXNv1 (○) and HXNv2 (x) diesel surrogate fuel models with the experimental measurements (●) for ambient temperatures of 900 K and 1000 K. 123

Figure 6-12: Predicted SVF contours and experimental soot cloud images at quasi-steady state for diesel combustion using the (a) HXNv1 and (b) HXNv2 diesel surrogate fuel models for ambient temperatures of 900 K and 1000 K. [**ppm denotes parts per million.] 125

Figure 6-13: Comparison of the computations of (a) LPL and (b) VPL with the measurements (--) using the biodiesel surrogate fuel fuel for SME (—) and RME (—) combustions..... 127

Figure 6-14: Comparison of the IDs and LOLs predicted by the (a) MCBSv1 and (b) MCBSv2 biodiesel surrogate fuel models with the experimental measurements for ambient temperatures of 900 K and 1000 K. 128

Figure 6-15: Predicted SVF contours and experimental soot cloud images at quasi-steady state for (i) SME and (ii) RME combustions using the (a) MCBSv1 and (b) MCBSv2 biodiesel surrogate fuel models for ambient temperatures of 900 K and 1000 K..... 130

Figure 7-1: Reactions with normalised temperature *A*-factor sensitivities for reduced mechanisms of (a) HMN and (b) CHX, with initial pressure of 60 bar, initial temperature of 950 K and Φ of 1. [Note: Red boxes indicate the reactions selected for adjustment of the *A*-factor values of Arrhenius parameters.]..... 139

Figure 7-2: Main reaction pathways of (a) HMN, (b) CHX and (c) toluene ($C_6H_5CH_3$) during fuel oxidation process for initial pressure of 60 bar, initial temperature of 950 K and Φ of 1..... 141

Figure 7-3: Sequential steps to formulate the multi-component diesel surrogate fuel models..... 143

Figure 7-4: Comparisons of ID calculated by the detailed (line) and reduced (\square) models of (a) HMN and (b) CHX for initial pressure of 60 bar and Φ of 0.5 (green), 1.0 (black), 2.0 (red)..... 147

Figure 7-5: Computed species profiles predicted by the detailed (\circ) and reduced (—) models of (a) HMN and (b) CHX under auto-ignition condition, with initial pressure of 60 bar, initial temperature of 950 K and Φ of 1..... 150

Figure 7-6: Computed species profiles predicted by the detailed (\circ) and reduced (—) models of (a) HMN and (b) CHX under JSR condition, with initial pressure of 60 bar, initial temperature of 950 K and Φ of 1..... 152

Figure 7-7: Computed and experimental species mole fractions obtained from the oxidation of (a) 0.07 % HMN and (b) 0.1 % CHX in a JSR. [Note: The associated operating conditions are depicted in Table 7-2.] 155

Figure 7-8: Comparisons of ID calculated by MCDS1 (Δ) and MCDS2 (\circ) with the detailed (line) models of (a) HXN, (b) HMN and (c) CHX for initial pressure of 60 bar and Φ of 0.5 (green), 1.0 (black), 2.0 (red)..... 158

Figure 7-9: Comparison of species profiles predicted by MCDS1 (\cdots) and MCDS2 (--) surrogate models with those of the detailed models (\circ) for (a) HXN, (b) HMN and (c) CHX under auto-ignition condition, with initial pressure of 60 bar, initial temperature of 950 K and Φ of 1..... 162

Figure 7-10: Comparison of species profiles predicted by MCDS1 (\cdots) and MCDS2 (--) surrogate models with those of the detailed models (\circ) for (a) HXN, (b) HMN and (c) CHX under JSR condition, with initial pressure of 60 bar, initial temperature of 950 K and Φ of 1..... 165

Figure 7-11: Computed and experimental species mole fractions (●) obtained from the oxidation of (a) 0.03 % HXN, (b) 0.07 % HMN and (c) 0.1 % CHX in a JSR using MCDS1 (X) and MCDS2 (○) surrogate models as well as the detailed model (—) for each fuel constituent. [Note: The associated operating conditions are depicted in Table 7-2.] 168

Figure 7-12: Comparisons of ID predicted by MCDS1 (Δ) and MCDS2 (○) surrogate models with the detailed mechanisms (lines) of (a) DPRF58^a [160] and (b) n-dodecane^b [7] for initial pressure of 40 bar, Φ of (i) 0.5, (ii) 1 and (iii) 2. [^aIDs of DPRF58 were computed by Perini et al. [160] using the detailed mechanism of Westbrook et al. [31] in a constant volume vessel using identical initial conditions; ^bThe mechanism of n-dodecane was extracted from the detailed mechanism of Westbrook et al. [7] for combustion of n-alkane hydrocarbons from n-octane to HXN.]..... 169

Figure 7-13: ID (black) and LOL (red) predictions against CN for the sensitivity tests using MCDS1 surrogate model for ambient temperatures of 900 K (X) and 1000 K (●)..... 173

Figure 7-14: ID (black) and LOL (red) predictions using MCDS1 (○) and MCDS2 (X) surrogate models in comparison with the experimental measurements (●) for D2 fuel combustion for ambient temperatures of 900 K and 1000 K..... 174

Figure 7-15: Qualitative comparisons of predicted SVF contours and experimental soot cloud images at quasi-steady state for D2 fuel combustion in a constant volume chamber using the (a) MCDS1 and (b) MCDS2 surrogate models. 175

Figure 7-16: Comparisons of the computed SVF along spray axis using MCDS1 (black) and MCDS2 (red) surrogate models at ambient temperatures of 900 K (⋯) and 1000 K (—)..... 176

Figure 7-17: Comparisons of C_2H_2 and C_6H_6 mass fractions at temperature increments of (a) 100 K, (b) 200 K, (c) 400 K, (d) 800 K and (e) 1000 K from the initial ambient temperatures as well as at (f) quasi-steady state using MCDS1 and MCDS2 surrogate models. [**Note: Mass fractions of C_6H_6 at $\Delta T = 100$ K, $\Delta T =$

200 K and $\Delta T = 400$ K are scaled down by a factor of 20, 10 and 5, respectively; [900 K] and [1000 K] denote initial ambient temperatures of 900 K and 1000 K, respectively.].....	179
Figure 8-1: 60° sector mesh of the combustion chamber for the light-duty diesel engine at Top Dead Centre (TDC).....	183
Figure 8-2: Measured and simulated pressure and HRR profiles using different mesh resolutions.	185
Figure 8-3: Measured and simulated pressure and HRR profiles using computational grids which are generated with/without field mapping.....	187
Figure 8-4: Measured and simulated pressure and HRR profiles using different time steps.	188
Figure 8-5: Measured and simulated pressure and HRR profiles using different C_S values.	189
Figure 8-6: Measured and simulated pressure and HRR profiles using different $C_{I\varepsilon}$ values.....	190
Figure 8-7: Experimental and simulated pressure and HRR curves.....	193
Figure 8-8: In-cylinder temporal soot evolutions for diesel and biodiesel combustions.	194
Figure 8-9: In-cylinder spatial soot evolutions for diesel and biodiesel combustions.	195
Figure 8-10: Predicted C_2H_2 (–) and O_2 (--) mass fractions for diesel (black) and biodiesel (red) fuel combustions.....	196

LIST OF TABLES

Table 1-1: Properties of typical North American diesel fuel [5,6].	2
Table 2-1: Compilation of the currently available surrogate mechanisms for straight-alkanes with short carbon chain (≤ 7 carbon atoms).	14
Table 2-2: Compilation of the currently available surrogate mechanisms for straight-alkanes with long carbon chain (> 7 carbon atoms).	15
Table 2-3: Compilation of the currently available multi-component diesel surrogate fuel mechanisms.	18
Table 2-4: Compilation of the currently available surrogate mechanisms for diesel fuel components such as aromatics, branched- and cyclo-alkanes.	19
Table 2-5: Compilation of the currently available biodiesel surrogate fuel mechanisms with short carbon chain (≤ 5 Carbon Alkyl Esters).	20
Table 2-6: Compilation of the currently available biodiesel surrogate mechanisms with long carbon chain (> 5 Carbon Alkyl Esters).	22
Table 2-7: Compilation of the currently available multi-component biodiesel surrogate fuel mechanisms.	24
Table 2-8: Reaction classes presented in the reaction mechanism.	26
Table 2-9: Advantages and disadvantages of the conventional mechanism reduction techniques.	31
Table 2-10: Advantages and disadvantages of the recent mechanism reduction techniques.	35
Table 3-1: Model constants used in standard k- ϵ model.	45
Table 3-2: Model constants used in RNG k- ϵ model.	47

Table 3-3: Summary of CFD sub-models employed in the 2-D spray combustion simulations and 3-D internal combustion engine simulations.	49
Table 4-1: Base mechanism for diesel and biodiesel surrogate fuels.	57
Table 4-2: Fuel components of RME and the proposed biodiesel surrogate fuel model along with their respective chemical formula, average composition and C:H:O ratio.	58
Table 4-3: Operating conditions applied for validation of each reduced mechanism.	59
Table 4-4: Selection of E_t as well as the resulting N_S and N_R of the reduced mechanisms for each stage of DRG reduction.	61
Table 4-5: Summary of the reduction performance for DRG, DRGASA, DRGEP and DRGEP SA.	69
Table 5-1: Test conditions applied for mechanism reduction as well as model validations of the diesel and biodiesel surrogate fuel models.	77
Table 5-2: Example of major isomers in reduced HXN and MDBIO mechanisms generated via DRGEP methodology.	78
Table 5-3: Comparison of the original and adjusted A-factor values of Arrhenius parameters.	83
Table 5-4: Operating conditions applied to for reduction of the ethylene mechanism.	96
Table 5-5: Test conditions applied for model validations of the reduced ethylene model.	99
Table 6-1: Experimental operating conditions and injector characteristics.	108
Table 6-2: Definitions of parameters.	109
Table 6-3: Numerical set-ups for parametric studies.	110

Table 6-4: Descriptions of mesh with different grading sizes.	112
Table 6-5: Model constants for different turbulence models.	115
Table 6-6: Best-fit numerical set-ups for non-reacting and reacting diesel/biodiesel fuel sprays.	120
Table 7-1: Fuel properties [17,178].	135
Table 7-2: Test conditions applied for mechanism reduction as well as validations of the diesel surrogate fuel models.	136
Table 7-3: Chemistry sizes of detailed/reduced chemical mechanism models used in the current work.	137
Table 7-4: Comparisons of the original and adjusted <i>A</i> -factor values of Arrhenius parameters in conjunction with their respective targeted functions for the diesel fuel components.	138
Table 7-5: Details of the multi-component diesel surrogate fuel models.	145
Table 7-6: (a) Sensitivity test with various CN using MCDS1 surrogate model; (b) Test matrix for validations of D2 fuel by applying different fuel blends; (c) Experimental operating conditions.	172
Table 8-1: Engine specifications and operating conditions.	183
Table 8-2: Numerical set-ups for parametric studies of diesel engine simulations.	184
Table 8-3: Details of meshes with different grid sizes.	185
Table 8-4: Best-fit numerical setups for 3-D engine simulations.	191
Table C-1: The HXNV2 diesel surrogate fuel model. Units are in mole, cm, s, K and cal.	236
Table C-2: The MCBSv2 biodiesel surrogate fuel model. Units are in mole, cm, s, K and cal.	241

Table C-3: The reduced ethylene mechanism. Units are in mole, cm, s, K and cal.	246
Table C-4: The MCDS1 multi-component diesel surrogate fuel model. Units are in mole, cm, s, K and cal.....	250
Table C-5: The MCDS2 multi-component diesel surrogate fuel model. Units are in mole, cm, s, K and cal.....	255

ACKNOWLEDGEMENTS

First and foremost, I would like to express my deepest gratitude to my supervisors, Prof. Ng Hoon Kiat and Prof. Gan Suyin, for their valuable advice and guidance throughout my studies in The University of Nottingham Malaysia Campus. I would also like to express my sincere thanks to Dr. Pang Kar Mun and Prof. Jesper Schramm for their contribution in providing assistance throughout the course of this study.

The scholarship awarded by the Ministry of Higher Education Malaysia to pursue my postgraduate study is acknowledged. The technical assistance in MATLAB programming provided by my friend, Mr. Lim Lian Hing, is also gratefully appreciated. Besides, I would also like to specially thank my colleagues and friends for their moral support and encouragement throughout my studies.

Last but not least, I would like to thank all of my family, especially mom and dad, for their unfailing support and understanding throughout my life.

CHAPTER 1

INTRODUCTION

1.1 Background

With the advancement in fuel processing technology, biodiesels have made considerable in-roads as a viable alternative to fossil fuels in order to alleviate growing concerns on environmental pollution and depleting oil reserves. Nevertheless, continued reliance on fossil fuels as the main energy source is expected in the foreseeable future although there are uncertainties surrounding their future availability [1,2]. In view of this, research into in-cylinder combustion of the diesel and biodiesel fuels for ground transportation purpose has offered many untapped opportunities for further development. In line with this, there are also considerable interests within the automotive industry to better understand the complex processes governing reacting spray jets of diesel and biodiesel fuels, which result in the observed engine-out measurements. Hence, detailed insights into the combustion and pollutant formation events for both diesel and biodiesel fuels inside the combustion chamber are essential. Numerical modelling, particularly Computational Fluid Dynamics (CFD) simulation, has been shown as the more cost-effective approach than experimental measurements to facilitate the investigation into these complex in-cylinder processes.

1.1.1 Coupling of Chemical Kinetics with CFD Modelling

For successful simulation of dynamic reacting sprays with appropriate representation of key species and reactions, the size of the chemical kinetic mechanisms describing this is typically large. These mechanisms normally consist of hundreds or thousands of species as they are usually tested with a wide range of experimental operating conditions. However, it is noted that to date most of the existing detailed mechanisms consist of redundant species and elementary reactions [3]. These additional species and reactions are included in the detailed mechanisms even though their importance to the key species is uncertain. As a consequence, the size of the detailed mechanisms has increased tremendously and

it is impractical to use them in CFD simulations owing to the high computational cost. This has been demonstrated in the study of Herbinet et al. [4] whereby approximately 160 hours is required to obtain one set of results for motored engine simulations using a detailed methyl decanoate (MD) mechanism with 3,012 species on a 4-GHz Intel Pentium four-processor PC. Apart from that, stiffness induced by the non-linear species coupling may also render a problem to the modelling work. There is a possibility to encounter divergence and code crash too if the detailed chemistries are integrated into the CFD code. In view of this, it is essential to formulate compact yet comprehensive diesel and biodiesel surrogate fuel mechanisms for multi-dimensional CFD applications while fulfilling the accuracy requirement. Hence, a systematic chemical kinetic mechanism reduction scheme is necessary to cope with such massive mechanisms for successful CFD simulations.

1.1.2 Development of Diesel Surrogate Fuel Model

Diesel fuel primarily comprises complex mixtures of different hydrocarbons that can be classified into several basic structural classes of compounds such as n-alkanes, iso-alkanes, polycyclic alkanes, aromatic compounds, olefins and naphthenes. Among all, n-alkanes have been studied extensively in diesel fuel combustion as these are important components in most practical transportation fuels. The chemical and physical properties of typical North American diesel fuel are demonstrated in Table 1-1.

Table 1-1: Properties of typical North American diesel fuel [5,6].

Property	Value
Cetane Number (CN)	40 – 56
Carbon Number Range	C ₁₀ – C ₂₄
Boiling Range [°C]	190 – 360
Composition:	
% normal-, iso-alkanes [%]	25 – 50
% cyclo-alkanes [%]	20 – 40
% aromatics [%]	15 – 40

Of late, there is growing interest to better understand the combustion of large hydrocarbons especially n-hexadecane (HXN). It is the primary reference fuel for diesel combustion with CN of 100. Surrogate fuel models with different CN values can hence be produced when HXN is blended with other fuels such as 1-methylnaphthalene with a CN of 0 and 2,2,4,4,6,8,8-heptamethylnonane (HMN) with a CN of 15. Besides, it is also a large n-alkane fuel which plays an important role in low temperature reactivity and early ignition kinetics. According to the research carried out by Westbrook et al. [7], the combustion characteristics of the large n-alkanes, such as n-octane to HXN (i.e. nC_8 to nC_{16}), are remarkably comparable such that the n-alkanes are interchangeable and can be used in simulations for a wide range of applications. While n-heptane (nHep) [8] has been successfully implemented as a single-component diesel surrogate fuel model in many application simulations, efforts are now focused on HXN, which is a better representative of large n-alkane component in the actual diesel fuels, especially in terms of the ignition rate and physical properties [9]. The boiling point of HXN extends to a wide range of the distillation curve of the No. 2 Diesel Fuel (D2) and it is also able to model the vaporisation characteristics of D2. Additionally, HXN is a less volatile fuel and its volatilities extend a substantial portion of the D2 fuel volatility range [10]. Moreover, it possesses longer liquid penetration length (LPL) as compared to short-chain hydrocarbons such as nHep. It is evident that the liquid penetration of diesel fuel jet is significant in enhancing in-cylinder processes of diesel engines [11]. The liquid-phase penetration is essential in promoting air/fuel mixing and consequently affects the levels of engine-out emissions. Based on these arguments, HXN is deemed as a good diesel surrogate fuel model.

However, it is common to assume that more accurate simulations can be achieved if fuel compositions and CN of the surrogate fuel match those of the actual diesel fuel within a typical range of 40 to 56, as demonstrated in Table 1-1. For this reason, nHep which has a CN of 55 is frequently employed as a single-component diesel surrogate fuel model. Nevertheless, the ignition characteristics of nHep might not be similar to the actual diesel fuels throughout a wide range of speed/load conditions as reported in some studies [12]. Additionally, nHep is a

more volatile fuel and this gives rise to significant variances in liquid spray penetration and vaporisation, which subsequently affect the local air/fuel ratio. Therefore, CN is not the only consideration when proposing a diesel surrogate fuel model for engine applications. Consequently, the combustion of long-chain hydrocarbons particularly HXN [7] has become the focal point in recent research works [9,13] as a promising component for diesel surrogate fuel model. Based on this, it is reasonable to appraise HXN as a possible diesel surrogate fuel model for diesel engine applications despite its high CN.

Nonetheless, it is evident that the Hydrogen/Carbon Molar Ratio (H/C) of HXN is different from that of the actual diesel fuels, in addition to the difference in CN. H/C ratio is a key property in simulation studies in order to replicate combustion properties such as heat of reaction, local air/fuel stoichiometric location, flame temperature and flame speed [14]. It is noteworthy that similar restriction is expected to hold for any other single-component diesel surrogate fuel models [15,16]. Apart from that, Polycyclic Aromatic Hydrocarbons (PAH) formation in diesel fuel combustion is not well described by a single-component diesel surrogate fuel model [12]. In the experiment carried out by Kook and Pickett [17], soot formation of a surrogate fuel comprising 23 % m-xylene and 77 % n-dodecane (by volume) was studied and the sooting tendency was subsequently compared to a conventional jet fuel under diesel-engine like conditions. Their planar laser induced incandescence (LII) measurement revealed that the soot level produced by the m-xylene/n-dodecane surrogate fuel is higher than that of the conventional jet fuel. For the combustion of fuels that do not contain aromatic compounds, the maximum local soot volume fraction (SVF) increases by a factor of approximately two when the ambient temperature rises from 900 K to 1000 K. Conversely, the maximum SVF increases by a factor of at least five for the combustion of fuels which consist of aromatic volume of 23 % to 27 %. This corresponds with the studies in [18–21] where the sooting tendency of a single-component surrogate model is comparatively less significant than an alkane/aromatic mixture. Single-component diesel surrogate fuel models which do not contain PAH chemistry in its original fuel composition are hence debatable since actual diesel fuels contain 20 % to 30 % of aromatic compounds [22].

Recognising the limitations of the single-component diesel surrogate fuel models, development of surrogate models with matching fuel compositions as the actual diesel fuels is necessary.

1.1.3 Development of Biodiesel Surrogate Fuel Model

With the growing awareness of environmental issues as well as future availability of oil reserves, there is considerable demand to pursue a resolution to reduce the environment impacts and find an alternative, clean fuel to overcome the fuel depletion crisis. Of late, biodiesel has become the centre of attention of governments, industries and research institutes as an alternative renewable fuel to petroleum diesel. Owing to its environment profits as well as its potential for greater regional development in third world countries, it can be observed that studies related to combustion and exhaust emission performances using biodiesel have actively progressed.

Biodiesel is a multiple-component blend of mono-alkyl esters which consists of long-chain fatty acids with various degree of unsaturation. It is primarily extracted from renewable sources such as vegetable oils, animal fats as well as waste cooking oils. One of the most commonly used biodiesel fuels is rapeseed methyl ester (RME) derived through trans-esterification of rapeseed oil with methanol. RME generally consists of five saturated and unsaturated methyl esters, namely methyl palmitate ($C_{17}H_{34}O_2$), methyl stearate ($C_{19}H_{36}O_2$), methyl oleate ($C_{19}H_{34}O_2$), methyl linoleate ($C_{19}H_{32}O_2$), and methyl linolenate ($C_{19}H_{30}O_2$). The average compositions of RME are illustrated in Figure 1-1.

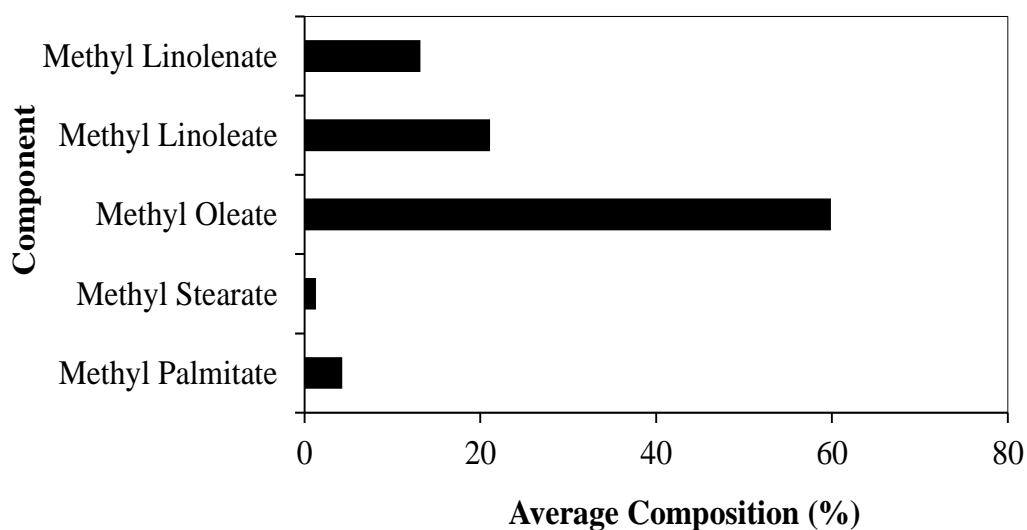


Figure 1-1: Average Compositions of RME.

The structures of the saturated and unsaturated methyl ester components are demonstrated in Figure 1-2. It is observed that the structures of these chemical species are relatively similar whereby each species contains a methyl ester which is attached to a large hydrocarbon fragment.

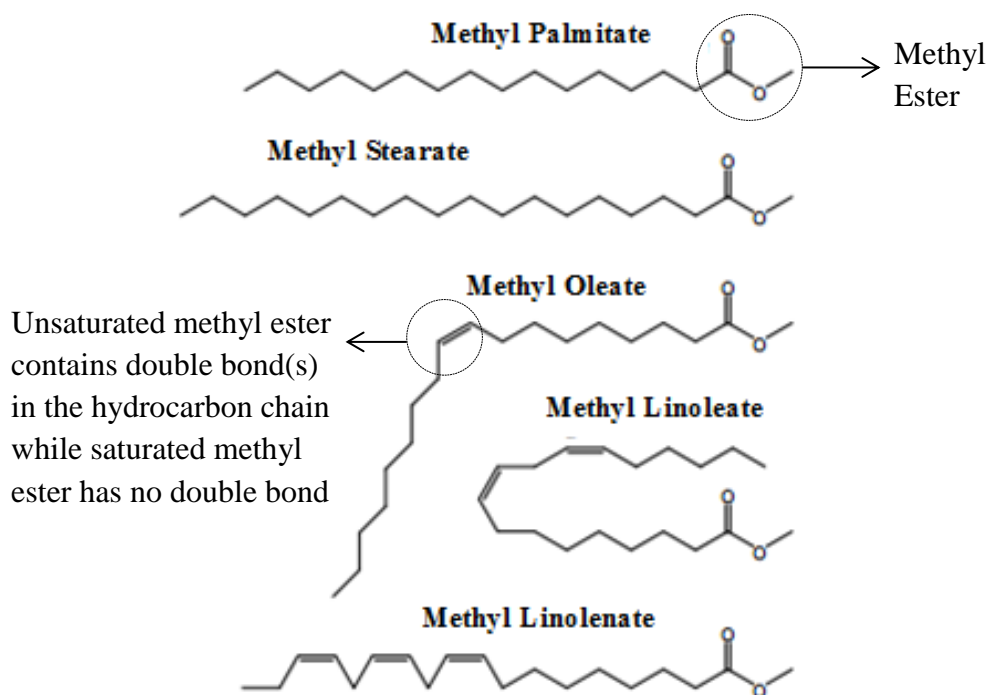


Figure 1-2: Structure of the methyl ester components in RME.

As observed in Figure 1-2, biodiesel fuel has a very large molecular size and the methyl ester components contain long carbon chains with various numbers of double bonds in the chain. As a result, the chemical kinetics of the biodiesel combustion is highly complex and poses a challenge for kinetic modelling.

Methyl butanoate (MB) has been widely employed as a biodiesel surrogate fuel model in many kinetic studies of biodiesel fuel combustion. It is a methyl ester with a chain of four carbon atoms attached to the methyl ester group. Although MB is able to replicate the kinetic features of the oxidation of methyl ester, it lacks the capability in reproducing the kinetic features of actual biodiesel fuels, which generally consist of a hydrocarbon chain of 16 to 18 carbon atoms [23]. Thus, recent studies have focused on a long-chain methyl ester, namely MD, which contains a hydrocarbon chain of ten carbon atoms that are connected to the methyl ester group. The kinetic modelling studies of MD have shown that MD is able to provide a closer reproduction of the features of actual biodiesel fuel kinetically as compared to MB. Apart from that, later development in kinetic studies of MD has permitted the flexibility in matching the physical and combustion properties of biodiesel from various feed-stocks by combining MD with methyl-9-decanoate (MD9D) and nHep. As such, compositions of the multi-component biodiesel surrogate fuel model can hence be adjusted to match the data of different biodiesel fuels.

1.1.4 In-cylinder Soot Formation

Soot particles which are mainly produced from the unburned hydrocarbons in fuel combustion [24] are solid substances comprising approximately eight parts of carbon and one part of hydrogen [25,26]. Generally, newly formed soot particles contain the highest hydrogen content with a Carbon/Hydrogen (C/H) ratio of as low as one. Then, the hydrogen content begins to decrease when soot evolves and matures. The density of soot is reported to be within the range of 1.8 g/cm^3 to 2 g/cm^3 [27,28].

The formation of soot in a diesel engine is a very complex process which is still under experimental exploration. The process generally involves numerous

intermediate steps which can be mainly divided into six stages including pyrolysis, nucleation, coalescence, surface growth, agglomeration, and oxidation. The schematic diagram of the soot formation process is presented in Figure 1-3.

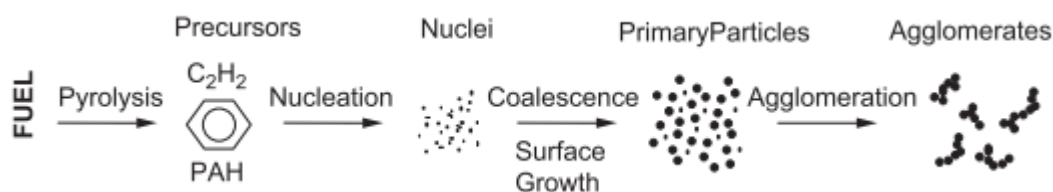


Figure 1-3: Schematic diagram of soot formation process [25].

With recent advances in chemical kinetic modelling, detailed chemistries describing the soot formation and oxidation processes have been incorporated in the chemical kinetic models of diesel and biodiesel fuels in many computational studies [29–33]. These detailed chemical kinetic models constitute a useful tool to better understand the phenomenology of soot formation and oxidation processes apart from the experimental investigations. In-cylinder soot formation events predicted by the models are thus compared against the combustion luminosity and temporal/spatial soot evolutions obtained from the optical diagnostic experiments for validation purposes.

1.2 Aim and Objectives

In view of the current state of knowledge, the present work aims to address issues related to kinetic modelling of both diesel and biodiesel surrogate fuel models, along with their applications in multi-dimensional CFD simulations concerning diesel and biodiesel spray combustions. The key objectives of this research study are to:

- i. appraise the existing chemical kinetic mechanism reduction techniques which are applicable for large-scale mechanisms such as the diesel and biodiesel surrogate fuel models*

In this study, the systematic algorithms for the currently available chemical kinetic mechanism reduction techniques have been developed using the MATLAB programming language (MathWorks, version R2012a). Accordingly, the performance of each mechanism reduction approach is evaluated through zero-dimensional (0-D) chemical kinetic simulations using CHEMKIN-PRO software by Reaction Design, which is a commercial software package for kinetic modelling. 0-D simulation approach is often applied to describe and assess the chemical kinetics of the surrogate models since it is able to take into account a huge number of different species and reactions with less computational cost.

ii. formulate an integrated chemical kinetic mechanism reduction scheme which is competent in producing compact yet comprehensive chemical kinetic mechanisms for diesel and biodiesel spray combustion modelling studies

Generally, there is only a single reduction technique applied in the mechanism reduction procedure. Therefore, only limited extent of reduction is achieved while the generated reduced mechanism typically consists of more than hundred species. For this reason, it is essential to formulate a reduction scheme which integrates different reduction techniques to construct a more effective and reliable approach that cope with larger mechanisms for successful CFD simulations. As such, greater reduction scale can be achieved and the weakness of each single reduction technique is compensated. Set against this background, an integrated chemical kinetic mechanism reduction scheme is introduced in this study to generate reduced mechanisms for both diesel and biodiesel fuels which are adequate for application in multidimensional CFD study.

iii. develop a generic chemical kinetic mechanism reduction scheme which is applicable for both large-scale and small-scale mechanism reductions

In this work, the systematic chemical kinetic mechanism reduction scheme formulated for large-scale mechanism reduction is applied to investigate its

performance in small-scale mechanism reduction. Here, one-dimensional (1-D) laminar flame-speed simulations are conducted to examine the flame temperatures of ethylene combustion under a wide range of equivalence ratio (Φ).

iv. develop multi-component diesel surrogate fuel models and integrate with CFD sub-models for diesel spray combustion modelling which are applicable across a wide range of engine conditions

Multi-component diesel surrogate fuel models which account accurately for both diesel fuel ignition and combustion across wider CN range of actual diesel fuels are developed in this study. The developmental work consists of several phases and two multi-component diesel surrogate fuel models with different fuel compositions and components are produced. Performance of each combination of the multi-component diesel surrogate models is evaluated through 0-D chemical kinetic simulations and 2-D spray combustion simulations. As such, the importance of each fuel component is determined. From here, an appropriate multi-component diesel surrogate fuel model is selected for the subsequent three-dimensional (3-D) CFD modelling study of diesel combustion in a light-duty, direct injection (DI) diesel engine.

v. compare the combustion characteristics and soot formation performances between the derived multi-component diesel and biodiesel surrogate fuel models in a light-duty, DI diesel engine

In this study, fidelity of the diesel and biodiesel surrogate fuel models are further assessed in the 3-D internal combustion engine simulations. The surrogate models are coupled with CFD sub-models in the OpenFOAM solver to simulate the combustion and soot formation processes in a light-duty, DI diesel engine. Here, a single main fuel injection strategy with retarded injection timing is applied. Then, the performance of the biodiesel fuel combustion is compared with diesel under the same operating conditions.

1.3 Layout of the Thesis

In the previous sections, the background to this project was defined, along with the corresponding scopes and objectives of the study. Set against this background, a detailed literature review is presented on the existing chemical kinetic mechanism reduction techniques which are commonly applied for large-scale mechanism reduction in Chapter 2 to deliver the background information. The current developments of diesel and biodiesel surrogate fuel models are also appraised in Chapter 2.

Accordingly, the theoretical backgrounds and the corresponding governing equations of the numerical models applied in the kinetics and CFD simulations are presented in Chapter 3.

In Chapter 4, the base mechanisms for the diesel and biodiesel surrogate fuel models applied in the numerical simulations are first selected. Then, the chemical kinetic mechanism reduction techniques which are applicable for large-scale mechanism reduction are appraised using these models. The comparison studies are conducted by means of 0-D chemical kinetic simulations using CHEMKIN-PRO software. The strengths and weaknesses of each reduction technique are discussed here.

Following that, a systematic integrated chemical kinetic mechanism reduction scheme is formulated in Chapter 5 to generate reduced yet comprehensive diesel and biodiesel surrogate fuel models for diesel engine applications. Model validations in 0-D simulations are also conducted. In addition, the reduction scheme is also applied on a small-scale mechanism to evaluate its performance.

In Chapter 6, mesh generation and grid independence studies for the 2-D spray combustion simulation are presented. Apart from that, the parametric studies to determine the constant values for various CFD sub-models are also reported. Fidelity of the reduced diesel and biodiesel surrogate fuel models developed in Chapter 5 are then evaluated in the 2-D simulations in this chapter.

Successively, Chapter 7 describes the procedures to develop multi-component diesel surrogate fuel models in order to achieve ignitibility and composition match to the actual diesel fuel. Validations of the surrogate models are also performed in 0-D chemical kinetic simulations as well as 2-D spray combustion simulations. On the other hand, the biodiesel surrogate fuel model applied in this current work is already a multi-component fuel blend. Hence, it is directly applied in the subsequent modelling studies.

In Chapter 8, fidelity of the multi-component diesel and biodiesel surrogate fuel models generated in the previous chapters are further evaluated in the 3-D internal combustion engine simulations. The combustion and soot formation processes of the diesel and biodiesel fuels in a light-duty, DI diesel engine are compared under the same operating conditions.

Lastly, the overall appraisals of the research work reported in this project are summarised in Chapter 9. Key conclusions from the numerical studies are highlighted and some recommendations for further work are presented too.

CHAPTER 2

LITERATURE REVIEW

2.1 Introduction

This chapter outlines the background information to the current research study in the form of a literature review. Here, the literature review covers the various chemical kinetic surrogate mechanisms employed for both diesel and biodiesel combustion modelling studies as well as the developmental work of chemical kinetic mechanism reduction techniques. These are presented in Section 2.2 and 2.3 respectively. Lastly, key points from the literature review are summarised in Section 2.4.

2.2 Chemical Kinetic Mechanisms

Chemical kinetic models are often coupled with the CFD models to simulate in-cylinder combustion processes. As it is unrealistic to employ practical fuel models with complex chemistries in multi-dimensional CFD modelling studies, surrogate fuel models are commonly favourable as alternatives to emulate the combustion behaviours. The simpler yet comprehensive surrogate fuel models are able to exhibit similar thermodynamics properties and combustion characteristics as compared to those of the actual fuels. In this section, chemical kinetic mechanisms which are developed and applied for diesel and biodiesel fuel combustion modelling studies are reviewed.

2.2.1 Diesel Surrogate Fuel Mechanisms

For the past decades, surrogate models for straight-alkanes with short carbon chain are generally employed as the representatives for diesel fuel owing to the limited availability of kinetic data and validation for longer carbon-chain fuels. The currently available surrogate mechanisms for straight-alkanes with short carbon chain are depicted in Table 2-1. As can be seen in Table 2-1, short-chain

straight alkanes (i.e. nC_nH_{2n+2}), such as n-butane and nHep, have been widely used as diesel surrogate fuel models. Among all, nHep has been comprehensively employed as a single-component surrogate fuel model in many diesel applications owing to its comparable CN of 55 to the practical diesel fuel [12].

Table 2-1: Compilation of the currently available surrogate mechanisms for straight-alkanes with short carbon chain (≤ 7 carbon atoms).

Composition(s)	N_s	N_R	Detailed/Reduced Chemistry	Author(s)	Ref
Straight Alkanes with Short Carbon Chain (≤ 7 Carbon Atoms)					
n-Butane (nC_4H_{10})	141	461	Detailed	Kojima	[34]
	54	94	Reduced	Strelkova et al.	[35]
nHep (nC_7H_{16})	550	2,450	Detailed	Curran et al.	[8]
	561	2,539	Detailed	LLNL	[36]
	654	2,827	Detailed	LLNL	[37]
	647	2,386	Detailed	Glaude et al.	[38]
	360	1,817	Detailed	Buda et al.	[39]
	211	1,044	Reduced	Niemeyer et al.	[40]
	153	691	Reduced	Niemeyer et al.	[40]
	173	868	Reduced	Niemeyer et al.	[40]
	108	406	Reduced	Niemeyer et al.	[40]
	188	842	Reduced	Lu and Law	[41]
	159	770	Reduced	Seiser et al.	[42]
55	283	Reduced	Lu and Law	[43]	
44	109	Reduced	Pang et al.	[44]	
171	1,011	Reduced	Müller et al.	[45]	

N_s and N_R denote total number of species and total number of elementary reactions, respectively. LLNL represents Lawrence Livermore National Laboratory. Ref represents Reference.

Nonetheless, it is found that surrogate fuels with short carbon chain are inadequate to represent the combustion kinetics of the actual fuels [12,15,46,47]. The carbon chain length is an important criterion in determining the suitability of a diesel surrogate fuel model as it has significant effects on the fuel ignition behaviours such as the low- and high-temperature kinetics on auto-ignition [12]. For instance,

fuels with long-chain n-alkanes exhibit higher reactivity at low temperatures as compared to those with short carbon chains. This is due to the higher ratio of secondary to primary hydrogen atoms which then increases the H-atom abstraction rate during the initiation phase of the oxidation of alkanes [48]. Subsequently, focus is then switched to the development of large surrogate models in recognition of the limitations of short carbon-chain surrogate models. The compilation of the currently available surrogate mechanisms for straight-alkanes with long carbon chain are depicted in Table 2-2.

Table 2-2: Compilation of the currently available surrogate mechanisms for straight-alkanes with long carbon chain (> 7 carbon atoms).

Composition(s)	N_s	N_R	Detailed/Reduced Chemistry	Author(s)	Ref
n-Decane (nC ₁₀ H ₂₂)	485	2,684	Detailed	Moréac et al.	[49]
	52	407	Reduced	Zeppieri et al.	[50]
	40	141	Reduced	Chang et al.	[51]
	715	3,872	Detailed	Buda et al.	[39]
	144	1,021	Reduced	Titova et al.	[52]
	202	846	Reduced	Niemeyer et al.	[40]
	51	256	Reduced	Niemeyer et al.	[40]
	940	3,878	Detailed	Westbrook et al.	[7]
	67	600	Reduced	Bikas and Peters	[53]
n-Dodecane (nC ₁₂ H ₂₆)	1,282	5,030	Detailed	Westbrook et al.	[7]
	105	420	Reduced	Luo et al.	[54]
	103	370	Reduced	Som et al.	[55]
n-Tetradecane (nC ₁₄ H ₃₀)	1,668	6,449	Detailed	Westbrook et al.	[7]
	1,701	5,396	Detailed	Mersin et al.	[56]
HXN (nC ₁₆ H ₃₄)	2,116	8,130	Detailed	Westbrook et al.	[7]
	2,115	8,157	Detailed	LLNL	[57]
	242	1,801	Detailed	Ristori et al.	[13]
	265	1,787	Detailed	Fournet et al.	[58]
	151	1,155	Reduced	Chaos et al.	[59]

Among the long-chain diesel surrogate fuel mechanisms presented in Table 2-2, n-decane is often used as a surrogate model in modelling studies since the mechanisms are well-validated across a wide range of operating conditions. It is noteworthy that the amount of data available for large hydrocarbons decreases when the carbon number of the fuel increases. Hence, n-decane serves as a good starting point for the developmental work of mechanisms with large hydrocarbons. Apart from n-decane, large mechanisms for straight-chain alkanes such as n-dodecane, n-tetradecane, and HXN are also developed as their boiling range fall within the diesel boiling range. Therefore, they can potentially be used as diesel surrogate fuel models in CFD modelling studies. In particular, HXN is the most favourable choice as it is the diesel primary reference fuel which permits fuel blending with a greater extent of CN range.

Based on the various diesel surrogate fuel mechanisms summarised in Table 2-1 and Table 2-2, it is observed that size of the mechanism increases tremendously as the carbon chain length increases. Furthermore, according to the studies carried out by Farrell et al. [12], three different targets of diesel surrogate fuel model formulation are presented, which are property targets, development targets and application targets. Property targets denote the important physical and chemical fuel properties such as H/C ratio and chemical composition. Meanwhile, development targets denote the kinetic and fluid dynamic processes which are essential to validate the surrogate mixture behaviours such as ignition delay (ID), LPL and spray vaporisations. Lastly, application targets denote the results obtained from engine experiments such as heat release, combustion efficiency and emissions. In general, it is a challenging task to meet the property targets as the wide-ranging properties of a practical fuel is difficult to be reproduced using a simplified single-component surrogate model. Similarly, in order to match the kinetic and fluid dynamic processes of a practical fuel, blending of several fuel components might be required for better predictions.

Additionally, while nHep is often used as a single-component diesel surrogate fuel model in many modelling studies due to its similar CN to the practical diesel fuel, it is reported that the ignition behaviours of nHep might differ from the practical

fuel over a wide range of diesel engine operating conditions despite its comparable CN [60]. The oxidation as well as pyrolysis kinetics of the practical diesel fuel are not well described by nHep and its C/H ratio are different from that of diesel too. Similar restrictions are expected to hold for any other single-component diesel surrogate fuel models. As a result, multi-component diesel surrogate fuel models are developed to overcome these drawbacks. Diesel fuel components such as branched-alkanes (i.e. iC_nH_{2n+2}), cyclo-alkanes (i.e. C_nH_{2n}) and PAH are integrated together with the straight-alkanes to develop the multi-component diesel surrogate fuel models.

In the earlier years, the number of components in a surrogate model was limited owing to the complexity in solving the stiff ordinary differential equations and the associated high computational cost. Additionally, huge quantity of work was required to develop the database and mechanistic understanding of the surrogate components for diesel fuels [12]. Fuel blends which are commonly employed in numerical simulations of diesel combustion are Integrated Diesel European Action (IDEA) mechanism [61–63], Primary Reference Fuels (PRF) mechanism [64–67] and Diesel Oil Surrogate (DOS) mechanism [68]. With rapid advancement in chemical kinetics as well as computing power, surrogate models with greater number of fuel components are established such as PRF+1 mechanism [69] and Toluene Reference Fuel/PAH (TRF-PAH) mechanism [70]. Nonetheless, PRF, PRF+1 and TRF-PAH surrogate models are predominantly developed for homogeneous charge compression ignition (HCCI) applications. In these chemical models, nHep is mainly employed to represent the n-alkane component. Although the component mass fraction in these fuel blends can be adjusted to generate diesel surrogate models with different CN, the maximum boundary of the CN range is constrained by the CN of nHep. Thus, they are not suitable to be used as surrogate models for fuels with higher CN such as a paraffinic diesel reference fuel blend [71] with a CN of 80. More recently, POLIMI_Diesel_201 mechanism has been developed by Ranzi et al. [72] which consists of toluene, xylene, methylnaphthalene and n-alkanes up to HXN. The mechanism is well validated in chemical kinetic simulations through comparison of the ID predictions with experimental measurements of a binary diesel surrogate mixture under auto-

ignition condition [73]. However, the performance of the surrogate model is yet to be tested in multi-dimensional CFD modelling studies. The aforementioned multi-component diesel surrogate fuel mechanisms are demonstrated in Table 2-3.

Table 2-3: Compilation of the currently available multi-component diesel surrogate fuel mechanisms.

Models	Compositions	$N_S; N_R$	Author(s)	Ref
IDEA	n-decane, 1-methylnaphthalene	118; 557	Hergart et al.	[63]
PRF	iso-octane, nHep	990; 4,060	Curran et al.	[64]
		58; 120	Kirchen et al.	[65]
		73; 296	Wang et al.	[66]
		1,034; 4,236	LLNL	[67]
Diesel_PRF	HXN, HMN	2,800; 11,000	Westbrook et al.	[31]
DOS	nHep, toluene	70; 305	Golovitchev et al.	[68]
PRF+1	iso-octane, nHep, toluene	469; 1,221	Chaos et al.	[69]
TRF-PAH	nHep, toluene, PAH	71; 360	Wang et al.	[70]
POLIMI Diesel_201	HXN, toluene, xylene, methylnaphthalene	201; 4,240	Ranzi et al.	[72]

Furthermore, it is noted that the actual diesel fuels generally consist of aromatics, straight-, branched- and cyclo-alkanes. Hence, diesel fuel components other than straight-alkanes are also developed and they are ready to be used for fuel blending. These mechanisms are depicted in Table 2-4.

Table 2-4: Compilation of the currently available surrogate mechanisms for diesel fuel components such as aromatics, branched- and cyclo-alkanes.

Composition(s)	N_s	N_R	Detailed/Reduced Chemistry	Author(s)	Ref
Branched Alkanes					
Iso-Octane (i-C ₈ H ₁₈)	860	3,600	Detailed	Curran et al.	[74]
	463	2,820	Detailed	Côme et al.	[75]
	233	959	Reduced	Lu and Law	[41]
	275	722	Reduced	Niemeyer et al.	[40]
	211	885	Reduced	Niemeyer et al.	[40]
	232	1,140	Reduced	Niemeyer et al.	[40]
	165	779	Reduced	Niemeyer et al.	[40]
	351	1,684	Detailed	Buda et al.	[39]
	857	3,606	Detailed	LLNL	[76]
Iso-Cetane/ HMN (i-C ₁₆ H ₃₄)	1,114	4,469	Detailed	LLNL	[77]
Cyclo-Alkanes					
Cyclohexane (C ₆ H ₁₂)	1,081	4,269	Detailed	LLNL	[78]
	107	771	Reduced	Bakali et al.	[79]
Aromatics					
Toluene (C ₇ H ₈)	46	143	Detailed	Bittker	[80]
	120	920	Detailed	Dagaut et al.	[81]
	349	1,631	Detailed	Pitz et al.	[82]

The branched-alkane, namely iso-octane, is a gasoline primary reference fuel. It is commonly applied to formulate diesel fuel blends such as PRF [64–67] and PRF+1 [69], as demonstrated in Table 2-3. By integrating the branched- and

straight-alkanes in the fuel blends, surrogate models with different CN can hence be generated. As compared to the straight-alkanes, the experimental studies conducted for branched-alkanes are relatively scarce to date [12], especially for larger branched-alkane such as iso-cetane (also known as HMN). Contrastingly, mechanisms for diesel fuel components such as cyclo-alkanes and aromatics are also developed to improve the predictions on soot productions. Cyclo-alkanes are reported to have an influence on soot formation which is intermediate between the influence of aromatics and straight-/branched-alkanes [83]. Toluene is an aromatic species which is widely applied to develop diesel surrogate fuel blends such as DOS [68], PRF+1 [69], TRF-PAH [70] and POLIMI_Diesel_201 [72] mechanisms, as shown in Table 2-3. Having one of the simplest molecular structures of the alkylated benzenes, toluene is considered as a good representative of the characteristics of aromatic fuels [82].

2.2.2 Biodiesel Surrogate Fuel Mechanisms

The currently available biodiesel surrogate fuel mechanisms with short carbon chain (≤ 5 Carbon Alkyl Esters) are summarised in Table 2-5. As shown, short-chain MB is a popular selection as the surrogate model for biodiesel fuels owing to its simple alkyl structure and hence requiring lower computational time-cost. MB is reported to be able to describe the reactivity level and behaviour of biodiesel fuel in the study of Fisher et al. [47].

Table 2-5: Compilation of the currently available biodiesel surrogate fuel mechanisms with short carbon chain (≤ 5 Carbon Alkyl Esters).

Composition(s)	N_s	N_R	Detailed/Reduced Chemistry	Author(s)	Ref
MB ($C_5H_{10}O_2$)	264	1,219	Detailed	Fisher et al.	[47]
	295	1,498	Detailed	Gail et al.	[84]
	41	150	Reduced	Brakora et al.	[85]
	88	363	Reduced	Golovitchev and Yang	[86]

Similar to diesel combustion, it is noteworthy that surrogate fuels with short carbon chain are inadequate to represent the combustion kinetics of the actual biodiesel fuels [47]. Although the MB surrogate models manage to capture the chain branching and chain propagation processes during fuel combustion, the combustion kinetic of an actual biodiesel fuel is not adequately represented by its short-carbon-chain structure. Furthermore, the reactivity level of MB is comparatively lower [87] and the Negative Temperature Coefficient (NTC) regions of the mechanisms are found to be marginal as compared to those of the actual biodiesel fuels [47,84,88,89]. For these reasons, the use of these short-chain biodiesel surrogate fuel models is not favourable for future CFD modelling studies in spite of the extensive developmental work of MB. In view of the limitation of short carbon chain length, development of long-carbon-chain surrogate model for biodiesel fuels is desired. The currently available biodiesel surrogate fuel mechanisms with long carbon chain are presented in Table 2-6.

Table 2-6: Compilation of the currently available biodiesel surrogate fuel mechanisms with long carbon chain (> 5 Carbon Alkyl Esters).

Composition(s)	N_s	N_R	Detailed/Reduced Chemistry	Author(s)	Ref
Methyl Hexanoate (MHex, C ₇ H ₁₄ O ₂)	435	1,875	Detailed	Dayma et al.	[90]
	401	2,440	Detailed	Glaude et al.	[91]
Methyl Heptanoate (MHep, C ₈ H ₁₆ O ₂)	1,087	4,592	Detailed	Dayma et al.	[92]
	531	3,236	Detailed	Glaude et al.	[91]
Methyl Octanoate (MOct, C ₉ H ₁₆ O ₂)	383	2,781	Detailed	Dayma et al.	[93]
MD (C ₁₁ H ₂₂ O ₂)	1,251	7,171	Detailed	Glaude et al.	[91]
	648	2,998	Reduced	Sarathy et al.	[94]
	125	713	Reduced	Seshadri et al.	[95]
	435	1,098	Reduced	Shi et al.	[96]
	2,276	7,086	Detailed	Diévert et al.	[97]
	238	1,244	Reduced	Diévert et al.	[97]
	3,012	8,820	Detailed	Herbinet et al.	[4]
	1,247	7,775	Detailed	Herbinet et al.	[98]
Methyl-5-Decenoate (MD5D, C ₁₁ H ₂₀ O ₂)	2,649	9,247	Detailed	Herbinet et al.	[99]
MD9D (C ₁₁ H ₂₀ O ₂)	3,298	6,904	Detailed	Herbinet et al.	[99]
Methyl Laurate (C ₁₃ H ₂₆ O ₂)	2,012	13,004	Detailed	Herbinet et al.	[98]
Methyl Myristate (C ₁₅ H ₃₀ O ₂)	3,061	20,412	Detailed	Herbinet et al.	[98]
Methyl Palmitate (C ₁₇ H ₃₄ O ₂)	4,442	30,425	Detailed	Herbinet et al.	[98]
Methyl Stearate (C ₁₉ H ₃₈ O ₂)	6,203	43,444	Detailed	Herbinet et al.	[98]

Among the long-chain biodiesel surrogate fuel mechanisms summarised in Table 2-6, MHex [90,100] and MD [4,95,97,98] are the most popular choices owing to their similar reactivity level to the actual biodiesel fuels. Nevertheless, most of these mechanisms are mainly applied in 0-D simulations only due to their large chemistry size. In contrast, MHep and MOct generated by Dayma et al. [92,93] are developed based on the detailed mechanism of MB [47]. These mechanisms are yet to be further validated under different operating conditions for model improvements. Other alkyl esters with long carbon chain are also developed by Herbinet et al. [98] which consists of methyl laurate, methyl myristate, methyl palmitate and methyl stearate. These mechanisms are found to be potential surrogate models for actual biodiesel fuel. In spite of this, it is essential to reduce the size of these mechanisms as it is unrealistic to apply such huge mechanisms in multi-dimensional CFD modelling studies.

Moreover, since biodiesel contains both saturated and unsaturated esters, surrogate model which combines these two components are recommended [87]. The currently available multi-component biodiesel surrogate fuel models are presented in Table 2-7. A surrogate model comprising MB which is a saturated ester as well as methyl(E)-2-butenate (MB2D) which is a unsaturated ester is developed by Gail et al. [87]. An increment in unsaturated species and soot precursors formation is observed owing to the additional double bond presented in the MB2D mechanism. Apart from that, change in molecular structures of the alkyl esters is also significant in identifying the ignition properties and formation of soot precursors [101]. Nonetheless, the development in unsaturated alkyl ester mechanisms is scarce to date which has resulted in limited progress in constructing a detailed multi-component biodiesel surrogate fuel model containing saturated and unsaturated components.

Additionally, in recognition of the limitation of small biodiesel surrogate fuel models with short carbon chain length (≤ 5 carbon alkyl ester) as well as the absence of unsaturated component in most of the model development, two large mechanisms for unsaturated methyl esters, i.e. MD5D and MD9D are developed by Herbinet et al. [99] based on the MD mechanism from LLNL [102] to

represent the different compositions of unsaturated fatty acid methyl esters (FAME) in biodiesel. Details of the MD5D and MD9D mechanisms are presented in Table 2-6. It is found that MD5D is less reactive as compared to MD9D and the importance of double bond in the unsaturated component on fuel reactivity is demonstrated. Consequently, an improved representative of biodiesel fuel [103] comprising MD, MD9D and nHep is formulated and it is extensively employed in application of in-cylinder CFD combustion modelling [23].

Table 2-7: Compilation of the currently available multi-component biodiesel surrogate fuel mechanisms.

Composition(s)	N_s	N_R	Detailed/Reduced Chemistry	Author(s)	Ref
Biodiesel Surrogates with Short Carbon Chain (≤ 5 Carbon Alkyl Esters)					
MB, MB2D	301	1,516	Detailed	Gail et al.	[87]
MB, MB2D, C ₇ H ₁₆	113	399	Reduced	Mohamed Ismail et al.	[89]
Biodiesel Surrogates with Long Carbon Chain (> 5 Carbon Alkyl Esters)					
MD, MD9D, C ₇ H ₁₆	3,299	10,806	Detailed	LLNL	[103]
	123	394	Reduced	Luo et al.	[104]
	118	837	Reduced	Luo et al.	[105]
	77	209	Reduced	Brakora et al.	[106]

2.2.3 Single-Component Diesel Surrogate Fuel Model – Detailed HXN Mechanism

Based on the literature review presented in Section 2.2.1, a long-chain straight alkane namely HXN is selected as the single-component surrogate fuel model for diesel fuel. This model will then serve as a base mechanism for development of multi-component diesel surrogate fuel model in Chapter 7 later. The detailed HXN mechanism consists of 2,115 species with 8,157 elementary reactions is applied in the present modelling studies. The model is derived from the composite mechanism established by Westbrook et al. [7] comprising all the detailed mechanisms for nine n-alkanes, including n-octane (nC₈H₁₈), n-nonane (nC₉H₂₀),

n-decane ($nC_{10}H_{22}$), n-undecane ($nC_{11}H_{24}$), n-dodecane ($nC_{12}H_{26}$), n-tridecane ($nC_{13}H_{28}$), n-tetradecane ($nC_{14}H_{30}$), n-pentadecane ($nC_{15}H_{32}$), and HXN ($nC_{16}H_{34}$) to describe the pyrolysis and oxidation process of the diesel fuel. The detailed composite mechanism has been validated against a wide range of operating conditions in various laboratory experimental devices such as shock tubes, flow reactors as well as jet stirred reactors (JSR). Since the detailed mechanisms for all these n-alkanes are presented as a single detailed mechanism, the corresponding mechanism for HXN is extracted out from the mechanism file.

HXN is easily ignited and it is remarkable for its ability to produce extensive amounts of low temperature reactivity. The low temperature reactivity is vital for its early ignition kinetics and this characteristic is governed by the low temperature reaction pathways which are mainly determined by alkylperoxy radical isomerisation. The mechanism is constructed based on the approach employed to develop nHep mechanism [8]. The elementary reactions are divided into 25 reaction classes in which reaction class 1 to 9 represent the high temperature regimes while reaction class 10 to 25 represent the low temperature regimes. The reaction classes are listed in Table 2-8.

Table 2-8: Reaction classes presented in the reaction mechanism.

Reaction Class	Reactions
<u>Low Temperature Mechanism</u>	
1	Unimolecular fuel decomposition
2	H-atom abstractions
3	Alkyl radical decomposition
4	Alkyl radical + O ₂ = olefin +HO ₂
5	Alkyl radical isomerisation
6	H-atom abstraction from olefins
7	Addition of radical species to olefins
8	Alkenyl radical decomposition
9	Olefin decomposition
<u>High Temperature Mechanism</u>	
10	Alkyl radical addition to O ₂
11	R + RO ₂ = RO + R'O
12	Alkylperoxy radical isomerisation
13	RO ₂ + HO ₂ = ROOH + O ₂
14	RO ₂ + H ₂ O ₂ = ROOH + HO ₂
15	RO ₂ + CH ₃ O ₂ = RO + CH ₃ O + O ₂
16	RO ₂ + RO ₂ = RO + R'O + O ₂
17	RO ₂ H = RO + OH
18	Alkoxy radical decomposition
19	QOOH decomposition and production of cyclic ethers
20	QOOH beta decomposition to produce olefin and HO ₂
21	QOOH decomposition to small olefin, aldehyde and OH
22	Addition of QOOH to molecular oxygen O ₂
23	Q ₂ QOOH isomerisation to carbonylhydroperoxide and OH
24	Carbonylhydroperoxide decomposition
25	Reactions of cyclic ethers with OH and HO ₂

R and R' denote the fuel components with same number of carbon atoms. The fundamental H₂/O₂ mechanism are developed by O'Conaire et al. [107] while the C₁ to C₄ sub-mechanisms are developed by Petersen et al. [108].

The 2,115-species HXN mechanism was applied to compute the species profiles for stirred reactor oxidation [7] and the results were compared to the work of

Ristori et al. [13]. 0.03 % mole fraction of HXN was diluted in N₂ with ϕ of 0.5, 1 and 1.5 at atmospheric pressure. The operating temperature range was set to 1000 K to 1250 K with a residence time of 0.07 s. Good agreement is reportedly achieved between the experimental measurements and the simulation results. Besides, the detailed mechanism of HXN was also employed to study the combustion of RME in a JSR [109]. The results obtained demonstrate overall good agreement between the experiments and simulations with evident deviations in CO₂ prediction at lower temperatures. It is suggested that the observed differences in results are caused by the different oxidation behaviour between RME and HXN at low temperatures. CO₂ is produced from the oxidation of CO during the oxidation of HXN while CO₂ is directly decomposed from the RME fuel which contributes to higher CO₂ concentration at low temperatures. Other than that, it is reported that n-alkanes such as the HXN is able to replicate various combustion characteristics of large methyl esters [7].

The proposed HXN mechanism of Westbrook et al [7] is a valuable chemical kinetic tool to study the combustion of practical hydrocarbon fuels as it is a representative of large n-alkanic fuel. Therefore, it is applied as a single-component diesel surrogate fuel model in this study to simulate diesel combustion and emission behaviours.

2.2.4 Biodiesel Surrogate Fuel Model – Detailed MD/MD9D/nHep Mechanism

Based on the literature review presented in Section 2.2.2, the detailed MD/MD9D/nHep mechanism developed by Herbinet et al. [99] with 3,299 species and 10,806 elementary reactions is selected as the base mechanism for rapeseed biodiesel fuel. From here, the surrogate mechanism is denoted as MDBIO for brevity. MD possesses similar ignition times and NTC behaviour to real biodiesel fuels. However, it is a saturated methyl ester with no double bond while most methyl esters in biodiesel fuel are unsaturated. The formation of unsaturated species, which are the soot precursors, are chiefly dependent on the presence of double bonds which subsequently influences the fuel reactivities.

Conversely, MD9D which is an unsaturated methyl ester acts as an important intermediate in the combustion of saturated FAME. MD9D is designated to represent the unsaturated component of biodiesel fuel as the location of its double bond is the same as that in methyl oleate and also the first double bond in methyl linoleate as well as methyl linolenate. Both MD and MD9D possess similar molecular structures with ten carbon atom chain as well as a methyl ester group except the absence of a double bond in the hydrocarbon chain of MD.

Furthermore, it is reported that blending of MD with nHep demonstrates reasonable predictions in fuel reactivity for oxidation of RME in a JSR [109]. In addition, good agreement is also obtained when the same model is applied to reproduce the oxidation of n-decane/methyl palmitate blend in a JSR. Thus, MD and MD9D are combined with the oxidation model of nHep in order to obtain an improved representative for biodiesel surrogate mechanism. The model can be employed to simulate different biodiesel fuels by changing the mole fractions of the fuel components in the reactant blend.

In view of the satisfactory species profile predictions of most species as compared to the experimental measurements, the proposed biodiesel surrogate fuel model of Herbinet et al. [99] is therefore applied in this study to model the combustion and emission processes of RME.

2.3 Chemical Kinetic Mechanism Reduction Techniques

This section provides an overview of the developmental work of currently available chemical kinetic mechanism reduction techniques. During the early stage of reduction effort, classical mechanism reduction techniques based on sensitivity analysis, reaction rate analysis and Jacobian analysis [3,110–113] are employed to generate simplified reaction mechanisms for multi-dimensional CFD applications. However, the application of these reduction techniques are limited to mechanisms with small and simple chemistries. As a result, mechanism reduction techniques with different approaches [40,114–116] have been introduced for reduction of mechanisms with complex and large chemistry size. The

development of the reduction techniques is further discussed in Sections 2.3.1 and 2.3.2.

2.3.1 Conventional Mechanism Reduction Techniques

In the earlier years, conventional mechanism reduction techniques such as the sensitivity analysis are often used to produce simplified kinetic models for multi-dimensional CFD simulations. Sensitivity analysis is useful to identify the influences of the studied parameters on the dynamic phenomena. It can be categorised based on the output of the studied kinetic model as a function of parameters. Hence, various types of sensitivity computations can be distinguished.

A review of applications of sensitivity analysis in chemical kinetic modelling studies is presented by Rabitz et al. [110]. This reduction technique offers an instant quantitative error measurement of the numerical modelling and thus providing more insights into the kinetic studies. Nevertheless, despite its simple application, sensitivity analysis requires additional postprocessing effort which is time-consuming, and it is only suitable to be used on small-scale mechanism reduction. These findings are supported by the work of Turányi [117] where the influence of parameter variations on the solution of mathematical models is studied using the sensitivity analysis. Concentration sensitivity, rate sensitivity and feature sensitivity analysis of spatially homogeneous constant-parameter reaction systems are discussed in his work. Brute-force method is introduced to calculate the local concentration sensitivity. However, huge computational power is required to perform the analysis [118] and thus this method is not recommended despite its simple usage. In contrast, rate sensitivity analysis involves the computation of species production rate using a sensitivity matrix [119]. The analysis provides the importance level of each elementary reaction to the kinetic systems and the main reaction pathways are discovered through the analysis. This permits an effective reduction in the mechanism size with adequate accuracy. Nonetheless, the use of sensitivity matrix also requires high computational time-cost and computing power when a complex reaction mechanism is involved.

Feature sensitivity analysis offers a different conception in the reduction procedure in comparison to the concentration sensitivity analysis. However, the analysis is not straightforward and generally brute-force method is employed in this application which is not in favour too due to its high consumption of computational power.

The reaction rate analysis is a simple technique to identify the redundant species and reactions in huge mechanisms. However, the approach requires validation for every single eliminated species which is not favourable for large-scale mechanism reduction. As a result, Jacobian-based methods [111,120,121] are introduced to overcome the drawbacks. The method of Jacobian analysis is able to identify species with strong coupling to the main species through computation of Jacobian matrix. Time-scale analysis such as Intrinsic Low-Dimensional Manifolds (ILDM) [122–124] and Computational Singular Perturbation (CSP) [125–128] methods are among the common techniques applied for mechanism reduction by computing Jacobian matrix. These approaches are able to decouple fast and slow subspaces, but they require high demand of computational time-cost as well as storage space. Furthermore, the arbitrary threshold value selection of Jacobian matrix might pose a problem to the user and system-dependent knowledge is often needed.

In addition, Principle Component Analysis (PCA) [129–131] is one of the methods used to determine redundant reactions too. During the reduction practice of PCA methodology, reduction criteria is carefully selected in order to control the accuracy of the reduced mechanism. The important kinetic data of species in a reacting system is extracted from the the linear sensitivity coefficients at several time steps. PCA method is able to identify the strong interacting reactions, and this key benefit permits elimination of unnecessary reactions from the detailed mechanism effectively. Nonetheless, the reduction technique is developed based on the approach of sensitivity analysis which involves resolution of sensitivity matrix and this has prohibited its usage on large-scale mechanisms.

The advantages and disadvantages of the conventional mechanism reduction techniques reviewed in this section are summarised in Table 2-9.

Table 2-9: Advantages and disadvantages of the conventional mechanism reduction techniques.

Reduction Techniques	Advantages	Disadvantages
Sensitivity Analysis	Simple and straightforward application	Involves additional post-processing effort which is time-consuming and it is unsuitable to be used on large-scale mechanism reduction
Reaction Rate Analysis	Simple technique to identify the redundant species and reactions in huge mechanisms	Computationally expensive since it requires validation for every single eliminated species
Jacobian Analysis	Able to identify species with strong coupling to the main species through computation of Jacobian matrix	Arbitrary threshold value selection might pose a problem to the user and system-dependent knowledge is often needed
PCA	Able to identify the strong interacting reactions with carefully selected reduction criterion to control the accuracy	High computational time-cost of solving the sensitivity matrices has prohibited its usage on huge mechanisms
ILDm	Compute Jacobian matrix which decouples fast and slow subspaces	Requires high demand of computational time-cost and storage space
CSP	Able to identify the steady-state species as well as the time scales of different mode effectively	Reference time criterion is required to separate the fast-slow subspaces and time-consuming when solving the Jacobian matrices

2.3.2 Recent Developments of Mechanism Reduction Techniques

In view of the shortcomings of the conventional mechanism reduction techniques shown in Table 2-9, different reduction approaches, such as the Directed Relation Graph (DRG) -based methods, are introduced later on to cope with larger kinetic models. These reduction methods are more favourable due to their straightforward chemical analysis and simpler application to kinetic modelling codes. Unimportant species as well as the associated elementary reactions are eliminated based on a predetermined numerical criterion using different types of graph searching (also known as graph traversal) algorithms. These search algorithms are the process of plotting an efficiently traversable path between multiple points (i.e. nodes) and are categorised by the order in which the nodes are visited.

Of late, the DRG method developed by Lu et al. [41,114] has received significant attention. In comparison with Jacobian analysis [113], both methods have similar approach in identifying major coupling between important species. However, Jacobian analysis consumes longer computational time since it requires iterative procedure [113] whereas DRG manages to identify all the candidate skeletal mechanisms with the time linearly proportional to the number of edges in the graph in a single run. Also, as compared to reaction rate analysis [3], DRG does not involve validation for each eliminated species that is assumed to be redundant. Thus, it significantly reduces the time cost for the reduction process. Other than that, DRG also provides a universally specifiable threshold value normalised between 0 and 1, which simultaneously states the upper error bound for the reduced mechanism. These features enable the reduction algorithm to be applicable in wider ranges of parametric space. It is reported that DRG is suitable to be used as the first stage to reduce detailed mechanism as it can effectively reduce the size of a huge mechanism quickly and in great extent. For instance, DRG has been successfully applied in the reduction of large-scale mechanisms such as nHep [8] and iso-octane [74].

Nonetheless, several drawbacks of DRG reduction method have been pointed out by Pepiot et al. [132]. Although DRG utilises coupling coefficient to resolve the error induced by removal of a single species to the production rate of another

species, the value is yet not directly correlated to an error measure. Additionally, DRG assumes that every selected species is correspondingly significant and hence the group of strongly coupled species has to be fully retained, which may not be necessary. Therefore, a novel method, namely DRG with Error Propagation (DRGEP) method, has been proposed by Pepiot et al. [132] to overcome the weaknesses of DRG. DRGEP has modified the approach of DRG by introducing a generalised coupling coefficient based on error propagations. Attention is paid on the transmission of error from a species to the targets. On top of that, selected species are no longer equally imperative whereby interrelated species that are situated far from each other might be more important than those directly connected to the targets. Similarly, DRGEP has also adopted a set of threshold value normalised between 0 and 1 to filter a subset of undesirable species.

It is noted that skeletal mechanisms developed by DRG are normally not nominal as it assumes upper-bound error propagation in the graph-searching procedure. Hence, DRG aided Sensitivity Analysis (DRGASA) method [115,118] is introduced to further reduce the species set to the minimal size. Other than that, isomer lumping approach is presented in this published work too. Generally, huge hydrocarbon fuels contain isomers that are important for low-temperature ignition. Thus, isomers with comparable thermal and diffusion properties are grouped together so that the number of species transport equations is reduced. As a consequence, isomers with group mass fractions that are smaller than a threshold value are eliminated. With the use of DRGASA, a reduced nHep mechanism with 55 species is successfully derived from a 78-species skeletal mechanism that is previously generated from DRG reduction technique.

Niemeyer et al. [20] has presented a novel mechanism reduction technique, namely DRG with Error Propagation and Sensitivity Analysis (DRGEPSA), which integrates the DRGEP and DRGASA methodologies together. It is demonstrated that the combination of DRGEP and DRGASA methods allows the DRGEPSA approach to overcome the weaknesses of each. It is reported that DRGEP is unable to identify all the unimportant species from the mechanism while DRGASA shields unimportant species from elimination. By merging these

two methods, DRGEPSA is capable to identify and eliminate more insignificant species than its precursors.

Another mechanism reduction scheme called Dynamic Adaptive Chemistry (DAC) is proposed by Liang et al. [133] based on the DRGEP method of Pepiot et al. [132]. This scheme allows on-the-fly mechanism reduction during reactive flow calculations and it reduces a globally valid detailed mechanism to a locally, instantaneously applicable smaller mechanism. Adaptive Chemistry (AC) [134–136] is one of the approaches established to exploit the time savings available through the use of locally and temporally valid reduced mechanisms. In their work, a more systematic and comprehensive evaluation of DAC scheme is discussed. It is found that removal of associated species that do not have a major influence on the total reaction rate can be achieved by eliminating species with very small mass fractions. However, sufficiently small reduction intervals are essential for calculation of fast problems.

Nagy et al. [137] has developed a new species reduction technique called Simulation Error Minimisation Connectivity Method (SEM-CM). In contrast to DRG-based mechanism reduction methods, SEM-CM utilises threshold values that are directly referring to the error of reduction. A mechanism building procedure is commenced by producing a small steady mechanism containing the important species and their elementary reactions with other species that are extracted from the detailed mechanism on the basis of the normalised Jacobian. In their research, reduction of detailed methane partial oxidation mechanism has been accomplished, and it is shown that smallest reduced mechanism is obtained at a given simulation error and the largest speed-up compared to DRG-based mechanism reduction techniques. Although this approach is capable of producing a minimal reduced mechanism for a specified error limit, its efficiency is restricted by the costly computational expenses.

Apart from species elimination reduction method, Selim et al. [138] has introduced a novel approach of Direct Elementary Reaction Error (DERE) to further reduce the kinetic mechanisms through elimination of insignificant reactions from the mechanisms. DRGEP method developed by Pepiot et al. [132]

has been employed as the initial step for skeletal mechanism reduction. Subsequently, DERE is applied to further reduce the mechanism by calculating the corresponding error of discarding a specific elementary reaction from the mechanisms. It is found that some reactions are not dominant, but they are identifiable due to other prominent active reactions. Thus, in this case, the methodology of error propagation will not be able to reduce the detailed mechanism any further. By employing this newly introduced approach into the system, the contribution of each single reaction will be taken into account. Thus, the slow reactions can be removed by applying an acceptable threshold. Nonetheless, huge computational time-cost is required to compute the error measure for every single reaction.

The advantages and disadvantages of the current mechanism reduction techniques reviewed in this section are summarised in Table 2-10.

Table 2-10: Advantages and disadvantages of the recent mechanism reduction techniques.

Reduction Techniques	Advantages	Disadvantages
DRG	Able to identify major species couplings and does not require validation for each removed species that is assumed to be redundant which then significantly reduces the time cost	Size of the reduced mechanism is not nominal since DRG assumes upper-bound error propagation in the graph-searching procedure and every selected species is assumed to be equally significant which might not be necessary
DRGASA	Further reduces the mechanism derived from DRG to minimal size by eliminating limbo species	Shields unimportant species from removal and the process of sensitivity analysis is time-consuming
DRGEP	Considers error propagated down the graph pathways owing to species elimination	Cannot detect all unimportant species and this method fails to identify the coupling between species when both

fast rate of production and consumption occur at the same time

DRGEPSA	Integrates DRGEP and DRGASA which absorbs the advantages of both reduction techniques	The overall reduction process requires high computational time cost
SEM-CM	Identifies the redundant species and elementary reactions of a large-scale mechanism by monitoring the error induced during species and reaction elimination procedure	Efficiency is restricted by the costly computational expenses
DAC	Allows on-the-fly mechanism reduction during reactive flow calculations	Requires small reduction intervals for calculation of fast problems
DERE	Further reduces mechanism by eliminating insignificant reactions through calculation of relative error of discarding a specific reaction from the mechanism	High computational time-cost is required to compute the error measure for every single reaction

2.4 Concluding Remarks

Based on the literature review conducted for diesel and biodiesel surrogate fuel mechanisms, it is found that mechanisms with long-carbon-chain structures are more suitable to be appraised as the surrogate models for diesel and biodiesel fuels. Hence, the HXN mechanism with 2,115 species and 8,157 elementary reactions as well as the MDBIO mechanism with 3,299 species and 10,806

elementary reactions are selected as the surrogate models for diesel and biodiesel fuels, respectively, for the present modelling studies.

Both conventional and current mechanism reduction techniques are reviewed in this chapter. It is found that the majority of the conventional mechanism reduction techniques requires high computational time-cost and computing power. Consequently, they are not applicable in reduction of large-scale mechanisms. In view of this, the current mechanism reduction techniques, particularly the DRG-based mechanism reduction techniques, are more favourable as they are able to achieve greater reduction scale with lower consumption of computing power. In Chapter 4, DRG, DRGASA, DRGEP and DRGEPSA are selected to perform mechanism reduction for both detailed diesel and biodiesel surrogate fuel models, and the performance of every reduction technique is appraised.

In addition, it is noted that the extent of reduction is restricted when only a single reduction technique is applied in the mechanism reduction procedure. Therefore, it is important to formulate a reduction scheme which incorporates different reduction techniques for greater reduction scale. As such, the incompatibility of each individual reduction technique is compensated. This will be further discussed in Chapter 5.

CHAPTER 3

GOVERNING EQUATIONS

3.1 Introduction

This chapter presents the governing equations of both the chemical kinetics and CFD models applied in this study. Two software packages, namely CHEMKIN-PRO and OpenFOAM, are employed. In Section 3.2, the governing equations applied in the CHEMKIN-PRO simulations are presented. CHEMIN-PRO is a FORTRAN-based chemical kinetics package which is employed to solve the gas-phase reactions involved in 0-D closed reactor systems. Meanwhile, OpenFOAM is an open-source code which is used as a CFD tool for multi-dimensional numerical simulations of constant volume combustion chamber and internal combustion engine. The sub-models and the correlated governing equations are presented in Section 3.3. Lastly, the numerical models applied in this study are summarised in Section 3.4.

3.2 Chemical Kinetics

In this work, a 0-D closed homogeneous batch reactor and an open perfectly-stirred reactor (PSR) models are applied throughout the kinetic studies. The closed homogeneous batch reactor is employed to simulate dynamic reactor conditions in which the controlling conditions vary with respect to time. Here, the ID timings predicted by the chemical kinetic models in a constant volume system along with the key species profiles are calculated as a function of time. In contrast, the open PSR model, which is also known as a continuously stirred tank reactor, is applied to simulate steady-state reactor systems from which species profiles as a function of ambient temperature are computed in this work.

The compositions of both batch and stirred reactors are presumed to be spatially uniform owing to high diffusion rates or forced turbulent mixing. As such, the

conversion rate of reactants to products is governed by chemical reaction rates instead of mixing processes.

3.2.1 0-D Closed Homogeneous Batch Reactor

A 0-D closed homogeneous batch reactor does not consist of any inlet or outlet flows. In this study, a batch reactor with constant-volume, adiabatic system is applied whereby there are no mass or heat exchanges between the reactor and its surroundings [139]. The system is essentially transient as the chemical state varies when production and destruction of species evolve through chemical reactions [140].

Based on the assumption that the compositions of the reactor are well-mixed, the material balance for i^{th} species, on the reactor can be represented by the following equation:

$$\frac{dn_i}{dt} = v_i \omega V \quad (3-1)$$

$$n_i = n_i^0 \text{ when } t = 0 \quad (3-2)$$

where V is the volume of the reactor, v_i is the species stoichiometric coefficient, n is number of mole of species, ω is the reaction rate and t is the time. The superscript 0 depicts the input to the reactor.

3.2.2 PSR

In contrast, the PSR is an open system which comprises of a chamber with inlet and outlet ducts. Here, flow reactor with constant-pressure, isothermal system is applied. It operates at steady-state, and the system is well-mixed to provide constant composition throughout the reactor [139]. The contents of the reactor are assumed to be equal to that of the effluent stream in which the reactions take place at this constant composition.

Therefore, the material balance for i^{th} species, on a PSR can be defined by:

$$v_i \omega = \frac{F_i - F_i^0}{V} \quad (3-3)$$

where F_i denotes the input molar flow rate of species i while F_i^0 denotes the output molar flow rate. The variance in species input and output flow rate is caused by the chemical reactions as the reactor is operating at steady state.

3.2.3 Chemistry Set

During pre-processing of gas-phase chemistry mechanism, the input data files for chemical kinetic mechanism (“chem.inp”) as well as the corresponding thermodynamic data (“therm.dat”) are imported into CHEMKIN-PRO. All these data input files will deliver the essential information of chemical reactions and thermodynamic properties for the simulation applications. The input file for chemical kinetic mechanism comprises of chemical species and elementary reactions with respective Arrhenius rate parameters to describe the gas-phase chemistry systems. Each chemical species is composed of chemical elements which are defined prior to the species data. The Arrhenius rate parameters stated for each reaction are applied to compute the production and consumption rates of each species which then determine the chemical pathways of the fuel combustion process. This will be discussed in Section 3.2.4.

Furthermore, the physical properties of each chemical species are described in the thermodynamic data file and they are used to compute specific heats, C_p , enthalpies, H and entropies, S of each species. The expressions of C_p , H and S are stated in Equation 3-4, 3-5 and 3-6 respectively.

$$\frac{C_p}{R} = a_1 + a_2 T + a_3 T^2 + a_4 T^3 + a_5 T^4 \quad (3-4)$$

$$\frac{H}{RT} = a_1 + \frac{a_2}{2} T + \frac{a_3}{3} T^2 + \frac{a_4}{4} T^3 + \frac{a_5}{5} T^4 + \frac{a_6}{T} \quad (3-5)$$

$$\frac{S}{R} = a_1 \ln T + a_2 T + \frac{a_3}{2} T^2 + \frac{a_4}{3} T^3 + \frac{a_5}{4} T^4 + a_7 \quad (3-6)$$

where R is the universal gas constant while T is the gas temperature. a_n is the polynomial fitted coefficient. The obtained C_p , H and S values are carried forward to calculate gas-phase chemical kinetic rates.

3.2.4 Gas-Phase Chemical Kinetic Rates

There are three Arrhenius coefficients provided by each reaction in the chemical kinetic mechanism to calculate the gas-phase chemical kinetic rates, namely pre-exponential factor, A , temperature exponent, β and the activation energy, E_a . By applying these Arrhenius parameters, the forward rate constant, k_f , of a reaction is obtained from the following Arrhenius temperature dependence:

$$k_f = AT_{gas}^{\beta} \exp\left(\frac{-E_a}{RT_{gas}}\right) \quad (3-7)$$

The production rate of i^{th} species, $\dot{\omega}_i$, involving j^{th} reaction is defined by the difference of the forward and reverse rates. This is expressed by the following equation:

$$\dot{\omega}_i = \sum_{j=1}^J v_{ij} \left\{ \underbrace{k_{f,j} \prod_i [X_i]^{v'_{ij}}}_{\text{forward reaction rate}} - \underbrace{k_{r,j} \prod_i [X_i]^{v''_{ij}}}_{\text{reverse reaction rate}} \right\} \quad (3-8)$$

$$v_{ij} = v''_{ij} - v'_{ij} \quad (3-9)$$

where k_r is the reverse rate constant, J is the total number of reactions and $[X_i]$ is the molar concentration of the i^{th} species. The superscript ' depicts forward stoichiometric coefficients, while '' depicts reverse stoichiometric coefficients.

k_r can be calculated from the following equation:

$$k_{r_j} = \frac{k_{f_j}}{K_{C_j}} \quad (3-10)$$

where K_{C_j} represents the equilibrium constant of j^{th} reaction given in concentration unit and it can also be expressed in pressure unit such as:

$$K_{c_j} = K_{p_j} \left(\frac{P_{atm}}{RT} \right)^{\sum_{i=1}^I v_{ij}} \quad (3-11)$$

$$K_{p_j} = \exp \left(\frac{\Delta S_j^0}{R} - \frac{\Delta H_j^0}{RT} \right) \quad (3-12)$$

where K_{p_j} is the equilibrium constant of j^{th} reaction given in pressure unit and Δ denotes the conversion that occurs in passing completely from reactants to products in the i^{th} species such as:

$$\frac{\Delta S_j^0}{R} = \sum_{i=1}^I v_{ij} \frac{S_i^0}{R} \quad (3-13)$$

$$\frac{\Delta H_j^0}{RT} = \sum_{i=1}^I v_{ij} \frac{H_i^0}{RT} \quad (3-14)$$

When a third body is involved in the reaction, the concentration of the effective third body is then added to the expression in Equation 3-8 with an extra term, α_{ij} and this is depicted in the following expression:

$$\dot{\omega}_i = \sum_{j=1}^J v_{ij} \left(\sum_{i=1}^I (\alpha_{ij}) [X_i] \right) \{ k_{f,j} \prod_i [X_i]^{v_{ij}} - k_{r,j} \prod_i [X_i]^{v'_{ij}} \} \quad (3-15)$$

where α_{ij} is equal to 1 if all species in the mixture contribute equally as third bodies.

3.3 CFD Sub-Models

In this section, CFD sub-models for constant volume spray combustion and diesel engine simulations are described. The CFD sub-models discussed here consist of primary and secondary droplet breakup models, turbulence model and soot model.

3.3.1 Spray Breakup Model – Reitz-Diwakar Model

Prediction of fuel droplets breakup is crucial to the modelling of fuel spray as it affects the subsequent air-fuel mixing process, and consequently influences the

engine performance and emissions. The Reitz-Diwakar model [141,142] is applied in this study to comprehend this phenomenon.

There are two major breakup regimes, namely primary breakup and secondary breakup. During the process of primary breakup, large droplets are formed from the breakup of intact liquid core immediately after exiting the spray nozzle. Meanwhile, large droplets break up into smaller droplets during the process of secondary breakup owing to the aerodynamic forces between fuel and the ambient gas. These regimes are dependent on the Weber number, We and it is expressed in the following equation:

$$We = \frac{u_{rel}^2 d \rho_g}{\sigma} \quad (3-16)$$

where u_{rel} is the relative velocity between liquid droplet and ambient gas. d is the droplet diameter, ρ_g is the gas density and σ is the surface tension.

In this work, the spray breakup process is simulated by Reitz-Diwakar model. The breakup model of Reitz and Diwakar is divided into two breakup regimes which are bag breakup and stripping breakup as defined by following the correlations:

$$\text{Bag breakup:} \quad We = \frac{u_{rel}^2 d \rho_g}{\sigma} > 6 \quad (3-17)$$

$$\text{Stripping breakup:} \quad \frac{We}{\sqrt{Re}} > 0.5 \quad (3-18)$$

Re is the Reynolds number defined as:

$$Re = \frac{2u_{rel}r}{\nu_g} \quad (3-19)$$

where ν_g is the kinematic viscosity of the gas and r is the droplet radius.

The lifetimes of unstable droplets for the bag and stripping modes are expressed as t_1 and t_2 in Equations 3-20 and 3-21, respectively.

$$t_1 = D_1 \sqrt{\frac{\rho_1 r^3}{\sigma}} \quad (3-20)$$

$$t_2 = D_2 \frac{r}{u} \sqrt{\frac{\rho_1}{\rho}} \quad (3-21)$$

The model constants D_1 and D_2 are of order unity [143].

3.3.2 Turbulence Model

In this study, standard k-epsilon (k - ϵ) model [144] and Re-Normalisation Group (RNG) k - ϵ model are applied in the 2-D spray combustion simulations and 3-D internal combustion engine simulations, respectively. The descriptions of the models are depicted in Sections 3.3.2.1 to 3.3.2.2.

3.3.2.1 Standard k - ϵ model

The standard k - ϵ model [144] is applied in the 2-D spray combustion simulations to model the turbulence flow conditions during combustion process. It is a two-equation semi-empirical model whereby two separate transport equations are resolved to determine the turbulent velocity and length scales individually. Several assumptions are made during the derivation of the standard k - ϵ model. The flow is assumed to be fully turbulent, and the influences of molecular viscosity are insignificant. Hence, the standard k - ϵ model is solely valid for fully turbulent flows.

The model is constructed based on the transport equations for turbulence kinetic energy, k and its dissipation rate, ϵ . The k and ϵ are obtained from the subsequent transport equations respectively:

$$\frac{\delta}{\delta t}(\rho k) + \frac{\delta}{\delta x_i}(\rho k u_i) = \frac{\delta}{\delta x_j} \left[\left(\mu + \frac{\mu_t}{\sigma_k} \right) \frac{\delta k}{\delta x_j} \right] + G_k + G_b - \rho \epsilon - Y_M + S_k \quad (3-22)$$

$$\frac{\delta}{\delta t}(\rho \epsilon) + \frac{\delta}{\delta x_i}(\rho \epsilon u_i) = \frac{\delta}{\delta x_j} \left[\left(\mu + \frac{\mu_t}{\sigma_\epsilon} \right) \frac{\delta \epsilon}{\delta x_j} \right] + C_{1\epsilon} \frac{\epsilon}{k} (G_k + C_{3\epsilon} G_b) - C_{2\epsilon} \rho \frac{\epsilon^2}{k} + S_\epsilon \quad (3-23)$$

where G_k is the generation of turbulence kinetic energy caused by mean velocity gradients while G_b is the generation of turbulence kinetic energy caused by buoyancy. Y_M depicts the contribution of the fluctuating dilatation in compressible turbulence to the overall dissipation rate. $C_{1\varepsilon}$, $C_{2\varepsilon}$ and $C_{3\varepsilon}$ are model constants whereas σ_k and σ_ε are the turbulent Prandtl numbers for k and ε , respectively. S_k and S_ε are the user-defined source terms.

μ_t is the turbulent viscosity and it is expressed in the following equation:

$$\mu_t = \rho C_\mu \frac{k^2}{\varepsilon} \quad (3-24)$$

where C_μ is a model constant.

The default values of the respective model constants are summarised in Table 3-1.

Table 3-1: Model constants used in standard k - ε model.

Model Constant	$C_{1\varepsilon}$	$C_{2\varepsilon}$	C_μ	σ_k	σ_ε
Default Value	1.44	1.92	0.09	1.0	1.3

3.3.2.2 RNG k - ε model

The standard k - ε model is frequently applied in numerical simulations of model flows with high Re . However, the major weakness of the standard k - ε model is that it is unable to simulate flows with low Re as well as flows in the near-wall region. Hence, the RNG k - ε model has been proposed by Yakhot and Orszag [145] to overcome these drawbacks. The model consists of an additional term in its ε equation which has significantly improved the accuracy of the model predictions for rapidly-strained flows. The swirling effects on turbulence are also incorporated in this model. As such, RNG k - ε model is found to be more accurate and reliable than the standard k - ε model for a wider range of flows. In addition, RNG k - ε model has also been reported to simulate the turbulence dynamics in an engine cylinder well [146,147]. As a result, it is applied in the current work to study the combustion and soot formation events in a light-duty, DI diesel engine.

The k equation in the RNG k - ε model is similar to that of standard k - ε model. Nonetheless, the ε equation of the RNG k - ε model is different from the standard version as it provides an analytical formula for turbulent Prandtl numbers rather than depending on empirically derived constants. Here, the k and ε of the RNG k - ε model are calculated using Equations 3-25 and 3-26, respectively.

$$\frac{\delta}{\delta t}(\rho k) + \frac{\delta}{\delta x_i}(\rho k u_i) = \frac{\delta}{\delta x_j} \left[\alpha_k \mu_{eff} \frac{\delta k}{\delta x_j} \right] + G_k + G_b - \rho \varepsilon - Y_M + S_k \quad (3-25)$$

$$\frac{\delta}{\delta t}(\rho \varepsilon) + \frac{\delta}{\delta x_i}(\rho \varepsilon u_i) = \frac{\delta}{\delta x_j} \left[\alpha_\varepsilon \mu_{eff} \frac{\delta \varepsilon}{\delta x_j} \right] + C_{1\varepsilon} \frac{\varepsilon}{k} (G_k + C_{3\varepsilon} G_b) - C_{2\varepsilon} \rho \frac{\varepsilon^2}{k} - R_\varepsilon + S_\varepsilon \quad (3-26)$$

where α_k and α_ε are the inverse effective Prandtl numbers for k and ε , respectively. R_ε in Equation 3-26 is the rate-of-strain term introduced in the RNG k - ε model to improve the model prediction in comparison to the standard k - ε model. Apart from that, μ_{eff} is the effective viscosity which is calculated using the following equations:

$$d \left(\frac{\rho^2 k}{\sqrt{\varepsilon \mu}} \right) = 1.72 \frac{\hat{v}}{\sqrt{\hat{v}^3 - 1 + C_v}} d \hat{v} \quad (3-27)$$

$$\hat{v} = \frac{\mu_{eff}}{\mu} \quad (3-28)$$

where C_v is a constant which has a value of approximately 100. Equations 3-27 and 3-28 are used to define the effective turbulent transport with respect to the variation of effective Re in order to achieve more accurate results for flows with low Re and flows in the near-wall region. Meanwhile, the effective viscosity for high Re is calculated using Equation 3-24, which is similar to that of the standard k - ε model. Nevertheless, the constant C_μ with a value of 0.0845 is obtained from the RNG theory, which is different from that of the standard k - ε model which yields a value of 0.09. Additionally, the model constant $C_{3\varepsilon}$ is defined as:

$$C_{3\varepsilon} = \tanh \left| \frac{v}{u} \right| \quad (3-29)$$

The default models constants employed in the RNG k - ε model are summarised in Table 3-2.

Table 3-2: Model constants used in RNG k - ε model.

Model Constant	$C_{1\varepsilon}$	$C_{2\varepsilon}$	C_μ	α_k	α_ε
Default Value	1.42	1.68	0.0845	1.393	1.393

In this study, the initial turbulence quantities at intake valve closure (IVC) such as k and ε are calculated using the following equations:

$$k = (\text{mean engine speed})^2 \quad (3-30)$$

$$\varepsilon = \frac{1.64k^{\frac{3}{2}}}{\text{Bore}} \quad (3-31)$$

The initial k and ε values of the RNG k - ε model calculated for the engine simulations (in Chapter 8) are $21 \text{ m}^2/\text{s}^2$ and $1840.1 \text{ m}^2/\text{s}^3$, respectively, with a mean engine speed of 4.587 m/s (i.e. 1600 rev/min) and a bore diameter of 0.086 m .

3.3.3 Soot Model – Multistep Model

The multistep soot model proposed by Leung et al. [148] is employed to capture soot inception, coagulation, surface growth and oxidation processes. First and foremost, the production of soot precursors and surface growth species are computed based on the gas-phase reactions. Following that, the calculated species concentrations are applied in the governing equation of multistep soot model to resolve the transport equations for particle number density, ϕ_N , as well as soot mass fraction, Y_{soot} . The transport equations for ϕ_N , and Y_{soot} are given in the following equations:

$$\frac{\delta}{\delta t}(\rho\phi_N) + \nabla \cdot (\rho\vec{v}\phi_N) = \nabla \cdot \left(\frac{\mu_t}{Sc_t} \nabla\phi_N \right) + \frac{1}{N_A} \frac{dN}{dt} \quad (3-32)$$

$$\frac{\delta}{\delta t}(\rho Y_{soot}) + \nabla \cdot (\rho\vec{v}Y_{soot}) = \nabla \cdot \left(\frac{\mu_t}{Sc_t} \nabla Y_{soot} \right) + \frac{1}{N_A} \frac{dM}{dt} \quad (3-33)$$

where \vec{v} depicts the fluid velocity and Sc_t is the turbulent Schmidt number. Additionally, N is the soot particle number density and M is the soot mass concentration. N_A is the Avogadro number and it has a value of $6.0223045 \times 10^{26} \text{ kmol}^{-1}$. dN/dt and dM/dt denote the instantaneous production rate of soot particles and net soot production in Equation 3-34 and 3-35, respectively. dN/dt is subjected to soot nucleation from the gas phase and coagulation in the free molecular regime, as expressed in the following equation:

$$\frac{dN}{dt} = C_\alpha \cdot N_A \left(\frac{X_{prec}P}{RT} \right) \exp\left(-\frac{21000}{T}\right) - C_\beta \left(\frac{24RT}{\rho_{soot}N_A} \right)^{1/2} \left(\frac{6M}{\mu\rho_{soot}} \right)^{1/6} N^{11/6} \quad (3-34)$$

where X_{prec} is the mole fraction of the soot precursor and it is calculated based on the chemical reactions. ρ_{soot} is the soot mass density which has a value of 2000 kg/m^3 [149]. C_α is the model constant for soot inception rate with a value of $10,000 \text{ s}^{-1}$. C_β is the model constant for coagulation rate and it has a value of 3.

Meanwhile, the dM/dt is depicted in the following expression:

$$\begin{aligned} \frac{dM}{dt} = & C_\alpha \cdot M_p \cdot \left(\frac{X_{prec}P}{RT} \right) \exp\left(-\frac{T_\alpha}{T}\right) \\ & + C_\gamma \cdot \left(\frac{X_{sgs}P}{RT} \right) \exp\left(-\frac{T_\gamma}{T}\right) \left[(\pi N)^{\frac{1}{3}} \left(\frac{6M}{\rho_{soot}} \right)^{\frac{2}{3}} \right]^{\frac{1}{2}} \\ & - C_{\omega,1} \cdot \eta_{coll} \left(\frac{X_{OH}P}{RT} \right) \sqrt{T} (\pi N)^{\frac{1}{3}} \left(\frac{6M}{\rho_{soot}} \right)^{\frac{2}{3}} \\ & - C_{\omega,2} \cdot \left(\frac{X_{O_2}P}{RT} \right) \exp\left(-\frac{T_{\omega,2}}{T}\right) \sqrt{T} (\pi N)^{\frac{1}{3}} \left(\frac{6M}{\rho_{soot}} \right)^{\frac{2}{3}} \end{aligned} \quad (3-35)$$

where C_γ is the surface growth rate scaling factor and it has a value of $72,000 \text{ kg/m}^{1/2}\text{-kmol-s}$. T_α is the activation temperature of soot inception with a value of $21,000 \text{ K}$ whereas T_γ is the activation temperature of surface growth with a value of $12,100 \text{ K}$. M_p is the mass of an initial soot particle which comprises of 100 carbon atoms and it has a value of 1200 kg/kmol . X_{sgs} is the mole fraction of the participating surface growth species and it is replaced by the mole fraction of C_2H_2 since it is the primary soot surface growth species in the chemistry. X_{OH} and

X_{OH} and X_{O_2} are the mole fractions for OH and O₂, respectively. Both species are designated as soot oxidants [150,151]. η_{coll} is the collision efficiency parameter and it is set to 0.13 in the numerical studies. Both $C_{\omega,1}$ and $C_{\omega,2}$ are model constant for soot oxidation due to OH and O₂, respectively. $C_{\omega,1}$ is set to 105.81 kg-m/kmol-K^{1/2}-s and $C_{\omega,2}$ is set to 8903.51 kg-m/kmol-K^{1/2}-s. $T_{\omega,2}$ is the activation temperature due to O₂ with a value of 19,778 K.

3.4 Concluding Remarks

In this chapter, the chemical kinetics and CFD sub-models along with their respective governing equations applied in the numerical study are described. The CFD sub-models applied in the subsequent diesel spray and engine combustion simulations are summarised in Table 3-3. The reduced chemical kinetic models employed to describe the combustion events are subsequently discussed in Chapter 4.

Table 3-3: Summary of CFD sub-models employed in the 2-D spray combustion simulations and 3-D internal combustion engine simulations.

Events	CFD Sub-Models
Combustion/Ignition	Reduced chemical kinetic models (Chapter 4)
Spray breakup	Reitz-Diwakar model
Turbulence	Standard k- ϵ model (2-D simulations) RNG k- ϵ model (3-D simulations)
Soot	Multistep model

CHAPTER 4

APPRAISAL OF CHEMICAL KINETIC MECHANISM REDUCTION TECHNIQUES

4.1 Introduction

In this chapter, theoretical backgrounds of the chemical kinetic mechanism reduction techniques are first described in Section 4.2 and subsequently, selection of the base mechanisms for mechanism reduction is presented in Section 4.3. Accordingly, performance of each technique is assessed in Section 4.4 using a 6-core PC with 16 GB RAM and 3.4 GHz processing speed. The prominent mechanism reduction techniques applied in this work are DRG [41,114], DRGASA [115,118], DRGEP [132] as well as DRGEPSA [40,152,153]. These reduction methods are commonly favoured for huge mechanism reduction owing to their straightforward chemical analysis as well as their simple application to prevailing kinetic modelling codes such as CHEMKIN-PRO. Following that, the performance of each reduction technique is compared and discussed in Section 4.5. Finally, concluding remarks are made in Section 4.6 to summarise the results obtained.

4.2 Theoretical Backgrounds

In this section, the reduction approach for each chemical kinetic mechanism reduction technique is presented in conjunction with the main governing equations used in the reduction procedure.

4.2.1 DRG

The DRG methodology established by Lu et al. [114] is a direct and efficient approach to identify the unimportant species from the mechanism with minimal requirement of system-dependent data by resolving couplings among species. By

applying the concept of DRG methodology, coupling between two species, say species x and species y , is quantified. The species coupling measure, r_{xy} , which is a normalised contribution of species y to the production rate of species x , is expressed in the following equation:

$$r_{xy} = \frac{\sum_{j=1, N_R} |v_{x,j} \omega_j \delta_{yj}|}{\sum_{j=1, N_R} |v_{x,j} \omega_j|} \quad (4-1)$$

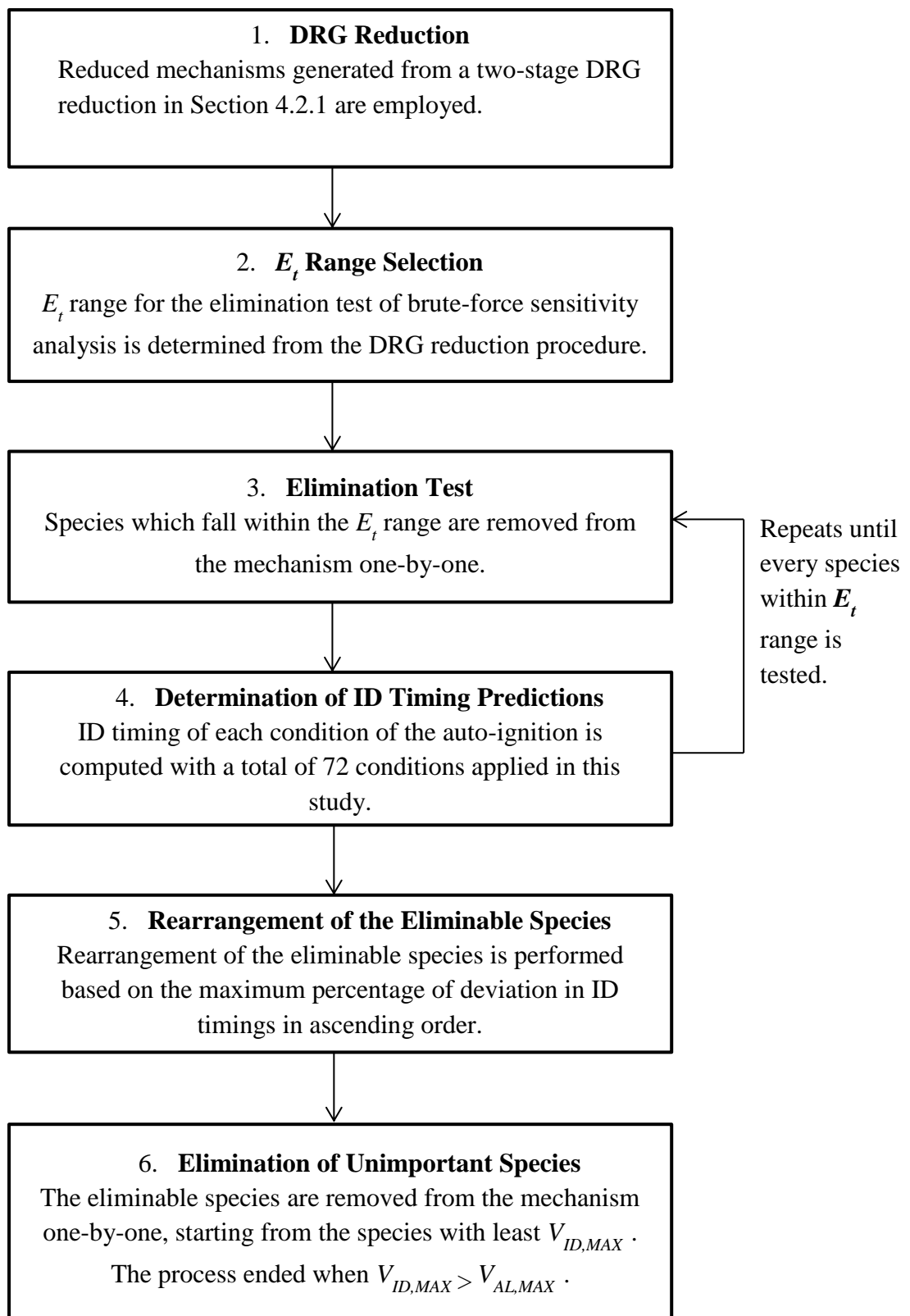
where N_R is the total number of elementary reactions in the mechanism. $v_{x,j}$ is the stoichiometric coefficient of species x while ω_j is the net reaction rate of j^{th} elementary reaction. δ_{yj} denotes the participation of species y in j^{th} elementary reaction and it is defined as:

$$\delta_{yj} = \begin{cases} 1, & \text{if the } j^{th} \text{ elementary reaction involves species } y; \\ 0, & \text{otherwise;} \end{cases} \quad (4-2)$$

As a results of the application of Equations 4-1 and 4-2, a universally specifiable threshold value, E_t , normalised between 0 and 1 is obtained. Species with $r_{xy} < E_t$ are eliminated along with the species group which are strongly coupled to them. Concurrently, the upper error bound for the reduced mechanism is specified and these features allow the reduction procedure to be applicable over extensive range of parametric space. Apart from that, when the number of species is large in the detailed mechanism, the DRG reduction can also be performed in several stages in order to further increase the reduction scale, such as the two-stage DRG and multi-stage DRG. The first stage of DRG reduction is the key reduction phase whereby a great number of species is removed from the detailed counterpart. On the other hand, the execution of the second stage is optional depending on the mechanism size. The written MATLAB code for DRG mechanism reduction technique can be found in Appendix A.

4.2.2 DRGASA

DRGASA is an extended methodology of DRG introduced by Zheng et al. [118]. While DRG assumes upper-bound error propagation in the graph-searching procedure, size of the reduced mechanism developed by DRG is usually not minimal. Apart from that, it is noted that not every species in the species group is equally important to the target species and global parameters. Thus, there is still a possibility to eliminate some of those species that have insignificant effects on other species. Hence, Zheng et al. [118] have introduced brute-force sensitivity to determine the entire set of eliminable species which is conserved during DRG reduction. The adapted reduction procedure of DRGASA is shown in Figure 4-1.



** $V_{ID,MAX}$ denotes maximum errors induced on ignition timings and $V_{AL,MAX}$ denotes maximum allowable induced error.

Figure 4-1: Adapted reduction procedure of DRGASA methodology [118].

4.2.3 DRGEP

As the species coupling coefficient adopted by DRG method does not directly associate to an error measure, Pepiot et al. [132] have established a new mechanism reduction method, namely DRGEP method, which takes account the transmission of error from a species to the targets. A Direct Interaction Coefficient (DIC) is introduced in this method whereby it refers to the dependency of a species on another based on its impact to the total production or consumption rate. DIC is expressed by the following equation:

$$\text{DIC} = \frac{|\sum_{j=1}^{N_R} v_{x,j} \omega_j \delta_y^j|}{\max(P_x, C_x)} \quad (4-3)$$

where P_x is the overall production rate of species x and C_x is the overall consumption rate of species x . Both P_x and C_x are described in Equations 4-4 and 4-5, respectively:

$$P_x = \sum_{j=1}^{N_R} \max(0, v_{x,j} \omega_j) \quad (4-4)$$

$$C_x = \sum_{j=1}^{N_R} \max(0, -v_{x,j} \omega_j) \quad (4-5)$$

Unlike DRG methodology, DRGEP takes distance from target species into consideration whereby the interrelated species are no longer equally significant to the target species. As such, an Overall Interaction Coefficient, R_{xy} , is introduced which is defined as the maximum of all dependency pathways for all species relative to the targets and it is expressed in the following equation:

$$R_{xy} = \max_{\text{all path } p} \left(\prod_{i=1}^{N_S-1} r_{s_i s_{i+1}} \right) \quad (4-6)$$

where i refers to the i^{th} species of pathway p . s is the placeholder for the intermediate species which starts at species x and ends at species y . r is equivalent to DIC presented in Equation 4-3.

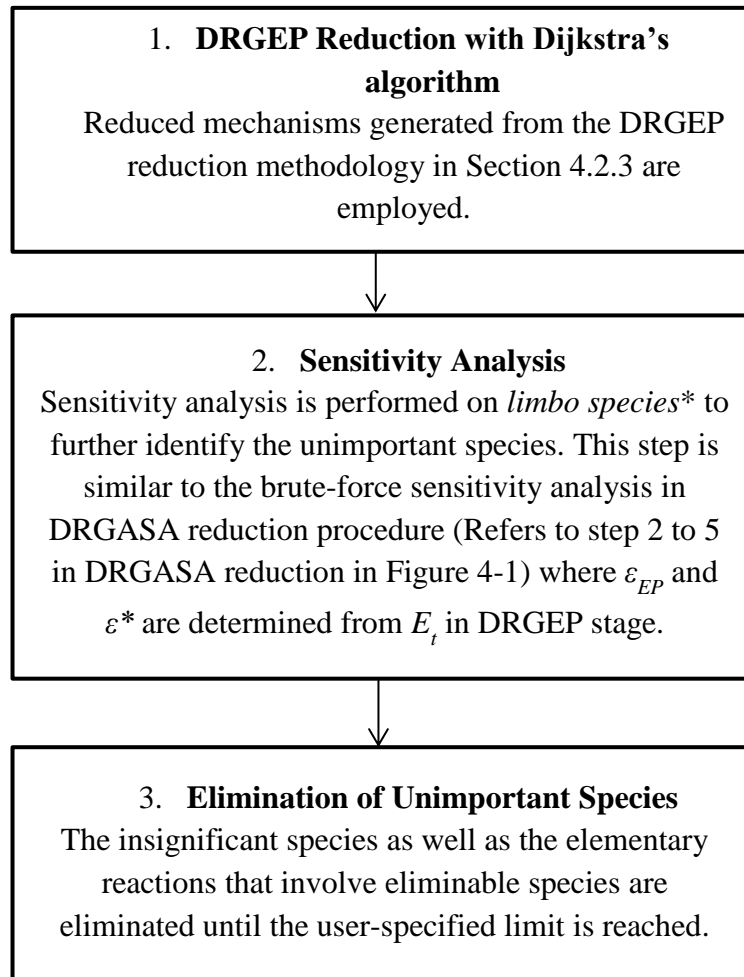
Moreover, Niemeyer and Sung [116] have carried out a study to inspect the performance of different graph searching algorithms applied in the DRGEP reduction methodology. The graph searching algorithms applied in their study are Depth First Search (DFS), Breadth First Search (BFS) [96,133,154,155] and

Dijkstra's algorithms [156,157]. DFS and BFS algorithms are commonly applied in majority of the DRGEP reduction work. DFS- and BFS-based algorithms initiate the searching procedure at a starting species to search species which are coupled to it according to pathways. In contrast, Dijkstra's algorithm calculates the shortest pathways from the target species to all other species. All search methods are found to have comparable performance in the study of Niemeyer and Sung [116], but Dijkstra's algorithm is able to generate the most compact reduced mechanism. The size of the reduced model generated using Dijkstra's algorithm is 3.4 and 1.6 times smaller than those produced from DFS and BFS algorithms, respectively [116]. Accordingly, DRGEP with Dijkstra's algorithm is selected to perform mechanism reduction in this work.

Furthermore, similar to DRG, DRGEP has also adopted a set of E_i normalised between 0 and 1 to filter a subset of undesirable species. However, DRG assumes that distance of species from targets is unimportant whereas DRGEP takes into account the importance of species further from targets. Hence, selection of starting species during DRGEP reduction procedure has to be done wisely in order to maximise the reduction scale. The written MATLAB code for DRGEP mechanism reduction technique can be found in Appendix B.

4.2.4 DRGEPSA

Niemeyer et al. [40] has presented a novel mechanism reduction technique namely DRGEPSA which combines both DRGEP and DRGASA in the new approach. By integrating DRGEP and DRGASA into DRGEPSA approach, weaknesses of the former two techniques are overcome. DRGEPSA is able to cope with the insufficiency of DRGEP in identifying all unimportant species as well as the shielding of unimportant species from elimination in DRGASA approach. Thus, DRGEPSA is able to detect more insignificant species than its precursors during the elimination process. The adapted reduction procedure of DRGEPSA is demonstrated in Figure 4-2.



**Limbo species* refers to species with R_{xy} values that satisfy $\epsilon_{EP} < R_{xy} < \epsilon^*$ (ϵ_{EP} is E_t during error propagation phase while ϵ^* is a higher value).

Figure 4-2: Adapted reduction procedure of DRGEP methodology [40].

4.3 Descriptions of the Base Mechanisms for Mechanism Reduction

In this section, the selected base mechanisms for both diesel and biodiesel surrogate fuel models are described. These are depicted in Table 4-1.

Table 4-1: Base mechanism for diesel and biodiesel surrogate fuels.

Surrogate Fuel	Base Mechanism	Mechanism Size		Ref
		N_S	N_R	
Diesel	HXN	2,116	8,130	[7]
Biodiesel	MDBIO	3,299	10,806	[99]

HXN mechanism [7] is chosen to represent diesel fuel since it is the primary reference fuel for diesel and it has a CN of 100 which could be varied over a wide range in fuel blending. Apart from that, it is more volatile and its boiling point is within the diesel boiling range. As discussed in Section 2.2.3, the HXN mechanism is included in the detailed chemical kinetic reaction mechanism established by Westbrook et al. [7] comprising nine n-alkanes. Hence, the corresponding mechanism for HXN is extracted out from the mechanism file.

Meanwhile, MDBIO mechanism is selected as the base mechanism for RME as MD produces similar ignition times and NTC behaviour to real biodiesel fuels. Additionally, Herbinet et al. [99] has established the importance of unsaturated methyl esters as an intermediate in the combustion of saturated FAME. Thus, MD9D is combined together with MD and oxidation model of nHep to attain an improved representative for rapeseed biodiesel blend surrogate mechanism. Here, the compositions of MD, MD9D and nHep are set to 3 %, 47 % and 50 % by volume, respectively. The composition of nHep is retained at 50 % in this work which is similar to the experimental study of RME oxidation in a JSR with dilute conditions [109]. The remaining 50 % of the surrogate fuel compositions is then divided accordingly based on the actual saturated and unsaturated compositions of RME. Components of the RME and the proposed biodiesel surrogate fuel model are listed in Table 4-2 along with their respective chemical formula, compositions and Carbon:Hydrogen:Oxygen (C:H:O) ratio.

Table 4-2: Fuel components of RME and the proposed biodiesel surrogate fuel model along with their respective chemical formula, average composition and C:H:O ratio.

Components	Chemical Formula	Saturated / Unsaturated	Avg Composition (%)	C:H:O
<u>RME</u>				
Methyl palmitate	C ₁₇ H ₃₄ O ₂	Saturated	4.3	1.00 : 2.00 : 0.12
Methyl linolenate	C ₁₉ H ₃₂ O ₂	Unsaturated	13.2	1.00 : 1.68 : 0.11
Methyl linoleate	C ₁₉ H ₃₄ O ₂	Unsaturated	21.1	1.00 : 1.79 : 0.11
Methyl oleate	C ₁₉ H ₃₆ O ₂	Unsaturated	59.9	1.00 : 1.89 : 0.11
Methyl stearate	C ₁₉ H ₃₈ O ₂	Saturated	1.3	1.00 : 2.00 : 0.11
Avg	C ₁₉ H _{35.15} O ₂	-	-	1.00 : 1.85 : 0.11
<u>Biodiesel Surrogate</u>				
MD	C ₁₁ H ₂₂ O ₂	Saturated	3	1.00 : 2.00 : 0.18
MD9D	C ₁₁ H ₂₀ O ₂	Unsaturated	47	1.00 : 1.82 : 0.18
nHep	C ₇ H ₁₆	-	50	1.00 : 2.29 : 0
Avg	C ₁₉ H _{38.1} O _{2.1}	-	-	1.00 : 2.00 : 0.11

Avg denotes average.

4.4 Validations in 0-D Chemical Kinetic Simulations

In this section, the reduced mechanisms for both diesel and biodiesel surrogate fuel models are derived from their corresponding detailed mechanism by applying DRG, DRGASA, DRGEP and DRGEP SA mechanism reduction techniques, respectively. MATLAB program is employed to develop the reduction algorithms and validations of the reduced mechanisms generated from the aforesaid reduction methodologies are carried out using 0-D closed homogeneous batch reactor model in CHEMKIN-PRO software. Efficiency of the mechanism in predicting auto-ignition is chosen as the basis for reduction. Here, maximum allowable induced error, $V_{AL,MAX}$, is set to 40 % as the error tolerance for large-scale mechanism reduction generally ranges from 30 % to 50 % [40,106,158,159]. The typical operating conditions for compression ignition diesel engine are applied, as shown in Table 4-3. The pressure range applied here is chosen based on the in-cylinder pressure values during the main fuel injection event for light-duty, DI diesel

engines. In this section, only results for 60 bar are shown as similar trends are obtained for pressures of 40 and 80 bar.

Table 4-3: Operating conditions applied for validation of each reduced mechanism.

Operating Condition	Range Evaluated
Φ (-)	0.5, 1.0, 2.0
Initial Pressure (bar)	40, 60, 80
Initial Temperature (K)	650 – 1350 (100 K increments)

4.4.1 DRG

DRG reduction is carried out as a function of number of stages. A total number of 216 sampling points are selected for each mechanism in order to facilitate the analysis of every representative reaction condition. It is observed that the number of sampling points applied in each reduction case is adequate for the specified accuracy. During the reduction procedure, each stage of DRG reduction process requires approximately 1 min in average to complete. $nC_{16}H_{34}$ is selected as the starting species for reduction of HXN mechanism whereas MD, MD9D and C_7H_{16} are selected as the starting species for reduction of MDBIO mechanism. The dependency of N_S in reduced mechanism on the user-defined E_t is demonstrated in Figure 4-3(a) for HXN mechanism and Figure 4-3(b) for MDBIO mechanism. In this reduction work, multi-stage DRG refers to a three-stage DRG.

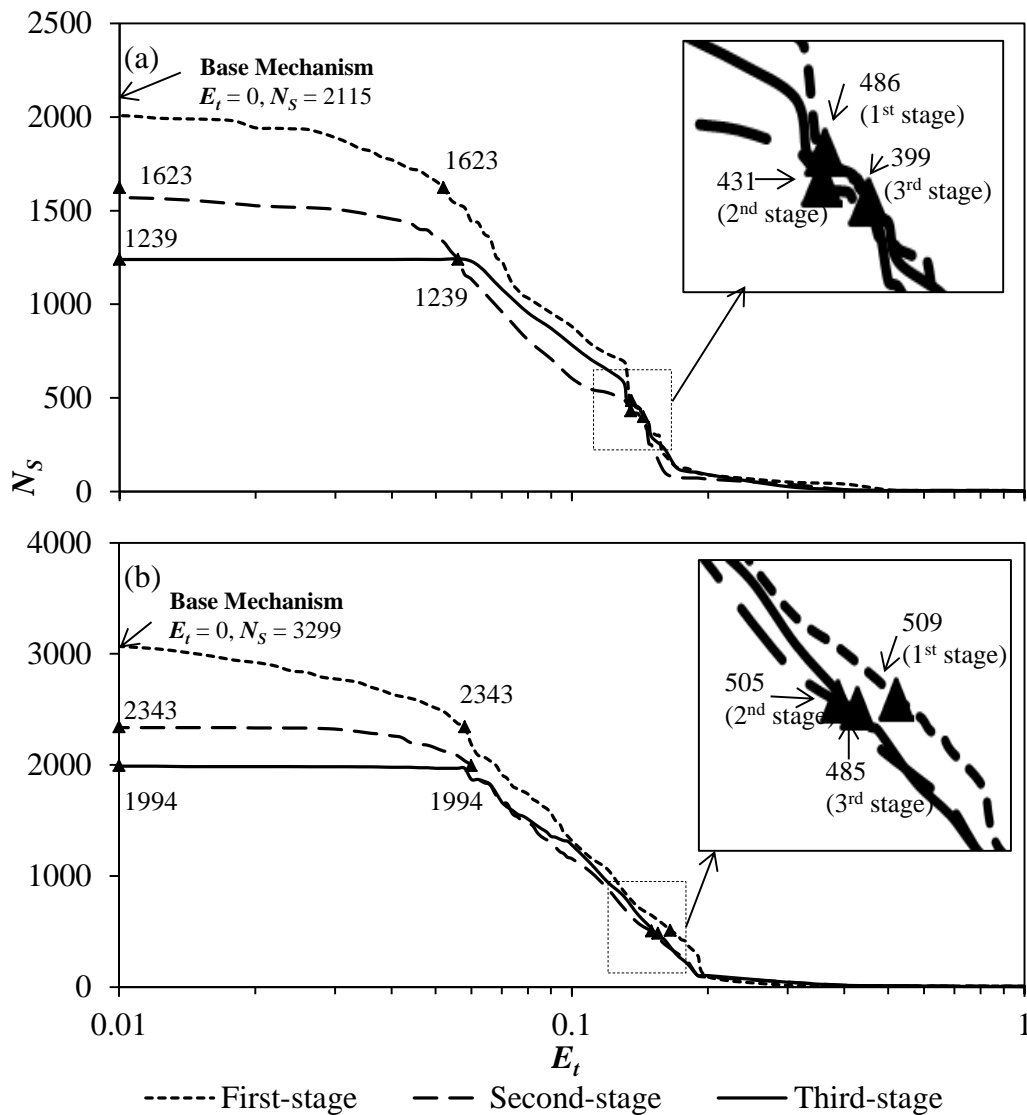


Figure 4-3: Dependency of N_s in the reduced mechanism of (a) HXN and (b) MDBIO on E_t for single-stage, two-stage and multi-stage DRG reduction to truncate weak relations of the species.

Based on the DRG reduction curves shown in Figure 4-3, it can be seen that when E_t approaches unity, only three species for MDBIO mechanism and one species for HXN mechanism are conserved. These are the starting species of the mechanisms designated at the beginning of the reduction procedure. On the contrary, when E_t is small, which is approximately 0.01, N_s in reduced mechanisms is very close to that of the detailed mechanisms. Besides that, “jumps” in N_s are observed at certain values of E_t due to the existence of species groups with strong coupling. For instance, there are “jumps” appear at $E_t = 0.058$

and 0.06 in Figure 4-3(a) for first-stage and second-stage DRG reduction of HXN, respectively. Therefore, the value of E_t should be chosen either before or after the “jump”. As such, species contained in the species group should either be kept or eliminated together. The E_t selection for each stage of DRG reduction and their respective reduction scale achieved are demonstrated in Table 4-4. For some cases, E_t is selected right before the “jump”. The reason is that it is essential to preserve the strongly coupled species for next stage of DRG reduction in order to minimise the errors induced on ID predictions. Conversely, E_t is selected after the “jump” for last stage of the DRG reduction to maximise the reduction scale while not exceeding $V_{AL,MAX}$.

Table 4-4: Selection of E_t as well as the resulting N_S and N_R of the reduced mechanisms for each stage of DRG reduction.

Detailed Mechanism	Reduction Method	E_t	Before / After “Jump”	N_S	N_R	
HXN	Single-stage DRG	0.134	After	486	2,225	
	Two-stage DRG	1 st stage	0.052	Before	1,623	6,797
		2 nd stage	0.135	After	431	1,788
	Multi-stage DRG	1 st stage	0.052	Before	1,623	6,797
		2 nd stage	0.056	Before	1,355	5,989
		3 rd stage	0.141	After	399	1,556
MDBIO	Single-stage DRG	0.165	After	509	2,144	
	Two-stage DRG	1 st stage	0.058	Before	2,343	8,536
		2 nd stage	0.15	After	505	2,075
	Multi-stage DRG	1 st stage	0.058	Before	2,343	8,536
		2 nd stage	0.06	Before	1,994	7,274
		3 rd stage	0.155	After	485	1,921

Successively, ID timings computed by the reduced MDBIO and HXN mechanisms are compared against those predicted by the detailed mechanisms, as illustrated in Figure 4-4.

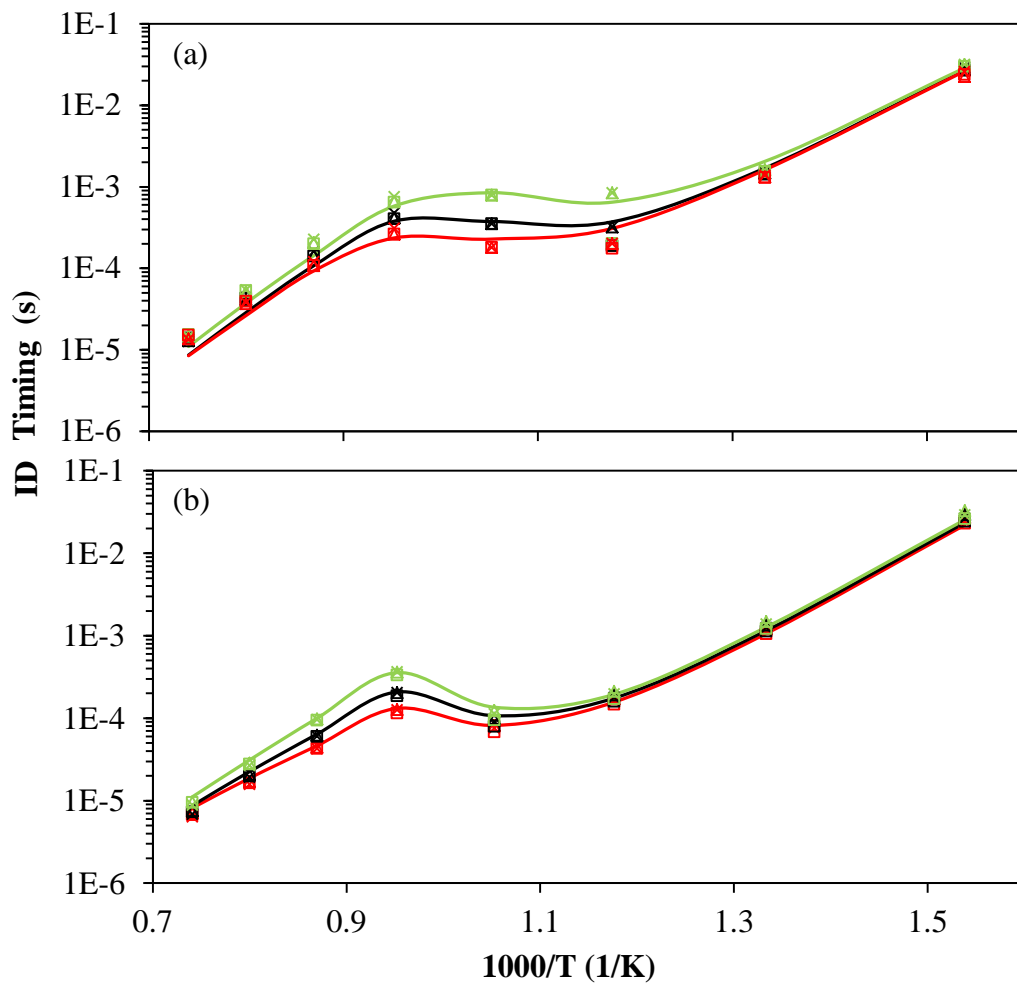


Figure 4-4: Comparisons of IDs computed by the detailed mechanisms (lines) with the predictions by the reduced (a) HXN and (b) MDBIO mechanisms generated from single-stage (□), two-stage (Δ) and multi-stage (x) DRG for initial pressure of 60 bar and Φ of 0.5 (green), 1.0 (black), 2 (red).

Based on the results shown in Figure 4-4, good agreements in ID predictions are observed between the reduced and detailed HXN and MDBIO mechanisms throughout the parametric range. Nevertheless, it is observed that two-stage and multi-stage DRG have superior performance in comparison with the single-stage DRG as their ID timing predictions in NTC region are more precise. For instance, referring to Figure 4-4(a), $V_{ID,MAX}$ at temperature of 950 K are 39.7 % for single-stage DRG, 20.7 % for two-stage DRG and 26.7 % for multi-stage DRG. This is because the implementation of two-stage and multi-stage DRG is able to preserve the strongly coupled species groups through first stage and second stage reductions, which might have been eliminated by single-stage DRG.

In cases in which great reduction scale is required for huge chemical kinetic mechanism reduction, there are views that more than two stages of DRG reduction is necessary to attain a set of converged reduced species [41]. However, the finding here agrees with the work carried out by Lu et al. [43] whereby two-stage DRG is sufficient to produce reduced mechanism with minimal size. Additionally, the execution of two-stage or multi-stage DRG will only contribute to minor raise in reduction scale since size of the reduced mechanism generated via single-stage DRG is already much smaller than that of the detailed mechanism. Hence, its impact on the reduction of computational runtime, T_C , in CHEMKIN-PRO simulations is insignificant with the presence of an additional DRG stage, as illustrated in Figure 4-5. T_C refers to the time taken for the CHEMKIN-PRO cases to complete.

Apart from that, the MATLAB runtime of an additional stage is comparatively high since it involves computations of a large number of sampling points (i.e. 216) as discussed earlier. Here, MATLAB runtime denotes the total processing time taken to perform the graph searching procedure to determine the correlations between N_S and E_t , as demonstrated in Figure 4-3. The entire reduction process requires additional 3 hours to complete. So, by considering these factors, two-stage DRG is fairly sufficient for DRG mechanism reduction.

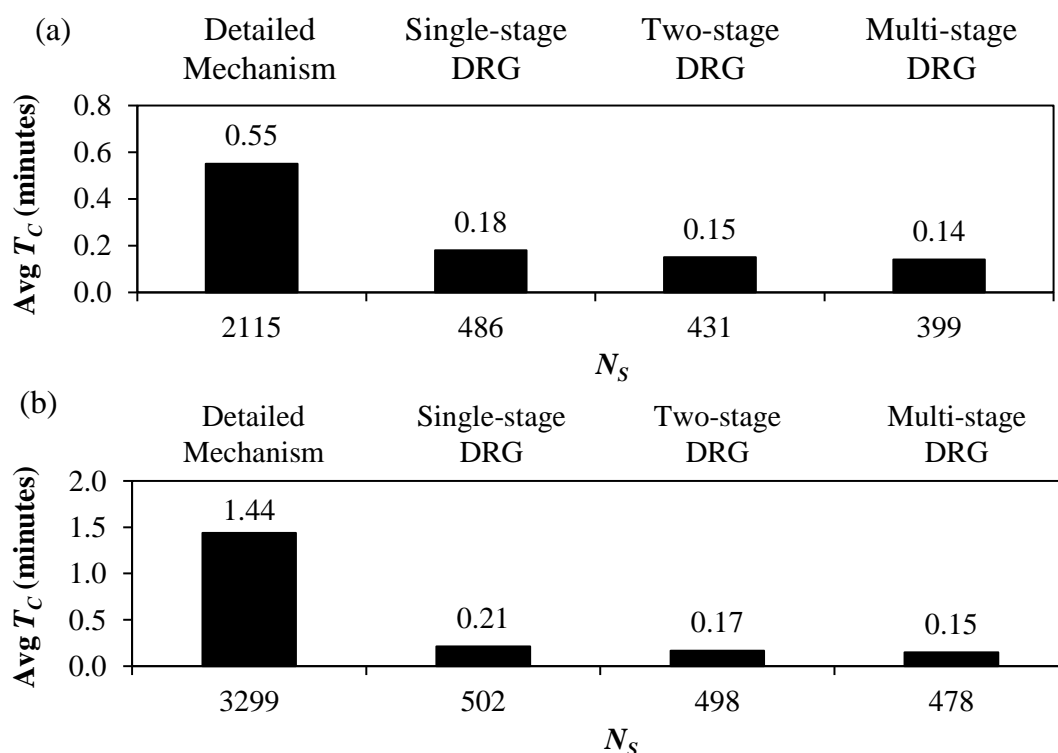


Figure 4-5: Average T_C for the detailed and reduced mechanisms of (a) HXN and (b) MDBIO mechanisms.

4.4.2 DRGASA

The reduced mechanisms generated from two-stage DRG reduction in Section 4.4.1 are applied in this section. During the DRG reduction procedure, it is verified that species with $E_t \leq 0.146$ for HXN mechanism and species with $E_t \leq 0.16$ for MDBIO mechanism are safely eliminated from the mechanisms. Furthermore, it is found that species with $E_t > 0.135$ for HXN mechanism reduction and $E_t > 0.15$ for MDBIO mechanism reduction are likely to have strong coupling with the target species. Once the species are removed, significant errors in ID timing predictions are encountered. Thus, species with these E_t are omitted from the elimination test. Accordingly, species with $0.135 \leq E_t \leq 0.146$ are selected for the elimination test for HXN mechanism and there are 78 participating species within the range. As for MDBIO mechanism, there is a total of 116 participating species within the threshold range of $0.15 \leq E_t \leq 0.16$ selected for the elimination test.

In this reduction work, a reduced HXN mechanism with 376 species and 1,501 elementary reactions as well as a reduced MDBIO mechanism with 466 species and 1,796 elementary reactions are successfully derived. Following that, ID timing predictions of the reduced HXN and MDBIO mechanisms are validated against those of the detailed mechanisms, using the parameter range shown in Table 4-3. The results are shown in Figure 4-6.

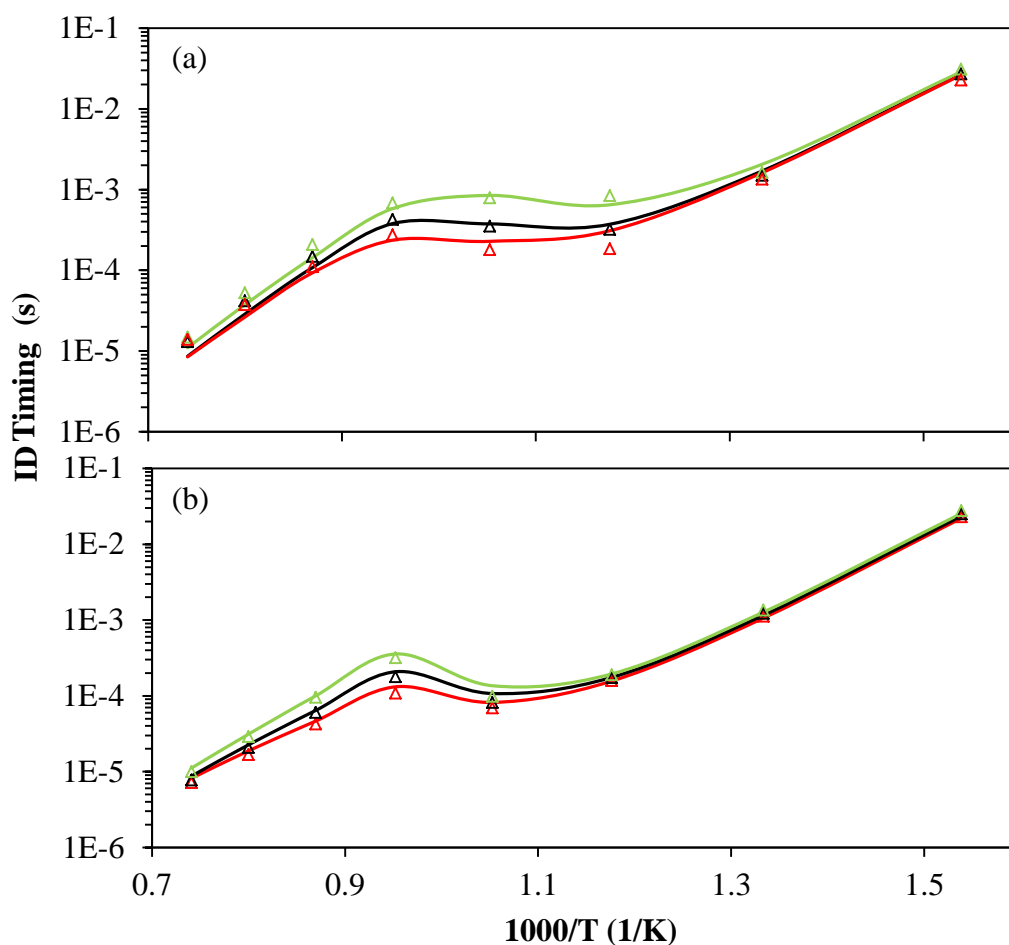


Figure 4-6: Comparisons of IDs computed by the detailed mechanisms (lines) with the predictions by the reduced (a) HXN and (b) MDBIO mechanisms (Δ) generated from DRGASA reductions for initial pressure of 60 bar and Φ of 0.5 (green), 1.0 (black), 2 (red).

Referring to the results shown in Figure 4-6, it can be observed that the ID timing predictions for both reduced mechanisms agree closely with those of their corresponding detailed mechanism throughout the parameter range. $V_{ID,MAX}$ for HXN mechanism is 33 % whereas $V_{ID,MAX}$ for MDBIO mechanism is 39.78 %.

Each CHEMKIN-PRO simulation in 0-D closed homogeneous batch reactor requires approximately 0.12 min and 0.14 min on average to complete for HXN and MDBIO mechanism reductions, respectively.

4.4.3 DRGEP

During DRGEP reduction, CO, CO₂, HCO, HO₂, H₂O₂, H₂, and N₂ are selected as target species for both HXN and MDBIO mechanisms. CO and CO₂ are the main emission species. HCO, HO₂ radical and H₂O₂ species are important in chain branching reactions. H₂ is selected to allow greater extension of reduction. N₂ is included such that it is retained consequently as it is not involved in any reactions. Working conditions as stated in Table 4-3 are applied in this section and there is a total of 216 sampling points applied for the analysis of reaction conditions for both mechanisms. The average times required to complete the reduction procedure for each sampling point are approximately 2.5 min for HXN mechanism and 3 min for MDBIO mechanism.

The predicted ID timings for the reduced HXN and MDBIO mechanisms are illustrated in Figure 4-7. During the reduction procedure of HXN mechanism, 0.0017 is selected as the optimal E_t to generate a reduced mechanism of 375 species and 1,454 elementary reactions while not exceeding $V_{AL,MAX}$. Contrarily, for the biodiesel case, E_t of 0.0056 is applied to produce a reduced MDBIO mechanism of 425 species and 1,281 elementary reactions.

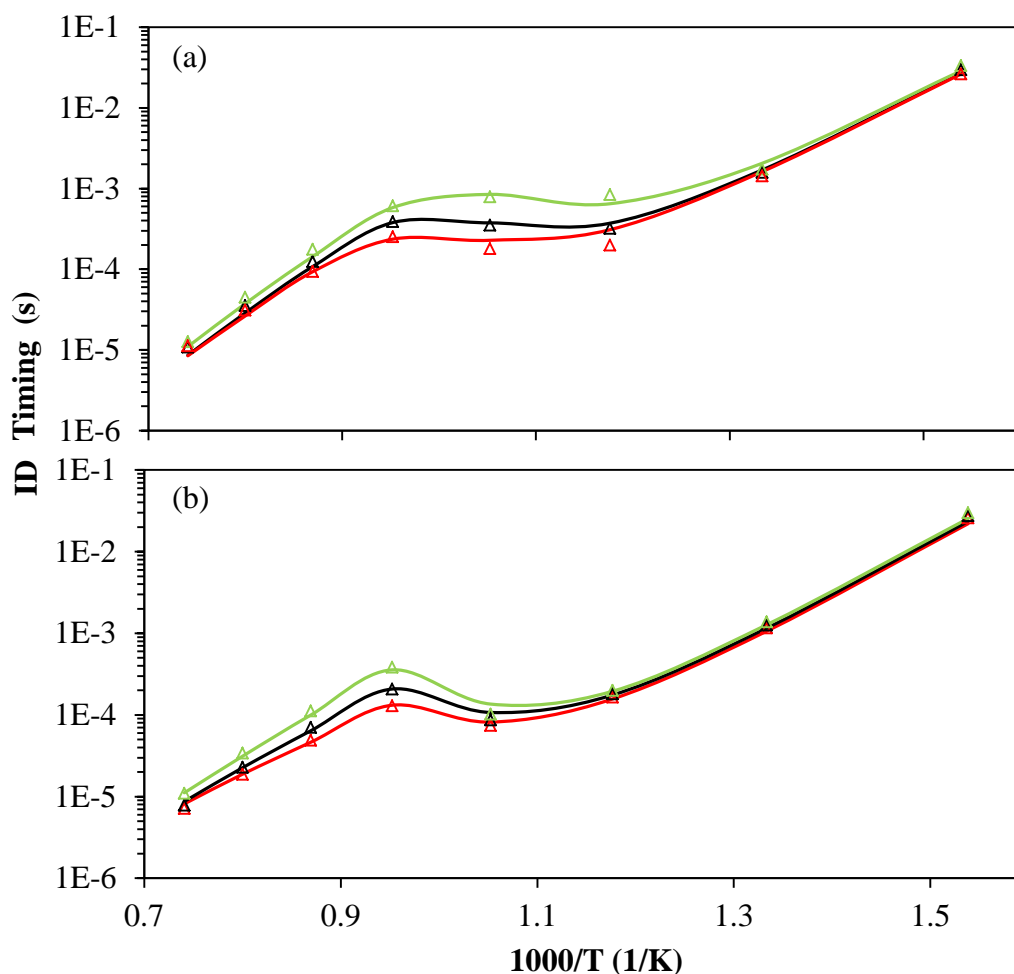


Figure 4-7: Comparisons of IDs computed by the detailed mechanisms (lines) with the predictions by the reduced (a) HXN and (b) MDBIO mechanisms (Δ) generated from DRGEP reductions for initial pressure of 60 bar and Φ of 0.5 (green), 1.0 (black), 2 (red).

Based on the results shown in Figure 4-7, it can be observed that ID timings of both reduced mechanisms match reasonably well with those of their corresponding detailed mechanism throughout the parametric range. The average T_C of the CHEMKIN-PRO simulations are 0.1 min and 0.13 min using the reduced HXN and MDBIO mechanisms, respectively.

4.4.4 DRGEP SA

The reduced mechanisms generated from DRGEP reduction in Section 4.4.3 are applied for sensitivity analysis in this section. Similar to the reduction exercise of

DRGASA in Section 4.4.2, 74 participating species from the HXN mechanism which fall between the range of $0.0017 \leq E_r \leq 0.004$ are selected for the elimination test. In contrast, 65 participating species with $0.0056 \leq E_r \leq 0.008$ are chosen for the elimination test of MDBIO mechanism reduction. Consequently, a reduced HXN mechanism with 364 species and 1,404 elementary reactions is attained whereas the size of the MDBIO mechanism is successfully reduced to 375 species and 1,146 elementary reactions. Accordingly, mechanism validations are performed and good agreements are achieved between the ID timing predictions and experimental measurements, as shown in Figure 4-8. Moreover, the average T_C in the 0-D simulations is greatly reduced from 0.55 min to 0.09 min for the diesel case while the average T_C for the biodiesel case is reduced from 1.44 min to 0.12 min.

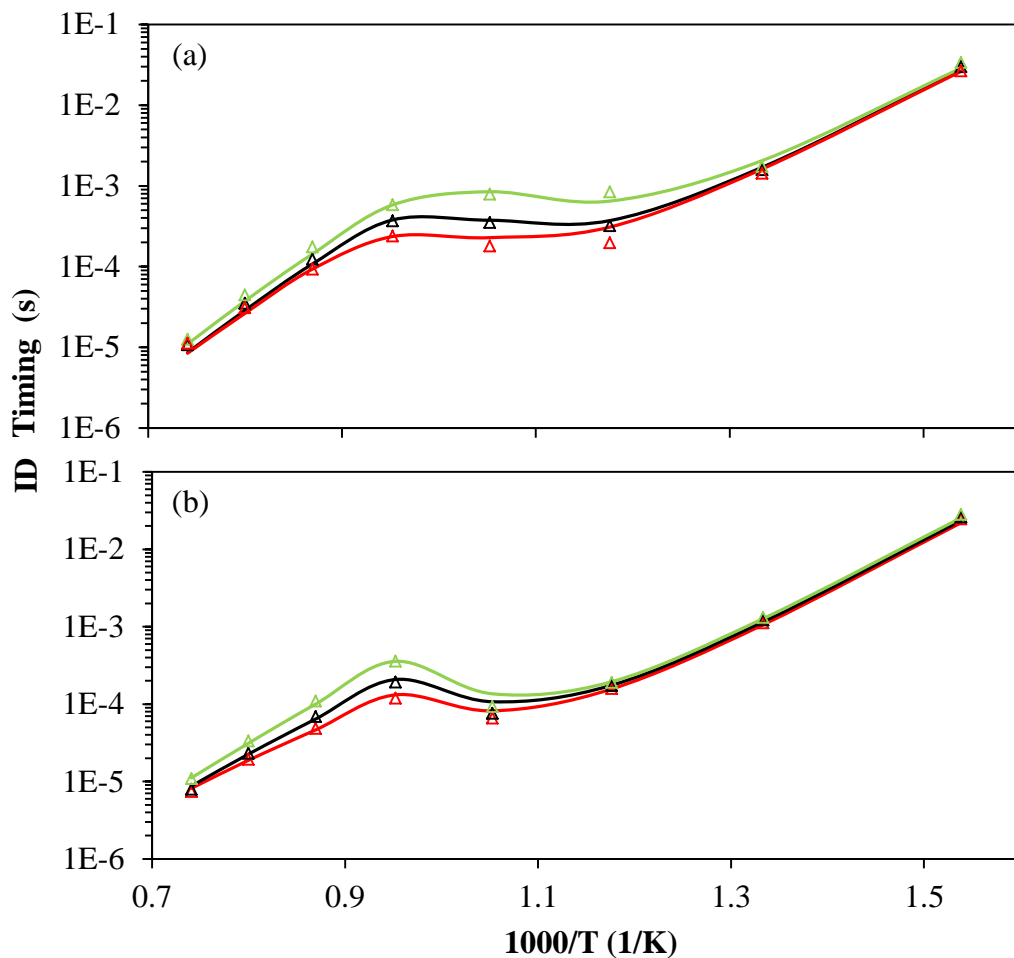


Figure 4-8: Comparisons of IDs computed by the detailed mechanisms (lines) with the predictions by the reduced (a) HXN and (b) MDBIO mechanisms (Δ)

generated from DRGEPSA reductions for pressure of 60 bar and Φ of 0.5 (green), 1.0 (black), 2 (red).

4.5 Performance Benchmarking

According to the reduction efforts carried out in Section 4.4, the performance of each reduction technique is summarised in Table 4-5 with respect to the percentage of reduction in N_S and T_C as well as accuracy in ID timing predictions.

Table 4-5: Summary of the reduction performance for DRG, DRGASA, DRGEP and DRGEPSA.

Model	Method	N_S	T_C (min)	Overall % reduction in N_S	Avg % reduction in T_C	$V_{ID,MAX}$
HXN	Single-stage DRG	486	0.18	77.02 %	67.27 %	21.41 %
	Two-stage DRG	431	0.15	79.62 %	72.73 %	15.51 %
	Multi-stage DRG	399	0.14	81.13 %	74.55 %	31.40 %
	DRGASA	376	0.12	82.22 %	78.18 %	33.00 %
	DRGEP	375	0.10	82.27 %	81.82 %	34.46 %
	DRGEPSA	363	0.09	82.84 %	83.33 %	34.47 %
MDBIO	Single-stage DRG	509	0.21	84.57 %	85.42 %	39.70 %
	Two-stage DRG	505	0.17	84.69 %	88.19 %	38.91 %
	Multi-stage DRG	485	0.15	85.30 %	89.58 %	32.46 %
	DRGASA	466	0.14	85.87 %	90.28 %	39.78 %
	DRGEP	425	0.13	87.12 %	90.74 %	29.20 %
	DRGEPSA	375	0.12	88.63 %	91.88 %	32.00 %

It can be seen that single-stage DRG has the lowest percentage of reduction in N_S as well as T_C while DRGEP SA achieves highest reduction scale in mechanism size and T_C . Moreover, the difference in $V_{ID,MAX}$ among each method is comparatively significant. According to the findings in Section 4.4.1, a two-stage DRG is adequate for large-scale mechanism reduction since the MATLAB processing time for multi-stage DRG reduction procedure is relatively high. The reduction procedure for third stage DRG requires additional 3 hours to complete, with only 1 – 2 % further reduction in mechanism size in terms of total number of species. On the other hand, the single-stage DRG is unable to retain most of the strongly coupled species groups. Hence, it is not practicable to apply single-stage and multi-stage DRG reductions in this work.

Since DRGASA is able to identify species with minor importance to the target species and global parameters, the size of the reduced mechanisms generated via DRGASA is smaller and T_C of CHEMKIN-PRO simulations is shorter too as compared to DRG methodology. Nevertheless, the application of brute-force sensitivity analysis of DRGASA is computationally expensive as species within the E_t range are tested individually for removal. Based on the reduction procedure illustrated in Figure 4-1, steps 3 and 4 are repeated until every species within the E_t range is tested in the elimination test. The simulation is performed for all the operating conditions whenever a species is removed from the kinetic model. Hence, it is not suggested to employ this method for reduction of large-scale mechanisms. Apart from that, species “shielding” during DRGASA reduction has prevented some eliminable species to be removed. This is because the DRG reduction phase of DRGASA does not take into account of distance from targets and can inflate species importance such that species are automatically retained instead of being evaluated with sensitivity analysis. Thus, the size of the reduced mechanism generated via DRGASA is not minimal yet.

Furthermore, based on the results shown in Table 4-5, it can be observed that DRGEP offers greater reduction in mechanism size and T_C as compared to DRG and DRGASA methodologies. Although DRG utilises species coupling coefficient to calculate error induced by elimination of a single species to the production rate of another species, the value is yet not directly associated to an error measure.

Other than that, distance from targets is not important in DRG provided that the selection of starting species enables directed graph to be populated by all species. This might result in the presence of unnecessary species in the reduced mechanisms. These weaknesses of DRG methodology are coped with by applying DRGEP reduction methodology.

Among all the mechanism reduction methodologies, DRGEP is found to be the most competent method to generate reduced mechanisms with minimal size. As DRGEP is unable to detect all unimportant species and DRGASA shields unimportant species from elimination, DRGEP approach has overcome the weaknesses of each by combining both methods. Again, the approach used in the sensitivity analysis of DRGEP is also time-consuming, and it is not favourable to be applied on large-scale mechanism reduction.

4.6 Concluding Remarks

In this chapter, the existing chemical kinetic mechanism reduction techniques are first evaluated with examples of large-scale mechanisms such as the biodiesel and diesel surrogate fuel models. The reduction techniques applied here are DRG, DRGASA, DRGEP, and DRGEP. Summarising from the performance of each reduction technique based on their reduction scale in mechanism size and T_C of the 0-D simulations, the mechanism reduction methods are arranged in descending order such that DRGEP > DRGASA > DRG. It is noted that the order of the performance ranking of the reduction methods would remain the same when different $V_{AL,MAX}$ is set. Smaller $V_{AL,MAX}$ would result in larger mechanism size as the required accuracy is higher and vice versa.

Nonetheless, the size of the reduced mechanisms generated via the aforesaid reduction methodologies is not minimal yet for the multi-dimensional CFD applications. For instance, in the study of Perini et al. [160], the application of a 47-species kinetic model in a 3-D non-reacting pilot injection simulation using a standard KIVA-ERC code involves 29.9 hours of CPU time on a single-core PC. While non-reacting simulations generally require lower amount of computational

runtime, it is expected that the application of kinetic mechanisms with 350 – 500 species in a reacting spray simulation would require hundreds of hours to complete. Thus, a new reduction scheme is desirable for further reduction. This will be discussed in the following chapter.

CHAPTER 5

DEVELOPMENT AND VALIDATION OF CHEMICAL KINETIC MECHANISM REDUCTION SCHEME

5.1 Introduction

Simulation results in the previous chapter show that only limited extent of reduction is achieved using a single reduction technique. Therefore, the generated reduced mechanisms typically consist of more than hundred of species. For this reason, it is essential to formulate a reduction scheme which integrates different reduction techniques to construct a more effective and reliable approach that copes with larger mechanisms for successful CFD simulations. In this chapter, a novel chemical kinetic mechanism reduction scheme is introduced in Section 5.2, followed by its applications on large-scale mechanism reductions such as the diesel and biodiesel surrogate fuel models in Section 5.3. Subsequently, the reduction scheme is employed on the ethylene mechanism in Section 5.4 in order to examine its applicability on reduction of small-scale mechanism. In the last section, the main findings of the chapter are presented.

5.2 Formulation of Chemical Kinetic Mechanism Reduction Scheme

In this section, a systematic chemical kinetic mechanism reduction scheme is formulated and presented for both small- and large- scale mechanism reductions. The reduction scheme consists of five stages which are DRGEP with Dijkstra algorithm, isomer lumping, reaction path analysis, DRG and adjustment of reaction rate constants. The reduction procedure is demonstrated in Figure 5-1.

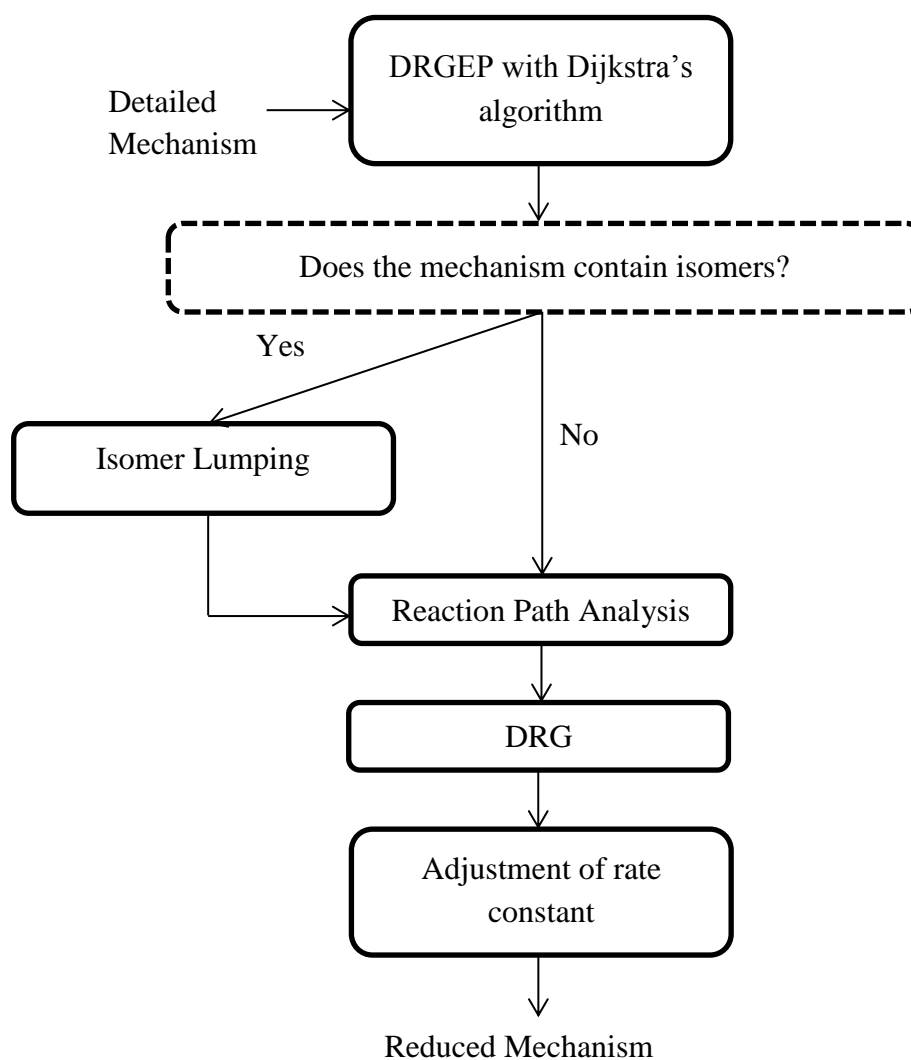


Figure 5-1: Flow chart of the novel integrated chemical kinetic mechanism reduction scheme.

First and foremost, DRGEP methodology is selected as the first step of mechanism reduction procedure. While the approach of sensitivity analysis in DRGEPSA method is laborious and thus is not favourable to be applied on large-scale mechanism reduction, DRGEP method with Dijkstra's algorithm is applied based on its superior performance as compared to other methods discussed in Section 4.5.

Following that, isomer lumping [43,106] is carried out whereby species with comparable thermodynamic as well as transport properties are grouped into a particular representative lump. As such, the size of the reduced mechanisms is significantly reduced. In this reduction exercise, isomers with very low

concentration level (1×10^{-10} mole/cm³) are removed. Then, the remaining isomer groups are brought forward to the next stage of reduction process for the selection of a representative isomer for each group.

Furthermore, it is noted that the order of the reduction strategies is imperative as it might affect the performance of the reduction scheme. In the study of Pepiot et al. [161], the effects of differences in the order of reduction techniques on the accuracy of final mechanism are investigated. The reduction strategies consist of DRGEP as well as lumping methods, and they are arranged in two ways, for instance, first DRGEP then lumping method and vice versa. It is found that both approaches are valid as the order of reduction techniques applied does not give a significant impact on the accuracy of final mechanism. However, the accuracy of the former technique is superior. Accordingly, isomer lumping is performed after DRGEP reduction in this proposed reduction scheme.

Once isomers are successfully lumped together, reaction path analysis is conducted in order to determine the major reaction pathways as well as the corresponding reactions. The reaction path analyser of CHEMKIN-PRO software is employed in this step to evaluate the relative contribution of each reaction pathway to the net production rate of the connecting species. In addition, selection of the representative isomers is performed based on the reaction path widths which quantify the production rate of the connecting species. The maximum production rate is scaled to the largest allowable line thickness while the minimum production rate corresponds to a line thickness of one. The intermediate production rate is measured by the line thickness on a log scale. Subsequently, the selection of reaction pathways is cautiously done based on the representative species.

Apart from that, the reaction path analyser of CHEMKIN-PRO software also provides the feature of sensitivity analysis. The first-order sensitivity coefficients of gas temperature and species mole fractions with respect to the reaction rate coefficients are taken into consideration. As a consequence, reactions of the associated species with low normalised temperature *A*-factor sensitivity are eliminated from the reduced mechanisms while analysing the reaction pathways.

The process is straightforward and it is not as laborious as the brute-force sensitivity analysis. The normalised A -factor sensitivity is expressed by the following equation:

$$\begin{aligned} & \text{Normalised Temperature } A \text{ – factor Sensitivity} \\ & = \frac{\text{Individual Temperature Sensitivity Coefficient Value}}{\text{Total Temperature Sensitivity Coefficient Value}} \quad (5-1) \end{aligned}$$

Next, after the reaction path analysis is accomplished, DRG method is employed by setting $E_t = 1$. The purpose of doing so is to eliminate the undesirable species which have lost pathway connection to the major species after isomer lumping and reaction path analysis.

Finally, appropriate adjustment of the reaction rate constants is performed. The reason is that elimination of species from mechanisms would cause deviations in the ID predictions. Hence, minor adjustment of the A -factor value of Arrhenius parameters is necessary. Here, reactions with high temperature A -factor sensitivity are chosen for adjustment of A -factor value.

5.3 Implementation of Chemical Kinetic Mechanism Reduction Scheme on Large-Scale Mechanism Reduction - Diesel and Biodiesel Surrogate Fuel Models

In this section, CHEMKIN-PRO software package is used to study the chemical kinetic interactions between the species presented in the diesel and biodiesel fuels. The reduced diesel and biodiesel surrogate fuel models are first derived in Section 5.3.1. Then, validations of the models are presented in Section 5.3.2.

5.3.1 Derivation of Reduced Models

Similar to the previous reduction effort in Section 4.4, a closed homogeneous batch reactor with constant volume is used to compute the ID timings for both diesel and biodiesel fuel combustions. Here, two case studies are conducted to investigate the effects of manipulating the reduction conditions on the

performance of the resulting mechanisms. For the first case study, only auto-ignition condition is selected as the data source for mechanism reduction. Meanwhile, both JSR and auto-ignition conditions are selected as the data source for reduction for the second case study. The operating conditions applied in the case studies are illustrated in Table 5-1.

Table 5-1: Test conditions applied for mechanism reduction as well as model validations of the diesel and biodiesel surrogate fuel models.

Operating Conditions		Range Evaluated
Auto-ignition ^a	Φ (-)	0.5, 1.0, 2.0
	Initial Pressure (bar)	40, 60, 80
	Initial Temperature (K)	650 – 1350 (100 K increments)
JSR ^a	Φ (-)	0.5, 1.0, 2.0
	Initial Pressure (bar)	40, 60, 80
	Residence Time ^c (s)	1
JSR ^b	Φ (-)	1.5 (diesel); 1.5 (biodiesel)
	Initial Pressure (bar)	1.01 (diesel); 1.01 (biodiesel)
	Residence Time (s)	0.07 (diesel); 0.1 (biodiesel)

^a Selected operating conditions for mechanism reduction and model validations against detailed models, based on the typical in-cylinder pressure values during the main fuel injection event for light-duty [162], direct-injection diesel engines.

^b Selected operating conditions based on the experimental results of HXN [13] and RME [109] oxidations in a JSR for model validations. The unit for pressure is converted from atm to bar (1 atm = 1.01 bar).

^c Selected residence time based on minimum extinction time at steady-state for combustion at low-, intermediate- and high-temperatures [163].

According to the mechanism reduction scheme demonstrated in Figure 5-1, DRGEP reduction is designated as the first stage of reduction procedure. Consequently, the reduced HXN mechanism with 375 species and the reduced MDBIO mechanism with 425 species generated in Section 4.2.3 are employed in this section for further reduction. The resulting mechanisms are generated by applying auto-ignition condition only. In contrast, a reduced HXN mechanism with 447 species and a reduced MDBIO mechanism with 460 species are obtained when both JSR and auto-ignition conditions are chosen as the data source for reduction. The difference in the resulting mechanism size is relatively minor for both case studies.

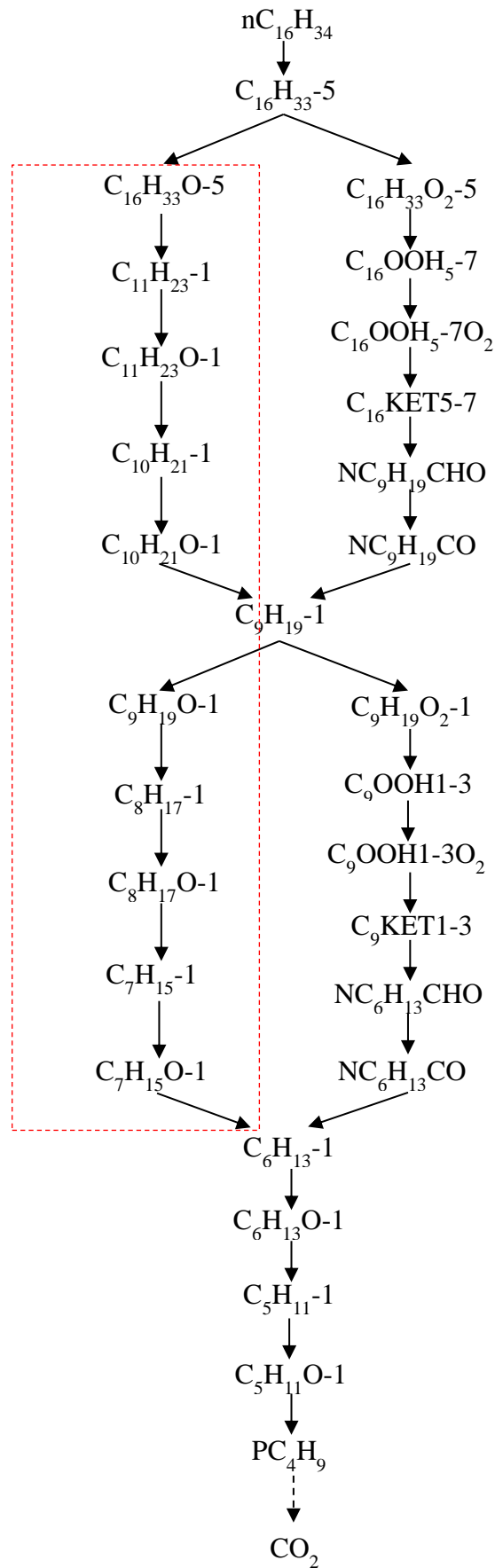
Accordingly, isomer lumping is conducted. $nC_{16}H_{34}$ from HXN mechanism and MD6J, MD9D6J, C_7H_{15-2} from MDBIO mechanism are selected as the representative isomers due to their high production rate. The isomer groups presented in the HXN and MDBIO mechanisms are shown in Table 5-2. The representative isomers are emphasised in bold and italic font.

Table 5-2: Example of major isomers in reduced HXN and MDBIO mechanisms generated via DRGEP methodology.

Mechanisms	Isomer Groups	Isomers
HXN	$nC_{16}H_{33}$	$nC_{16}H_{33-2}$, $nC_{16}H_{33-3}$, $nC_{16}H_{33-4}$, <i>$nC_{16}H_{33-5}$</i> , $nC_{16}H_{33-6}$, $nC_{16}H_{33-7}$, $nC_{16}H_{33-8}$
MDBIO	MD	MD2J, MD3J, MD4J, MD5J, <i>MD6J</i> , MD7J, MD8J, MD9J, MDMJ
	MD9D	MD9D2J, MD9D3J, MD9D4J, MD9D5J, <i>MD9D6J</i> , MD9D7J, MD9D8J, MD9D9J, MD9DMJ
	C_7H_{16}	C_7H_{15-1} , <i>C_7H_{15-2}</i> , C_7H_{15-3} , C_7H_{15-4}

Following that, major reaction pathways during the fuel oxidation process are analysed using the reaction path analyser of CHEMKIN-PRO software and they are illustrated in Figure 5-2. The highlighted reaction pathways in Figure 5-2 have been included when JSR condition is added as a criterion of data source for mechanism reduction instead of using only auto-ignition condition. It is found that predictions of ID as well as species concentration profiles have been improved. However, this also causes a dramatic increment in mechanism size. Moreover, based on the reaction pathway analysis, it is observed that H-atom abstractions on the fuel by OH, H and O radicals are more dominant as compared to thermal decompositions of the fuel for fuel-lean conditions throughout the temperature range. This importance also increases with temperature. In contrast, for fuel-rich conditions, thermal decompositions of the fuel are more prevalent especially in high temperature. On the contrary, for stoichiometric conditions, H-atom abstractions are prevailing for low temperature whereas thermal decompositions are more significant when temperature is high.

(a)



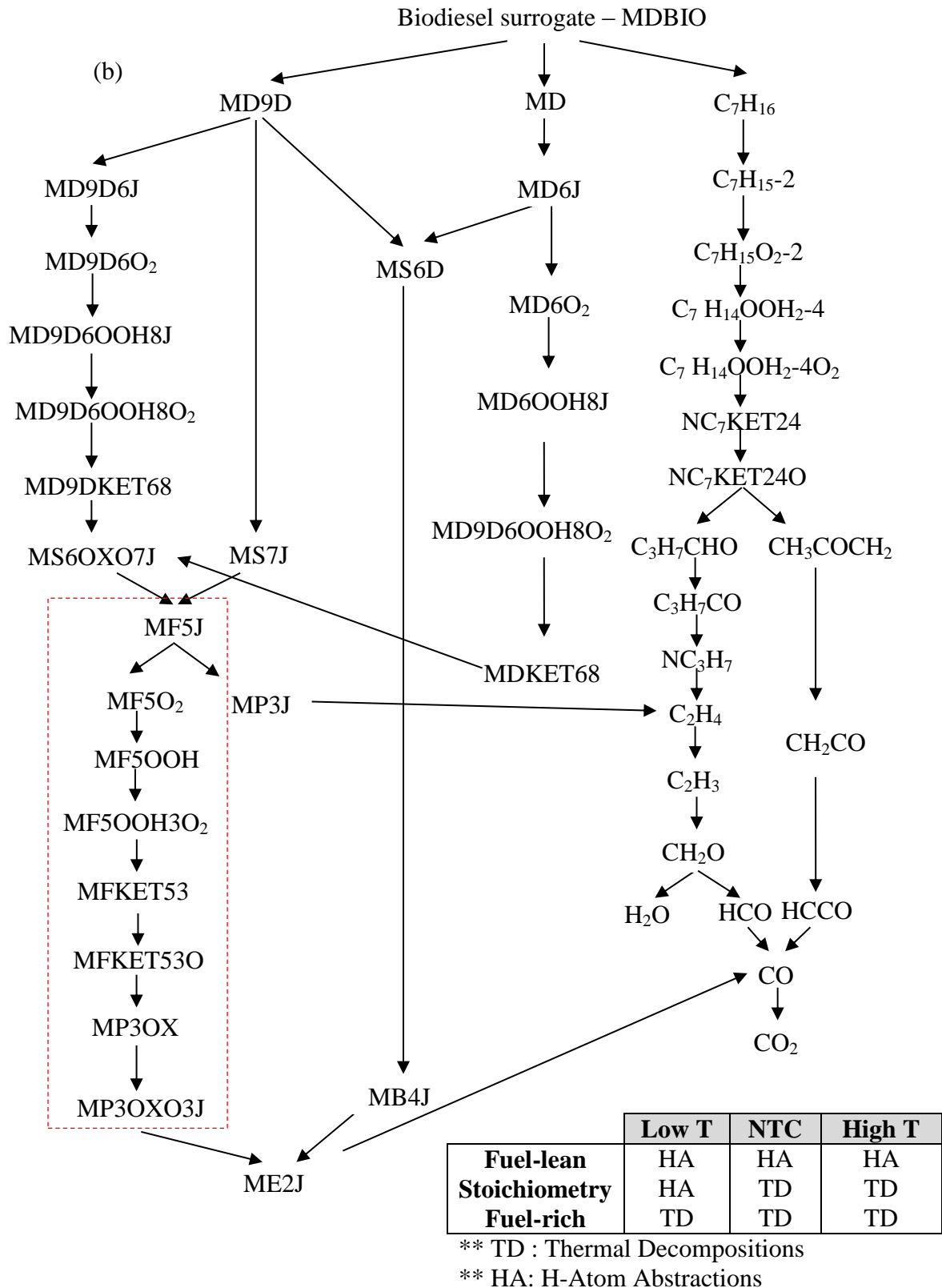


Figure 5-2: Main reaction pathways of (a) HXN and (b) MD/MD9D/nHep oxidations for initial pressure of 60 bar, initial temperature of 950 K and Φ of 1.

Next, species which have lost pathway connection to the major species are eliminated through DRG, and this is followed by adjustment of reaction rate constants. The adjusted *A*-factor values for the diesel and biodiesel surrogate fuel models are illustrated in Table 5-3. The results here provide a clearer description on the rate constant tuning procedure. As discussed in Section 5.2, the optimisation of reaction rate constants is performed based on reactions with high normalised temperature *A*-factor sensitivity, as demonstrated in Figure 5-3.

As a result of the reduction effort, a final reduced HXN mechanism with 49 species and 97 elementary reactions is generated using only auto-ignition condition as the data source for mechanism reduction. Meanwhile, a final reduced HXN mechanism with 79 species and 289 elementary reactions is obtained when both auto-ignition and JSR conditions are applied as criteria of data source for mechanism reduction. The 49-species and 79-species surrogate models are henceforth represented by HXNv1 and HXNv2, respectively, for brevity. Likewise, a final reduced MDBIO mechanism with 68 species and 163 elementary reactions is produced when auto-ignition condition is applied solely as the data source for mechanism reduction. Conversely, a final reduced MDBIO mechanism with 80 species and 252 elementary reactions is generated when both auto-ignition and JSR conditions are applied. They are henceforth denoted as MCBSv1 and MCBSv2, respectively.

Table 5-3: Comparison of the original and adjusted A-factor values of Arrhenius parameters.

Condi- tions	Models	Reactions	A-factor values		
			Original	Adjusted	
Auto- ignition	HXNv1	$nC_{16}H_{34} + OH = C_{16}H_{33-5} + H_2O$	9.400×10^7	9.400×10^6	
		$C_{16}H_{33}O_2-5 = C_{16}OOH5-7$	2.500×10^{10}	2.500×10^{11}	
		$C_{16}OOH2-5O_2 = C_{16}OOH5-7 + O_2$	1.367×10^{23}	4.800×10^{24}	
		$C_{10}H_{21-1} + C_6H_{13-1} = NC_{16}H_{34}$	8.000×10^{12}	2.200×10^{15}	
	MCBSv1	$MD + OH = MD6J + H_2O$	4.670×10^7	4.670×10^8	
		$MD9D6O2 = MD9D6OOH8J$	1.250×10^{10}	6.250×10^9	
		$MD9D6OOH8O2 = MD9DKET68 + OH$	1.250×10^{10}	1.250×10^{12}	
		$C_7H_{16} + OH = C_7H_{15-2} + H_2O$	9.400×10^7	9.400×10^5	
	Auto- ignition and JSR	HXNv2	$HXN + OH = C_{16}H_{33-5} + H_2O$	9.400×10^7	6.400×10^8
			$HXN + HO_2 = C_{16}H_{33-5} + H_2O_2$	1.120×10^{13}	5.120×10^{14}
$C_6H_{12-1} + C_{10}H_{21-1} = C_{16}H_{33-5}$			1.000×10^{11}	1.000×10^{12}	
$C_{16}KET5-7 = OH + NC_4H_9COCH_2 + NC_9H_{19}CHO$			1.050×10^{16}	4.050×10^{16}	
MCBSv2		$MD + OH = MD6J + H_2O$	4.670×10^7	4.670×10^8	
		$NC_3H_7 + MS6D = MD6J$	8.800×10^3	8.800×10^4	
		$MD9D6J = C_3H_5-A + MS6D$	3.310×10^{13}	1.310×10^{14}	
		$C_7H_{14}OOH_2-4O_2 = NC_7KET24 + OH$	1.250×10^{10}	1.250×10^9	
			$MD9D + OH = MD9D6J + H_2O$	4.670×10^7	4.670×10^8

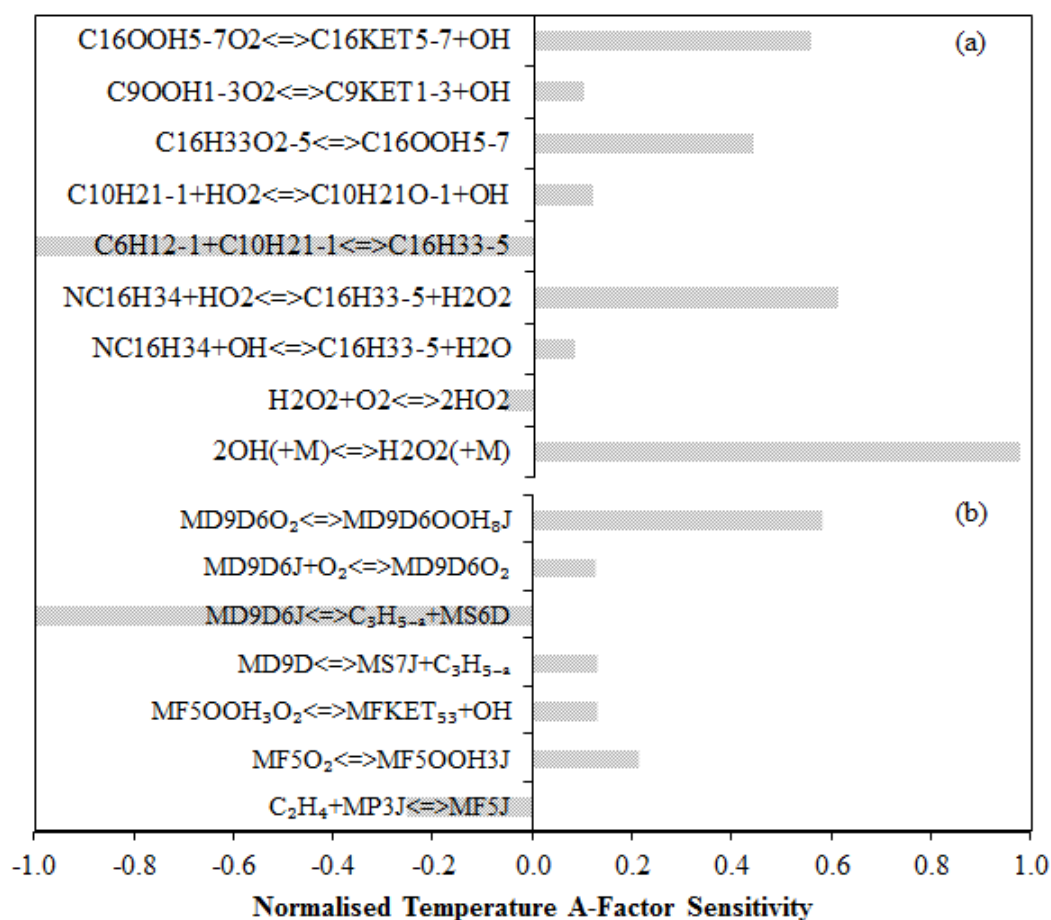


Figure 5-3: Normalised temperature A-factor sensitivity for (a) HXNV2 and (b) MCBSv2 for initial pressure of 60 bar, initial temperature of 950 K and ϕ of 1. [Only results for HXNV2 and MCBSv2 are demonstrated here for clearer description of the reaction rate optimisation procedure.]**

The reduction procedures have contributed to approximately 97 % reduction in the mechanism size and T_C using the generated reduced diesel and biodiesel surrogate fuel models. Each CHEMKIN-PRO simulation takes approximately 1 s to accomplish using a 6-core PC with 16 GB RAM and 3.4 GHz processing speed. Subsequently, model validations are performed in the next section to assess their performance in 0-D simulations.

5.3.2 Model Validations in 0-D Chemical Kinetic Simulations

0-D simulation approach is often applied to describe and assess the chemical kinetics of the surrogate model since it is able to take into account a huge number of different species and reactions with less computational cost. Here, the performance of the reduced diesel and biodiesel surrogate fuel mechanisms is compared to their corresponding detailed mechanisms with respect to ID and relative species mole fractions in 0-D chemical kinetic simulations. The results are demonstrated in Figure 5-4 and Figure 5-5, respectively. Based on the results obtained in Figure 5-4, it can be observed that the predicted ID timings of each reduced mechanism are in good agreement with their respective detailed mechanism for both diesel and biodiesel fuels. The maximum deviation between the reduced and detailed mechanisms is maintained to within 40 % which is reasonable for large-scale mechanism reduction as discussed earlier.

In Figure 5-5, fuel species such as HXN, MD, MD9D, nHep and oxidiser species O_2 are included in order to monitor their concentrations during combustion. CO_2 are the main emission species while C_2H_2 is the soot precursor species. HO_2 radical is important in chain branching reactions while OH radical is a highly reactive chemical intermediate during fuel oxidation process. Here, only results at initial pressure of 60 bar, initial temperature of 950 K and ϕ of 1 are shown as similar trends are obtained for other test conditions stated in Table 5-1.

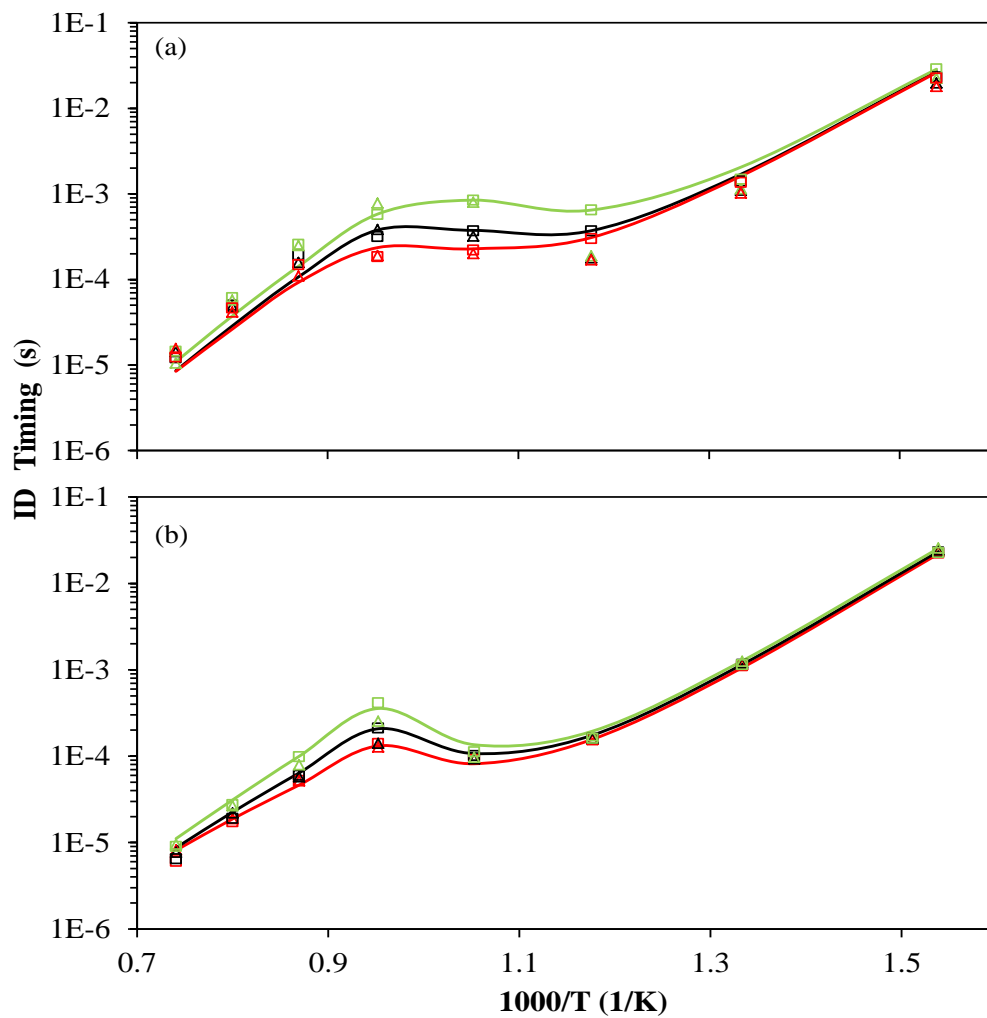
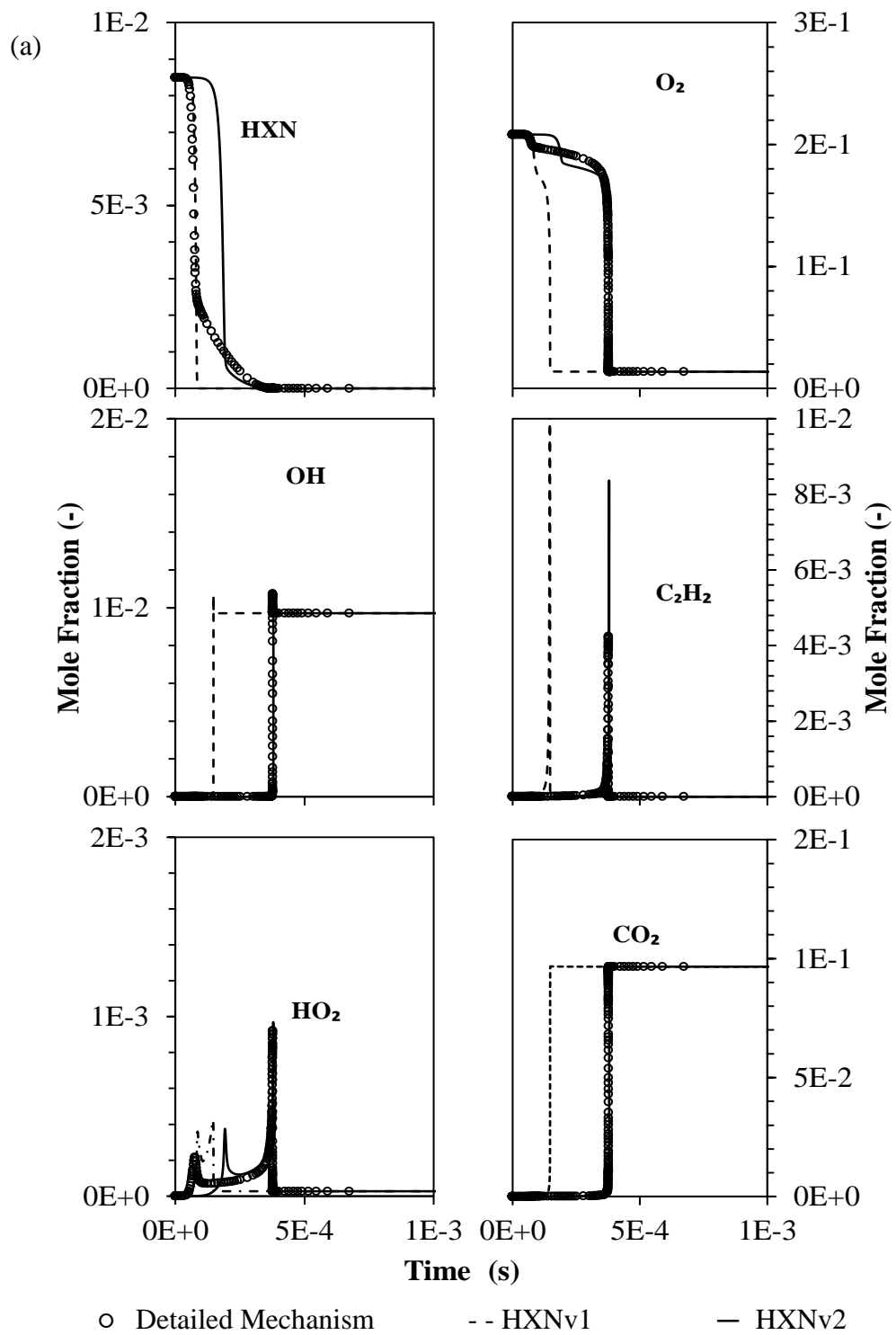


Figure 5-4: Comparisons of ID calculated by the detailed (line) and reduced (a) HXNv1 (Δ) / HXNv2 (\square) diesel surrogate fuel models and (b) MCBSv1 (Δ) / MCBSv2 (\square) biodiesel surrogate fuel models for initial pressure of 60 bar and Φ of 0.5 (green), 1.0 (black), 2.0 (red).



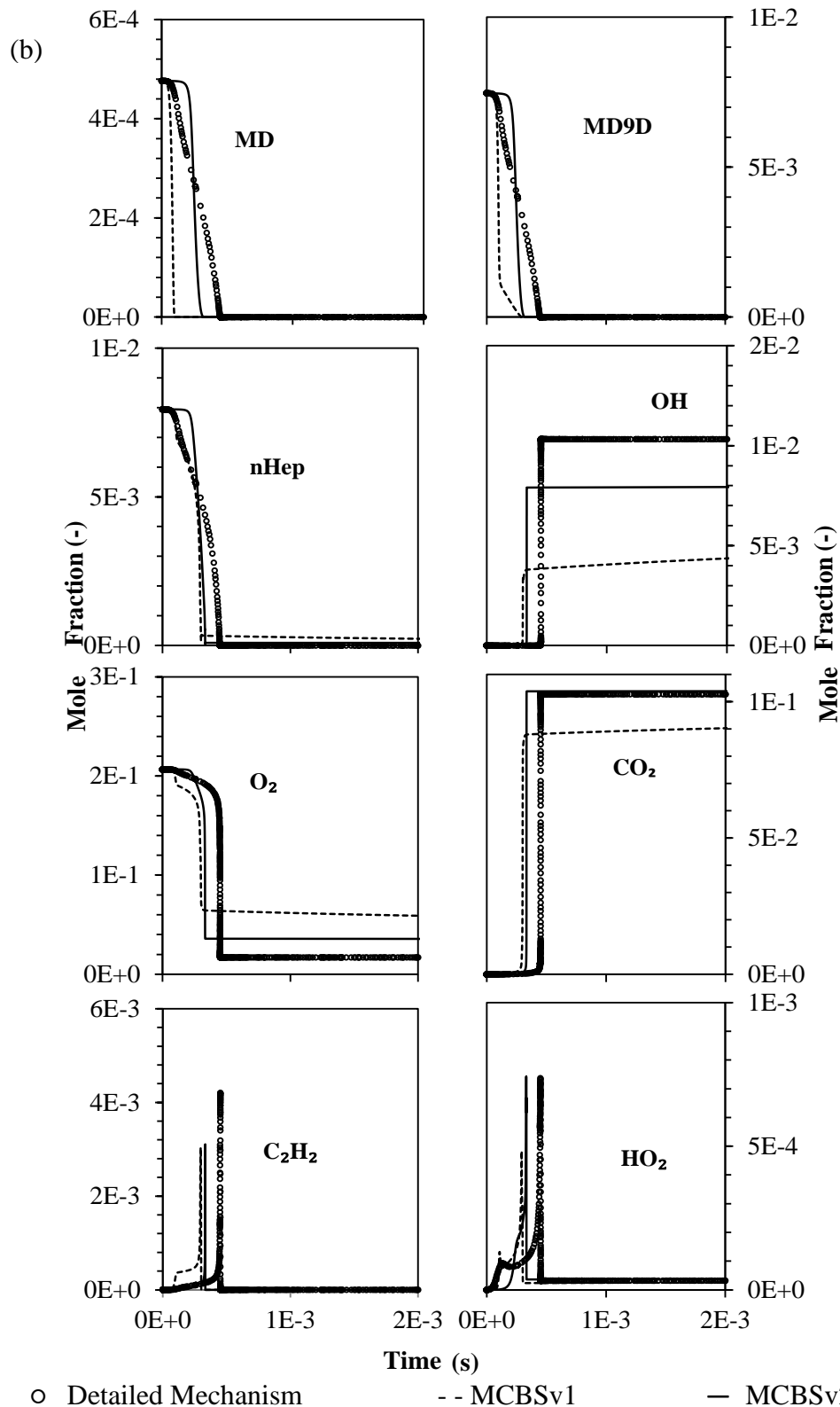
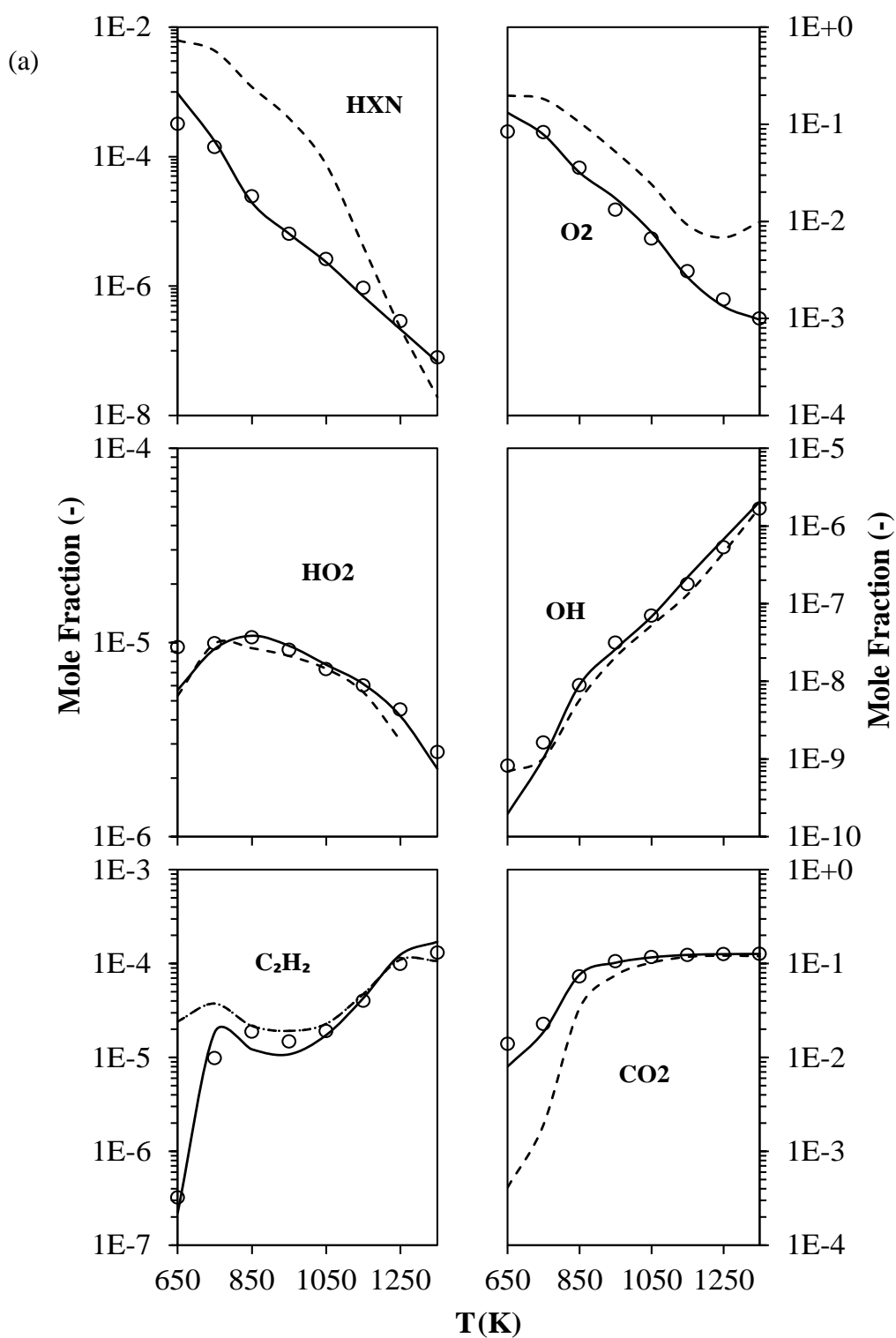


Figure 5-5: Comparison of the predicted species mole fractions between the reduced and detailed (a) diesel and (b) biodiesel surrogate fuel mechanisms under auto-ignition condition for initial pressure of 60 bar, initial temperature of 950 K and Φ of 1.0.

Based on the results shown in Figure 5-5, it is observed that the selected species mole fractions are reasonably replicated under the auto-ignition condition with the use of HXNv1 and HXNv2 for diesel combustion. The distance between the predicted species profiles can be attributed to the difference in ID predictions by the reduced and detailed mechanisms. Apart from that, in comparison to HXNv1, it is found that the species profiles computed by HXNv2 are in better agreement with those of the detailed model. This can be attributed to the inclusion of JSR as an additional data source for mechanism reduction on top of auto-ignition condition, which consequently improves the model predictions.

Nonetheless, noticeable deviations in O_2 , OH and CO_2 concentrations at steady-state are observed between the predictions by the MCBSv1 and detailed models. The present results show that MCBSv2 yields better predictions in species concentration profiles as compared to MCBSv1 for biodiesel combustion under auto-ignition condition. Additionally, it is seen that the temporal evolution trends of fuel species predicted by both reduced models are slightly different from those computed by the detailed model. The observed trends can be attributed to the elimination of isomers during mechanism reduction procedure. This can be improved by retaining more isomers in the reduced models. However, it will consequently increase the mechanism size which is not favourable for the complex CFD simulations. The findings obtained in this work have demonstrated an acceptable compromise in terms of mechanism size and results accuracy.

Comparison of species concentration profiles between the reduced and detailed mechanisms under JSR condition is illustrated in Figure 5-6. Similarly, only results at initial pressure of 60 bar and ϕ of 1 are demonstrated as similar temporal evolution trends in the results are observed for other conditions.



○ Detailed Mechanism

--- HXNv1

— HXNv2

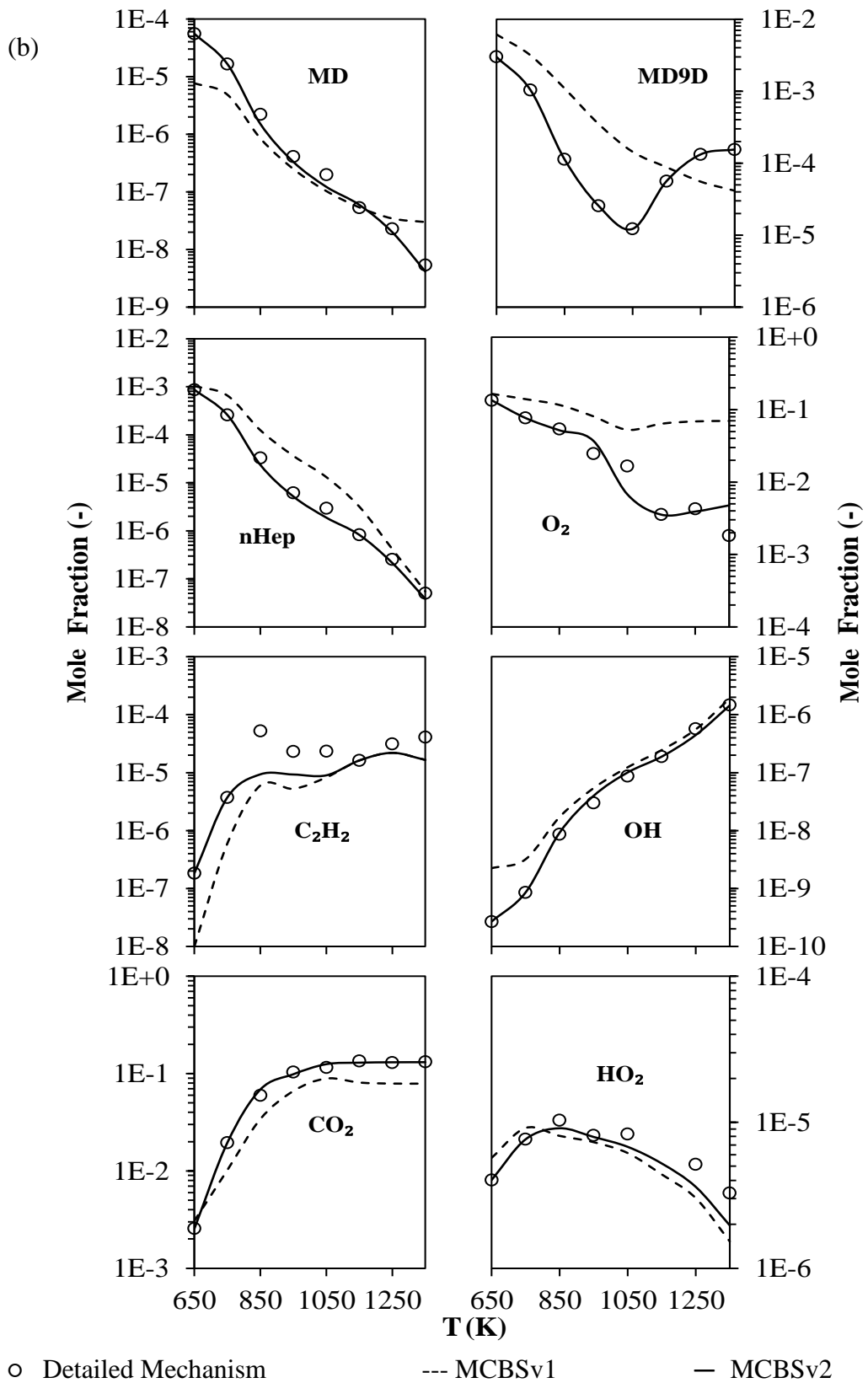


Figure 5-6: Comparison of species profiles predicted by the reduced (a) diesel and (b) biodiesel surrogate fuel mechanisms with the respective detailed

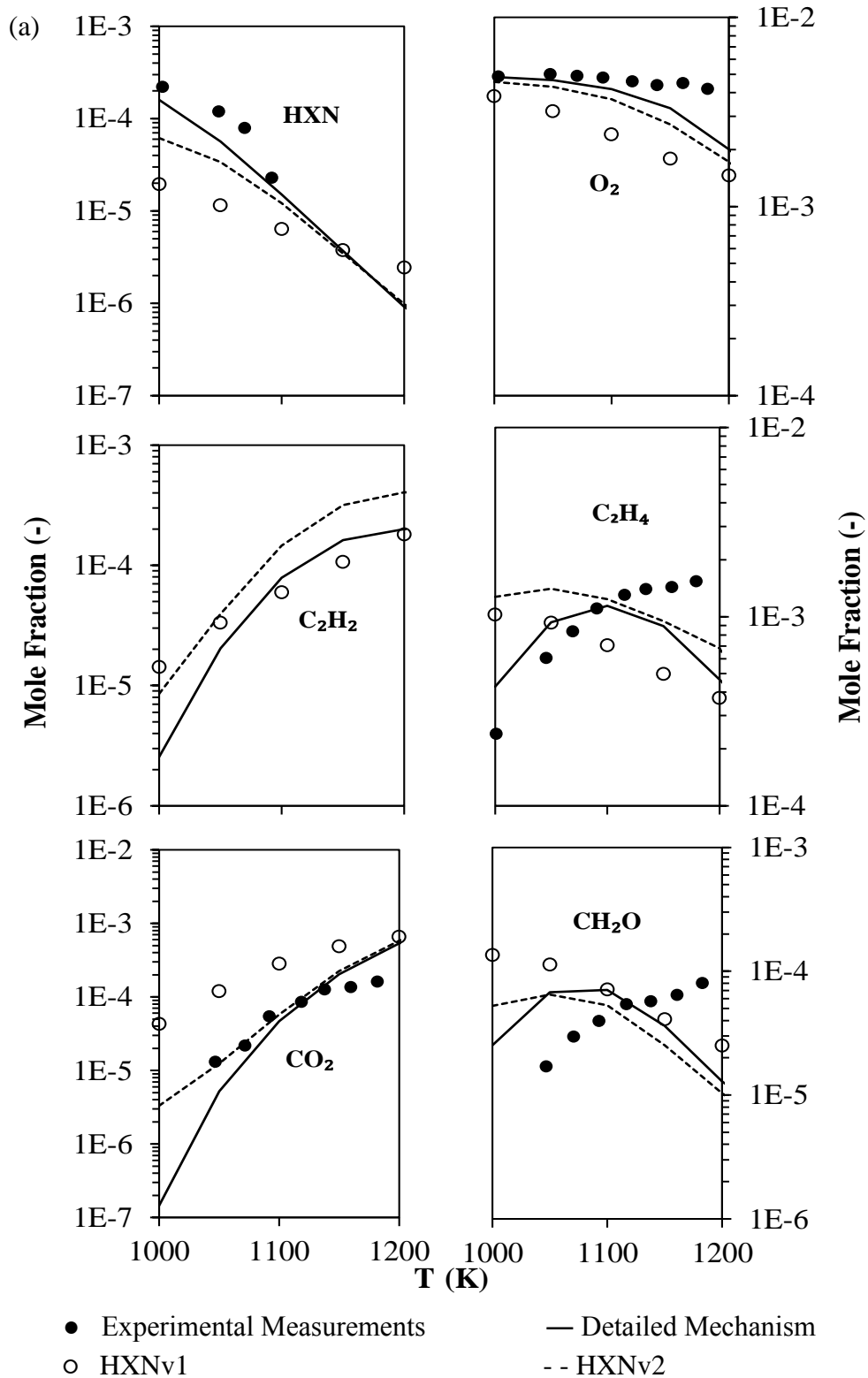
mechanisms under JSR condition as a function of temperature, with initial pressure of 60 bar and Φ of 1.

The results in Figure 5-6 show that HXNv2 and the MCBSv2 are able to reproduce species concentration profiles more accurately as compared to HXNv1 and MCBSv1, respectively, for both auto-ignition and JSR conditions. In both circumstances, the inaccuracies seem to be more obvious when initial temperature is low. The deviations in mole fractions between HXNv1 and the detailed HXN mechanism for the stated species are significant with errors greater than 80 %. Similar trend is encountered too for MCBSv1. In contrast, the relative error for each species concentration is comparatively smaller by applying HXNv2 and MCBSv2. Although discrepancies are perceived in low temperature regions, close agreements are achieved in NTC and high temperature regions for the latter occasion. Apart from that, referring to species profiles of HXN and MD9D in Figure 5-6, it can be seen that the application of HXNv1 as well as MCBSv1 has over-predicted the fuel concentration, especially at low temperature and NTC regions. Owing to these circumstances, A-factor constants of the reactions such as ‘ $C_{16}H_{34} + OH = C_{16}H_{33-5} + H_2O$ ’ and ‘ $MD9D + OH = MD9D6J + H_2O$ ’ have been adjusted. These reactions have been tested to give significant influence in fuel concentration predictions during combustion process.

In addition, it is observed that reaction such as ‘ $C_9H_{19-1} + C_7H_{15-1} = nC_{16}H_{34}$ ’ which play an important role during thermal decomposition is not incorporated in the HXNv1 diesel surrogate fuel model. Therefore, by including reactions from this class, ID predictions for high temperature have been improved. Furthermore, the addition of species MF5J along with the corresponding elementary reactions has also improved the ID predictions of MCBSv2 at low temperatures.

Following that, further validations of the surrogate models are performed by comparing the computed species profiles to the experimental results of D2 [13] and RME [109] oxidations in a JSR for fuel-oxygen mixtures, diluted by nitrogen. The associated test conditions are demonstrated in Table 5-1. The species selected for validation exercise here are important reactant and product species which are selected based on the availability of the experimental measurements. These

species are validated in order to ensure that the proposed surrogate models are able to provide a reasonable representation of the kinetics of the fuel oxidations. The results are shown in Figure 5-7.



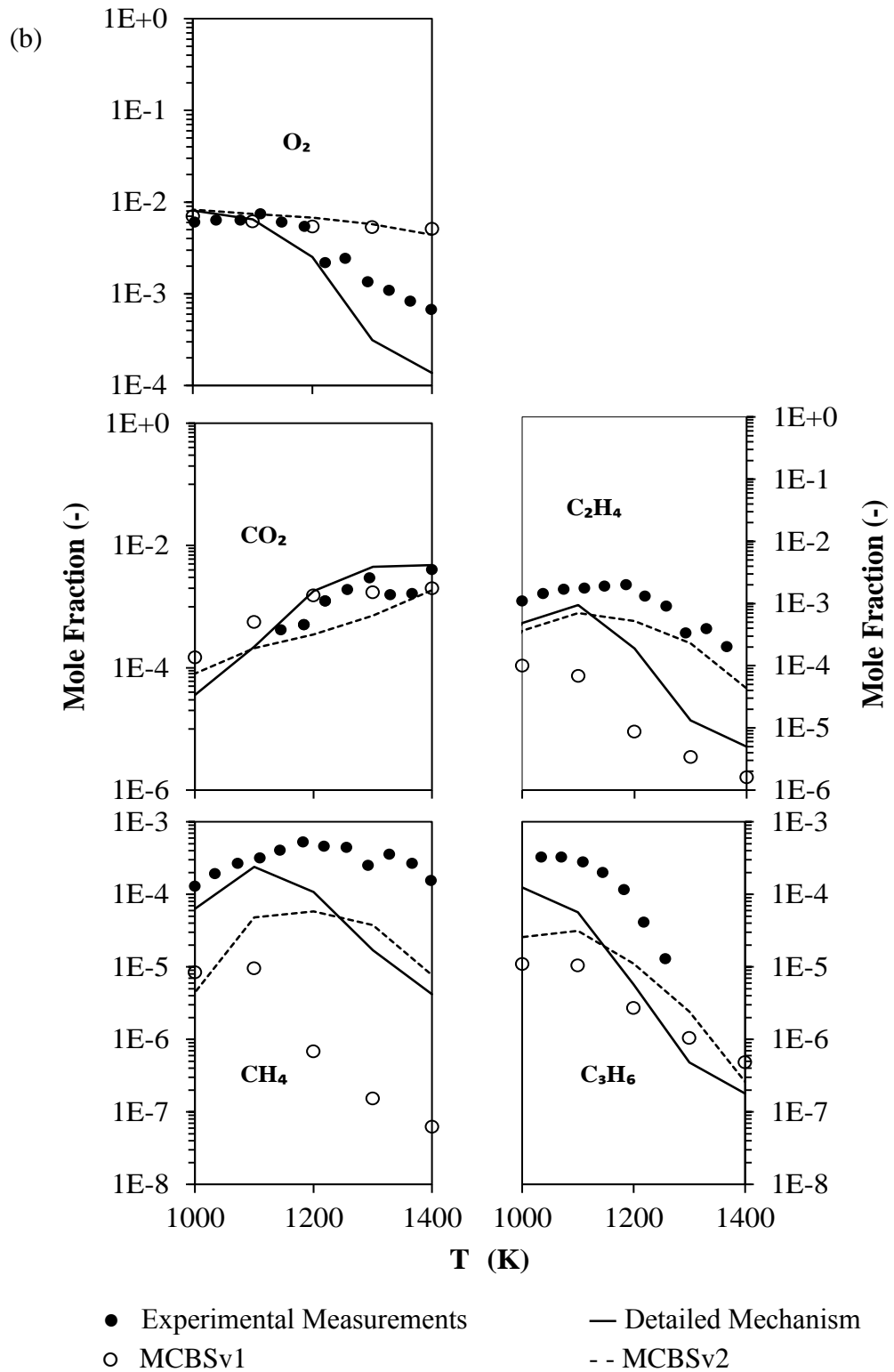


Figure 5-7: Computed and experimental species mole fractions obtained from the oxidation of (a) 0.03 % HXN and (b) 0.05 % of RME in a JSR. [Note: The associated operating conditions are depicted in Table 5-1.]

Figure 5-7(a) shows that both HXNv1 and HXNv2 are able to reproduce the species concentration profiles and kinetics of the fuel oxidation adequately in view of their simplified fuel chemistry. The species profile trends predicted by the reduced models are similar with minor deviations in absolute values. It is also observed that the computed fuel profiles are comparable with the experimental measurements in which the fuel concentration decreases with temperature. However, the fuel concentration for HXN oxidation at high temperatures (≥ 1000 K) is under-predicted. Owing to the different fuel consumption rate, the formation of product species such as CH_2O also differs from the experimental profiles across the temperature range. An opposite trend is also observed for C_2H_4 and CH_2O profiles between experimental data and those predicted by the reduced models, where the measured concentrations increase with increasing temperatures. This may be expected since the detailed model also predicted an opposite trend for these species, where decreasing trends are observed at high temperature region. The patterns produced by the reduced and detailed models are however consistent. Also, C_2H_4 and CH_2O are produced from the decomposition/consumption of HXN. Thus, their concentration levels reduce with decreasing HXN concentration. In addition, the species concentration profiles predicted by the reduced mechanisms are also compared with those of the detailed mechanism. Consistency in species profile trends is observed between the computed results using the reduced and detailed mechanisms.

In contrast, it is observed that the species mole fractions computed by MCBSv2 are comparable with those obtained from the experiments with maximum deviations of approximately one order of magnitude in the absolute values, as shown in Figure 5-7(b). Moreover, the predictions by the surrogate models are also compared with those calculated by the detailed model. Similar trend in temporal evolution is obtained when MCBSv2 is employed. Nonetheless, the computation results generated by MCBSv1 are seen to be relatively different from the measurements. Variations in species concentrations of CH_4 and C_2H_4 are more evident where both species concentrations are under-predicted across the temperature range. This can be attributed to the elimination of essential intermediate species and reactions during the mechanism reduction procedure.

Despite the variations in absolute values, the predicted species profiles by HXNv2 and MCBSv2 are consistent with those of the experiments and detailed models. The validation results are deemed acceptable in consideration of its simplified fuel chemistries. The HXNv2 diesel surrogate fuel mechanism and the MCBSv2 biodiesel surrogate fuel mechanism are compiled in Appendix C.

5.4 Implementation of Chemical Kinetic Mechanism Reduction Scheme on Small-Scale Mechanism Reduction - Ethylene

In view of the promising performance of the reduction scheme on large-scale mechanisms such as the diesel and biodiesel surrogate fuel models, the integrated chemical kinetic mechanism reduction scheme introduced in Section 5.2 is employed on the ethylene mechanism in this section in order to examine its applicability on reduction of small-scale mechanism.

5.4.1 Derivation of Reduced Model

The ethylene mechanism [164] which consists of 111 species and 784 elementary reactions is applied to investigate the flame temperatures under a wide range of Φ . The premixed laminar burner stabilised flame model of CHEMKIN-PRO software is employed, and the simulation setup is selected based on the experimental work done by Ivarsson and Schramm [165]. The operating conditions applied in this 1-D laminar flame-speed simulations are summarised in Table 5-4.

Table 5-4: Operating conditions applied to for reduction of the ethylene mechanism.

Operating Conditions	Range Evaluated
Φ (-)	0.5 – 2.5 (0.1 increments)
Initial Pressure (atm)	1
Initial Temperature (K)	300
Height above Burner (mm)	8.5

Here, capability of the mechanism in flame temperature predictions is selected as the basis of mechanism reduction. This is different from the previous section whereby capability of the mechanism in auto-ignition predictions is designated as the basis of mechanism reduction. The data source of mechanism reduction is carefully chosen based on the target applications such as auto-ignition simulations in Section 5.3.1 and laminar flame speed simulations in this section.

Similar to the reduction exercise in Section 5.3.1, mechanism reduction is conducted using the reduction scheme demonstrated in Figure 5-1. After the DRGEP reduction, a reduced mechanism with 55 species is generated with a maximum deviation of 2.5 % in temperature prediction. Following that, the second step of reduction procedure (i.e. isomer lumping) is ignored as there are no isomers presented in the mechanism. Thus, reaction pathway analysis is performed right after DRGEP reduction. The major reaction pathways during ethylene combustion are illustrated in Figure 5-8.

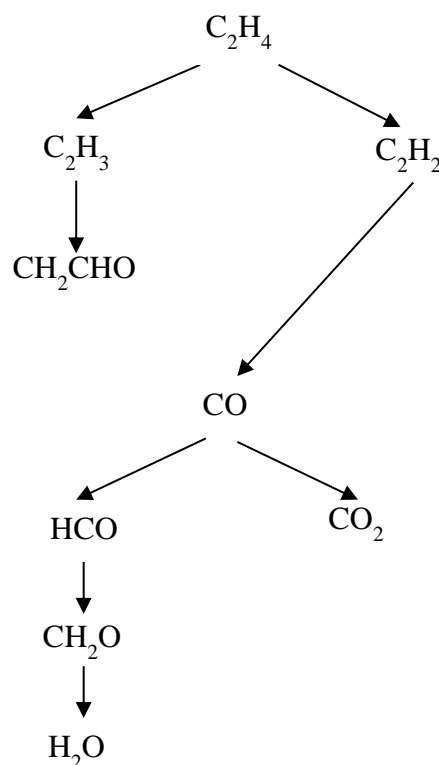


Figure 5-8: Main reaction pathways during ethylene combustion.

Here, A-factor constant for reaction ' $C_2H_2 + O = CH_2 + CO$ ' is optimised to improve the flame temperature predictions throughout the tested Φ range. The resulting reduced ethylene mechanism consists of 27 species and 147 elementary reactions. Successively, the reduced mechanism is validated against those of the detailed ethylene mechanism and the results are shown in Figure 5-9.

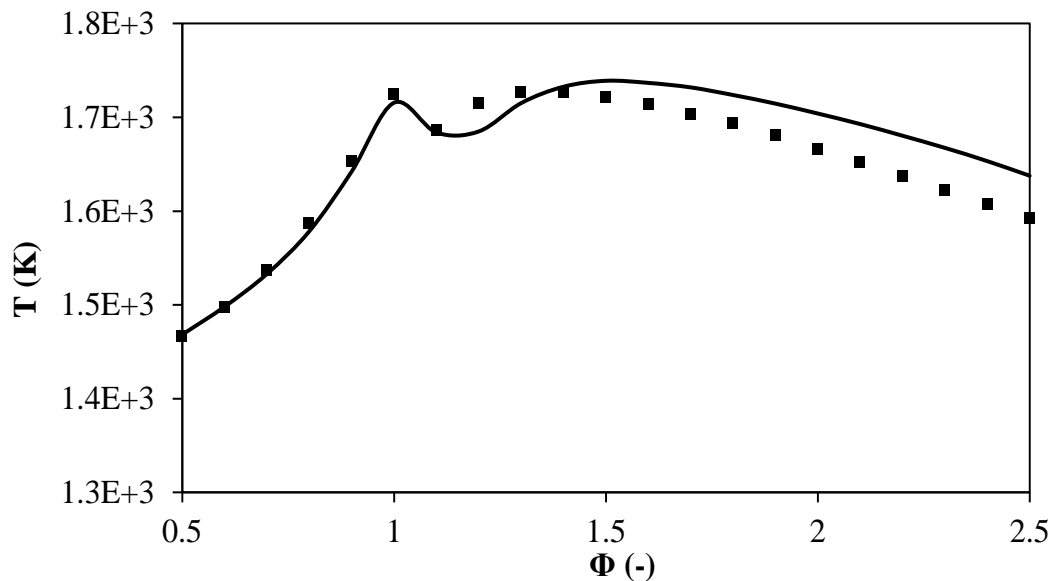


Figure 5-9: Comparison of the flame temperature profiles generated by the reduced (■) and detailed (—) ethylene mechanisms.

The flame temperature profile is seen to remain intact and good agreement between the reduced and detailed ethylene mechanisms is observed with maximum 2.8 % deviation in temperature predictions. In addition, each CHEMKIN-PRO simulation requires approximately 2 s on average to complete and this contributes to a 97 % reduction in T_C as compared to that of the detailed ethylene mechanism.

5.4.2 Further Validations in 0-D Chemical Kinetic Simulations

Subsequently, the 27-species reduced ethylene mechanism developed in the previous section is further validated with respect to:

- ID predictions under auto-ignition conditions (Figure 5-10);
- species mole fraction predictions under auto-ignition conditions (Figure 5-11);

- c) species mole fraction predictions under JSR conditions (Figure 5-12); and
 d) species mole fraction predictions against JSR experimental data of Dagaut et al. [166] (Figure 5-13).

Operating conditions listed in Table 5-5 is applied here.

Table 5-5: Test conditions applied for model validations of the reduced ethylene model.

Operating Conditions		Range Evaluated
Auto-ignition ^a	Φ (-)	0.5, 1.0, 2.0
	Initial Pressure (bar)	13.5, 41.0
	Initial Temperature (K)	650 – 1350 (100 K increments)
JSR ^a	Φ (-)	0.5, 1.0, 2.0
	Initial Pressure (bar)	13.5, 41.0
	Residence Time (s)	1
JSR ^b	Φ (-)	2
	Initial Pressure (bar)	5.05
	Initial Temperature (K)	1080

^a Operating conditions selected for model validations against the computations of the detailed model.

^b Operating conditions selected for model validations according to the experimental results of fuel oxidation in a JSR [166].

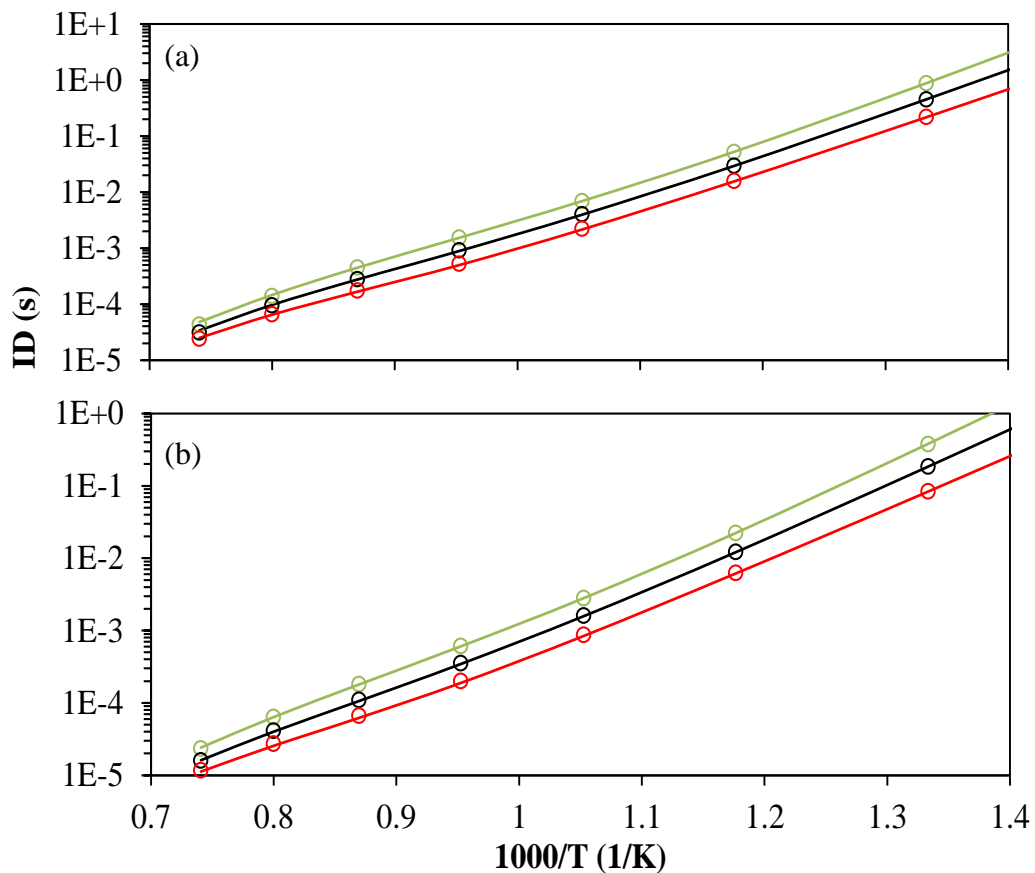


Figure 5-10: Comparisons of the respective ID timing predictions with the detailed mechanisms (lines) using the reduced ethylene mechanism (○) generated from the integrated reduction scheme for initial pressure of (a) 13.5 bar and (b) 41 bar and Φ of 0.5 (green), 1.0 (black), 2 (red).

Based on the results shown in Figure 5-10, good agreement in ID predictions are observed between the reduced and detailed models throughout the test conditions. Here, the conditions applied cover low to high pressures and temperatures so that the model can be used in wider range of CFD applications. Apart from that, satisfactory results are also obtained in species concentration predictions between the reduced and detailed models for fuel oxidations under auto-ignition and JSR conditions. The results are demonstrated in Figure 5-11 and Figure 5-12, respectively. In this section, only results for Φ of 1 are presented since similar temporal evolution trends in the results are obtained for both Φ of 0.5 and 2.

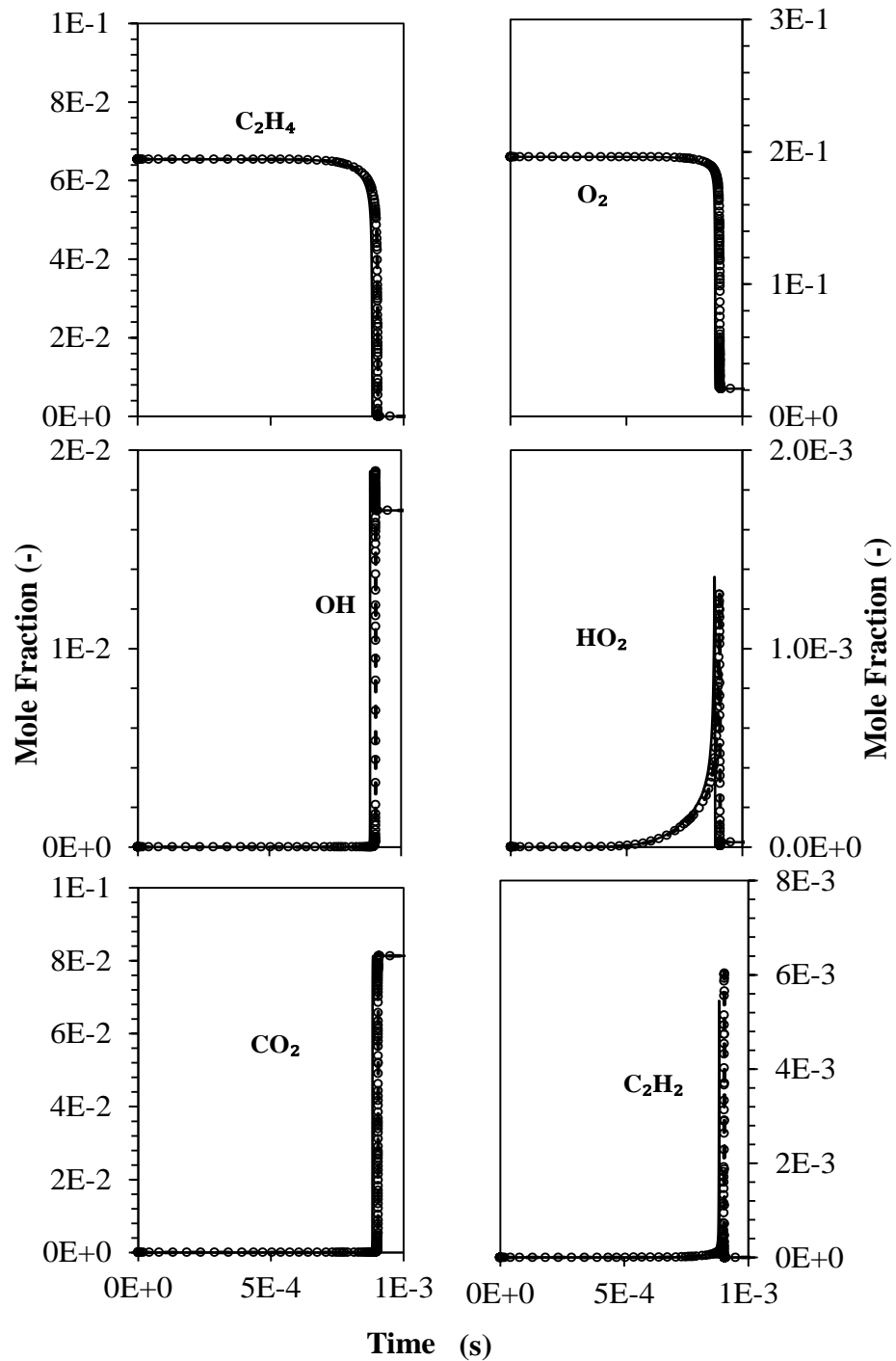


Figure 5-11: Comparison of species profiles of the reduced (—) and detailed (○) ethylene mechanisms under auto-ignition condition as a function of temperature, with initial pressure of 41 bar, initial temperature of 1050 K and Φ of 1.

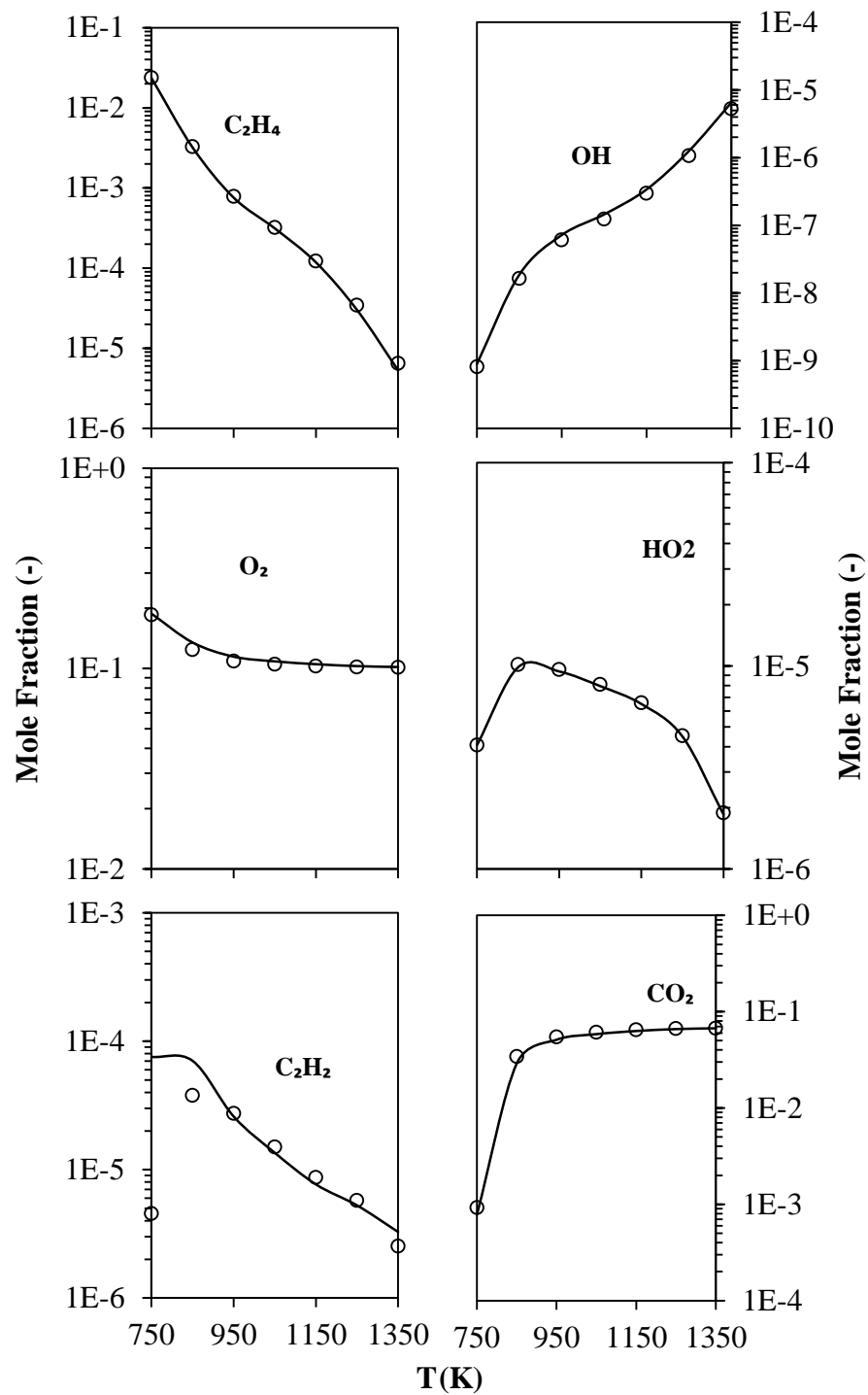
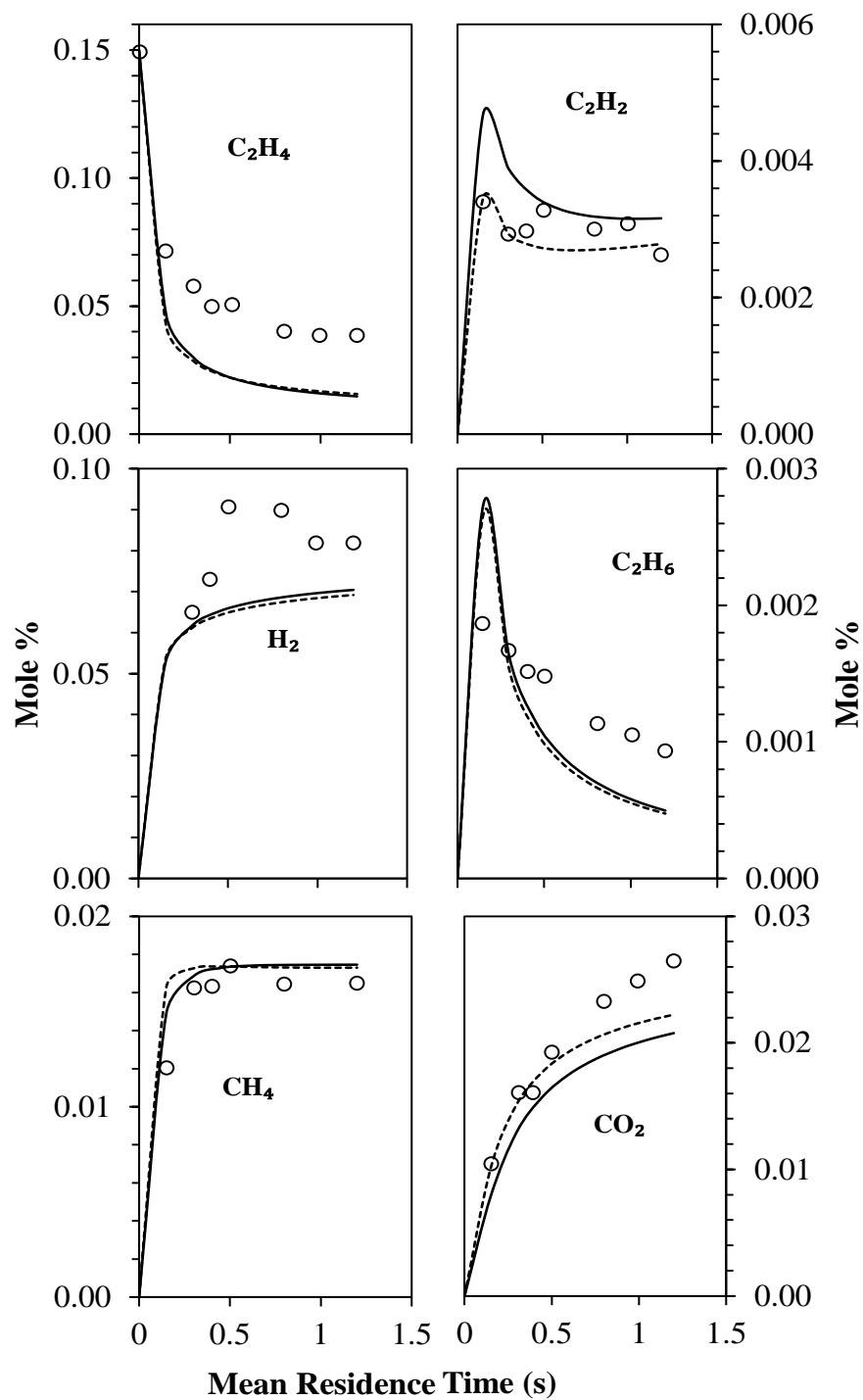


Figure 5-12: Comparison of species profiles of the reduced (—) and detailed (○) ethylene mechanisms under JSR condition as a function of temperature, with initial pressure of 41 bar and Φ of 1.

In addition, the reduced ethylene mechanism is further validated using the JSR experimental results of Dagaut et al. [166]. The validation results are depicted in Figure 5-13 by comparing the species concentration predictions to the experimental data for fuel-oxygen mixtures, diluted by nitrogen. Selection of species for comparison studies here depends on the availability of the experimental data. Species such as CH_4 , CO_2 , C_2H_2 , C_2H_4 , C_2H_6 and H_2 are validated to ensure that the proposed surrogate model is able to provide a reasonable representation of the kinetics of the fuel oxidations.

Figure 5-13 shows that the reduced ethylene model is able to reproduce the species profiles and kinetics of the fuel oxidation satisfactorily. The fuel concentrations computed by the reduced model are comparable with the measurements in which a decreasing trend with respect to the mean residence time is obtained. However, it is also observed that C_2H_4 concentrations are under-predicted as compared to the measurements when the mean residence time increases. As a result of the different fuel consumption rate, the formation of CO_2 and H_2 also varies from the experimental profiles. Besides, it is seen that the C_2H_2 concentrations computed by the reduced model are comparatively lower than those of the detailed model and they are in closer agreement with the experimental data. Consequently, the lower C_2H_2 concentration predictions by the reduced model might yield lower soot production during ethylene combustion as C_2H_2 is often used as the soot precursor/surface growth species to capture soot onset and soot formation processes. Apart from that, while CO_2 formation is also dependent on C_2H_2 , as shown in Figure 5-8, decrement in exhaust CO_2 levels is also anticipated. Apart from the comparison with the experimental measurements, the species profile trends computed by the reduced mechanism are also consistent with those predicted by the detailed mechanism. Despite the variation between the computations and measurements, the results of the predicted species concentrations are deemed acceptable in view of its simplified fuel chemistries [66]. The reduced ethylene mechanism with 27 species is provided in Appendix C.



○ Experimental Measurements — Detailed Mechanism
 ... Reduced Mechanism

Figure 5-13: Computed and experimental species mole fraction obtained from the oxidation of 0.15 % C₂H₄ in a JSR at pressure of 5 atm and Φ of 2.

5.5 Concluding Remarks

In this study, an integrated chemical kinetic mechanism reduction scheme which consists of five reduction stages is formulated for large-scale mechanism reduction such as the diesel and biodiesel surrogate fuel models. Here, it is found that the applications of both auto-ignition and JSR conditions as the data source of mechanism reduction permit better agreement in species profiles predictions, instead of using auto-ignition condition only. As such, a 79-species HXNv2 diesel surrogate fuel model and an 80-species MCBSv2 biodiesel surrogate fuel model are successfully derived from their detailed mechanisms, respectively. Good agreement is achieved between the reduced and detailed mechanisms in ID predictions, with a maximum relative error of 40 %. The reduced mechanisms are also able to reproduce the species concentration profiles of the detailed mechanisms satisfactorily.

In view of the adequate reduction performance on the diesel and biodiesel surrogate fuel models, the mechanism reduction scheme is henceforth applied on the 111-species ethylene mechanism in order to examine its applicability on small-scale mechanism reduction. Flame temperatures under a wide range of Φ are examined using the premixed laminar burner stabilised flame model of CHEMKIN-PRO software. Consequently, a resulting mechanism with 27 species is generated. Close agreements are achieved between the reduced and detailed mechanisms with a maximum deviation of 2.8 % in flame temperature predictions. Additionally, further validations of the model in 0-D simulations are performed and satisfactory results are obtained in view of its simplified chemistry.

CHAPTER 6

VALIDATIONS OF THE DIESEL AND BIODIESEL SURROGATE FUEL MODELS IN 2-D SPRAY COMBUSTION SIMULATIONS

6.1 Introduction

In this chapter, 2-D spray combustion simulations are performed to further evaluate the fidelity of the developed diesel and biodiesel surrogate fuel models. In Section 6.2, the numerical formulations and setups applied in the 2-D simulations are described. Subsequently, the diesel and biodiesel fuel spray combustion characteristics as well as their soot formation performances in a constant volume combustion chamber are assessed in Section 6.3. Lastly, the results obtained in this phase of work are summarised in Section 6.4.

6.2 Numerical Formulations and Setups

Spray combustion within a constant volume combustion chamber is studied by performing 2-D simulations using the OpenFOAM software package. *dieselFOAM*, which is the OpenFOAM-2.0.x solver for diesel spray and combustion is used in this study. The diesel and biodiesel surrogate fuel models generated in Chapter 5 are directly coupled into the CFD solver. The chemical reactions are modelled as source terms in the species transport equation while the reaction rates are determined through the Arrhenius expressions.

The combustion chamber is a well-stirred reactor. It is a 108 mm cube with a common-rail, single-hole injector mounted in a metal side-port which directs a spray into the centre of the combustion chamber [167], as illustrated in Figure 6-1.

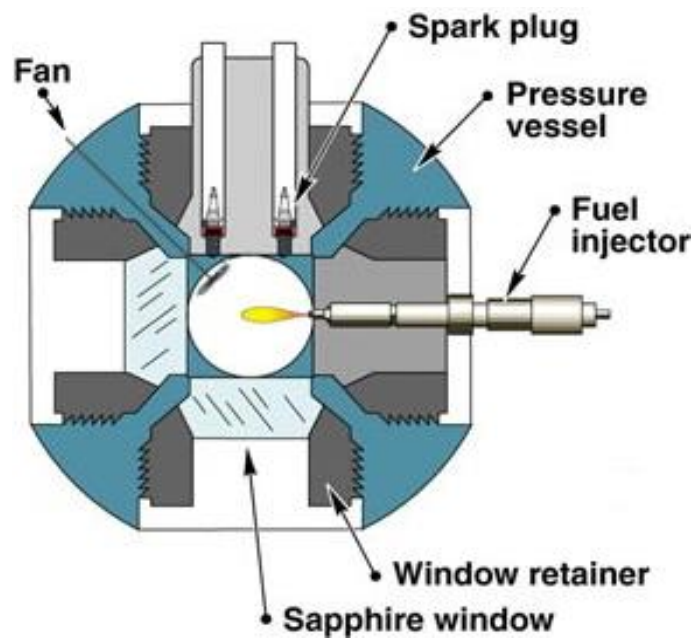


Figure 6-1: Schematic cross-section of the constant volume combustion chamber [167].

Following that, the simulation results are compared to the experimental data of D2 [17,168] for diesel fuel combustion and soy methyl ester (SME) [169] for biodiesel fuel combustion. The associated experimental operating conditions as well as the fuel injector characteristics are shown in Table 6-1.

Table 6-1: Experimental operating conditions and injector characteristics.

(a) Experimental Operating Conditions	
Ambient Temperature (K)	900/1000
Ambient Density (kg/m ³)	22.8
Ambient Pressure (MPa)	6/6.7
Ambient Composition (%):	
Non- Reacting	O ₂ = 0 %; CO ₂ = 6.52 %; H ₂ O = 3.77 %; N ₂ = 89.71 %
Reacting	O ₂ = 15 %; CO ₂ = 6.23 %; H ₂ O = 3.62 %; N ₂ = 75.15 %
(b) Injector Characteristics	
Type	Bosch common rail, 2nd generation
Nozzle	Single hole, KS1.5/86, Min-sac type
Nozzle Diameter (µm)	90
Injector Pressure (MPa)	150
Orifice Diameter (mm)	0.09
Injector Duration (ms)	7
Fuel Temperature (K):	
SME	363
D2	373

Here, the non-reacting condition is chosen for simulations in order to ensure accurate mixing and vaporisation processes [23]. Contrastingly, the purpose of selecting the ambient gas conditions (i.e. reacting conditions) is to simulate the operating conditions for the latest generation of low-emission diesel engines, such as the turbocharged engine with exhaust gas recirculation system. In this work, LPL and vapour penetration length (VPL) are simulated for non-reacting fuel spray whereas ID, lift-off length (LOL) and SVF distribution are simulated for reacting diesel spray. Definitions of the parameters applied in this section are shown in Table 6-2 based on the references given on the Engine Combustion Network (ECN) website [167].

Table 6-2: Definitions of parameters.

Parameters	Definitions
LPL	Axial location from the injector to the location where 99 % of the total liquid mass is found.
VPL	Axial location from the injector to the location where fuel vapour mixture fraction ≥ 0.001 .
ID	Maximum dT/dt gradient of the temperature profile. This corresponds to ignition at $T > 2000$ K.
LOL	Distance from the injector to the closest layer where OH mass fraction reaches 0.02 %.

Next, parametric studies are performed using the non-reacting fuel spray condition to obtain a set of optimum configurations for the CFD simulations. The numerical set-ups for the parametric studies are tabulated in Table 6-3. Here, only results for the diesel surrogate fuel model are shown as similar trends are captured using the biodiesel surrogate fuel model. The simulations are conducted using ambient temperature of 900 K.

Table 6-3: Numerical set-ups for parametric studies.

Models/ Parameters	Selected Configurations	Parametric Studies				
		I	II	III	IV	V
Turbulence Model	Standard k - ε ($C_I = 1.44$)	✓	✓	○	✓	✓
Breakup Model	Reitz Diwakar ($C_s = 5$)	✓	✓	✓	○	✓
Grid	Grading; 0.25 mm x 0.25 mm (minimum), 4 mm x 2 mm (maximum) in both radial and axial directions	○	✓	✓	✓	✓
Time Step	1e-6 s	✓	○	✓	✓	✓
No. of Parcels	80,000	✓	✓	✓	✓	○
Initial k	0.735	✓	✓	✓	✓	✓
Initial ε	3.5	✓	✓	✓	✓	✓

‘✓’ represents fixed parameter constants; ‘○’ represents constants varied for parametric studies; I, II, III, IV and V refer to the parametric studies performed in Sections 6.2.1 to 6.2.5, respectively.

Initial k and ε are calculated using Equations 6-1 and 6-2, respectively:

$$\varepsilon = C_\mu^{0.75} k^{1.5} / l \quad (6-1)$$

$$k = 1.5u_{rms}^2 \quad (6-2)$$

l is the turbulence length scale and u_{rms} is approximately 0.7 m/s based on the experimental data.

6.2.1 Parametric Study I: Grid Independence Test

Grid independence test is carried out using three different mesh sizes of 0.25 mm, 0.5 mm and 1 mm, which represent fine, semi-fine and coarse mesh, respectively. The results are shown in Figure 6-2.

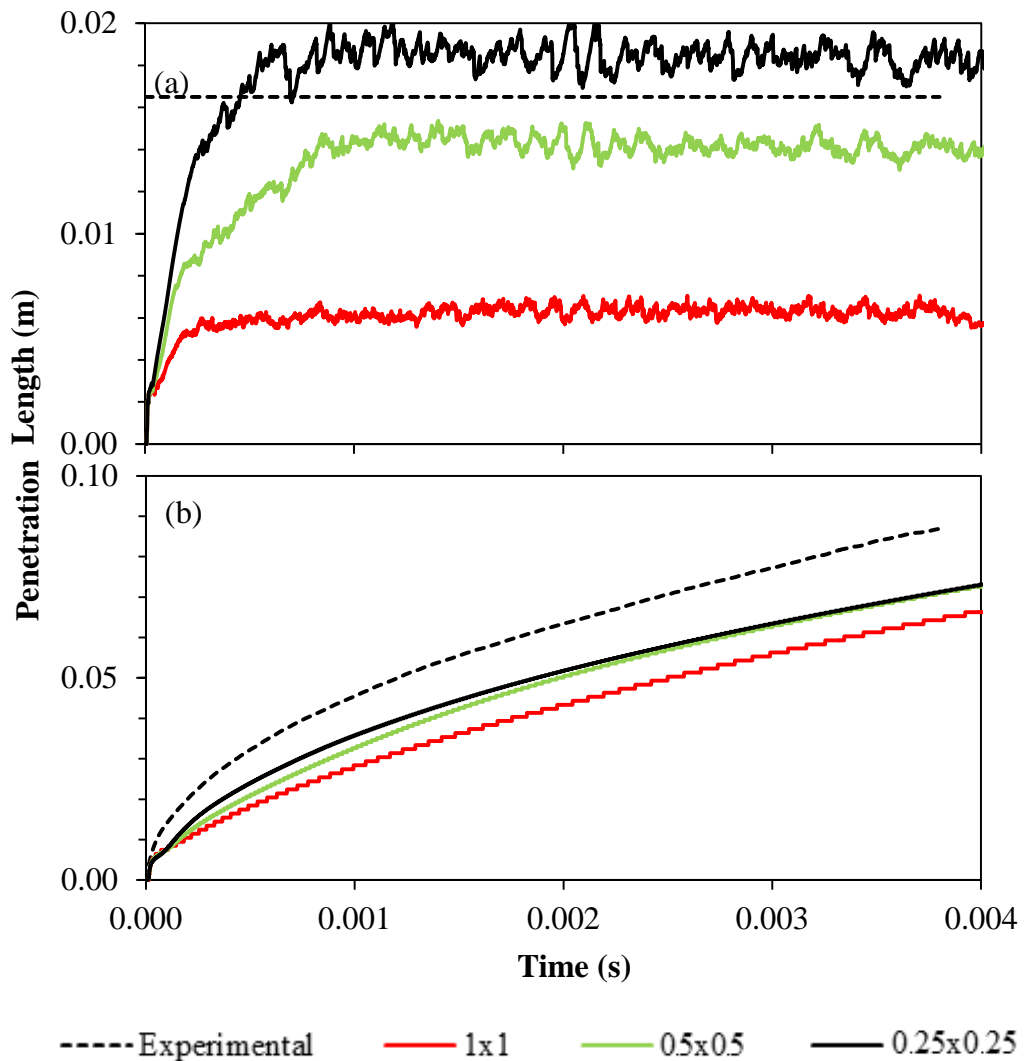


Figure 6-2: Comparison of the predicted (a) LPL and (b) VPL with the measurements using different grid sizes.

Based on the results shown in Figure 6-2, it is perceived that the mesh with finer grid size produces higher LPL and VPL as compared to the mesh with coarser grid size. The difference in penetration length is more obvious when a grid size of 1 mm is applied. Both LPL and VPL are the lowest, and liquid length fluctuations are obvious. The results are grid dependent for the grid size range studied. While discrepancy with the experimental data is usually the largest at the early part of vapour penetration profile, grids which are located near the injector tip have to be sufficiently small so that the early stage of vapour penetration is well captured. Meanwhile, it is not necessary to apply fine grid throughout the entire mesh as both liquid and vapour penetrations are captured near the injector tip. Thus, mesh

grading is recommended in order to reduce the total number of cells involved and thus the resulting computational time. Table 6-4 shows the details of mesh with different grading sizes.

Table 6-4: Descriptions of mesh with different grading sizes.

Grids	Baseline	Mesh 1	Mesh 2	Mesh 3	Mesh 4
Minimum Grid Size (mm):					
Radial	0.25	0.25	0.25	0.25	0.25
Axial	0.25	0.25	0.25	0.25	0.25
Maximum Grid Size (mm):					
Radial	0.25	4	4	2	2
Axial	0.25	2	4	4	2
Total Number of Cells	119,232	8,856	5,454	6,868	11,152

Mesh with uniform grid size of 0.25 mm is thus selected as the baseline in this numerical study since fine grids are required for better prediction of penetration length at the beginning part of penetration profiles. The results are shown in Figure 6-3.

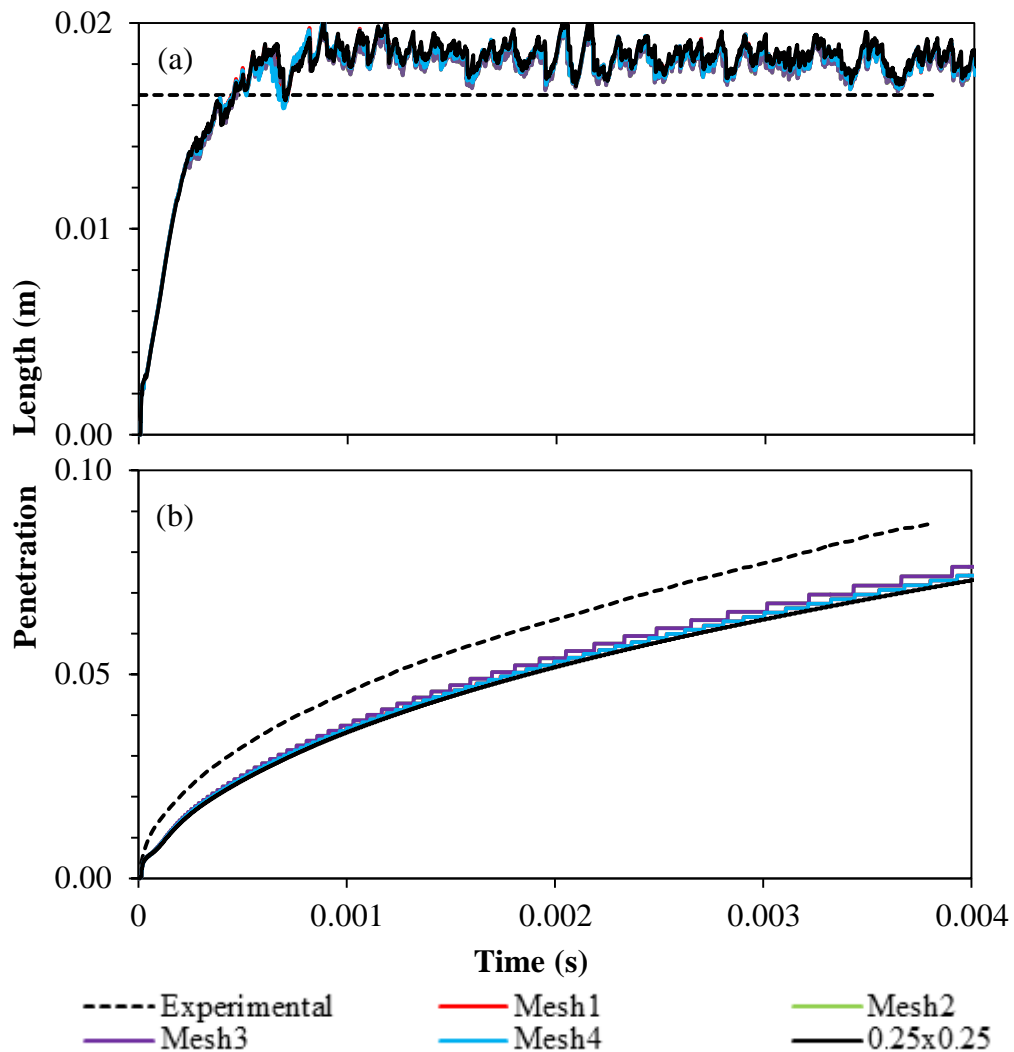


Figure 6-3: Comparison of the predicted (a) LPL and (b) VPL with the measurements using different mesh gradings.

Referring to Figure 6-3, it is observed that there are only slight differences in LPL and VPL. As such, it can be said that size of the grids located further from the diesel spray gives negligible effects on spray penetrations. Mesh 1 is selected for further parametric studies and its total number of cells is fourteen times lesser than the uniform mesh (i.e. 0.25 mm grid size) while maintaining the accuracy in spray penetration length predictions. Here, Mesh 2 is not selected for the subsequent modelling studies as a smaller grid size in axial location is preferable to account for better soot location predictions, despite the fact that it contains the least number of cells. On the other hand, grid size in radial direction further from injector tip is maximised as it does not affect the penetration profiles. Conversely,

grid size in axial direction further from injector tip is comparatively smaller than that in the radial direction for better prediction of the LOL.

6.2.2 Parametric Study II: Time Step

The effects of applying different computational time steps on spray penetration lengths are studied and the results are illustrated in Figure 6-4.

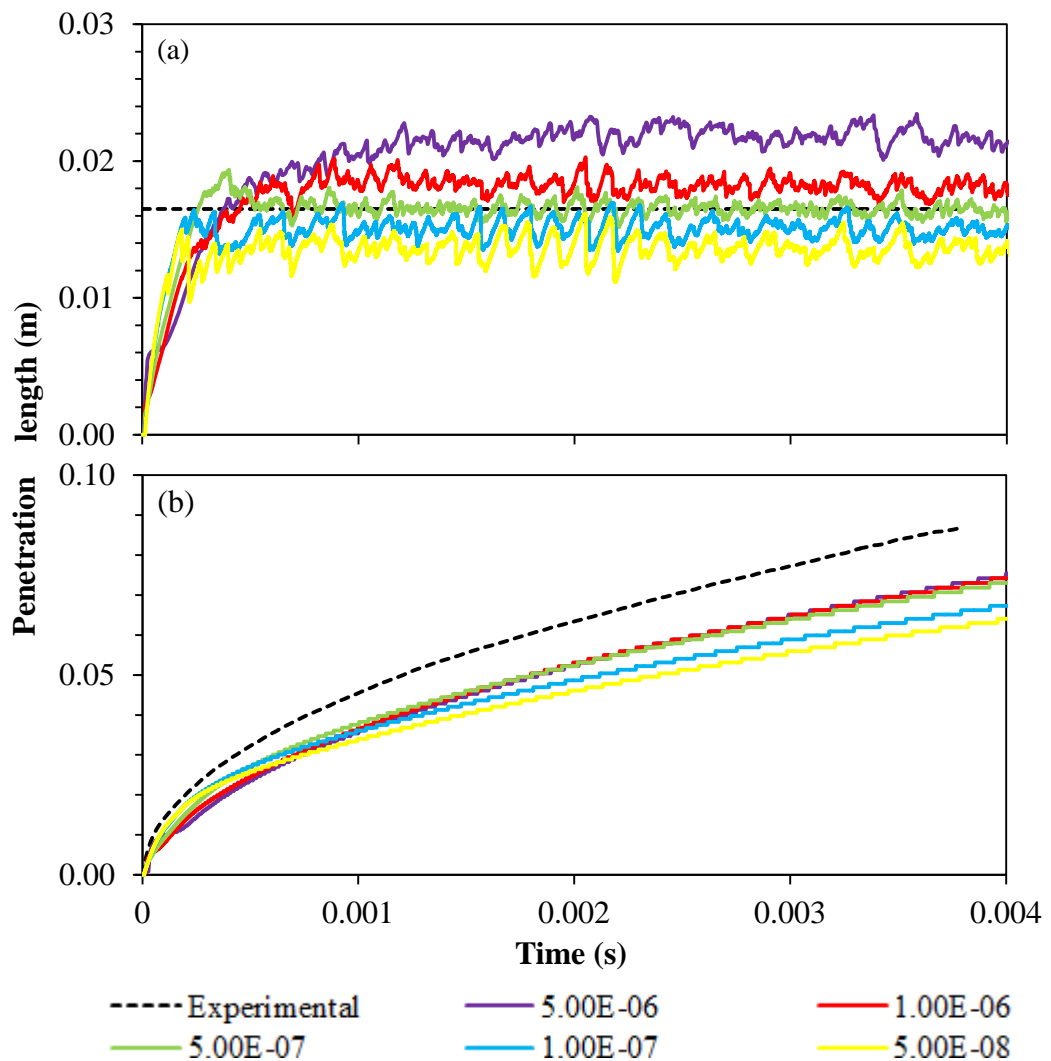


Figure 6-4: Comparison of the predicted (a) LPL and (b) VPL with the measurements using different time steps.

Figure 6-4 demonstrates that huge computational time step such as 5×10^{-6} s can cause instability to the LPL with higher magnitude. Further refinement in computational time step leads to lower and more stable LPL as well as lower

VPL. However, fluctuation in LPL is noticeable when a computational time step of 5×10^{-8} s is applied as the use of smaller time step provides a higher resolution to capture the instability. This trend shows that spray penetration is sensitive to the change of computational time step in this study. Time steps of 1×10^{-6} s and 5×10^{-7} s are more favourable as the resultant LPL are more stable and trends of the vapour penetration profiles are closer to the experimental measurements.

6.2.3 Parametric Study III: Turbulence Model

Performance of three different turbulence models, i.e. standard $k-\varepsilon$ model, RNG $k-\varepsilon$ model as well as realisable $k-\varepsilon$ models are compared. The model constants for each turbulence model are listed in Table 6-5.

Table 6-5: Model constants for different turbulence models.

Turbulence Models	Model Constants
Standard $k-\varepsilon$	$C_\mu = 0.09$; $C_{1\varepsilon} = 1.44$; $C_{2\varepsilon} = 1.92$; $C_{3\varepsilon} = -0.33$; $\sigma_k = 1$; $\sigma_\varepsilon = 1.3$
RNG $k-\varepsilon$	$C_\mu = 0.0845$; $C_{1\varepsilon} = 1.42$; $C_{2\varepsilon} = 1.68$; $C_{3\varepsilon} = -0.33$; $\sigma_k = 0.71942$; $\sigma_\varepsilon = 0.71942$; $\eta = 4.38$; $\beta = 0.012$
Realisable $k-\varepsilon$	$C_\mu = 0.09$; $C_{2\varepsilon} = 1.9$; $A_0 = 4$; $\sigma_k = 1$; $\sigma_\varepsilon = 1.2$

The effects of using different turbulence models on the predictions of LPL and VPL are demonstrated in Figure 6-5.

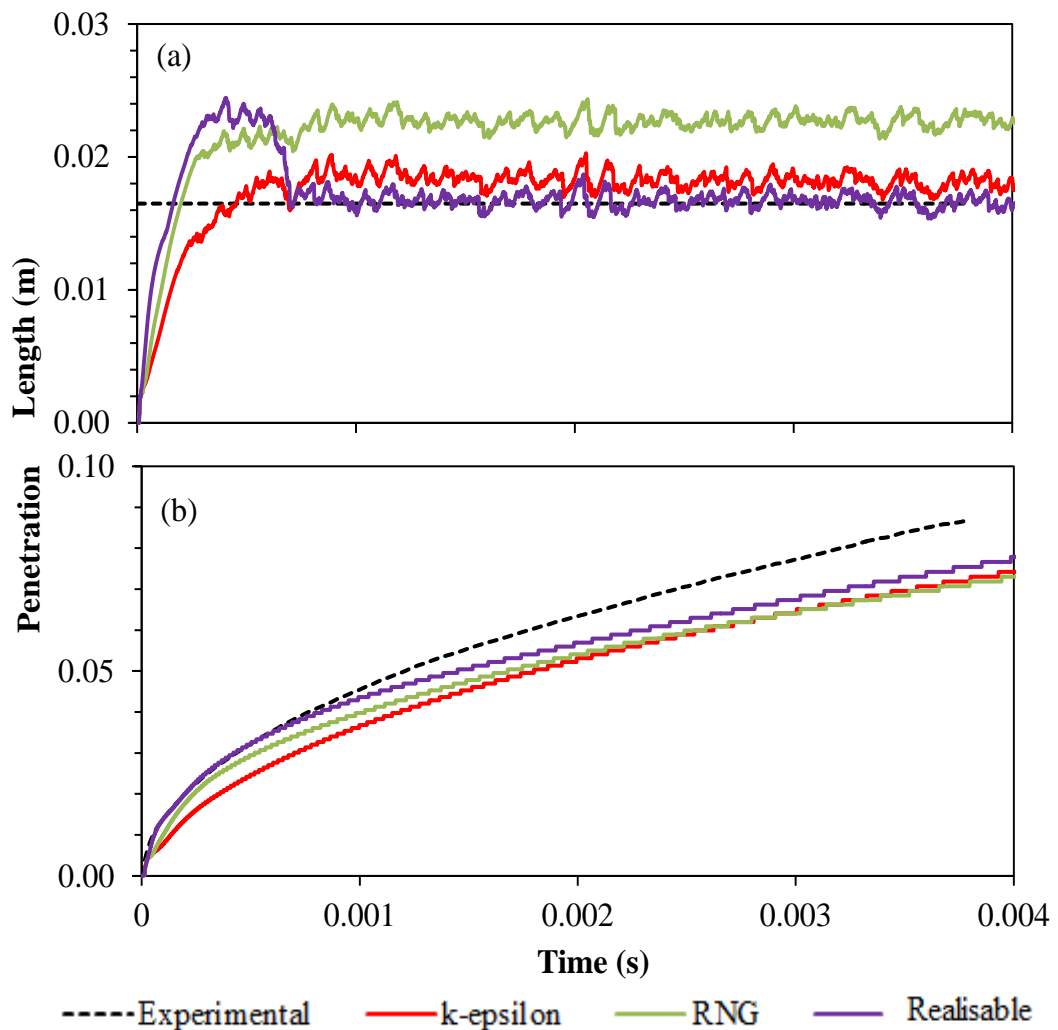


Figure 6-5: Comparison of the predicted (a) LPL and (b) VPL with the measurements using different turbulence models.

Liquid penetration peaks at early part of the injection and subsequently drops to a stable level throughout the injection period while vapour penetration during the starting part of injections is over-predicted with the use of realisable $k-\varepsilon$ model. In contrast, although RNG $k-\varepsilon$ model is able to accurately predict the early stage of spray penetrations, the variation in VPL gets larger towards the end of fuel injection. The standard $k-\varepsilon$ model produces results that provide a better fit with the experimental data, especially for the changes of vapour penetration with time. Based on the results obtained, standard $k-\varepsilon$ model is chosen for further simulations in the present work, and the effects of changing the corresponding constant value $C_{1\varepsilon}$ are demonstrated in Figure 6-6.

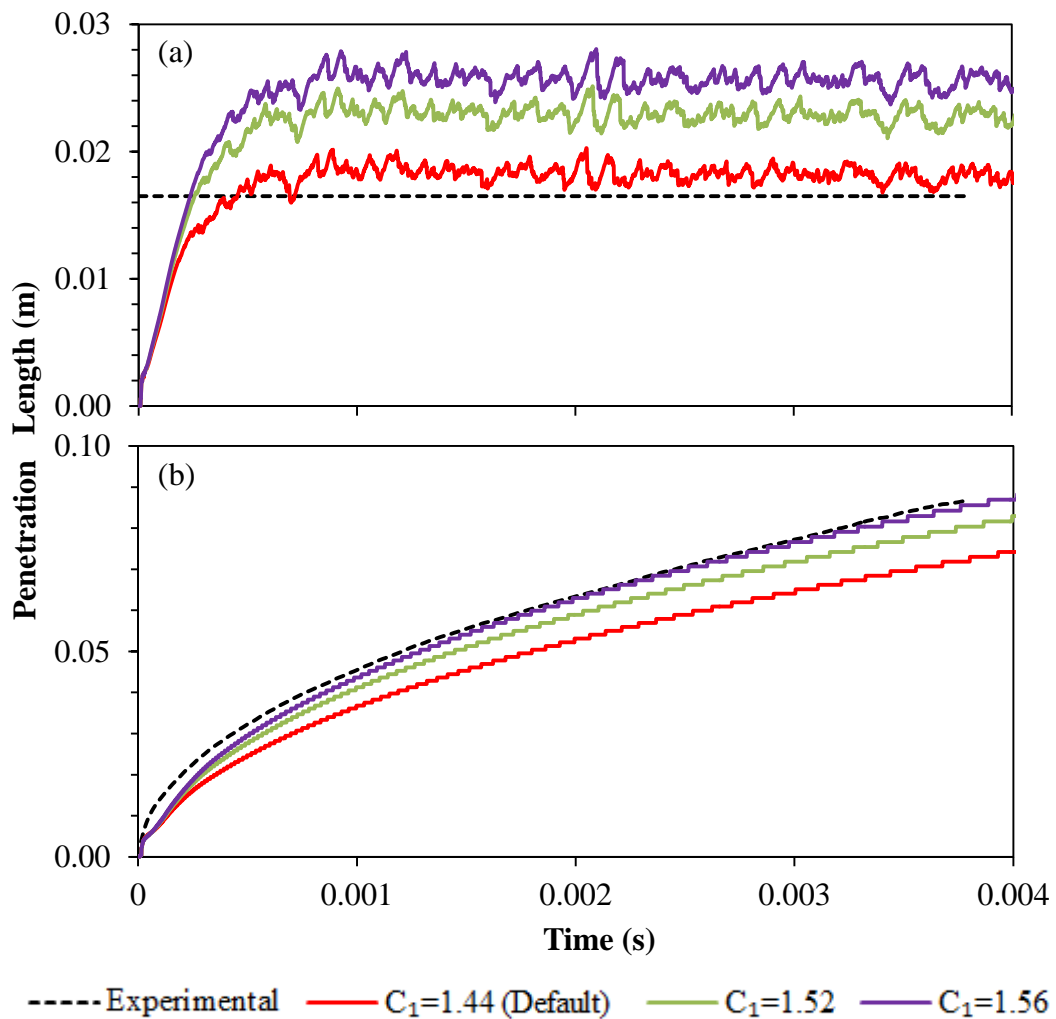


Figure 6-6: Comparison of the predicted (a) LPL and (b) VPL with the measurements using different $C_{1\epsilon}$ values of standard $k-\epsilon$ model.

In Figure 6-6, it is observed that both LPL and VPL are highly sensitive to the changes in $C_{1\epsilon}$ value whereby both lengths increase with the increment of $C_{1\epsilon}$ values. $C_{1\epsilon}$ is selected for the parametric studies in order to adjust the spreading of the spray jet to match the experimental data. The slope of the vapour penetration profile for each variable is similar to that of the experimental data. Consequently, it is found that trend of the vapour penetration profile using $C_{1\epsilon}$ of 1.56 agrees closely with the experimental data in this case.

6.2.4 Parametric Study IV: Droplet Breakup Model

Reitz and Diwakar breakup model is applied here and model constant C_s is varied to provide best-fit results, as illustrated in Figure 6-7.

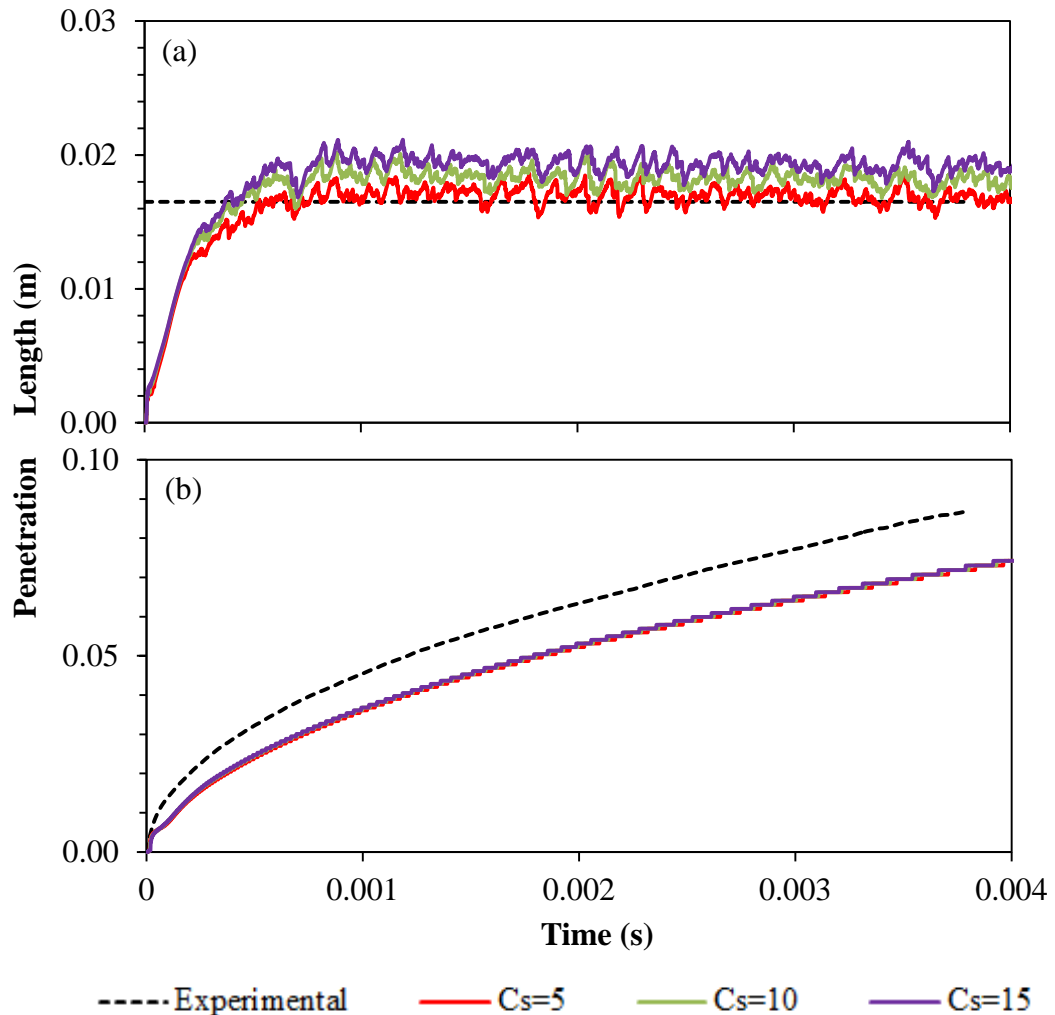


Figure 6-7: Comparison of the predicted (a) LPL and (b) VPL with the measurements using different C_s values of Reitz and Diwakar breakup model.

Referring to Figure 6-7, LPL varies with C_s value while VPL is not dependent on C_s value. C_s is the time factor constant for stripping breakup whereby liquid is sheared or stripped from the droplet surface. The empirical coefficient C_s is in the range of 2 to 20 [170]. It is observed that LPL increases as C_s is increased. This causes the increment in characteristic time scale of the break-up process, and consequently reduces the breakup rate. Thus, LPL is higher when C_s is increased.

6.2.5 Parametric Study V: Number of Parcels

A parcel is a group of droplets with similar characteristics. By applying a fixed number of parcels in the numerical calculations, the computational load can be reduced as it does not involve resolving of equations for every single droplet. Nonetheless, determination of number of parcels in the numerical computation is important as it will lead to an appropriate resolution of the flow. When a low amount of parcels is applied, droplets with diverse characteristics are grouped together during calculations. This might cause apparent discrepancies to the computed results. Penetration lengths for different number of parcels are shown in Figure 6-8.

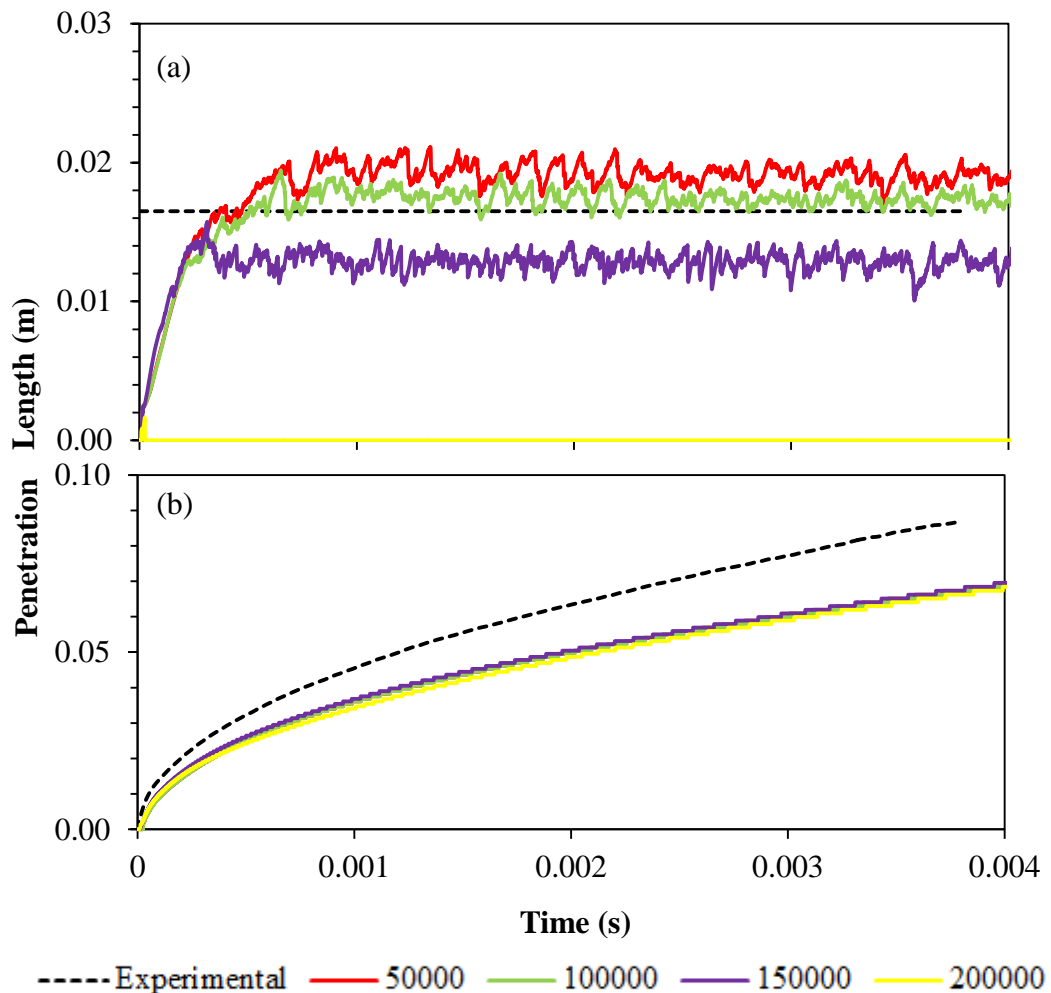


Figure 6-8: Comparison of the predicted (a) LPL and (b) VPL with the measurements using different number of parcels injected.

Based on the results obtained in Figure 6-8, it is observed that LPL is sensitive to number of parcels injected while it has no effect on the VPL predictions. Liquid penetration tends to be more stable with less fluctuation as the number of parcels increases. However, as the amount of parcels injected into the system is increased to more than 150,000 parcels, errors in calculation of LPL occur as no liquid mass is found in the system shortly after the beginning of the injection time.

6.2.6 Best-Fit Numerical Setups

Based on the parametric studies performed in Sections 6.2.1 to 6.2.5, a set of best-fit numerical set-up for the non-reacting and reacting diesel/biodiesel fuel sprays is obtained, as shown in Table 6-6.

Table 6-6: Best-fit numerical set-ups for non-reacting and reacting diesel/biodiesel fuel sprays.

Models/Parameters	Diesel	Biodiesel
Grid	Grading ; 0.25mm x 0.25mm (minimum), 4mm x 2mm (maximum) in both radial and axial directions	
Turbulence Model	Standard $k-\varepsilon$ ($C_{1\varepsilon} = 1.54$)	Standard $k-\varepsilon$ ($C_{1\varepsilon} = 1.59$)
Atomisation Model	Blobs Sheet Atomisation	
Breakup Model	Reitz Diwakar ($C_s = 12$)	Reitz Diwakar ($C_s = 15$)
Soot Model	Multistep	
Time Step (s)	5×10^{-7}	
Number of Parcels	100,000	
Initial k (m^2/s^2)	0.735	
Initial ε (m^3/s^3)	3.5	

The computational grid applied in this work is illustrated in Figure 6-9.

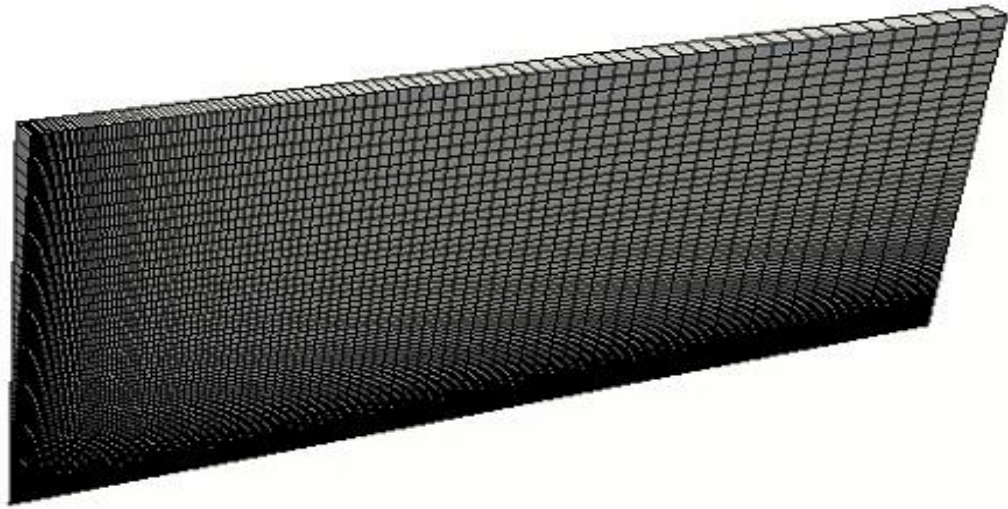


Figure 6-9: Wedge mesh of the constant volume combustion chamber applied in the 2-D simulations.

6.3 Non- Reacting and Reacting Diesel/Biodiesel Sprays

Following that, the non-reacting and reacting diesel/biodiesel fuel spray simulations are performed. The results are discussed in Sections 6.3.1 and 6.3.2 for diesel and biodiesel fuel combustions, respectively.

6.3.1 Diesel Fuel Spray Combustion

First and foremost, the simulated spray penetration lengths generated by the HXNv1 and HXNv2 diesel surrogate fuel models are compared with the experimental measurements of D2 fuel [13] under non-reacting condition, as demonstrated in Figure 6-10. Since both LPL and VPL of the HXNv1 diesel surrogate fuel model are essentially the same as those of the HXNv2 diesel surrogate fuel model in non-reacting environment, only results for the HXNv2 are shown in Figure 6-10.

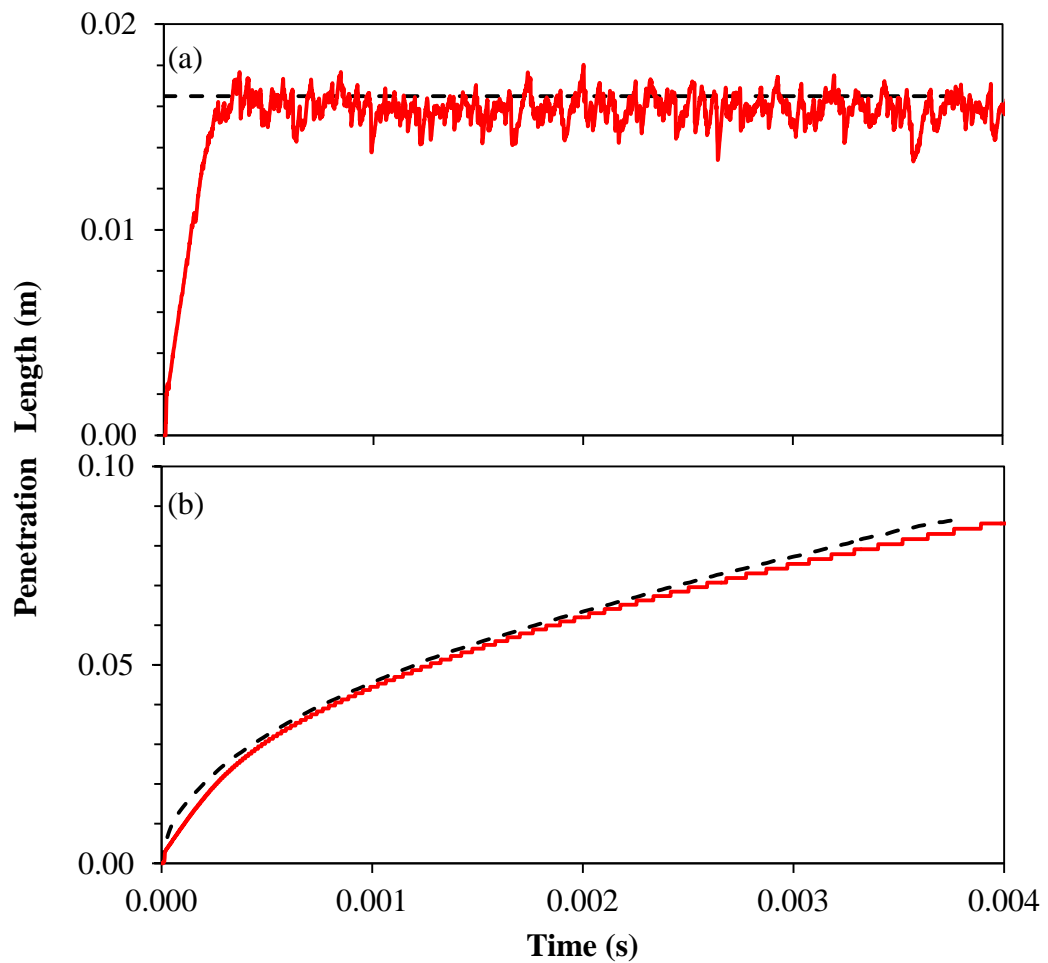


Figure 6-10: Comparison of the computations (—) of (a) LPL and (b) VPL with the measurements (--) using the diesel surrogate fuel fuels.

Referring to Figure 6-10, it is observed that the LPL and VPL computed by the diesel surrogate fuel model are compatible with the experimental measurements under non-reacting condition. Therefore, the numerical models are carried forward to the following section to study the performance of the surrogate models under reacting fuel spray conditions. ID and LOL predictions of the HXNv1 and HXNv2 diesel surrogate fuel models are shown in Figure 6-11.

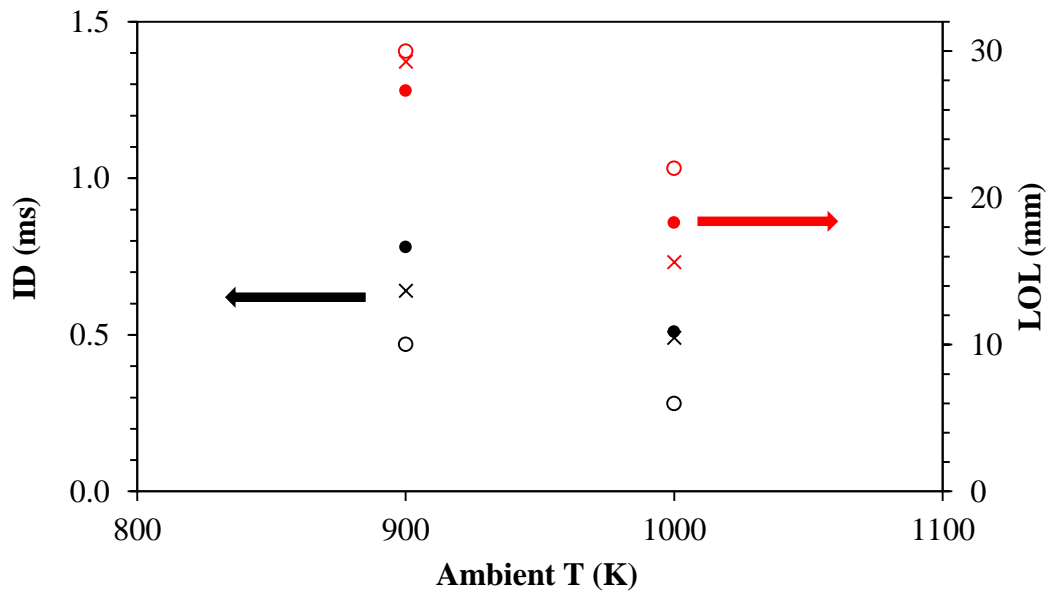


Figure 6-11: Comparison of the IDs and LOLs predicted by the HXNv1 (○) and HXNv2 (x) diesel surrogate fuel models with the experimental measurements (●) for ambient temperatures of 900 K and 1000 K.

In Figure 6-11, significant improvements are observed in ID and LOL predictions when the HXNv2 diesel surrogate fuel model is applied in the reacting diesel fuel spray simulations as compared to the HXNv1 diesel surrogate fuel model. In addition, it is found that the computed IDs by both the diesel surrogate fuel models are brought forward as compared to the measurements. Maximum deviations of 45 % and 18 % are recorded between the measurements and computations by HXNv1 and HXNv2, respectively. LOLs predicted by HXNv2 are in closer agreements with the experimental measurements as compared to HXNv1. As discussed in Section 5.3.2, species concentration profiles for both open PSR and 0-D closed homogeneous batch reactor simulations are not reproduced well by applying the HXNv1 diesel surrogate fuel model, especially the concentration predictions of fuel and oxidiser. Both species concentrations are over-predicted and thus, this leads to higher fuel oxidation rate and consequently shorter ID when the model is applied in the 2-D spray combustion simulations.

The computed SVF distributions are compared with the experimental measurements in Figure 6-12. Here, C_2H_2 is designated as the soot precursor species as well as soot surface growth species. It is seen that SVF distribution

predicted by the HXNv2 diesel surrogate model is in good agreement with that of the D2 fuel as compared to HXNv1, whereby shape and location of the computed soot contours mimic the experimental measurements. Highest SVF is found to be located at the centre region of soot clouds which matches the fuel-rich zone of the fuel jet. However, the quantitative trends of the soot production are not well captured as the density of soot particles is unknown and only C_2H_2 is applied as a precursor for soot formation. Therefore, only qualitative trends are compared here.

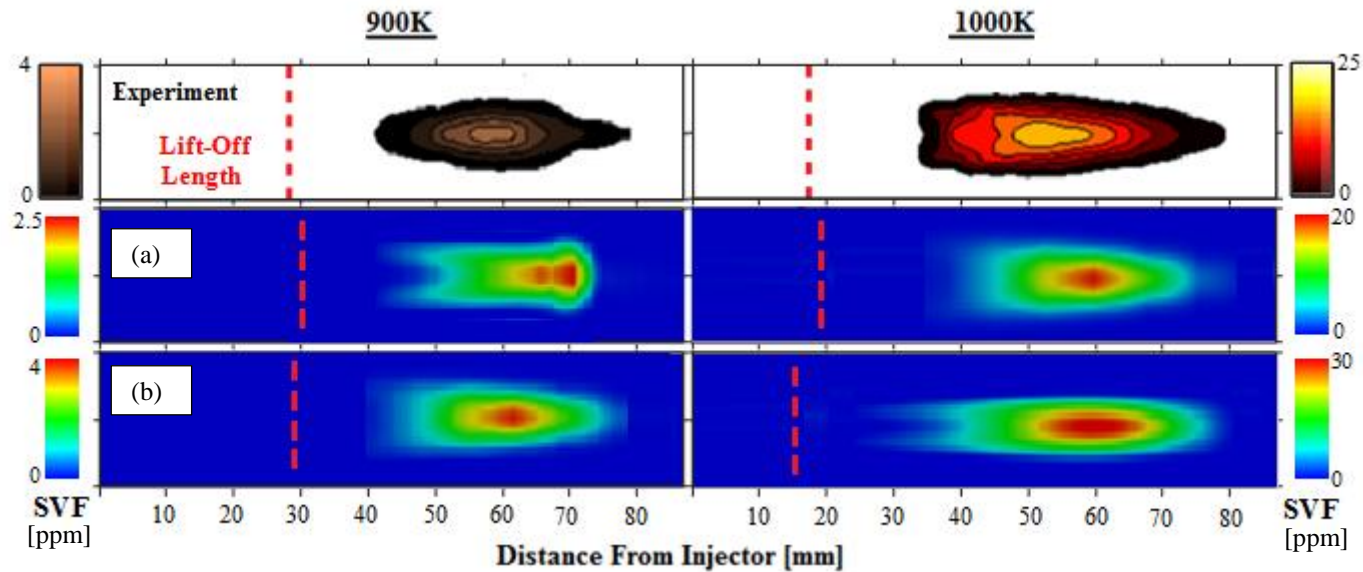


Figure 6-12: Predicted SVF contours and experimental soot cloud images at quasi-steady state for diesel combustion using the (a) HXNv1 and (b) HXNv2 diesel surrogate fuel models for ambient temperatures of 900 K and 1000 K. [ppm denotes parts per million.]**

6.3.2 Biodiesel Fuel Spray Combustion

In this section, model validations of the MCBSv1 and MCBSv2 biodiesel surrogate fuel models in spray combustion phenomena are carried out using the experimental measurements of Nerva et al. [171]. The experiment was conducted in a constant volume combustion chamber using SME. It is evident that the biodiesel feed-stock applied in the experiment is different from the target fuel (i.e. RME) applied in this work. Therefore, the models are first validated against the experimental results by setting the fuel compositions according to those of SME [171]. In this case, the compositions of MD, MD9D and nHep are set to 6 %, 44 % and 50 % by volume, respectively. This is followed by the simulations using fuel compositions of RME while retaining the same numerical setups. As discussed in Chapter 4, the compositions of MD, MD9D and nHep for RME are set to 3 %, 47 % and 50 % by volume, respectively. The actual thermo-physical properties for RME and SME are applied for accurate predictions of the biodiesel fuel spray development.

Firstly, the computed LPL and VPL by the MCBSv1 and MCBSv2 biodiesel surrogate fuel models are validated against the experimental measurements. The results are demonstrated in Figure 6-13. Similar to the diesel fuel spray simulations, the predicted spray penetrations by the MCBSv1 and MCBSv2 biodiesel surrogate fuel models are comparable under non-reacting environment. Hence, only results for the MCBSv2 biodiesel surrogate fuel model are shown in Figure 6-13.

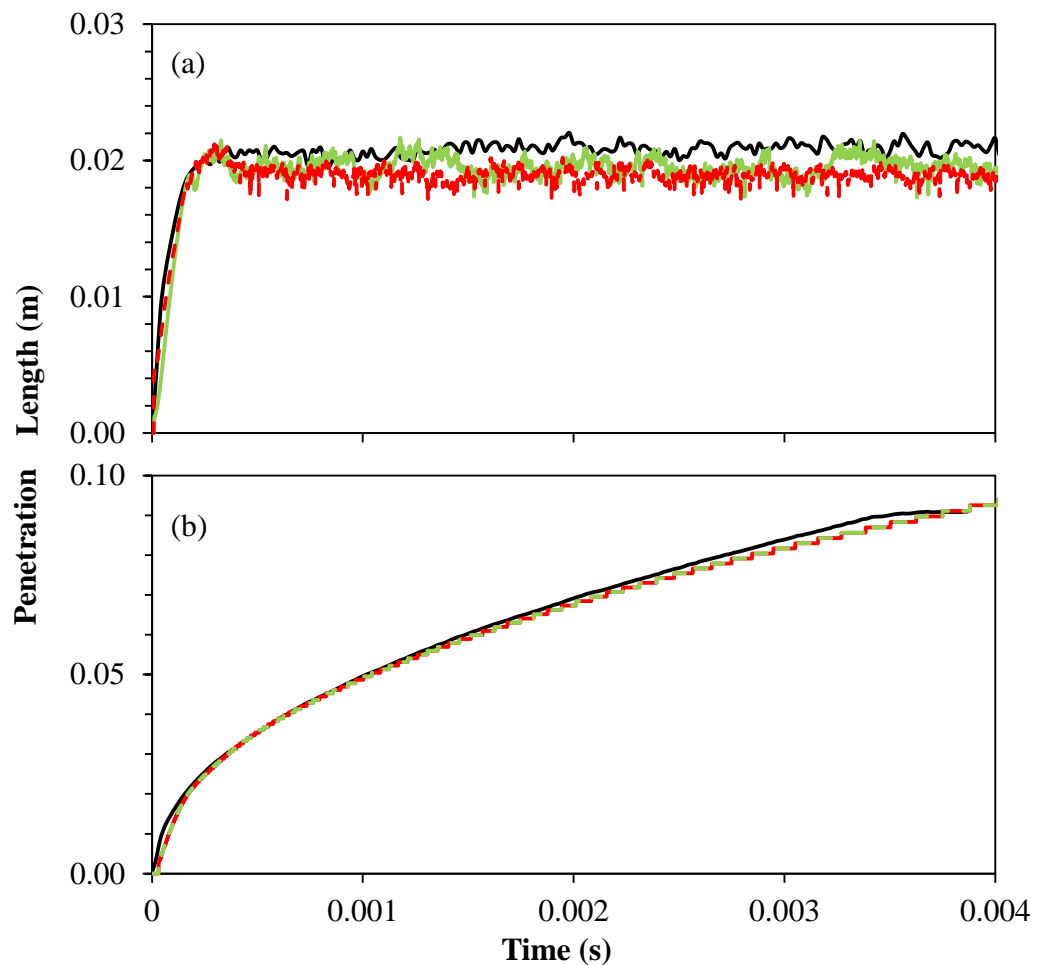


Figure 6-13: Comparison of the computations of (a) LPL and (b) VPL with the measurements (--) using the biodiesel surrogate fuel fuel for SME (—) and RME (—) combustions.

The results obtained show that the LPL and VPL predicted by MCBSv2 for both SME and RME cases match reasonably well with the experimental measurements. The maximum deviations between the predictions and measurements are maintained to within 10 % for both cases.

Subsequently, the predicted IDs and LOLs by both MCBSv1 and MCBSv2 for SME and RME fuel combustions at ambient temperatures of 900 K and 1000 K are demonstrated in Figure 6-14.

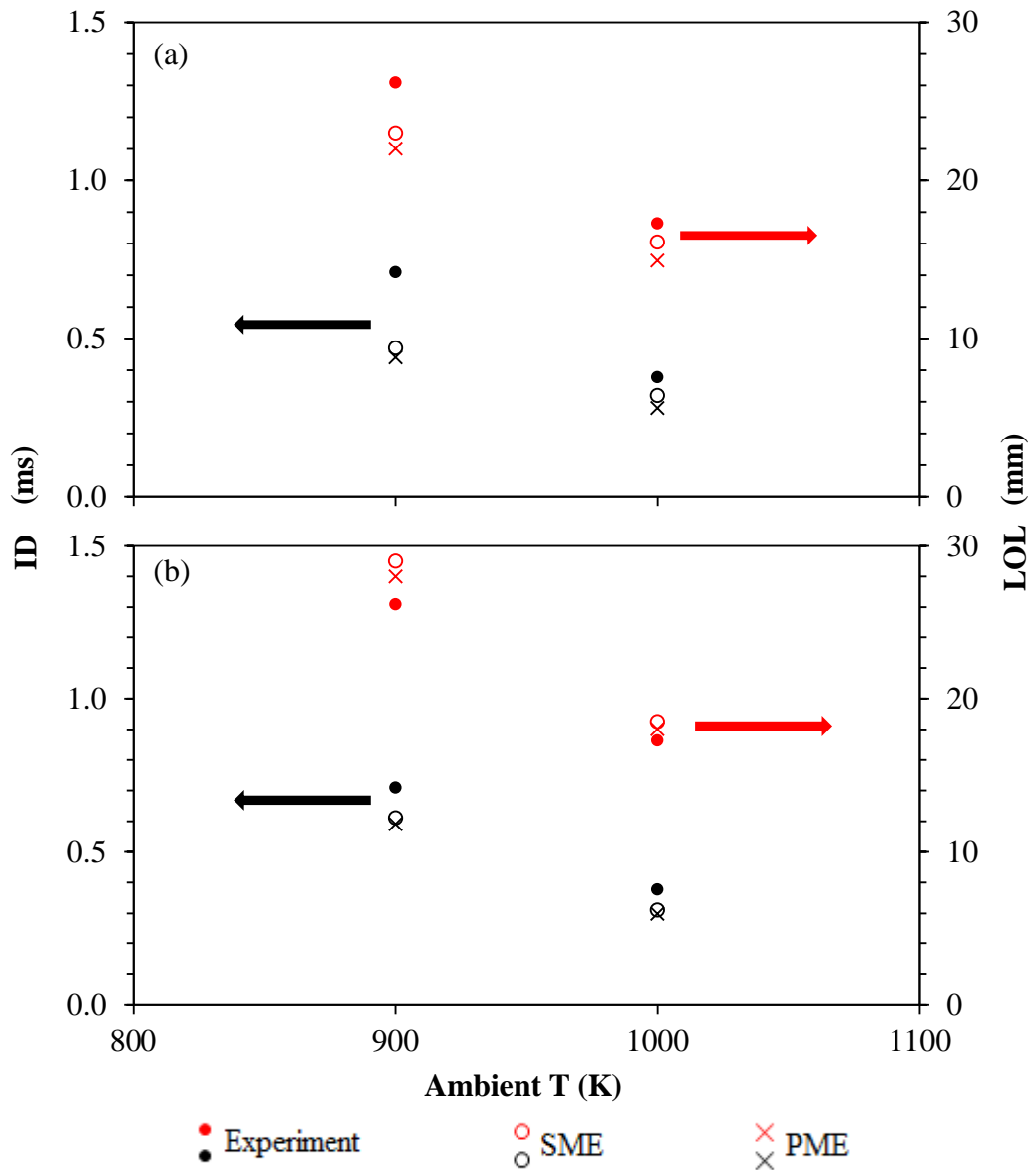


Figure 6-14: Comparison of the IDs and LOLs predicted by the (a) MCBSv1 and (b) MCBSv2 biodiesel surrogate fuel models with the experimental measurements for ambient temperatures of 900 K and 1000 K.

From Figure 6-14, it is observed that the computed IDs for both cases are under-predicted as compared to the experimental measurements with the use of MCBSv1 and MCBSv2. On the contrary, LOLs are under-predicted for both SME and RME combustions using the MCBSv1 biodiesel surrogate fuel model. Maximum deviations of 33.7 % and 37.9 % between the measurements and predictions of IDs are obtained for SME and RME combustions, respectively. In addition, the maximum deviations between the measured and computed LOLs for

both SME and RME cases are recorded at 12.1 % and 16 %, respectively. In contrast, the application of MCBSv2 as the surrogate model has over-predicted the LOLs for both cases. The maximum deviations between the simulated and experimental IDs and LOLs for SME combustion are 17.8 % and 15.2 %, respectively. For RME combustion, maximum deviations of 21 % and 18.6 % are recorded for IDs and LOLs, respectively. The improvements in ID predictions of the biodiesel fuel spray combustion are apparent when the MCBSv2 biodiesel surrogate fuel model is applied instead of MCBSv1. This corresponds with the improved predictions in species concentration profiles under auto-ignition and JSR conditions using the MCBSv2 surrogate model, as discussed in Chapter 5.

Furthermore, it is also found that the IDs predicted for RME combustion are shorter than those of SME combustion at both ambient temperatures. This can be attributed to the higher content of MD9D in RME which promotes faster chain branching process owing to its location of double bond at the end of the hydrocarbon chain [99]. As a result, the LOLs predicted for RME combustion are comparatively shorter due to shorter IDs.

Following that, the SVF contours computed by the surrogate models are compared with those measured from the experiments at quasi-steady state for ambient temperatures of 900 K and 1000 K. The comparisons are illustrated in Figure 6-15 for both SME and RME combustions.

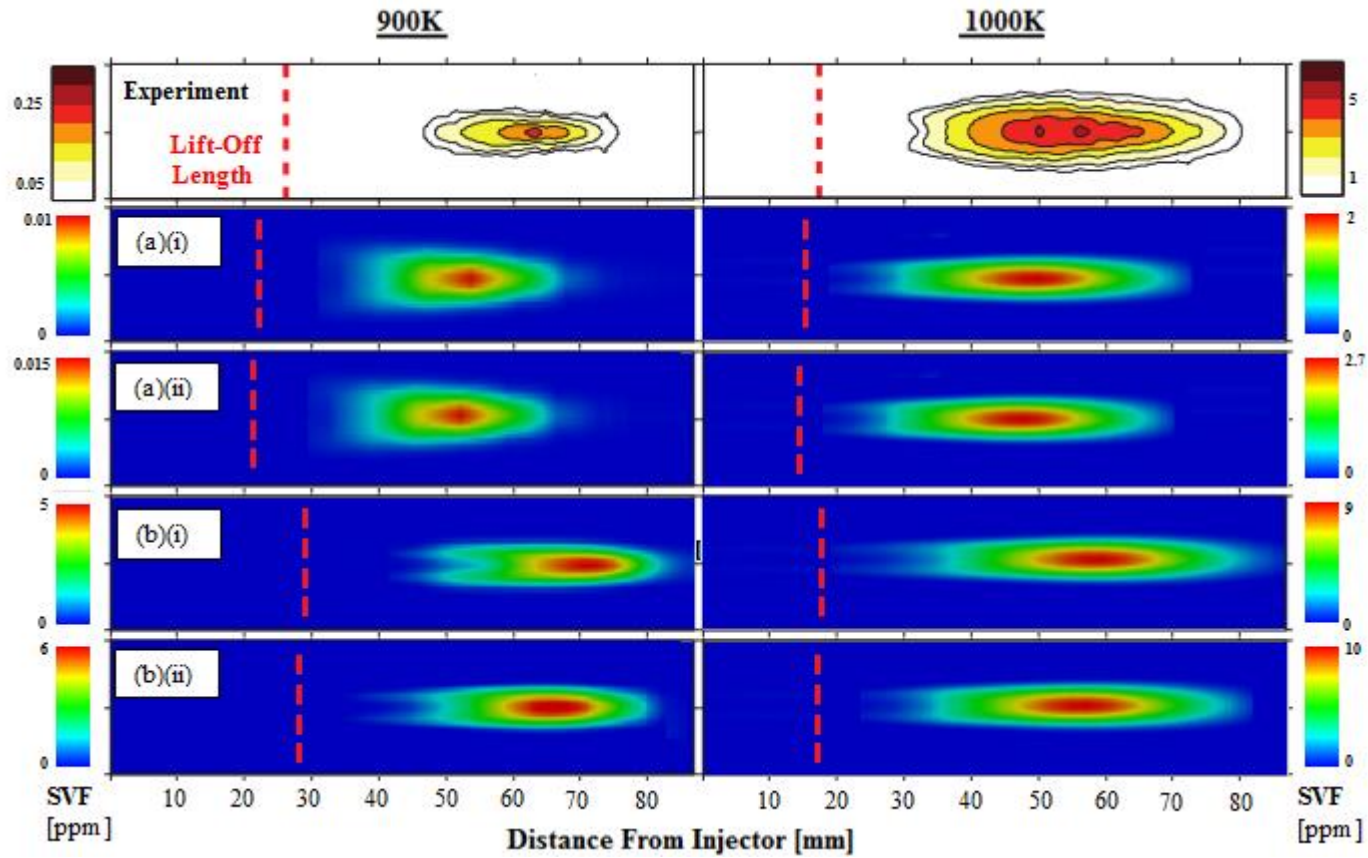


Figure 6-15: Predicted SVF contours and experimental soot cloud images at quasi-steady state for (i) SME and (ii) RME combustions using the (a) MCBSv1 and (b) MCBSv2 biodiesel surrogate fuel models for ambient temperatures of 900 K and 1000 K.

Figure 6-15 shows that the predicted soot contours of MCBSv2 are in better agreement with the experimental measurements as compared to those computed by MCBSv1. Highest SVF is captured at the centre region of soot clouds which corresponds with the fuel-rich region of the fuel jet. Here, only qualitative trends are compared as the quantitative soot formation predictions are not well captured. This can be attributed to the uncertain soot particle density as well as the application of C_2H_2 only as the soot precursor species, as mentioned in the previous section.

Furthermore, the difference in the computed soot distributions between SME and RME combustions is less apparent apart from the small deviations in soot locations. This can be attributed to the corresponding LOLs in which soot is formed nearer to the injection tip as LOL is shorter. It is observed too that the predicted SVFs from SME combustion are lower since it contains less double-bond as a result of lower amount of unsaturated fatty acids. Here, quantitative comparison is performed between the simulated results in order to demonstrate the difference between the computations for SME and RME combustions. Quantitative assessments with the measurements are not involved.

6.4 Concluding Remarks

2-D CFD simulations are performed to study the spray combustion phenomena within a constant volume combustion chamber. LPL and VPL are replicated for non-reacting diesel/biodiesel fuel sprays. For reacting diesel/biodiesel fuel sprays, ID, LOL and SVF distributions are simulated. The simulation results are compared to the experimental data of D2 and SME for both diesel and biodiesel combustions, respectively. IDs computed by all the surrogate models are advanced when ambient temperatures of 900 K and 1000 K are applied. Additionally, the SVF predictions in terms of the shape and location of the soot clouds agree well with the experimental data of D2 and SME fuels when the HXNv2 diesel surrogate fuel model and the MCBSv2 biodiesel surrogate fuel model are applied.

The current results suggest that further improvement is necessary on the HXNv2 diesel surrogate fuel model where the effect of aromatic chemistry should be taken into consideration to improve the predictions of the complex soot formation phenomenon. Additionally, multi-component diesel surrogate fuel model is recommended to match the chemical compositions of the actual diesel fuels in order to achieve better agreement in kinetic performance and pollutant formation, particularly the soot formation events. In contrast, MCBSv2 is a better surrogate model for biodiesel fuel as it is able to reasonably capture the variation of SVF with respect to the change of ambient temperature in comparison with the MCBSv1 surrogate model. Thus, it is ready to be used for the subsequent internal combustion engine modelling studies.

CHAPTER 7

DEVELOPMENT OF MULTI-COMPONENT DIESEL SURROGATE FUEL MODELS

7.1 Introduction

Chapter 7 outlines the procedures of developing multi-component diesel surrogate fuel models which are applicable for multi-dimensional diesel engine applications. Since the biodiesel surrogate fuel model applied in this presented work is already a multi-component fuel blend, it will be directly applied in the engine modelling studies in the following chapter. The typical fuel constituents of a commercial diesel fuel (i.e. D2) are described in Section 7.2. Successively, a reduced model for each diesel fuel constituent is derived using the chemical kinetic mechanism reduction scheme formulated in Chapter 5. This is demonstrated in Section 7.3. In Section 7.4, the process of generating the multi-component diesel surrogate fuel models is discussed. Following that, validations of the surrogate models for each diesel fuel constituents as well as the fuel blends in 0-D chemical kinetic simulations are presented in Section 7.5. In Section 7.6, the fidelity of the multi-component diesel surrogate fuel models are further assessed in 2-D spray combustion simulations. Lastly, significant findings in the numerical formulations are highlighted in Section 7.7.

7.2 Descriptions of the Diesel Fuel Constituents

Since a single-component diesel surrogate fuel model does not match the actual diesel fuel behaviour in terms of H/C ratio and CN as discussed in Chapter 2, fuel blending has been suggested to match the ignitibility and composition of the actual diesel fuels [12,68]. Even though it is not necessary for a surrogate model to possess all the representative components in actual diesel fuels, a match in chemical composition may provide better agreement in kinetic performance and pollutant formation [12]. Furthermore, since the H/C ratio of a single-component

diesel surrogate fuel model differs from that of actual fuels, the local mixing phenomenon is not well represented under stoichiometric condition [12]. Thus, fuel blending is proposed in this study to mimic the actual behaviour of a commercial diesel fuel namely D2 which consists of aromatic compounds, straight-, branched- and cyclo-alkanes as well as a small amount of olefins. Among all these components, straight-alkanes are usually the most abundant components in liquid fuels [172,173]. Branched alkanes which are also known as iso-alkanes are hydrocarbons containing branched carbon chains. The branched alkanes in diesel fuels usually contain only one or two methyl substituents on a long carbon chain [172,173]. Meanwhile, the cyclo-alkanes consist of carbon atoms combined together by single bonds in a ring structure [174]. Olefins refer to straight-chain hydrocarbons which are characterised by one or double carbon-carbon bonds [175]. Lastly, aromatic compounds are cyclic, planar hydrocarbons with alternating double and single bonds between carbon atoms, forming a continuous ring [172].

In this work, HXN [7], HMN [176], cyclohexane (CHX) [177] and toluene [177] are proposed to represent the diesel fuel components. The straight-alkane, HXN, and the branched-alkane, HMN (also known as iso-cetane), are diesel primary reference fuels. HMN has a CN of 15 and its combination with HXN provides the capability to vary the CN of the diesel surrogate fuel models. CHX is selected to represent the cycloalkane component in diesel fuel as it is capable of representing the major reaction characteristics of cycloalkane oxidation process even though it is the simplest cycloalkane [177]. Apart from that, it may also have a greater effect on soot production as compared to non-cyclic alkane whereby the oxidation routes directly yield aromatic species as intermediates [12]. Toluene has one of the simplest molecular structures of the alkylated benzenes and it is regarded as a good representative of the characteristics of aromatic fuels [82]. Hence, it is integrated into the multi-component surrogate model to improve soot predictions as well as to achieve compositional match. The properties of D2 fuel and each diesel fuel component [17,178] are presented in Table 7-1.

Table 7-1: Fuel properties [17,178].

Properties	D2	HXN	HMN	CHX	Toluene
Chemical Formula	C ₃ -C ₂₅	n-C ₁₆ H ₃₄	i-C ₁₆ H ₃₄	C ₆ H ₁₂	C ₇ H ₈ (C ₆ H ₅ CH ₃)
Type of Hydrocarbon	33.8 % ^a / 27 % ^b Aromatics, 65 % ^a Alkanes, 1.2 % ^a Olefins	Straight-alkane	Branched-alkane	Cyclo-alkane	Aromatic
CN	46 (40-56)	100	15	-	-
Molecular Weight [g/mol]	~200.000	226.446	226.446	84.161	92.141
H/C Ratio	1.800	2.125	2.125	2.000	1.143

^aComposition of aromatic compounds provided in the study of Farrell et al. [12]

^bComposition of aromatic compounds provided in the study of Kook and Pickett [168]

7.3 Derivation of Reduced Models for Fuel Constituents

Detailed models of HXN, HMN and CHX developed by Westbrook et al. [7], Oehlschlaeger et al. [176] and Silke et al. [177], respectively, are employed in this section. The reduced model for HXN, namely HXNv2, has been derived in Section 5.3 and thus it is directly applied here. Also, the elementary reactions for toluene are subset of the detailed mechanism of CHX. Both CHX and toluene are important components for benzene production, which act as a ‘connecting species’ between them through several reaction pathways. As such, the reduction procedures are only carried out for the detailed mechanisms of HMN and CHX in this study.

Similar to the previous mechanism reduction exercise, the five-stage chemical kinetic mechanism reduction scheme developed in Chapter 5 is applied to derive a reduced mechanism for each diesel fuel constituent. Capability of the mechanisms

in auto-ignition predictions is selected as the basis for reduction. Both JSR and auto-ignition conditions are then chosen as data source for mechanism reduction, where sampled data points are obtained over a wide range of initial pressure, initial temperature and Φ . The conditions applied for mechanism reduction are summarised in Table 7-2.

Table 7-2: Test conditions applied for mechanism reduction as well as validations of the diesel surrogate fuel models.

Operating Conditions		Range Evaluated
Auto-ignition ^a	Φ (-)	0.5, 1.0, 2.0
	Initial Pressure (bar)	40, 60, 80
	Initial Temperature (K)	650 – 1350 (100 K increments)
JSR ^a	Φ (-)	0.5, 1.0, 2.0
	Initial Pressure (bar)	40, 60, 80
	Residence Time ^c (s)	1
JSR ^b	Φ (-)	2 (HMN); 1.5 (CHX)
	Initial Pressure (bar)	10.1 (HMN, CHX)
	Residence Time (s)	1 (HMN); 0.5 (CHX)

^a Selected operating conditions based on the typical in-cylinder pressure values during the main fuel injection event for light-duty [162], direct-injection diesel engines.

^b Selected operating conditions based on the experimental results of HMN [179] and CHX [180] oxidations in a JSR for mechanism validations. The unit for pressure is converted from atm to bar (1 atm = 1.01 bar).

^c Selected residence time based on minimum extinction time at steady-state for combustion at low-, intermediate- and high-temperatures [163].

JSR is included in this study as an additional data source for mechanism reduction as it is important in modelling the steady-state extinction process of the combustion process [163]. Closed homogeneous batch reactor and open PSR models of CHEMKIN-PRO software are applied. The size of each diesel fuel constituent, including that of the HXNv2 model derived in Chapter 5 is tabulated in Table 7-3.

Table 7-3: Chemistry sizes of detailed/reduced chemical mechanism models used in the current work.

Chemistry Sizes	HXNv2	HMN	CHX
Detailed mechanism (N_S ; N_R)	2,116; 8,130	1,114; 4,469	1,081; 4,269
Final reduced mechanism (N_S ; N_R)	79; 289	89; 319	80; 287

Next, appropriate optimisation of the reaction rate constants are carried out such that the influence of the eliminated reactions is incorporated in the Arrhenius rate constants of the retained reactions in order to maintain accuracy of the model predictions [29,66,68]. This reaction rate constant optimisation approach has also been successfully demonstrated in the modelling studies of Wang et al. [66] and Golovitchev et al. [68]. The approach had significantly improved their model predictions where the reaction rate constants of H-atom abstraction from the fuel species was include as one of their optimisation targets, as with this study. The optimised rate constants for important reactions in these reduced mechanisms and the associated targeted functions are detailed in Table 7-4. The optimised rate constants for HXNv2 can be found in Table 5-3 in Chapter 5. The rate constant tuning is carried out for reactions with high normalised temperature A -factor sensitivity across all the test conditions. The results shown in Figure 7-1 are calculated based on the temperature sensitivity coefficient values with initial pressure of 60 bar, initial temperature of 950 K and Φ of 1. The results here provide a clearer description on the rate constant tuning procedure.

Table 7-4: Comparisons of the original and adjusted A-factor values of Arrhenius parameters in conjunction with their respective targeted functions for the diesel fuel components.

Reactions	A-factor values		Targeted Functions
	Original	Adjusted	
<u>HMN</u>			
$TC4H9 + FC12H25 = HMN$	8.000×10^{12}	4.000×10^{12}	Improved ID prediction at high temperature ^c
$HMN + H = HMN-R8 + H2$	7.340×10^5	7.340×10^6	Improved fuel concentration prediction
$IC4H8 + FC12H25 = HMN-R8$	1.000×10^{10}	5.000×10^9	Improved ID prediction at NTC ^b
$HMN-R8O2 = HMN-R8 + O2$	3.465×10^{20}	7.465×10^{19}	Improved ID prediction at NTC ^b
$HMNOOH8-5O2 = HMNOOH8-5 + O2$	4.734×10^{27}	4.734×10^{26}	Improved ID prediction at low temperature ^a
$HMNOOH8-5O2 = HMNKET8-5 + OH$	3.125×10^9	2.125×10^{10}	Improved ID prediction at low temperature ^a
<u>CHX</u>			
$C6H5CH3 + OH = C6H5CH2J + H2O$	5.190×10^9	5.190×10^7	Improved concentration prediction of toluene
$CHXO2J = CHX1Q3J$	1.860×10^{11}	2.860×10^{11}	Improved ID prediction at low temperature ^a

^aLow-temperature region: 650 – 850 K

^bNTC region: 850 – 1050 K

^cHigh-temperature region: 1050 – 1350 K

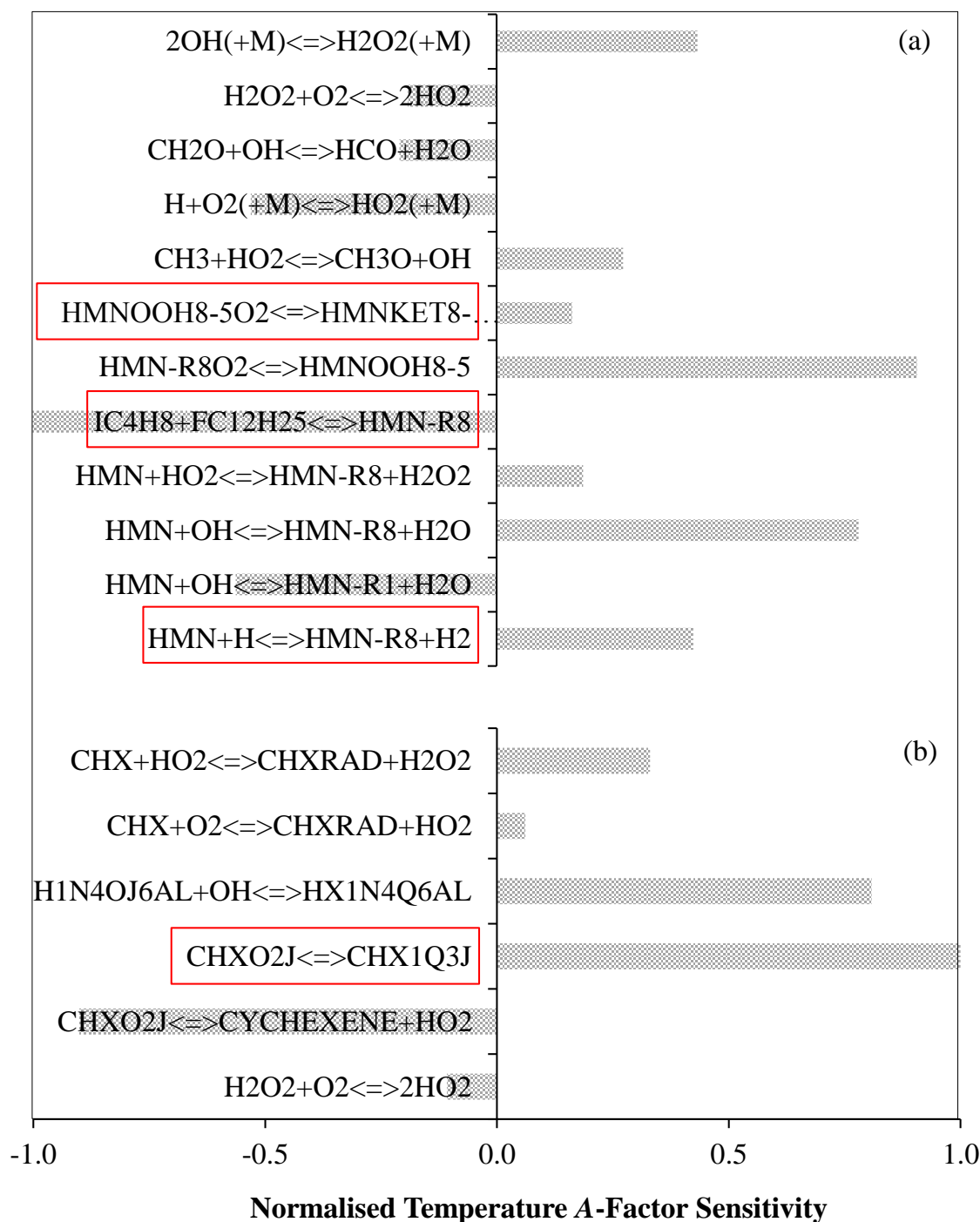


Figure 7-1: Reactions with normalised temperature A-factor sensitivities for reduced mechanisms of (a) HMN and (b) CHX, with initial pressure of 60 bar, initial temperature of 950 K and ϕ of 1. [Note: Red boxes indicate the reactions selected for adjustment of the A-factor values of Arrhenius parameters.]

In Figure 7-1, it is observed that not all of the reactions with high temperature sensitivity coefficient values are selected for rate constant tuning. The procedure is performed according to the targeted functions such as improvement of ID at low temperatures and thus changes in ID at other temperature regimes are undesirable. As a result, reactions with high temperature sensitivity coefficient values which alter IDs at other temperature regimes are not taken into consideration in this case. In order to ensure the IDs at other temperature regimes across all the test conditions are not affected, the 0-D simulations are repeated whenever the rate constant is adjusted.

The major reaction pathways for each diesel fuel component are illustrated in Figure 7-2. The key reaction pathways of the fuel combustion are obtained from reaction pathway analysis during the mechanism reduction process. As observed in the fuel oxidation pathways under similar conditions, the oxidation of n-alkanes varies from that of branched-alkanes in terms of the products formation. However, it is observed that the chemical kinetics of fuel oxidations for HXN, HMN and CHX are similar. For instance, H-atom abstractions on the fuel components are prevailing under fuel-lean conditions while thermal decompositions of the fuel components are more dominant under fuel-rich conditions. For stoichiometric conditions, H-atom abstractions are dominant when temperature is low whereas thermal decompositions are more prevalent when temperature is high [13,179,180].

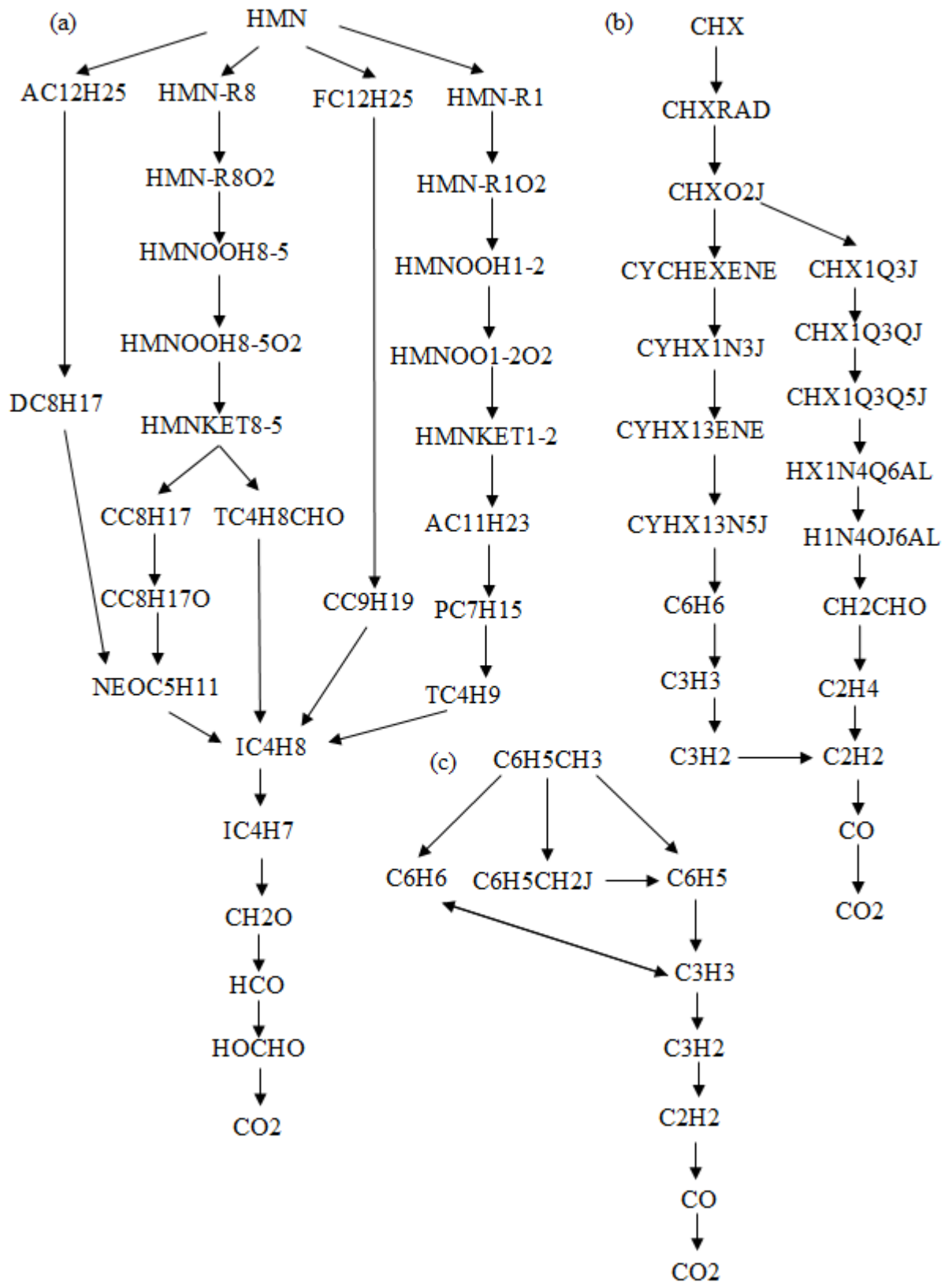


Figure 7-2: Main reaction pathways of (a) HMN, (b) CHX and (c) toluene ($C_6H_5CH_3$) during fuel oxidation process for initial pressure of 60 bar, initial temperature of 950 K and Φ of 1.

In this section, the reduced models of the fuel constituents are successfully derived using the five-stage chemical kinetic mechanism reduction scheme. The application of the reduction scheme has contributed to at least 92 % reduction in N_S and 93 % reduction in N_R in the reduced mechanisms as compared to the detailed mechanisms for each fuel constituent. Appropriate optimisation of selected reaction rate constants are performed to minimise the influence of eliminated species and reactions associated to the drastic mechanism reduction that has been carried out. Following that, the surrogate models are carried forward to the next section to formulate multi-component diesel surrogate models.

7.4 Derivation of Multi-Component Diesel Surrogate Fuel Models

The sequential procedure to formulate the multi-component diesel surrogate fuel models is illustrated in Figure 7-3. The procedure is similar to the model construction scheme of Slavinskaya et al. [181]. Here, a ‘reduced-then-combined’ model construction strategy is employed where the reduced models for each of the fuel components are first derived from the respective detailed models and are subsequently combined together to generate the multi-component diesel surrogate models. As such, the reduced models for each of the components are constructed and may be used for other applications. This strategy also limits errors and complications generated from reducing the combined, detailed surrogate models with more than 3,500 species.

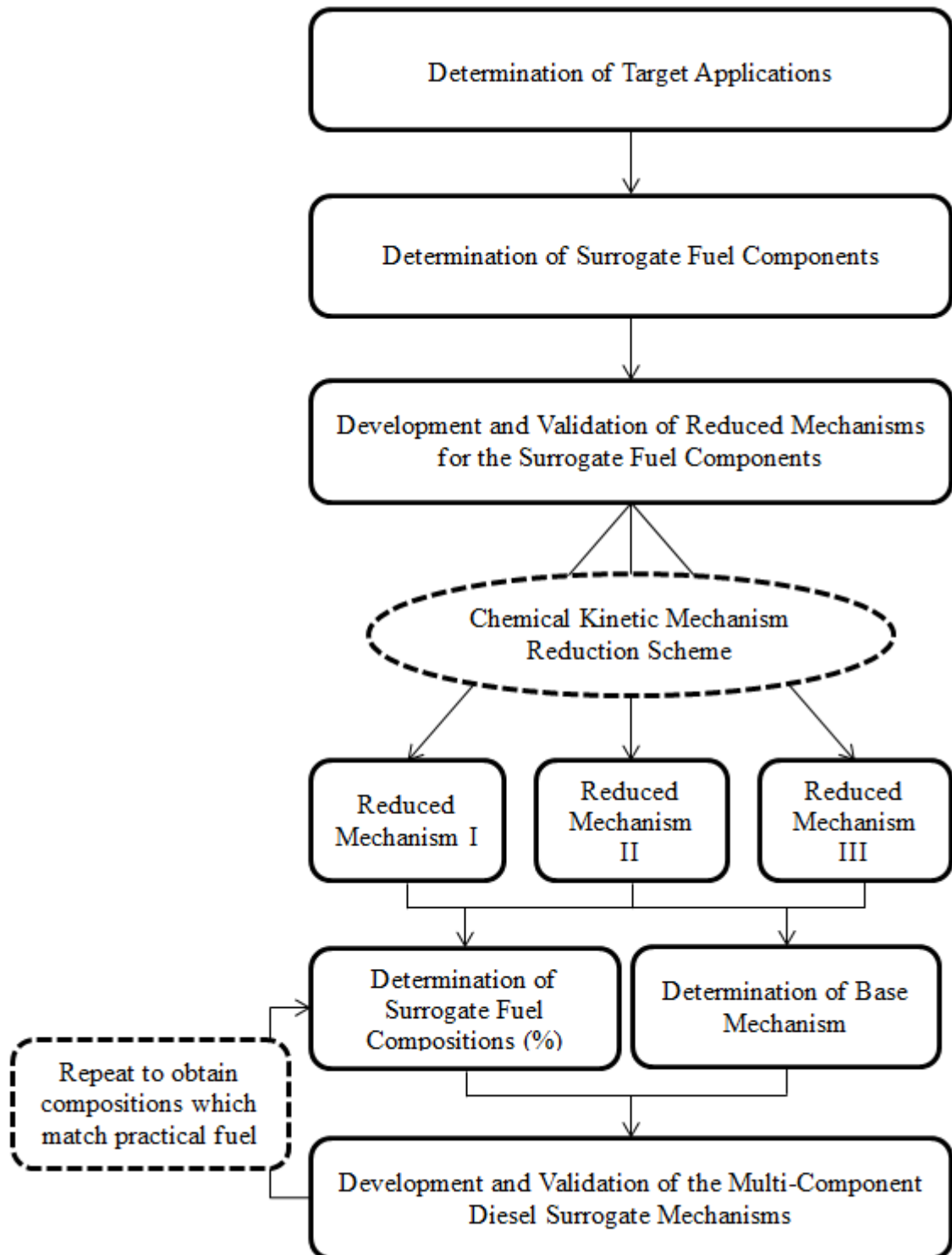


Figure 7-3: Sequential steps to formulate the multi-component diesel surrogate fuel models.

The target applications of this work focus on chemical composition match as well as mimicking the combustion and soot precursor formation behaviours of actual diesel fuels such as D2. In this work, the reduced mechanism of HXN is designated as the base mechanism as it is the most abundant and largest hydrocarbon among the fuel constituents. Subsequently, the reduced mechanisms for other diesel fuel constituents are added to the base mechanism to generate two combinations of multi-component diesel surrogate fuel models:

- (a) Multi-Component Diesel Surrogate No. 1 (MCDS1): HXN + HMN;
- (b) Multi-Component Diesel Surrogate No. 2 (MCDS2): HXN + HMN + toluene + CHX.

These two models are proposed to investigate the combustion and soot formation performances with and without the presence of aromatic formation pathways. It is important to note that MCDS1 is a pure alkanic surrogate fuel model whereas MCDS2 consists of important reaction pathways for aromatic production with the integration of CHX and toluene. The reduced mechanisms of HXN, HMN and CHX generated from the previous sections are employed. It is worth mentioning that the base chemistries of the fuel constituents are essentially similar as the reactions mechanisms are constructed based on the hierarchical nature of hydrocarbon–oxygen systems [7,176,177] in order to ensure that the results may not be affected when the base model is replaced by different models. The approach is similar to the model construction of the detailed mechanisms of nHep and iso-octane by Curran et al. [8,74].

The CN of MCDS1 is calculated using Equation 7-1:

$$\text{CN of mixture} = [F_{\text{HXN}} + 0.15F_{\text{HMN}}] \times 100 \quad (7-1)$$

F_{HXN} is the mass fraction of HXN and F_{HMN} is the mass fraction of HMN. The CN and compositions of MCDS1 are determined based on those of Diesel Primary Reference Fuel (DPRF58) [160]. DPRF58 is a fuel mixture of 42 % HXN and 58 % HMN by mass, corresponding to a CN of 50.7. It was found to yield the same ID timings as the D2 fuel experimentally [182,183]. However, Equation 7-1 is not applicable for fuel model which considers other components. The compositions of

MCDS2 are hence determined based on those of the D2 fuel. The composition of toluene is fixed at 28 % which is close to the aromatic composition of D2 provided in the study by Kook and Pickett [168] and it is also approximately the average value of the aromatic composition of typical North American diesel fuels [12]. Subsequently, mass fractions of the remaining fuel components such as HXN, HMN and CHX are iterated to match the IDs of D2. The properties of MCDS1 and MCDS2 surrogate models as well as the size of the surrogate models are presented in Table 7-5.

Table 7-5: Details of the multi-component diesel surrogate fuel models.

Properties	MCDS1	MCDS2
Chemical Formula	42 % n-C ₁₆ H ₃₄ + 58 % i-C ₁₆ H ₃₄	42 % n-C ₁₆ H ₃₄ + 20 % i-C ₁₆ H ₃₄ + 28 % C ₇ H ₈ + 10 % C ₆ H ₁₂
Type of Hydrocarbon	Straight- and branched-alkanes	Straight-, branched- and cyclo-alkanes, aromatic
Molecular Weight [g/mol]	226.446	174.612
H/C Ratio	2.125	1.838
Size of final reduced mechanism (N_S ; N_R)	128; 408 ^a 88; 284 ^b	169; 545 ^a 129; 411 ^b

^aBefore elimination of unimportant species and reactions upon integration

^bAfter elimination of unimportant species and reactions upon integration

Upon the construction of the multi-component diesel surrogate fuel models, the relative contribution of each reaction pathway to the net production rate of each species has altered as compared with that of the respective single-component model. The reaction pathways of each fuel species in the multi-component diesel surrogate fuel mechanisms are hence reassessed using reaction pathway analysis. It is observed that there are certain species which can be removed from the mechanisms owing to their insignificant effect on the predictions of fuel oxidation process upon integration. Thus, the unimportant species and their corresponding reactions are eliminated. One of the examples of the eliminated species is the

alkyl radical of HMN, namely HMN-R1. It is formed mainly through H-atom abstraction and alkyl radical decomposition from the fuel specie. During the reduction of detailed mechanism of HMN, two isomers of HMN are retained during chain-branching process such as HMN-R8 and HMN-R1, as demonstrated in Figure 7-2. However, when HMN is combined with other fuel components in the MCDS1 and MCDS2 surrogate mechanisms, influence of HMN-R1 onto the formation of intermediate species during chain branching process has become less significant. Therefore, HMN-R1, together with its corresponding reactions and connected species are removed from the mechanism.

Here, the model accuracy in ID and species profile predictions is selected as the criterion for the elimination procedure. A species is eliminated provided if the normalised temperature *A*-factor sensitivities for all its corresponding reactions are lower than the user-specified threshold value (i.e. 0.05) throughout all the test conditions. It is important to note that the species for H₂/CO and small hydrocarbon oxidations are not considered in the elimination procedure as these pools of important species are shared by the fuel constituents in the integrated models. The maximum relative error tolerance between the model predictions before and after elimination procedure is retained to within 5%. The sizes of the final, reduced multi-component diesel surrogate mechanisms are provided in Table 7-5. The MCDS1 and MCDS2 multi-component diesel surrogate fuel mechanisms are presented in Appendix C.

7.5 0-D Chemical Kinetic Simulations

In this section, validations of the chemical kinetic mechanisms are carried out in 0-D chemical kinetic simulations. The validation results are discussed in Sections 7.5.1 and 7.5.2 for each individual diesel fuel constituent and multi-component diesel surrogate fuel models, respectively. The test conditions applied for the mechanism validations in 0-D simulations are described in Table 7-2.

7.5.1 Validation of Individual Diesel Surrogate Fuel Component

Validation results for HXNv2 are already presented in Chapter 5. Thus, only results for HMN and CHX are shown here. Firstly, validations of the reduced models are performed by comparing the IDs and species profile predictions of important species to those of the detailed mechanisms. In addition, only results for the initial pressure of 60 bar are presented. Same pattern is observed for the ID timing plots at initial pressures of 40 bar and 80 bar, which is characterised by the S-shaped curve for ID profiles. Comparisons of ID timing predictions between the reduced and detailed mechanisms are demonstrated in Figure 7-4.

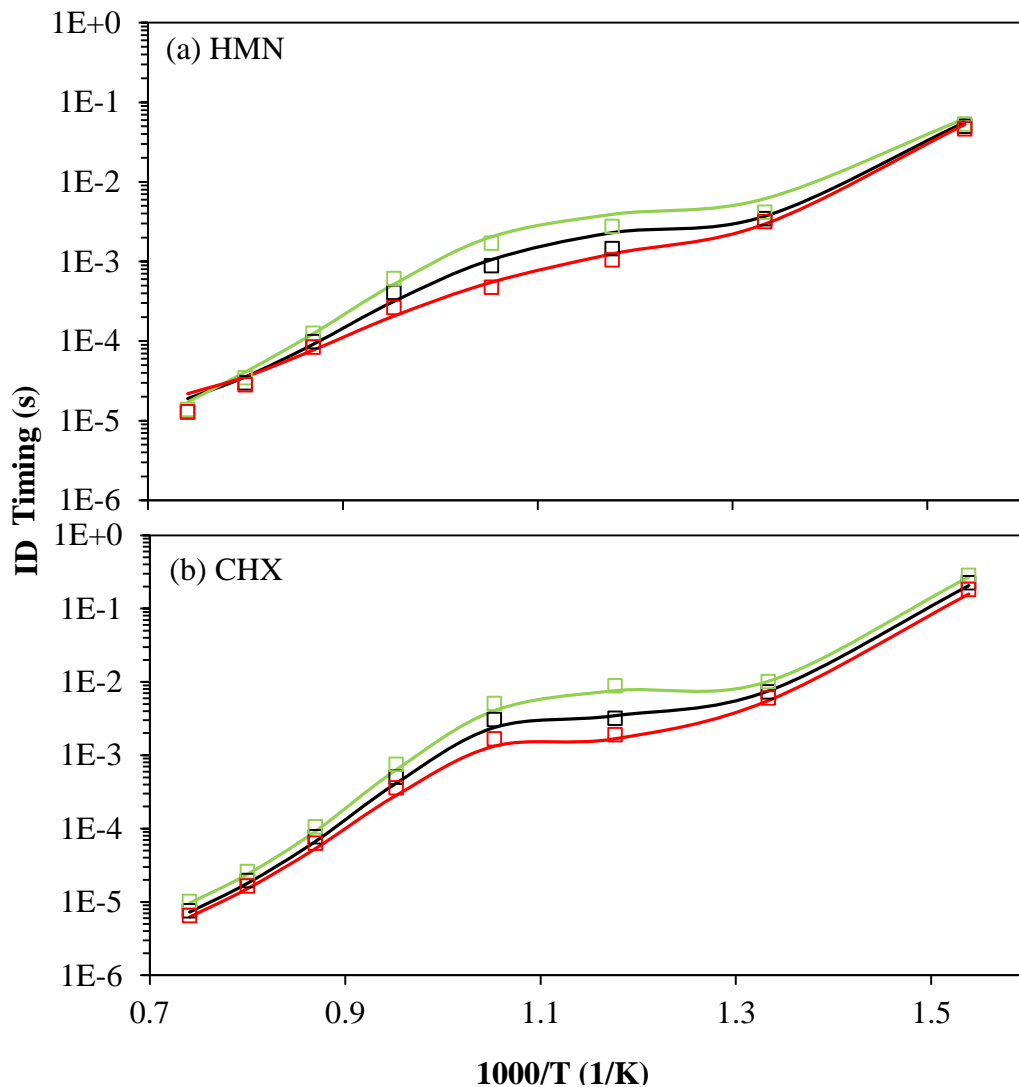
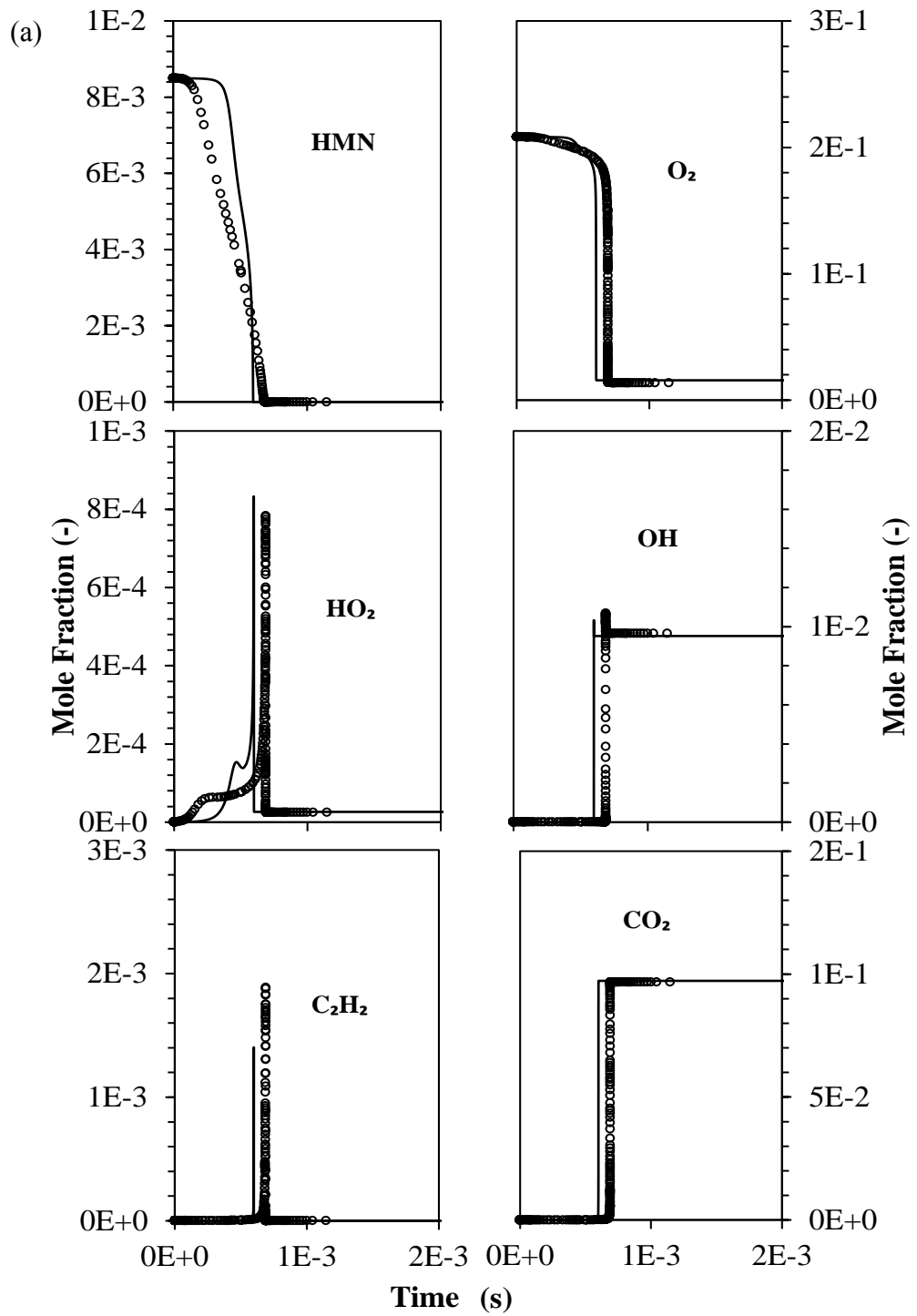


Figure 7-4: Comparisons of ID calculated by the detailed (line) and reduced (□) models of (a) HMN and (b) CHX for initial pressure of 60 bar and Φ of 0.5 (green), 1.0 (black), 2.0 (red).

It is observed that reasonably good agreements are achieved between the reduced and detailed mechanisms in ID predictions for each diesel fuel constituent. In this reduction work, deviations in ID are relatively evident at low and intermediate temperatures for auto-ignition conditions. Hence, further reduction will deteriorate the ID predictions as reaction pathways are more complex at this temperature range. The current results are considered satisfactory as the induced error for each prediction retains within the error tolerance of 40 % [40,106,158,159].

In addition, capability of the reduced model for each fuel constituent in replicating concentration of important combustion products is monitored throughout this reduction work. Comparisons of the reduced and detailed mechanisms with respect to species concentration profiles for auto-ignition as well as JSR conditions are shown in Figure 7-5 and Figure 7-6, respectively. Only results for Φ of 1 are presented since similar temporal evolution trends in the results are obtained for both Φ of 0.5 and 2.

Figure 7-5(a) shows that the selected species mole fractions are reasonably replicated for the HMN auto-ignition condition. On the other hand, a consistent distance between the computed species mole fraction using the reduced and detailed CHX models is observed in Figure 7-5(b). This is due to the shorter ID calculated by the reduced CHX model as shown earlier in Figure 7-4(b). In spite of this, the computed absolute species mole fractions agree with those of the detailed counterpart. Besides, satisfactory results are also obtained in species concentration predictions between the reduced and detailed models for fuel oxidations under the JSR condition, as demonstrated in Figure 7-6. However, slight deviations are observed in the computed C_2H_2 profiles by the reduced model as compared to the detailed counterpart when temperature is greater than 850 K, as shown in Figure 7-6(a). This can be attributed to the elimination of fuel isomers which are significant for C_2H_2 productions during the mechanism reduction procedure. The findings here demonstrate an acceptable compromise in terms of mechanism size and results accuracy.



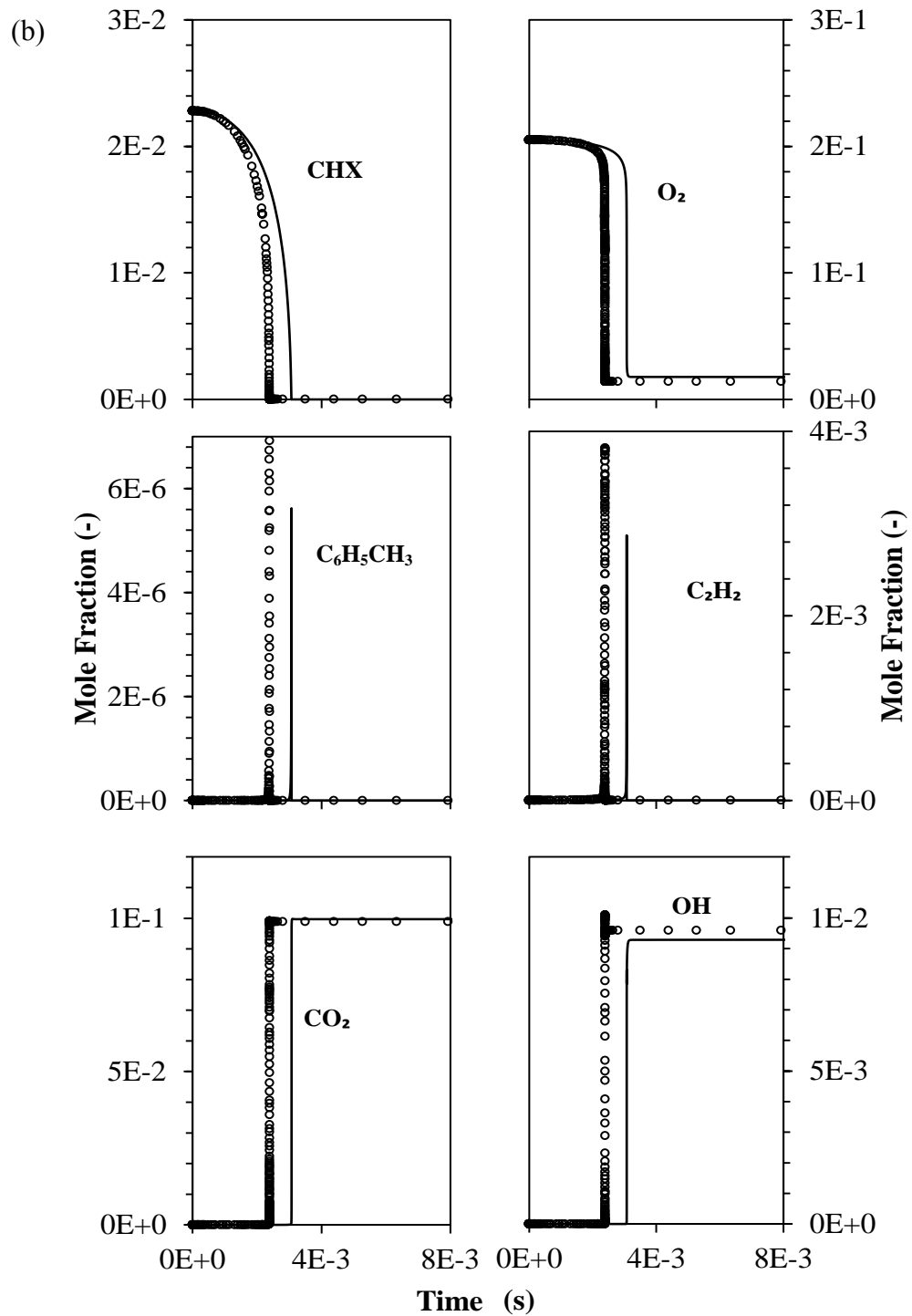
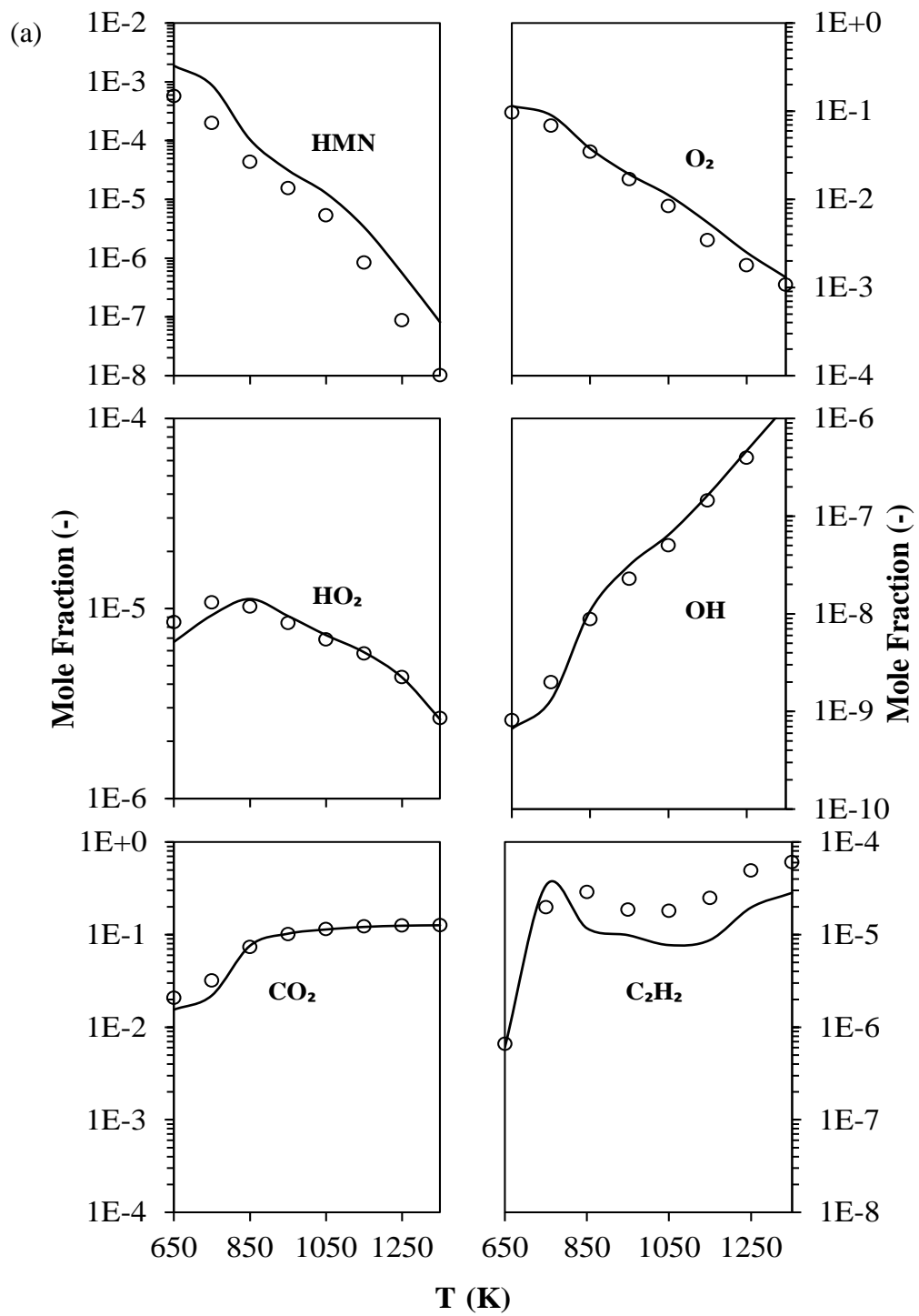


Figure 7-5: Computed species profiles predicted by the detailed (\circ) and reduced ($-$) models of (a) HMN and (b) CHX under auto-ignition condition, with initial pressure of 60 bar, initial temperature of 950 K and Φ of 1.



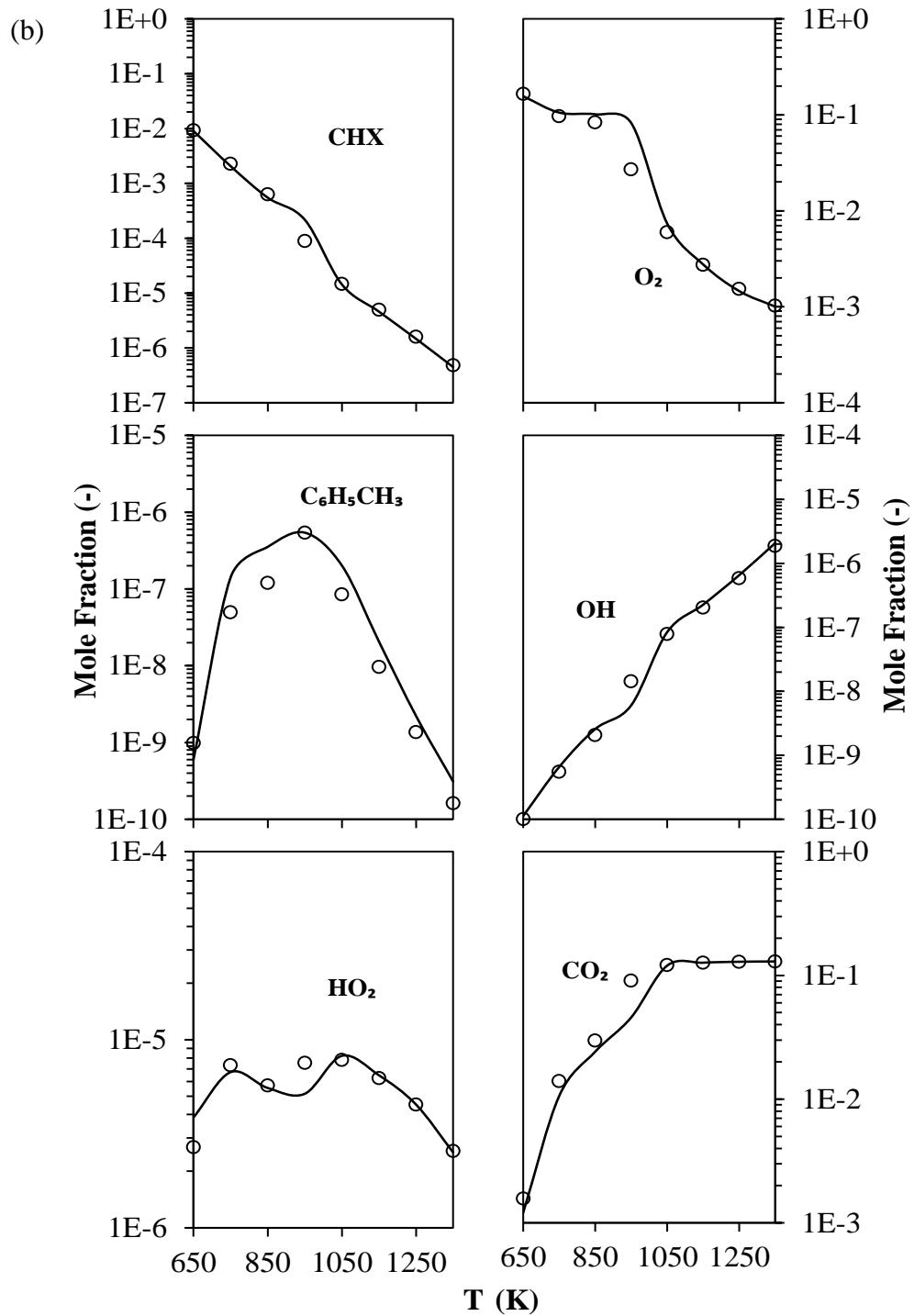
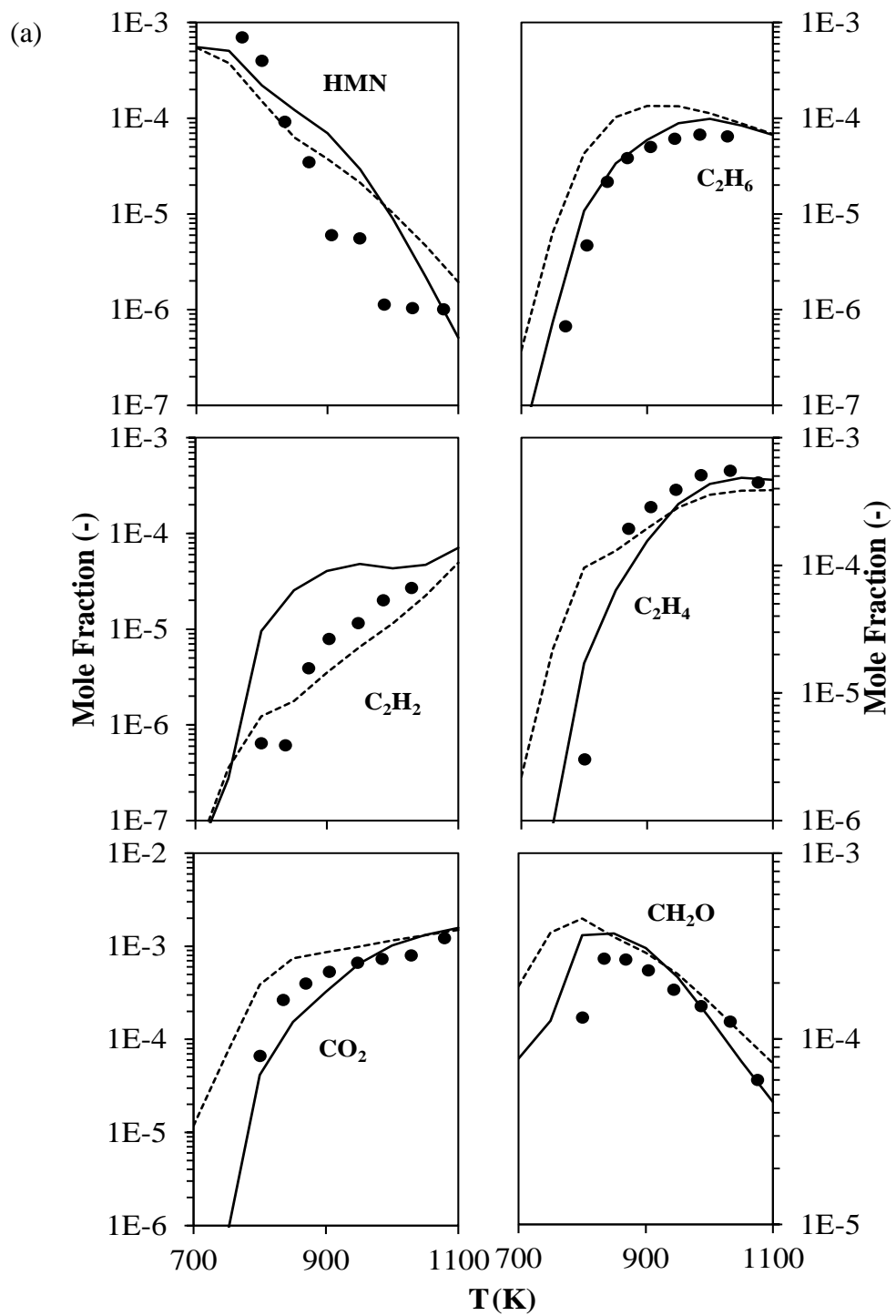


Figure 7-6: Computed species profiles predicted by the detailed (○) and reduced (—) models of (a) HMN and (b) CHX under JSR condition, with initial pressure of 60 bar, initial temperature of 950 K and Φ of 1.

Furthermore, the reduced mechanisms for the diesel surrogate fuel components are further validated using the JSR experimental results of HMN and CHX oxidations carried out by Dagaut et al. [179] and Voisin et al. [180], respectively. The validation results are depicted in Figure 7-7 by comparing the computed species concentrations to the corresponding experimental measurements for fuel-oxygen mixtures, diluted by nitrogen. The selected species for comparison studies here are reactants (i.e. HMN, CHX, O₂), oxygenated products (i.e. CO₂, CH₂O) as well as important products under fuel-rich region (i.e. C₂H₂, C₂H₄ and C₆H₆). These species concentrations are validated to ensure that the proposed surrogate models are able to provide a reasonable representation of the kinetics of the fuel oxidations. Apart from that, concentration profiles of C₂H₂, C₂H₄ and C₆H₆ are monitored as they are the major species involved in the soot formation. Both C₆H₆ and C₂H₂ are commonly used as soot precursors while the latter is also the soot surface growth species which is important to soot mass addition during surface growth process. Additionally, C₂H₄ is the most abundant alkene among all the measured alkenes and it plays an important role in the formation of C₂H₂. Thus, validation of concentration profiles of these rich combustion products is expected to aid soot formation predictions for the subsequent multi-dimensional CFD modelling studies. As soot is mainly formed in fuel-rich condition, Φ of 1.5 is applied in the subsequent validation exercise.



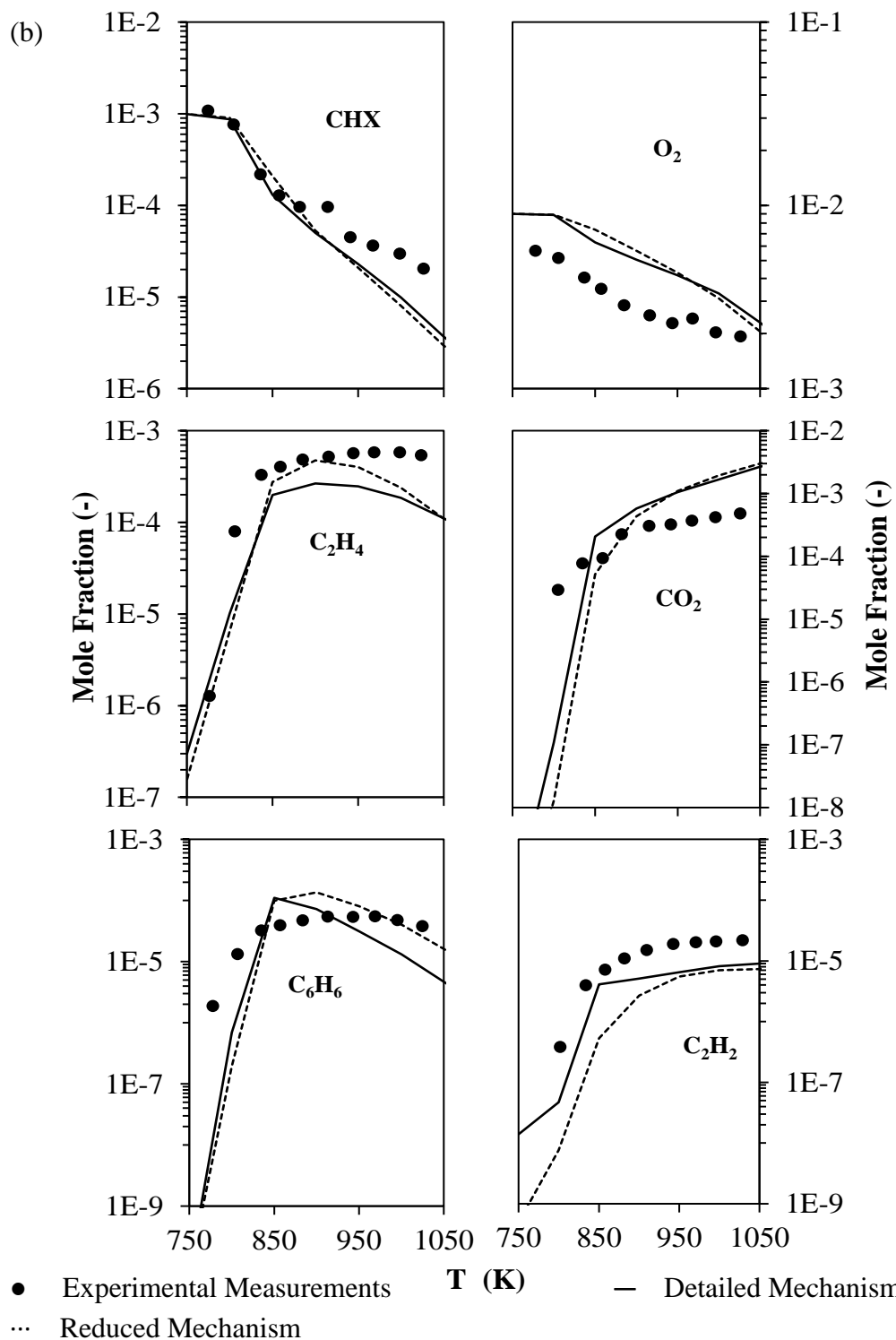


Figure 7-7: Computed and experimental species mole fractions obtained from the oxidation of (a) 0.07 % HMN and (b) 0.1 % CHX in a JSR. [Note: The associated operating conditions are depicted in Table 7-2.]

Figure 7-7(a) demonstrates that the HMN concentration decreases when ambient temperature increases. Nonetheless, the computed fuel concentration using the reduced chemistry is over-predicted at $800 \text{ K} < T < 1000 \text{ K}$ as compared to the experimental measurements. The deviations between the computed results and the experimental measurements are within one order of magnitude in the absolute values. In spite of this, the species profiles for the resulting product species such as C_2H_2 , C_2H_4 and C_2H_6 are seen to be consistent and identical. Similar temporal evolution trends are observed between the reduced and detailed mechanisms. Additionally, it is observed that the C_2H_2 concentrations predicted by the reduced model are much lower than those computed by the detailed model and the profile is seen to be closer to the experimental measurements when $T > 800 \text{ K}$. This can be attributed to the elimination of kinetic reactions associated to C_2H_2 formation during the mechanism reduction process, leading to lower production rate of C_2H_2 .

Furthermore, based on the results obtained for CHX oxidation in Figure 7-7(b), decreasing trend in fuel profile is obtained and fuel concentrations at $T > 850 \text{ K}$ are under-predicted. Overall agreement is achieved between the species concentration predictions and the experimental measurements. The species profile trends predicted by the reduced mechanism are also consistent with those of the detailed mechanism.

Although variation of the computed concentrations could reach as high as one order of magnitude as compared to the JSR experimental measurements, the results of the predicted species concentrations are deemed acceptable in view of their simplified fuel chemistries. The overall agreements between the experimental and predicted species profiles for HMN and CHX are achieved. These fuel constituent models are henceforth used in the successive exercise to construct multi-component diesel surrogate fuel models.

7.5.2 Validation of Multi-Component Diesel Surrogate Fuel Models

In this section, mechanism validations are performed using the MCDS1 and MCDS2 diesel surrogate fuel models for:

- i) ID timing of each diesel fuel component such as HXN, HMN and CHX (Figure 7-8);
- ii) species concentration profiles of each diesel fuel component under auto-ignition (Figure 7-9) and JSR conditions (Figure 7-10);
- iii) species concentration profiles of each diesel fuel component in a JSR (Figure 7-11); and
- iv) ID timing of DPRF58 [160] and n-dodecane ($n\text{-C}_{12}\text{H}_{26}$) [7]. (Figure 7-12)

It is noteworthy that computation results generated by both the multi-component models are plotted together with those predicted by the detailed model for each fuel constituent. The purpose here is to demonstrate that the performance in predicting the ID timings and species concentrations retains after mechanism integration is carried out.

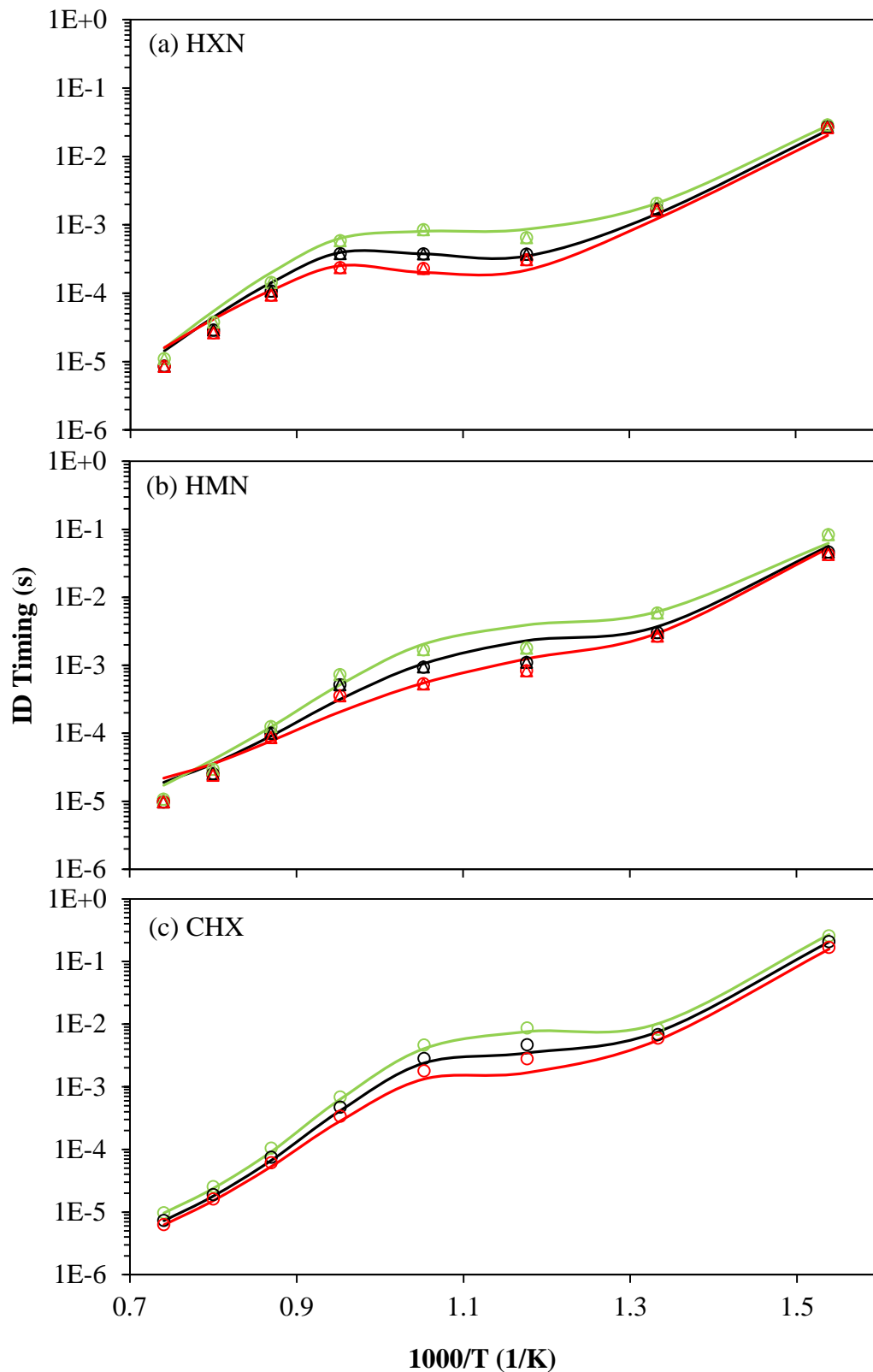
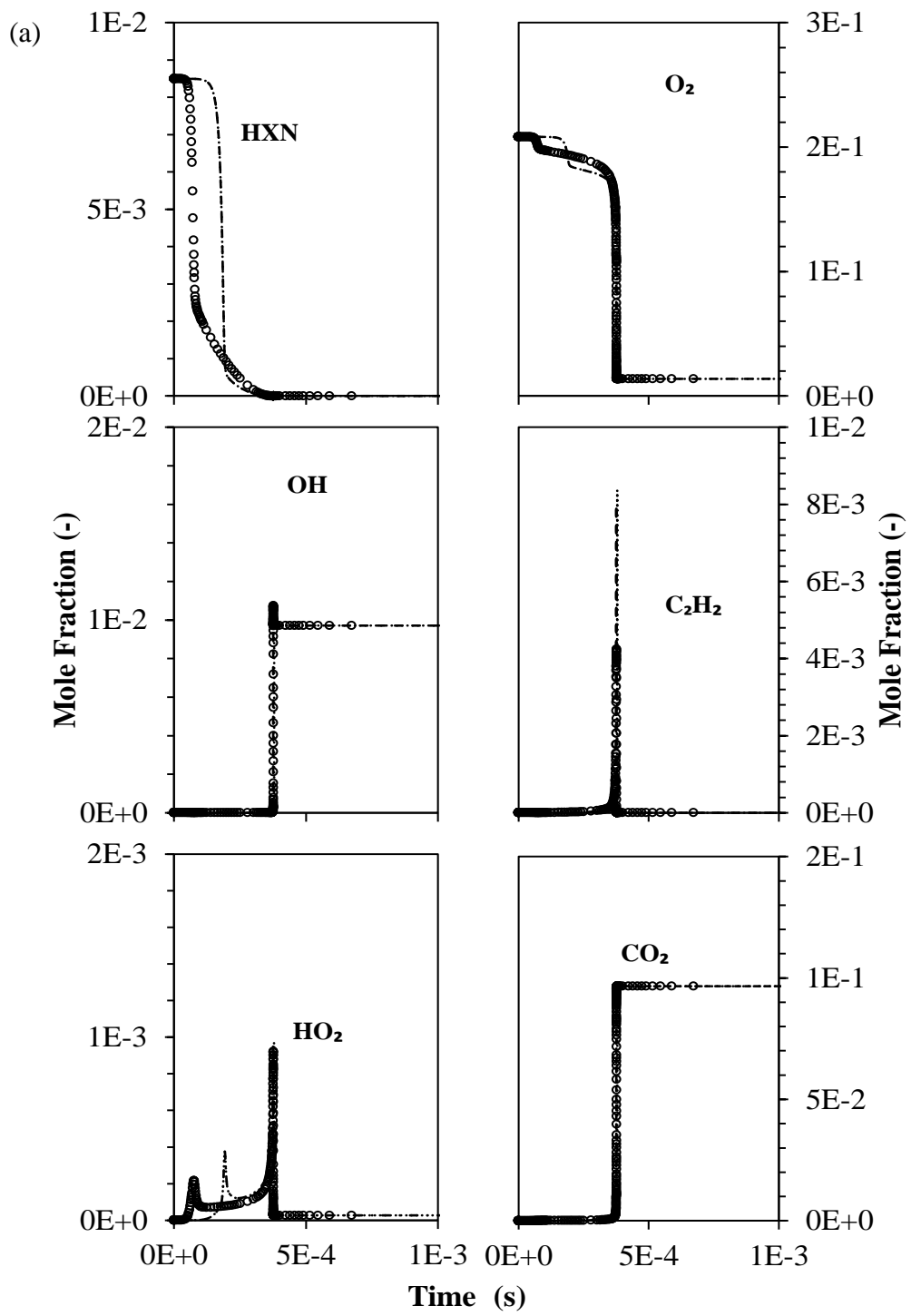
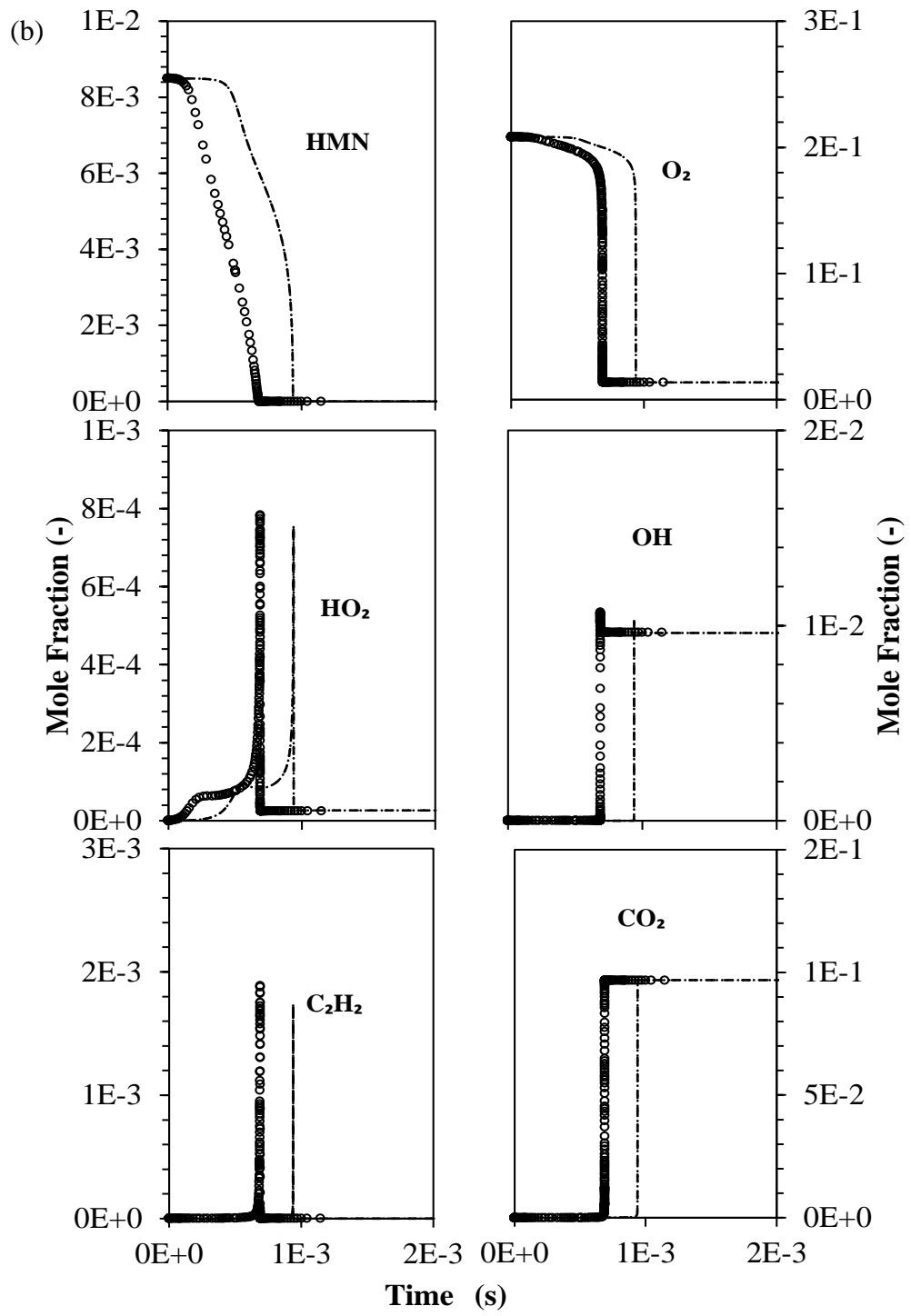


Figure 7-8: Comparisons of ID calculated by MCDS1 (Δ) and MCDS2 (\circ) with the detailed (line) models of (a) HXN, (b) HMN and (c) CHX for initial pressure of 60 bar and Φ of 0.5 (green), 1.0 (black), 2.0 (red).

In Figure 7-8, the computed ID for HXN and HMN oxidations using MCDS1 and MCDS2 surrogate models are similar as the elementary reactions for HXN and HMN in these two mechanisms are the same. Comparison of ID timings and species profiles with those of CHX detailed mechanism is only performed using MCDS2 as MCDS1 does not contain elementary reactions for CHX. It is observed that the predicted ID timings for each surrogate model agree reasonably well with those of the surrogate components. In addition, trend of the species concentration profiles for both auto-ignition and JSR conditions is retained using both the multi-component surrogate models in comparison with those of each individual diesel fuel component, as illustrated in Figure 7-9 and Figure 7-10, respectively. As can be seen, the results for MCDS1 are comparable with those of MCDS2 with only about $\pm 5\%$ deviations.

Apart from that, it is observed that the species concentration profiles in a JSR for each surrogate component are reproduced using the MCDS2 surrogate model, as seen in Figure 7-11. However, opposite trends are observed in Figure 7-11(a) between the computed and measured species profiles of C_2H_4 and CH_2O during HXN oxidation. As mentioned in Section 5.3.2, C_2H_4 and CH_2O are formed during the HXN decomposition and consumption processes. While the kinetic reactions of HXN are integrated into the multi-component surrogate models, similar trend to that of HXNv2 is expected whereby the C_2H_4 and CH_2O concentrations decrease when HXN concentration reduces. Furthermore, the deviations in the species concentration predictions between the multi-component surrogate models and the individual detailed model for each fuel constituent can be attributed to the influence of kinetic reactions of other fuel components upon model integration. Despite the apparent difference in the absolute values, the relative trends of the species profiles computed by the detailed model are reasonably reproduced by the multi-component surrogate models.





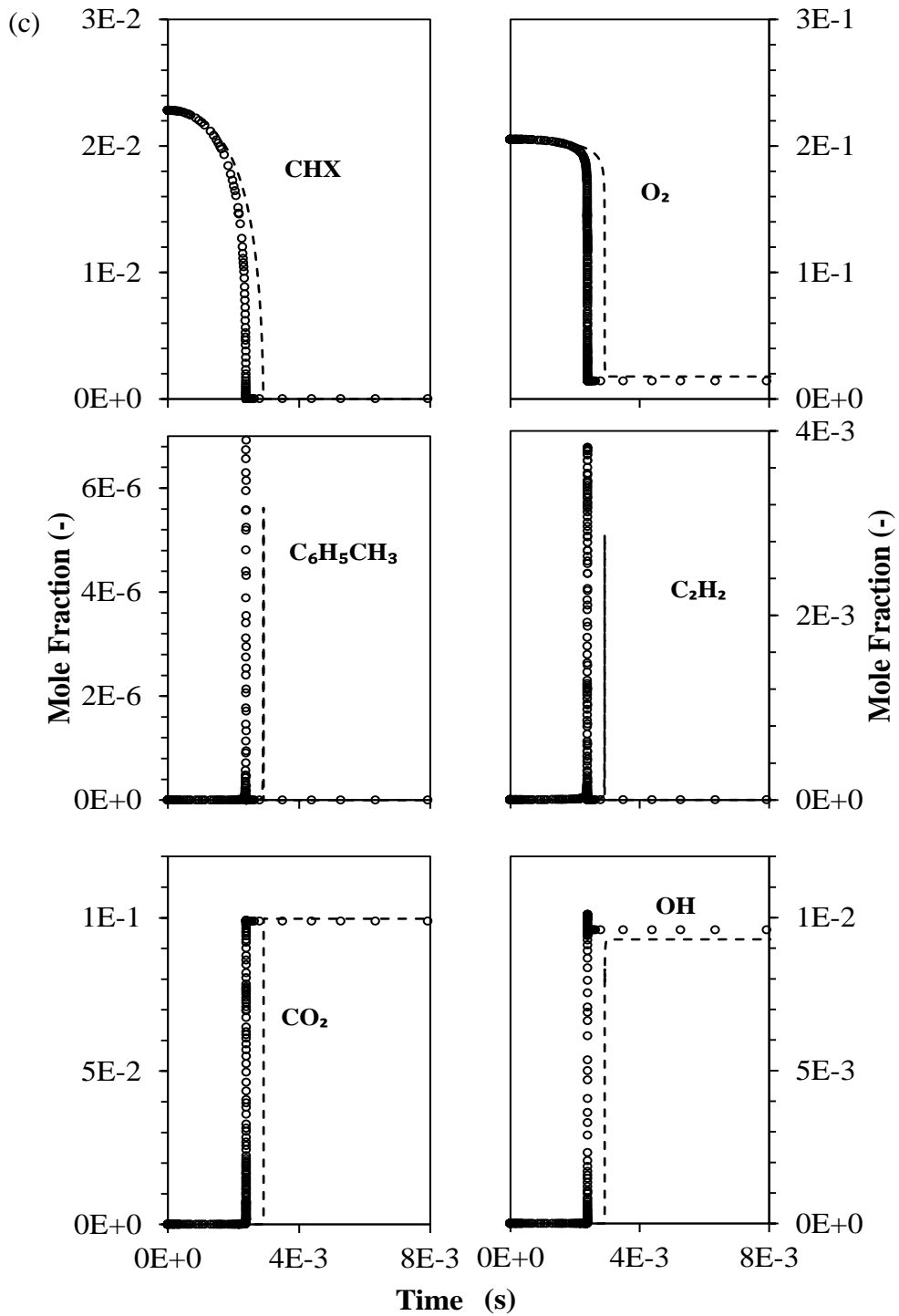
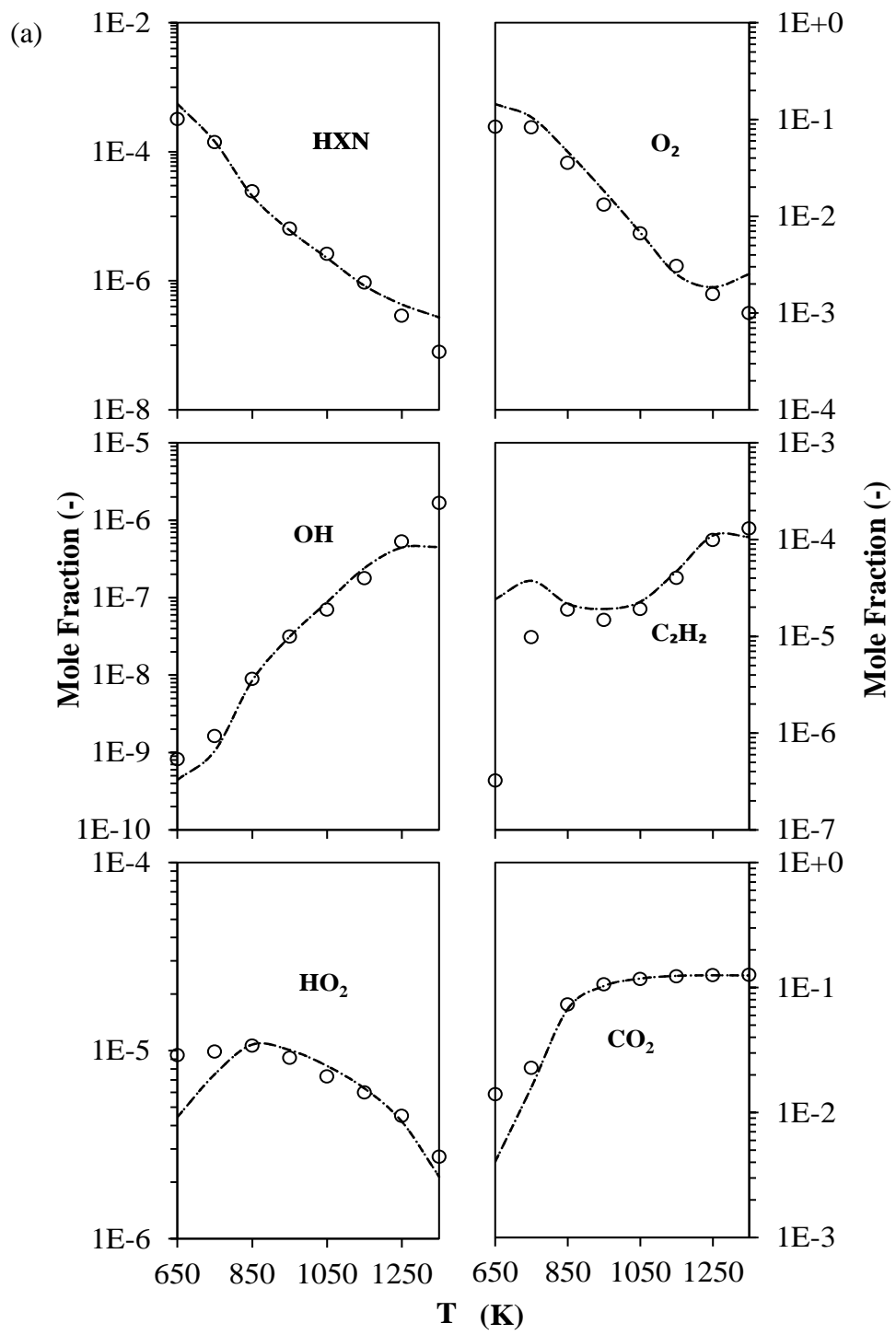
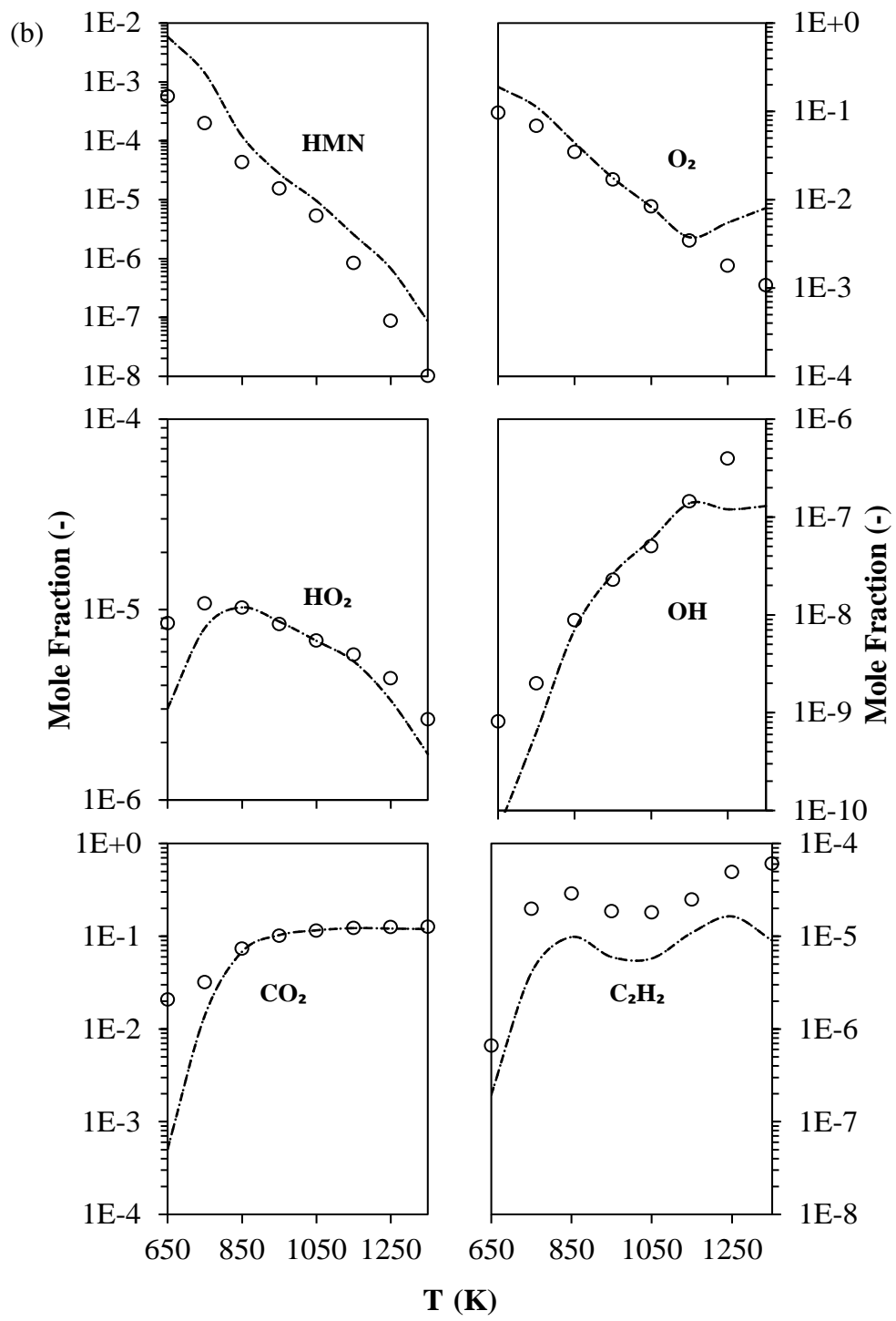


Figure 7-9: Comparison of species profiles predicted by MCDS1 (···) and MCDS2 (--) surrogate models with those of the detailed models (○) for (a) HXN, (b) HMN and (c) CHX under auto-ignition condition, with initial pressure of 60 bar, initial temperature of 950 K and Φ of 1.





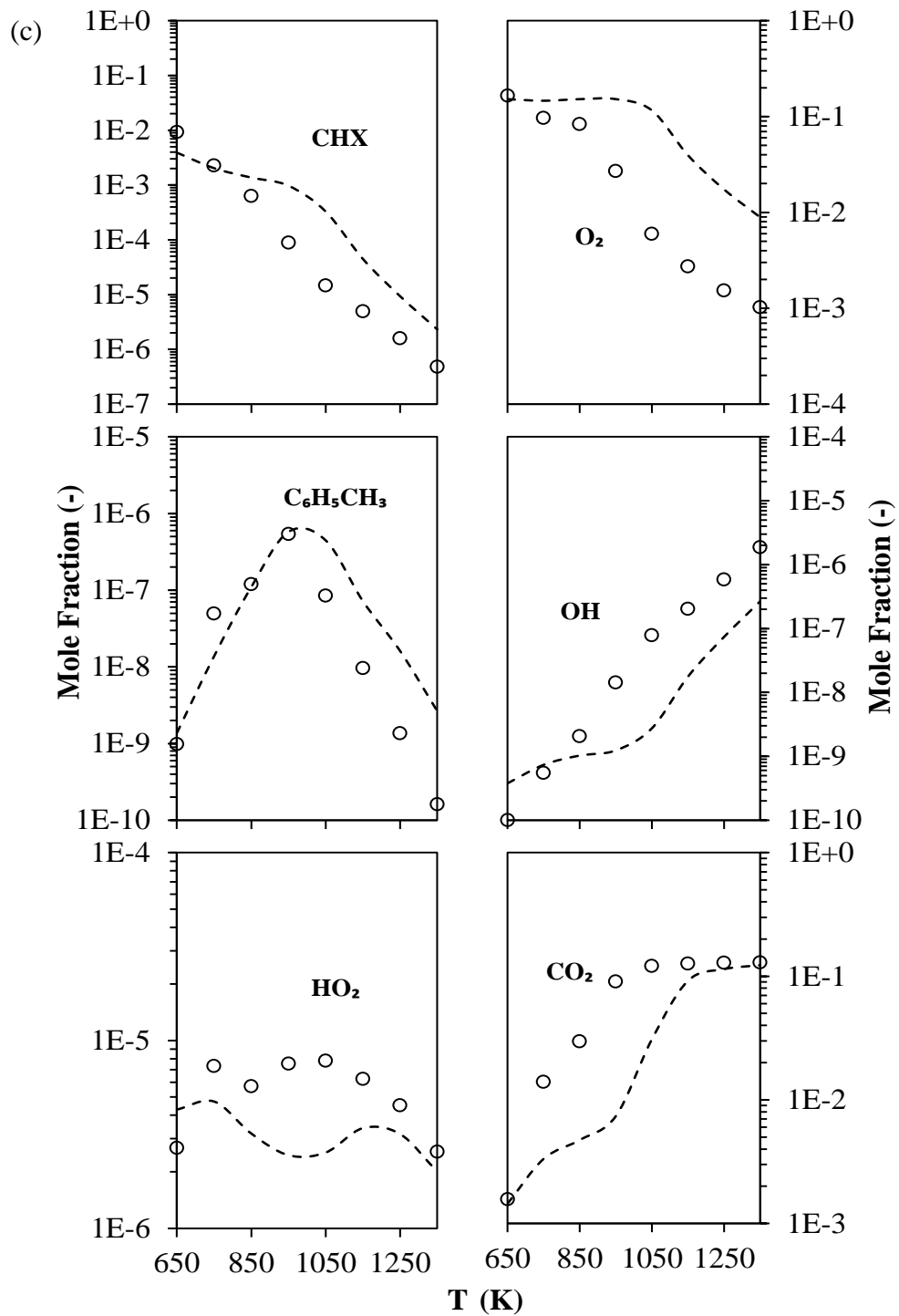
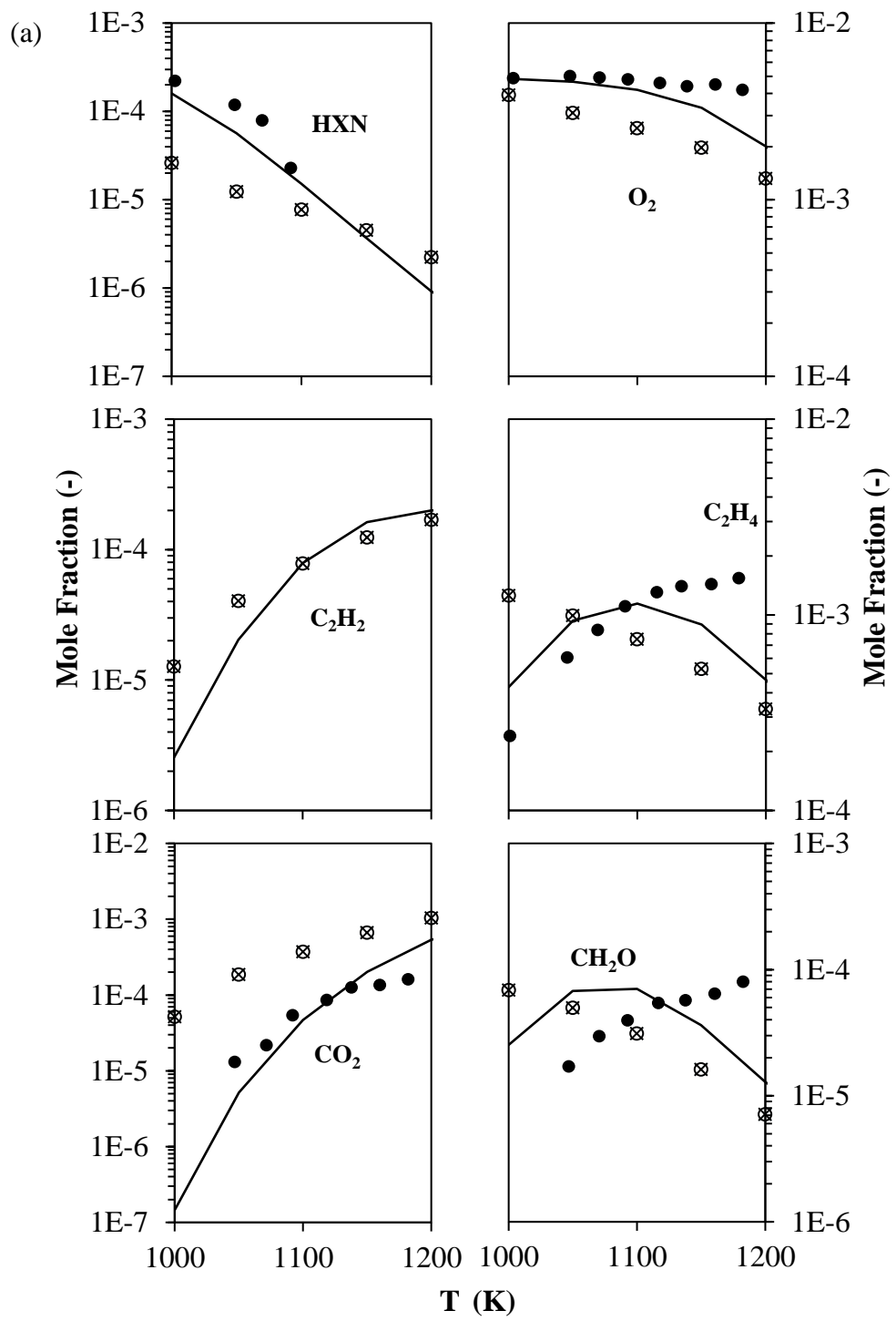
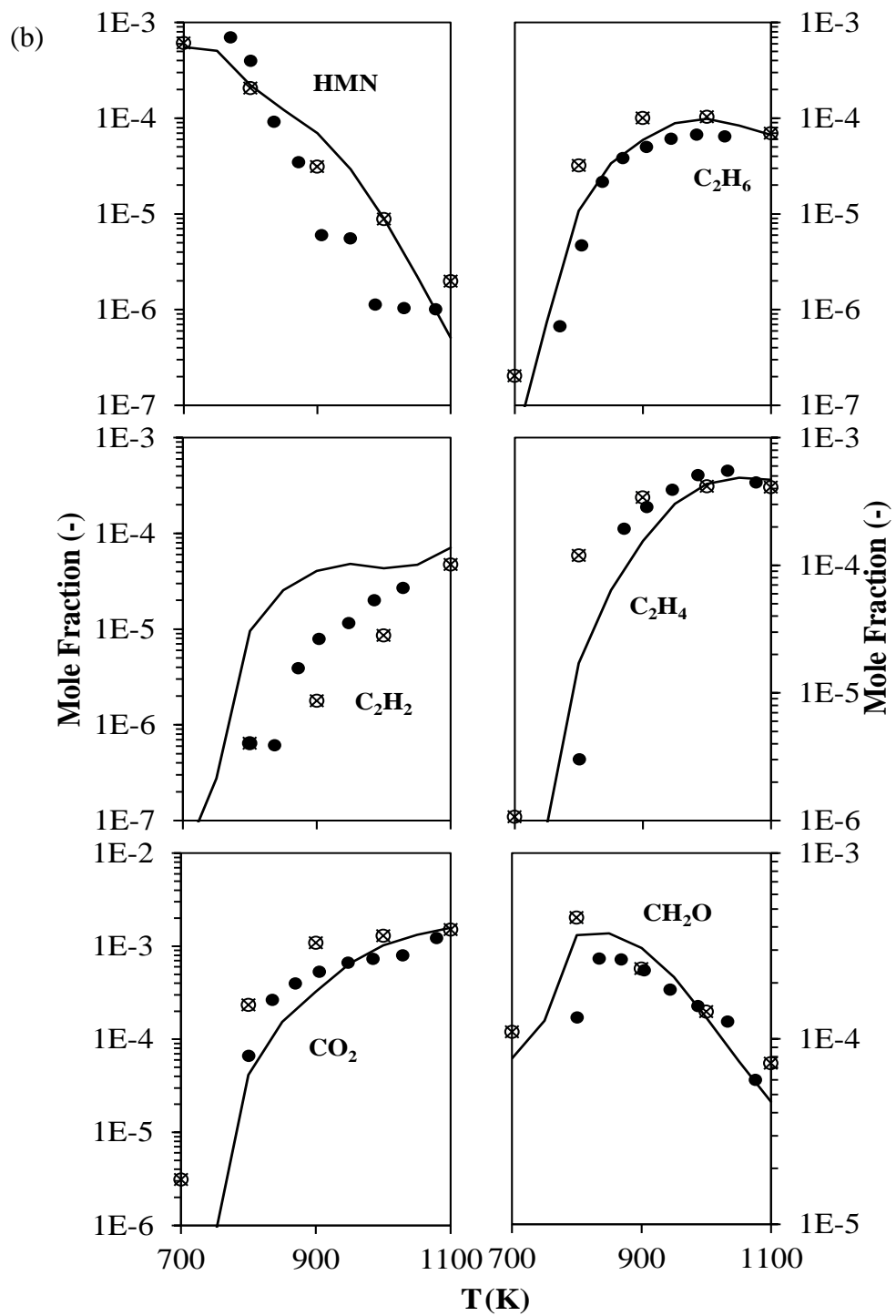


Figure 7-10: Comparison of species profiles predicted by MCDS1 (···) and MCDS2 (--) surrogate models with those of the detailed models (o) for (a) HXN, (b) HMN and (c) CHX under JSR condition, with initial pressure of 60 bar, initial temperature of 950 K and Φ of 1.





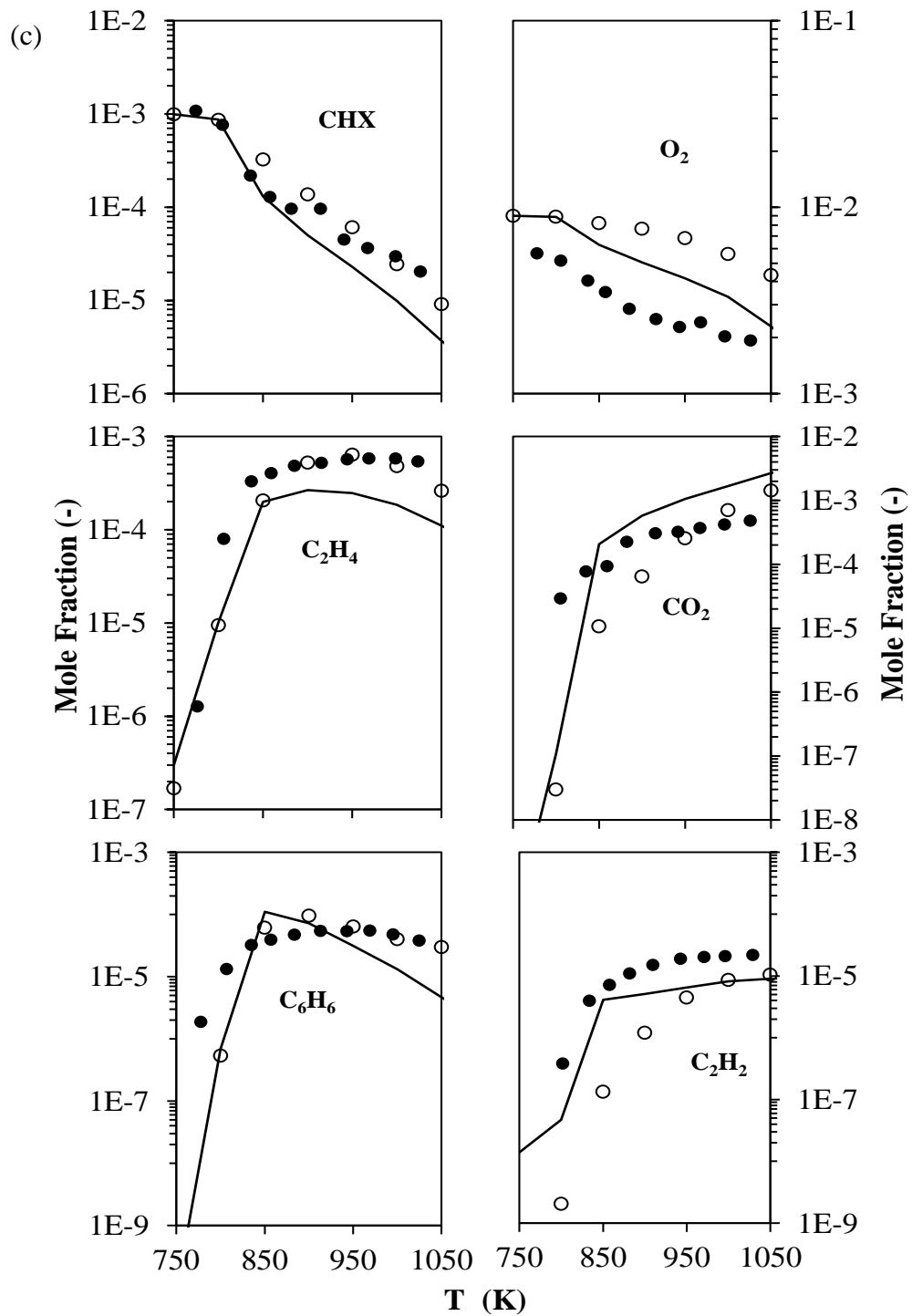
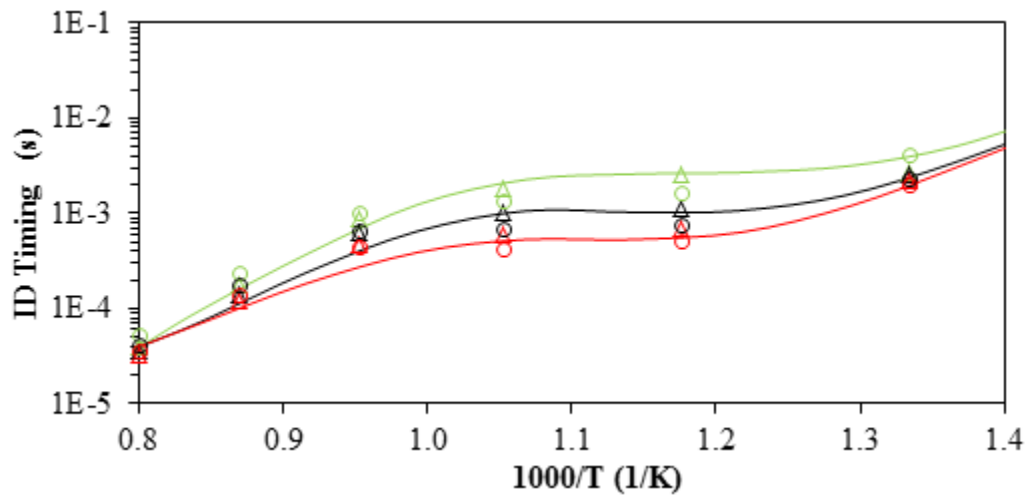
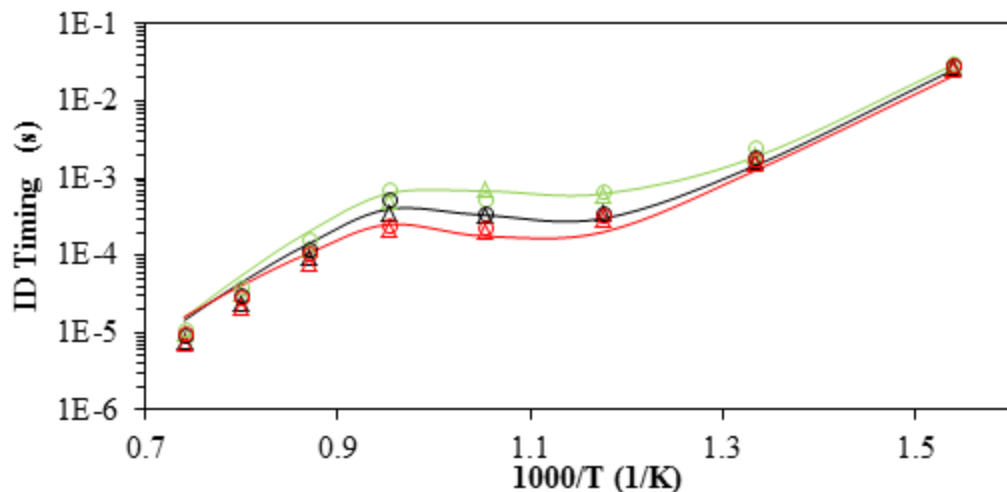


Figure 7-11: Computed and experimental species mole fractions (●) obtained from the oxidation of (a) 0.03 % HXN, (b) 0.07 % HMN and (c) 0.1 % CHX in a JSR using MCDS1 (X) and MCDS2 (○) surrogate models as well as the detailed model (—) for each fuel constituent. [Note: The associated operating conditions are depicted in Table 7-2.]

Comparisons of the ID predictions between the surrogate models and DPRF58 are demonstrated in Figure 7-12(a). It is observed that agreement is achieved between the multi-component surrogate and DPRF58 mechanisms in ID predictions throughout the test conditions, with maximum deviations maintained to within 40 %. This is reasonable since the error tolerance for large-scale mechanism reduction generally ranges from 30 % to 50 % [40,106,158,159]. Apart from that, it is found that MCDS2 with compositions of $F_{H_{2XN}}:F_{H_{2MN}}:F_{C_7H_8}:F_{CH_4}$ set to 0.42:0.20:0.28:0.10 yields similar ID timing predictions as DPRF58. In other words, its ignition behaviour is compatible with that of D2.



(a)



(b)

Figure 7-12: Comparisons of ID predicted by MCDS1 (Δ) and MCDS2 (\circ) surrogate models with the detailed mechanisms (lines) of (a) DPRF58^a [160] and (b) n-dodecane^b [7] for initial pressure of 40 bar, Φ of (i) 0.5, (ii) 1 and

(iii) 2. [^aIDs of DPRF58 were computed by Perini et al. [160] using the detailed mechanism of Westbrook et al. [31] in a constant volume vessel using identical initial conditions; ^bThe mechanism of n-dodecane was extracted from the detailed mechanism of Westbrook et al. [7] for combustion of n-alkane hydrocarbons from n-octane to HXN.]

The multi-component diesel surrogate mechanisms are further validated in closed homogeneous batch reactor simulations by varying their CN. ID timing predictions are compared in Figure 7-12(b) with respect to the detailed n-dodecane mechanism (CN of 87). Composition of $F_{\text{HXN}}:F_{\text{HMN}}$ is set to 0.85:0.15 for MCDS1, corresponding to a CN of 87.25. Conversely, the fuel composition for MCDS2 is fixed at 0.85:0.15:0:0 for $F_{\text{HXN}}:F_{\text{HMN}}:F_{\text{C7H8}}:F_{\text{CHX}}$. It is observed that the projected ID timings are well replicated using both MCDS1 and MCDS2 diesel surrogate models. Upon the model validation under a series of different test conditions in the 0-D kinetic simulations, the proposed MCDS1 and MCDS2 surrogate models are coupled with CFD models in the next section to simulate spray combustion and soot formation under diesel-engine like conditions.

7.6 2-D Spray Combustion Simulations Using the Derived Multi-Component Diesel Surrogate Fuel Models

In this section, 2-D multi-dimensional CFD simulations are carried out to simulate spray combustion and soot formation processes using both the multi-component diesel surrogate fuel models. The spray combustion solver in OpenFOAM-2.0.x is used and a multistep soot model is integrated into the solver [184,185]. The numerical setups for the reacting diesel fuel sprays are described in Table 6-6. In this work, the physical properties of the aromatic compounds are represented by those of toluene. In contrast, the physical properties of the alkanes are represented by the physical properties of n-tetradecane as its physical properties are close to those of real diesel fuels. Thus, influence of the fuel physical properties is isolated and effect of the chemical kinetics of the reaction models can be studied.

Based on the sensitivity study shown in [185], the spatial and temporal evolutions of fourth aromatic ring PAH, pyrene, is similar those of smaller PAHs or C_2H_2 when the flame temperature is relatively high, i.e. when no or low EGR is used. Here, C_2H_2 is selected as the soot precursor in the numerical simulations using the MCDS1 surrogate model as this mechanism does not contain PAH mechanism. Implementation of C_2H_2 as soot precursor is usually a good compromise between results accuracy and simplicity when the PAH chemistry is absent [184,186–188]. On the contrary, C_6H_6 is present in the MCDS2 surrogate model when CHX mechanism is integrated into the multi-component mechanism during the model development. With the presence of the PAH chemistry in the surrogate model, C_6H_6 is thus designated as the soot precursor species in the respective modelling studies. In order to simulate the mass addition on soot particle surface, C_2H_2 is consistently used as the soot surface growth species when MCDS1 and MCDS2 are applied. OH and O_2 are set as the soot oxidant species for the calculation of soot mass destruction.

In this section, the numerical simulations are separated into two parts. First and foremost, MCDS1 surrogate model is applied in a sensitivity test to examine its reactivity towards variation in CN. Mass fractions of HXN and HMN as well as the corresponding CN are shown in Table 7-6(a). It is then followed by the validation of both MCDS1 and MCDS2 using the measurements of D2 fuel [17,168] from constant volume combustion chamber experiments. Mass fraction of each component is varied to mimic the actual fuel properties and these details are provided in Table 7-6(b). Operating conditions used for this validation exercise are demonstrated in Table 7-6(c). Measurements are available for reacting spray test cases at 15 % O_2 mole fraction. This condition represents a reactive environment of air diluted with exhaust gas recirculation. The ambient temperature varies from 900 K to 1000 K while the ambient density is fixed at 22.8 kg/m^3 . The computed ID, LOL and SVF are compared to the experimental data. For the simulation results, ID is defined as the maximum dT/dt gradient of the temperature profile. Meanwhile, LOL is defined as the distance from the injector to the closest layer where OH mass fraction reaches 2 % of its maximum

value in the domain. These definitions correspond with those recommended by ECN [167].

Table 7-6: (a) Sensitivity test with various CN using MCDS1 surrogate model; (b) Test matrix for validations of D2 fuel by applying different fuel blends; (c) Experimental operating conditions.

(a) Sensitivity Test with Various CN		
Test	Compositions ($F_{\text{HXN}}:F_{\text{HMN}}$)	CN
1	1:0	100
2	0.75:0.25	78.75
3	0.50:0.50	57.5
4	0.25:0.75	36.25
5	0:1	15
(b) Test Matrix for Fuel Validations		
Surrogate Fuel	Compositions	
MCDS1	$F_{\text{HXN}}:F_{\text{HMN}} = 0.42:0.58$	
MCDS2	$F_{\text{HXN}}:F_{\text{HMN}}:F_{\text{C7H8}}:F_{\text{CHX}} = 0.42:0.20:0.28:0.10$	
(c) Experimental Operating Conditions		
Ambient Temperature (K)	900/1000	
Ambient Density (kg/m^3)	22.8	
Ambient Pressure (MPa)	6/6.7	
Orifice Diameter (mm)	0.09	
Ambient Composition (%)	O ₂ = 15 %; CO ₂ = 6.23 %; H ₂ O = 3.62 %; N ₂ = 75.15 %	
Injection Duration (ms)	7	

F denotes mass fraction.

7.6.1 Sensitivity Test of the MCDS1 Surrogate Model on CN Variations

The effects of variation in CN on LOL and ID predictions are demonstrated in Figure 7-13. As the CN increases, it is expected that the ID becomes shorter. As a result, the ignition occurs at a location closer to the injection tip and the associated flame lift-off is hence shorter. The trend is replicated by the model. Based on the results in Figure 7-13, it is observed that the kinetics of MCDS1 surrogate model is sensitive to changes in CN ranging from 15 to 100. MCDS1 serves as a promising surrogate model for diesel fuels with various CN.

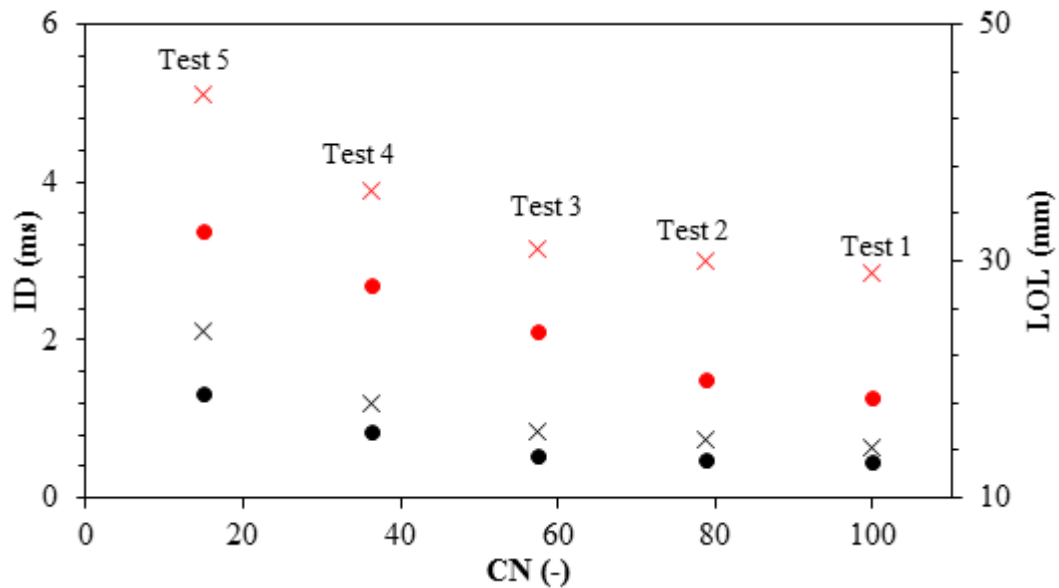


Figure 7-13: ID (black) and LOL (red) predictions against CN for the sensitivity tests using MCDS1 surrogate model for ambient temperatures of 900 K (X) and 1000 K (•).

In the next section, the MCDS1 model is further validated using the D2 fuel data. Its performance is also compared against that of the counterpart MCDS2 which considers CHX and toluene reactions.

7.6.2 Validation using D2 experimental data

The predicted IDs and LOLs by MCDS1 and MCDS2 surrogate models for D2 fuel combustion at ambient temperatures of 900 K and 1000 K are demonstrated in Figure 7-14. It is observed that the predictions follow the overall trend where the calculated ID and LOL decrease with increasing ambient temperature. The maximum deviations in ID and LOL predictions with respect to the experimental measurements retain within 15.4 % and 23 %, respectively. Shorter LOLs are however, captured for D2 fuel combustion in both 900 K and 1000 K cases when using the MCDS1 surrogate model. The predicted LOLs are slightly longer for both cases when the MCDS2 surrogate model is applied. Toluene is a compound which is difficult to ignite. As it is integrated to the MCDS2, the resulting ID becomes longer. The flame hence stabilizes at a location further downstream from the injection tip, yielding a longer LOL. The deviations between the experimental

and computed LOLs for D2 fuel combustion using the MCDS2 surrogate model are less pronounced, where deviations of 3.5 mm and 2.5 mm are recorded for ambient temperatures of 900 K and 1000 K, respectively. The results here correspond well with the ID predictions where shorter ID yields shorter LOL and vice versa.

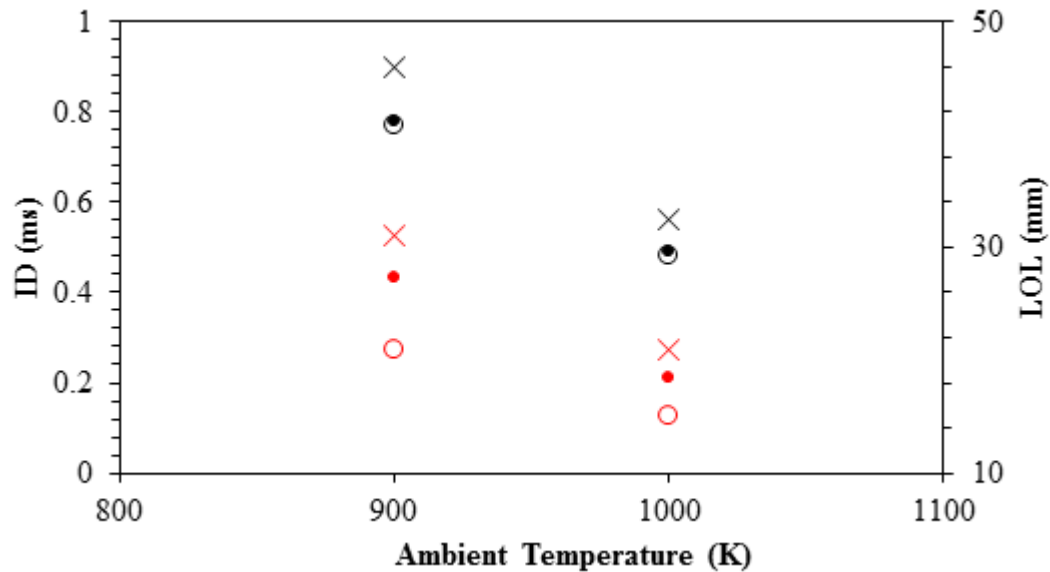


Figure 7-14: ID (black) and LOL (red) predictions using MCDS1 (○) and MCDS2 (×) surrogate models in comparison with the experimental measurements (●) for D2 fuel combustion for ambient temperatures of 900 K and 1000 K.

In addition, the SVF predictions of D2 fuel using the MCDS1 and MCDS2 surrogate models are demonstrated in Figure 7-15. The predictions are compared with the experimental soot clouds obtained at quasi-steady state, i.e. 4 ms after start of injection (ASI), for ambient temperatures of 900 K and 1000 K. These experimental soot images are obtained from the PLII measurement which provides two-dimensional information of SVF distributions for D2 fuel. The red dashed lines on the images indicate the flame LOLs and only qualitative information of soot distribution in the fuel jets is provided based on the images obtained from the experiment. In Figure 7-15, it is observed that size of the soot cloud predicted by the MCDS2 surrogate model is similar to that of the experimental measurements for D2 fuel combustion at ambient temperatures of

900 K and 1000 K. In contrast, the simulated soot clouds appear to be larger than the soot clouds observed in the experiments for both cases when the MCDS1 surrogate model is employed. In comparison to the MCDS2 surrogate model's prediction, the soot clouds predicted by the MCDS1 surrogate model are formed at further upstream locations closer to the injection tip. This can be attributed to the associated shorter LOLs.

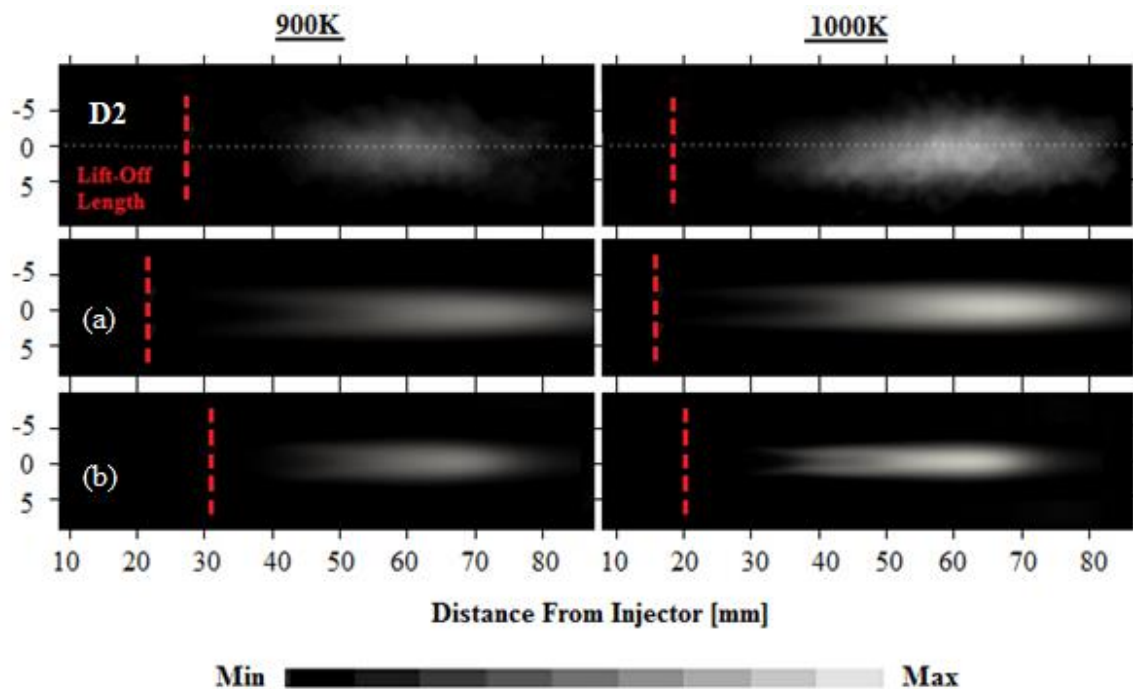


Figure 7-15: Qualitative comparisons of predicted SVF contours and experimental soot cloud images at quasi-steady state for D2 fuel combustion in a constant volume chamber using the (a) MCDS1 and (b) MCDS2 surrogate models.

Subsequently, quantitative SVF predictions along spray axis at quasi-steady state for D2 fuel combustion are demonstrated in Figure 7-16. Figure 7-16 shows that the local SVF values produced by MCDS1 and MCDS2 are different. MCDS1 estimates maximum local SVF values of 15 ppm and 24 ppm for the 900 K and 1000 K test cases, respectively. On the other hand, the maximum local SVF values predicted by MCDS2 for the 900 K and 1000 K test cases are 5.8 ppm and 12.2 ppm, respectively. It is observed that the local SVF given by MCDS1 is higher than that of MCDS2. This can be attributed to several reasons. First of all, the LOLs predicted by MCDS1 are shorter. The associated amount of air

entrained into the fuel rich core region is lesser. Besides this, MCDS1 utilises C_2H_2 as soot precursor while MCDS2 uses C_6H_6 . The mass concentration of C_2H_2 is commonly higher than that of PAH, leading to higher level of soot inception rate and hence soot mass gained. Lastly, as compared to MCDS1, the amount of branched-alkane (i.e. HMN) used in the initial fuel composition of the MCDS2 model is lower. As a consequence, the production rate of C_2H_2 drops and the soot mass gained through the soot surface growth process decreases correspondingly, yielding lower SVF values.

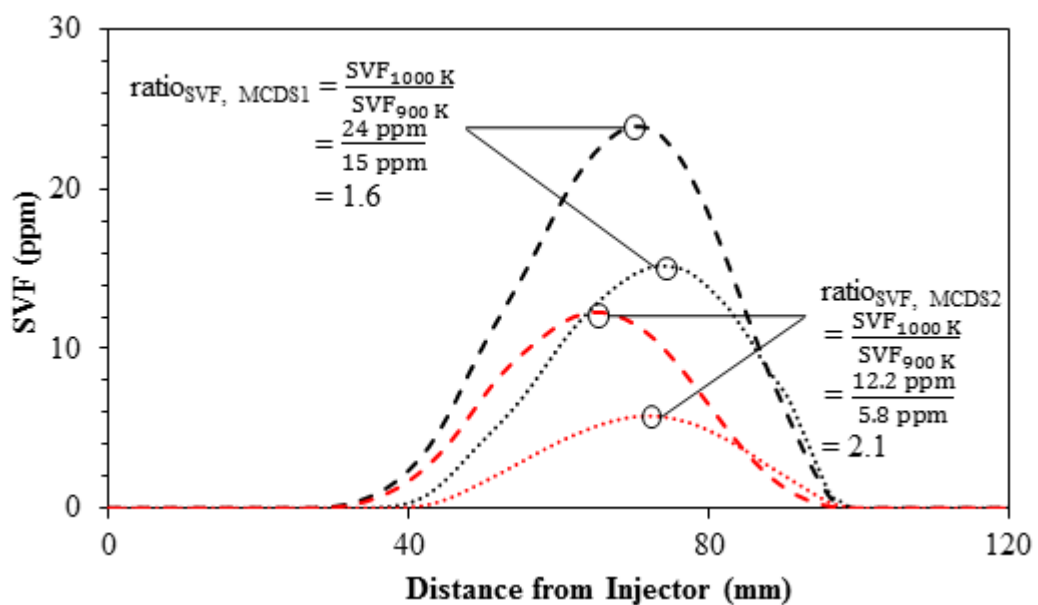


Figure 7-16: Comparisons of the computed SVF along spray axis using MCDS1 (black) and MCDS2 (red) surrogate models at ambient temperatures of 900 K (---) and 1000 K (—).

The next parameter used to evaluate the performance of the multi-component surrogate models is the soot formation behaviour at different ambient temperatures. The results indicates that the predicted maximum local SVF increases by a factor of 1.6 as the ambient temperature is raised from 900 K to 1000 K when MCDS1 is applied. The use of MCDS2 increases the maximum local SVF by a factor of 2.1. The ratio of increment in maximum SVF from ambient temperature of 900 K to 1000 K is henceforth represented by $ratio_{SVF}$ for brevity. Based on the measurement presented by Kook and Pickett [17], the experimental $ratio_{SVF}$ is more than three for D2 fuel combustion. The use of

MCDS2 is found to improve the overall simulated ratio_{SVF}. This can be attributed to the inclusion of aromatic and cyclo-alkane components in the initial fuel composition in MCDS2. At different ambient temperatures, the production of C₂H₂ is different when the aromatic and cyclo-alkane components are considered and omitted. This is further elaborated in the subsequent section.

Numerical analysis of C₂H₂ and C₆H₆ formations is performed at times when temperature rises by 100 K, 200 K, 400 K, 800 K and 1000 K from the initial ambient temperatures. The results are demonstrated in Figure 7-17 and the temperature tolerance for this comparison study is ± 20 K. Besides these, C₂H₂ and C₆H₆ formations at quasi-steady state are also provided, in which the computed results are obtained at 4ms after the time of injection to ensure that the formation of the selected species in all test cases reaches a quasi-steady state. The discussions of the C₂H₂/C₆H₆ formations at various temperature increments from the initial ambient temperatures are presented in a sequential order as below for clarity:

- (i) Results in Figure 7-17(a) show that the amount of C₂H₂ produced at the temperature rise of 100 K from the initial ambient temperatures of 900 K and 1000 K is lower than C₆H₆ when both MCDS1 and MCDS2 are applied. C₆H₆ is mainly produced through the breakdowns of cyclo-paraffin ring as well as toluene via R7-1 to R7-4.

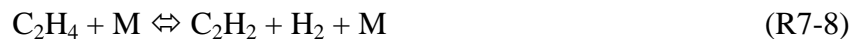


- (ii) At temperature interval of 200 K from the initial ambient temperatures, it is observed that the maximum values of C₂H₂ calculated using MCDS2 are approximately two-fold and five-fold greater than those predicted by MCDS1 in the 900 K and 1000 K cases, respectively. This is depicted in Figure 7-17(b). The apparent differences in the predicted C₂H₂ levels can be attributed to the significant amount of C₆H₆ produced by MCDS2, which subsequently leads to higher production rate of C₂H₂ as compared to that of MCDS1. The

key formation pathways to C_2H_2 from C_6H_6 are described by reactions R7-5 to R7-7.



(iii) In Figure 7-17(c), it is observed that the peak mass fractions of C_2H_2 in the 1000 K cases are consistently higher than those in the 900 K cases when the initial ambient temperatures increase by 400 K, disregards the use of MCDS1 and MCDS2. This is due to the higher production rate of C_2H_2 from the dissociation of C_6H_6 by R7-5 to R7-7 using MCDS2 as well as the consumption of C_2H_4 using both MCDS1 and MCDS2 in the 1000 K cases. The formation of C_2H_2 is significantly dependent on C_2H_4 and the main formation pathways from C_2H_4 to C_2H_2 are described by reactions R7-8 to R7-10.



- (iv) At temperature interval of 800 K from the initial ambient temperatures, the associated mass fractions of C_2H_2 predicted by MCDS1 start to grow significantly and the peak values match with those produced by MCDS2, as demonstrated in Figure 7-17(d). As discussed in the previous section, MCDS1 contains higher amount of branched-alkane in the initial fuel composition. As a result, the production rate of C_2H_2 becomes higher than that of MCDS2, which eventually results in the current observation.
- (v) Same observation as of Figure 7-17(d) persists until approaching ignition points.
- (vi) The associated mass fractions of C_2H_2 continue to rise and eventually those predicted by MCDS1 become higher for both 900 K and 1000 K cases upon reaching a quasi-steady state, as illustrated in Figure 7-17(f). This corresponds well with the earlier findings in Figure 7-16, in which SVF predictions by MCDS2 are lower for both 900 K and 1000 K cases.

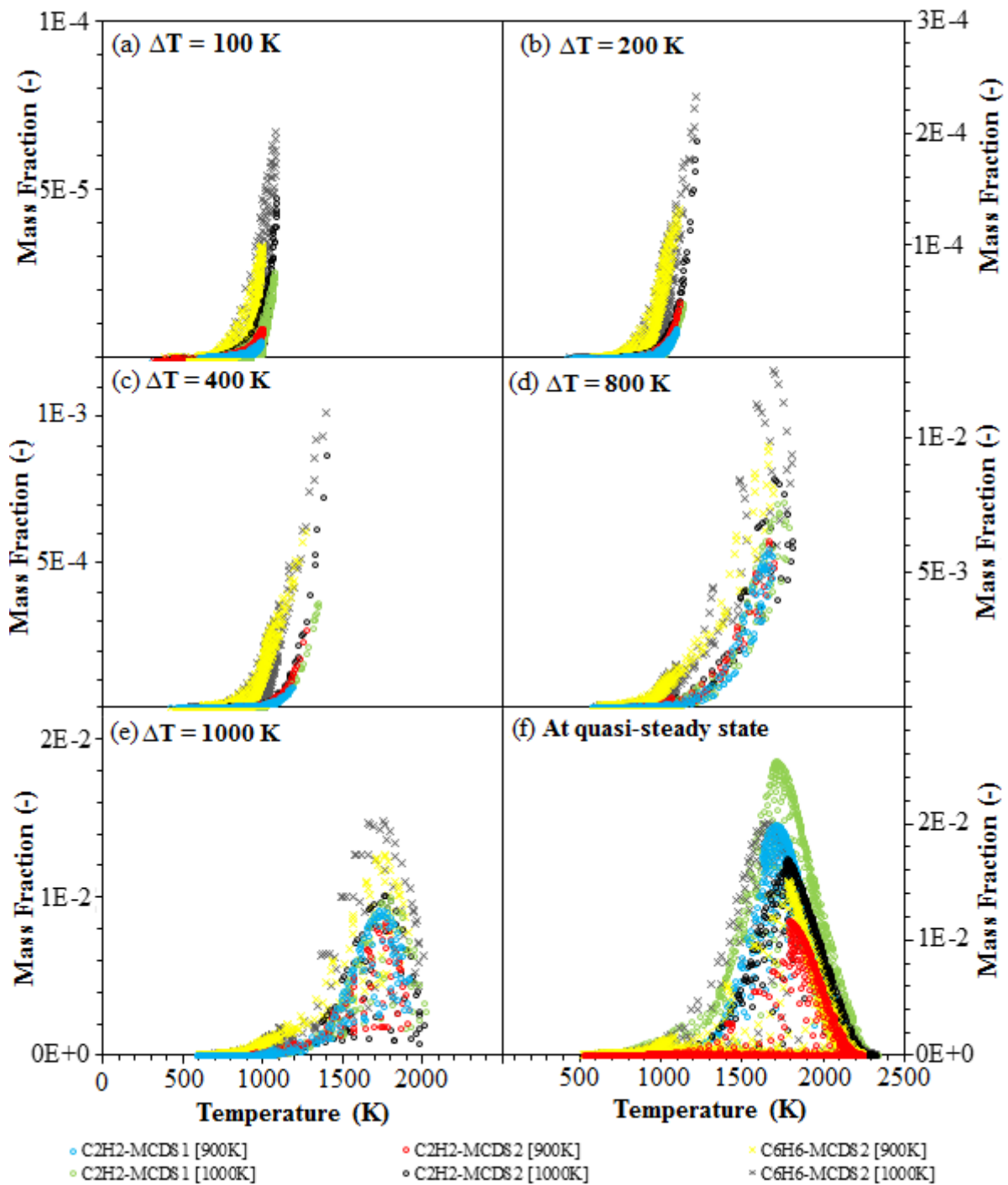


Figure 7-17: Comparisons of C₂H₂ and C₆H₆ mass fractions at temperature increments of (a) 100 K, (b) 200 K, (c) 400 K, (d) 800 K and (e) 1000 K from the initial ambient temperatures as well as at (f) quasi-steady state using MCDS1 and MCDS2 surrogate models. [Note: Mass fractions of C₆H₆ at ΔT = 100 K, ΔT = 200 K and ΔT = 400 K are scaled down by a factor of 20, 10 and 5, respectively; [900 K] and [1000 K] denote initial ambient temperatures of 900 K and 1000 K, respectively.]**

The current results suggest that the MCDS1 model is useful for the soot formation simulations where the effect of aromatic chemistry plays a less significant role. For instance, Vishwanathan and Reitz [149] reasonably captured the variation of SVF with respect to the change of injection pressure and injector diameter using a single-component surrogate model, namely nHep, showing that the presence of aromatic compounds has less pronounced impact on such application. In contrast, this work demonstrates that by considering cyclo-alkane and aromatic compounds have improved the overall soot formation prediction. The revised counterpart, MCDS2 is found to predict a higher $\text{ratio}_{\text{SVF}}$ when the ambient temperature varies.

7.7 Concluding Remarks

In this chapter, two compact yet comprehensive multi-component diesel surrogate fuel models for CFD spray combustion modelling studies are developed. Here, HXNv2 which has been derived in Chapter 5 using the five-stage chemical kinetic mechanism reduction scheme is designated as the base mechanism. The same scheme is used to develop reduced models of other surrogate components for diesel fuels including HMN, CHX and toluene. They are then combined to produce two different versions of multi-component diesel surrogate models in the form of MCDS1 (HXN + HMN) and MCDS2 (HXN + HMN + toluene + CHX). All the fuel constituent reduced mechanisms and the integrated mechanisms namely MCDS1 and MCDS2 are comprehensively validated in 0-D chemical kinetic simulations under a wide range of shock tube and JSR conditions. Subsequently, the fidelity of the surrogate models is further evaluated in 2-D CFD spray combustion simulations. Simulation results show that ID prediction corresponds well to the change of fuel constituent mass fraction which is calculated to match the CN. In addition, comparisons of the simulation results to the experimental data of D2 fuel in a constant volume combustion chamber show that IDs and LOLs are reasonably well replicated by the models. The MCDS2 model is also found to perform better in the soot formation prediction in D2 fuel combustion as the model contains aromatic and cyclo-alkane components which provide an additional pathway to the formation of rich species such as C_2H_2 and

C_6H_6 . Implementation of MCDS2 predicts an increase of maximum local SVF by a factor of 2.1 when the ambient temperature increases from 900 K to 1000 K, while the prediction by MCDS1 is lower at 1.6. This trend qualitatively agrees with the experimental observation. This work demonstrates that MCDS1 serves as a potential surrogate fuel model for diesel fuels with different CN. It also shows that MCDS2 is a more appropriate surrogate model for fuels with aromatics and cyclo-paraffinic contents, particularly when soot calculation is of main interest.

CHAPTER 8

VALIDATIONS OF THE MULTI-COMPONENT DIESEL AND BIODIESEL SURROGATE FUEL MODELS IN 3-D INTERNAL COMBUSTION ENGINE SIMULATIONS

8.1 Introduction

Simulation results presented in the previous chapter demonstrate that the MCDS2 diesel surrogate fuel model is able to reproduce the combustion and soot formation/oxidation processes adequately in 2-D spray combustion simulations. Hence, the fidelity of the surrogate model is further assessed in 3-D internal combustion engine simulations in terms of combustion and soot formation performances in a light-duty, DI diesel engine. In addition, the MCBSv2 biodiesel surrogate fuel model developed in Chapter 5 is also applied here to evaluate the performance of biodiesel combustion under the same operating conditions as diesel combustion. In this chapter, the numerical formulations and setups are first presented in Section 8.2. This is followed by the numerical simulations of diesel and biodiesel combustions in a light-duty, DI diesel engine in Section 8.3. The computational results are compared with the experimental measurements [189]. The main findings of the chapter are summarised in the last section.

8.2 Numerical Formulations and Setups

In this chapter, simulations are performed to model the combustion of diesel and biodiesel fuels in a single-cylinder, DI, light-duty diesel engine. A six-hole injector is installed centrally in the test engine which delivers an injection scheme comprising a pilot injection preceding a main fuel injection with a split main ratio of 98/2. As shown in Figure 8-1, a 60° sector mesh is employed to represent one-sixth of the combustion chamber since the injection nozzle is equally spaced with

six injector holes. The engine and injector specifications as well as the operating conditions applied in the test engine are illustrated in Table 8-1.

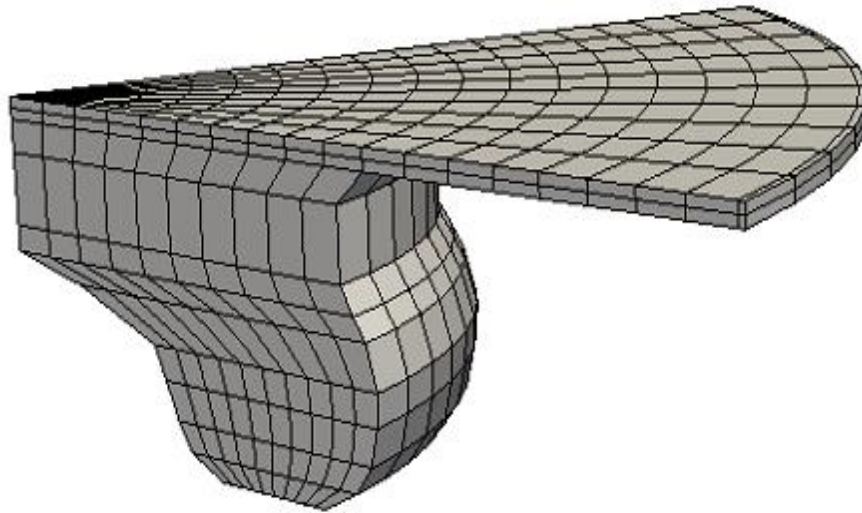


Figure 8-1: 60° sector mesh of the combustion chamber for the light-duty diesel engine at Top Dead Centre (TDC).

Table 8-1: Engine specifications and operating conditions.

Engine Specifications	
Bore X Stroke [mm]	86 x 86
Displacement [L]	0.5
Compression Ratio	18.2:1
Number of Hole	6, Equally spaced
Nozzle Orifice Diameter [mm]	0.149
Spray Pattern Included Angle	154°
Operating Conditions	
Engine speed [rev/min]	1,600
SOI ^a [° ATDC ^b]	+2
Injection quantity [mg]	27.6
Initial temperature [K]	313
Initial pressure [bar]	1.01

^aSOI represents start of injection; ^bATDC represents After Top Dead Centre.

It is noted that accurate predictions of the combustion characteristics and soot formation events cannot be achieved with the use of the default model constants. Additionally, a computational mesh for the combustion chamber with reasonable grid size is required in order to reasonably capture the complex in-cylinder processes. Thus, parametric studies are conducted to select an appropriate grid size for the computational mesh as well as to obtain a set of optimal numerical setups in order to improve the simulated results for the subsequent modelling studies. The parametric studies which are discussed in Sections 8.2.1 to 8.2.4 are performed using the MCDS2 diesel surrogate fuel model, and the results are compared against the pressure and heat release rate (HRR) profiles obtained from experiments [189]. The numerical set-ups for the parametric studies are illustrated in Table 8-2.

Table 8-2: Numerical set-ups for parametric studies of diesel engine simulations.

Model/Parameter	Selected Configurations	Parametric Study			
		I	II	III	IV
Grid	2 mm	0	✓	✓	✓
Time Step	0.005 CAD	✓	0	✓	✓
Breakup Model (Reitz Diwakar)	$C_S = 3$	✓	✓	0	✓
Turbulence Model (RNG $k-\epsilon$)	$C_{I\epsilon} = 1.42$	✓	✓	✓	0

‘✓’ represents fixed parameter constants; ‘0’ represents constants varied for parametric studies; CAD represents Crank Angle Degrees.

8.2.1 Parametric Study I: Grid Independence Test

Grid independence test is performed using three different mesh sizes of 1 mm, 1.5 mm and 2 mm, which represent fine, semi-fine and coarse mesh, respectively. The computed pressure and HRR profiles are compared with the experimental measurements in Figure 8-2. In addition, details of the computational meshes with three different grid sizes are provided in Table 8-3.

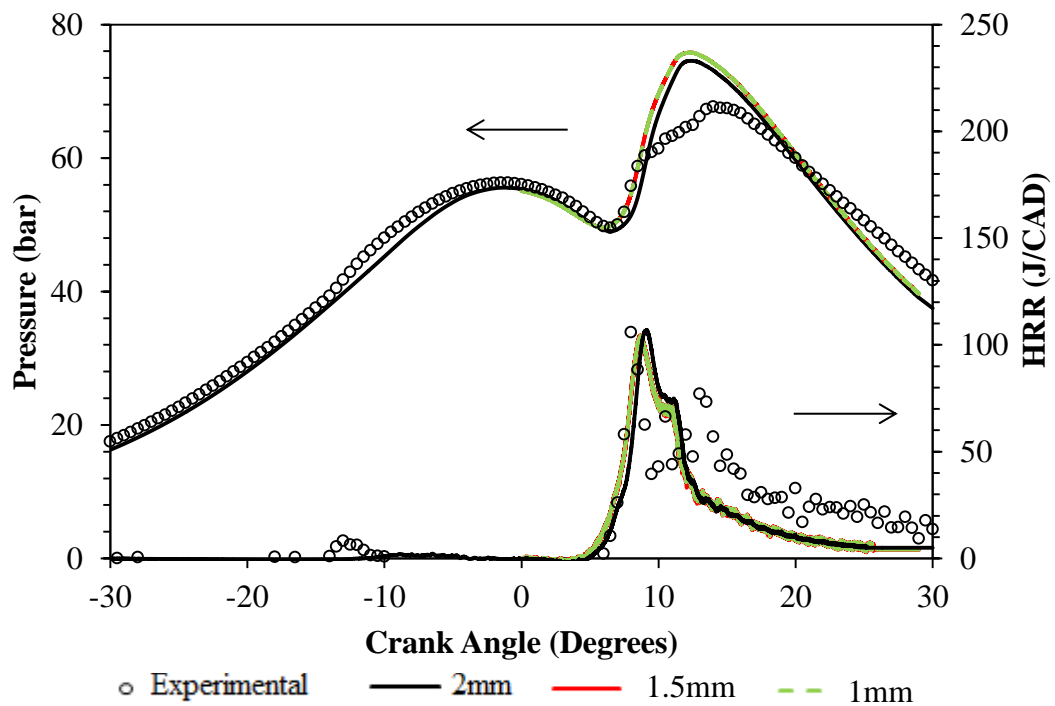


Figure 8-2: Measured and simulated pressure and HRR profiles using different mesh resolutions.

Table 8-3: Details of meshes with different grid sizes.

Grid Size	Number of grids at TDC	Estimated Runtime from -30° to +30° ATDC (Hours ^a)
2 mm	11,532	35
1.5 mm	16,284	78
1 mm	23,940	160

^aSimulations are performed using a 6-core PC with 16 GB RAM and 3.4 GHz processing speed without the use of parallel computing.

Figure 8-2 reveals that the computed pressure and HRR profiles before SOI are identical. However, slight deviations in ID predictions are observed whereby mesh with coarse grids produces longer ID as compared to the semi-fine and fine meshes. Here, ID is defined as the time interval between the SOI and the start of combustion (SOC) where fuel/air mixture is ignited. When the grid size is reduced, improvements in ID predictions are obtained with good agreement with the measurements. In spite of these, the estimated T_C for semi-fine and fine meshes are approximately 2.2 times and 4.5 times greater than that of the coarse mesh, respectively, as demonstrated in Table 8-3. Nonetheless, the coarse mesh configuration is not implemented here despite its corresponding shorter T_C . Based on the results shown in Figure 8-2, grid independence is achieved when semi-fine mesh is applied, and further mesh refinement does not contribute to significant improvement in the predictions. The associated computational time cost using the semi-fine mesh is still significantly high which requires approximately 78 h to complete the simulations from -30° to $+30^\circ$ ATDC. Therefore, the mapFields utility of OpenFOAM-2.0.x solver is applied to map the corresponding fields of a finer mesh to a coarser mesh. As such, the number of cells in the sector mesh is greatly reduced while retaining the accuracy of the target fields. Here, the semi-fine mesh with 1.5 mm grid size is selected as the source for field mapping and the resulting mesh consists of 2,028 grids at TDC. As demonstrated in Figure 8-3, a high level of result accuracy is retained in the predictions of pressure and HRR profiles and this mesh is hence selected for the subsequent engine simulations in Section 8.3.

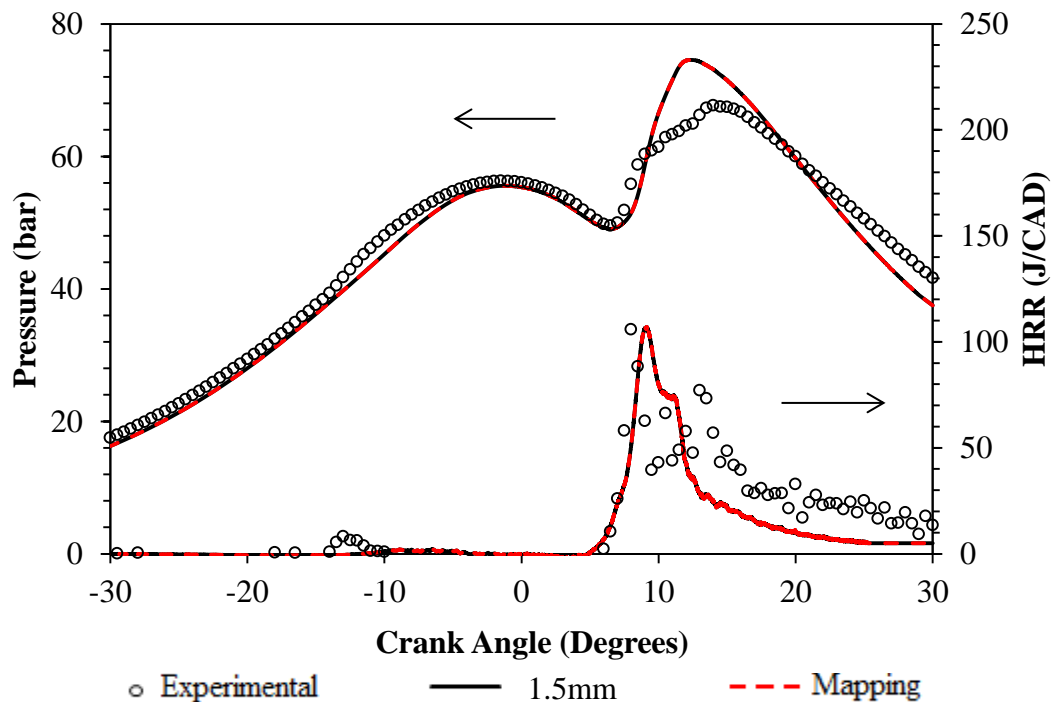


Figure 8-3: Measured and simulated pressure and HRR profiles using computational grids which are generated with/without field mapping.

8.2.2 Parametric Study II: CFD Time Step

It is noteworthy that an adequately small CFD time-step size is essential to accurately resolve the fuel combustion and soot emission characteristics. Consequently, three CFD time-step sizes are examined in this section, which include time-step sizes of 0.005 CAD, 0.002 CAD and 0.001 CAD. The CADs can be converted into seconds using the following equation:

$$1 \text{ CAD } [^\circ] = \frac{1}{6 \times \text{Engine Speed } [\text{rev}/\text{min}]} [\text{s}] \quad (8-1)$$

Engine speed of 1,600 rev/min is employed in this study. Hence, the associated time-step sizes of 0.005 CAD, 0.002 CAD and 0.001 CAD are equivalent to 0.5 μs , 0.2 μs and 0.1 μs , respectively. It is found that independent results are obtained when time-step size of 0.002 CAD is applied in the simulations, as demonstrated in Figure 8-4. Implementation of smaller time-step size than that does not provide significant improvement on the results. As a result, time-step size of 0.002 CAD is chosen for the subsequent modelling work in Section 8.3.

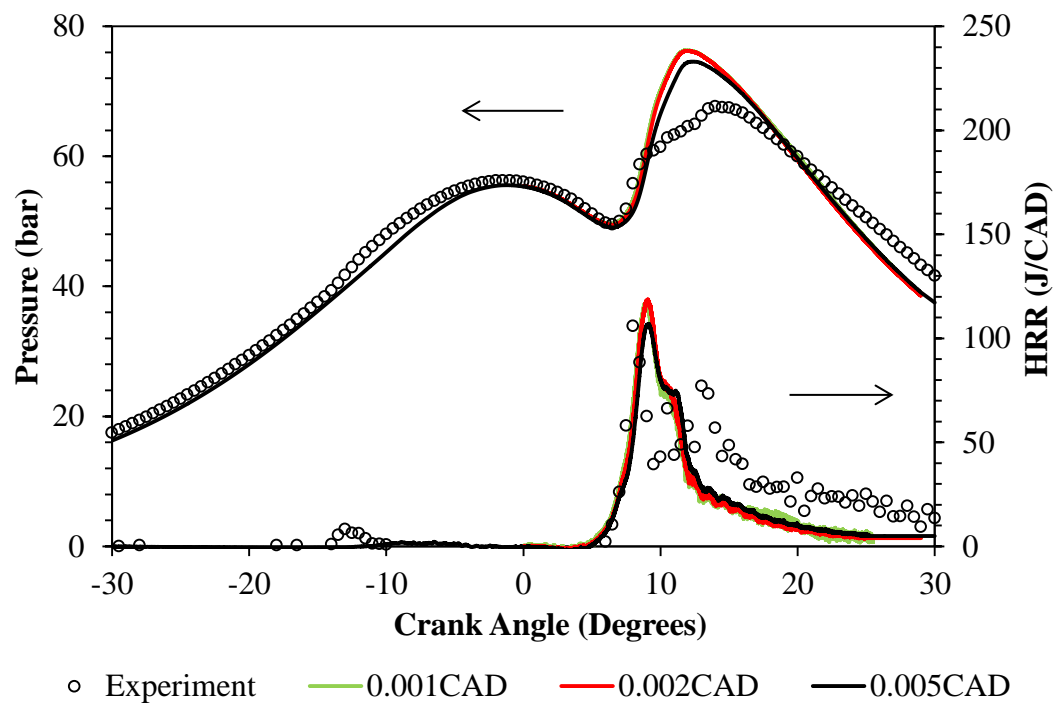


Figure 8-4: Measured and simulated pressure and HRR profiles using different time steps.

8.2.3 Parametric Study III: Droplet Breakup Model

In this study, the Reitz and Diwakar model is applied to simulate the fuel droplet breakup process. Here, the time factor constant for stripping breakup, C_S , is varied and the corresponding influences on the pressure and HRR predictions are shown in Figure 8-5.

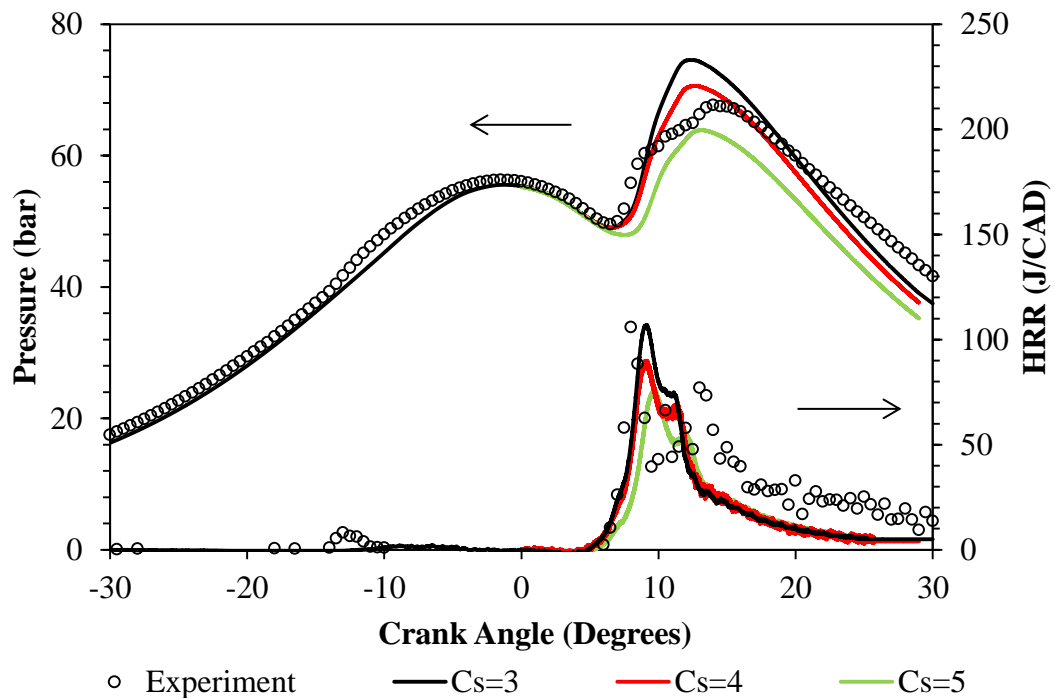


Figure 8-5: Measured and simulated pressure and HRR profiles using different C_S values.

Based on the results shown in Figure 8-5, decrement in peak pressure is observed when C_S value is increased. Similar trend is also observed in the simulated peak HRR. As discussed in Section 6.2.4, increment in C_S value leads to longer characteristic time scale, τ_b , of the break-up process. As a consequence, the fuel droplet breakup rate is decreased which reduces the amount of fuel burned during premixed combustion (PMC) phase, leading to lower peak pressure and HRR. In this study, C_S of 3.8 is selected for the subsequent engine simulations.

8.2.4 Parametric Study IV: Turbulence Model

The RNG k - ϵ turbulence model is employed in this study. Here, the turbulence model constant, $C_{1\epsilon}$, is varied and its effects on the simulated pressure and HRR profiles are monitored. The results are demonstrated in Figure 8-6.

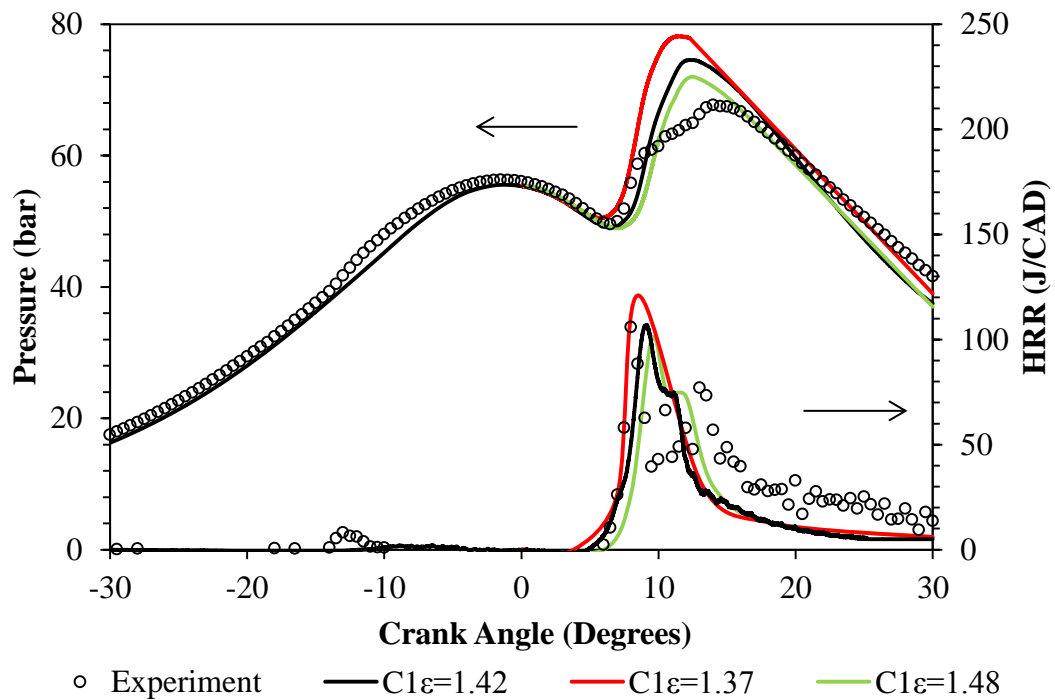


Figure 8-6: Measured and simulated pressure and HRR profiles using different $C_{1\varepsilon}$ values.

In Figure 8-6, it is observed that the computed peak pressure and HRR decreases with increasing $C_{1\varepsilon}$ value. In this study, the default $C_{1\varepsilon}$ value of the RNG $k-\varepsilon$ model, which has a value of 1.42, is selected for the following modelling studies. The default value is found to be sufficient to reproduce the pressure and HRR profiles in this work.

8.2.5 Best-Fit Numerical Setups

Based on the parametric studies performed in Sections 8.2.1 to 8.2.4, a set of best-fit numerical setups for the successive 3-D internal combustion engine simulations is obtained. This is listed in Table 8-4.

Table 8-4: Best-fit numerical setups for 3-D engine simulations.

Numerical Setups	Details
Mesh resolution [mm]	0.25 mm at TDC
Timestep [CAD]	0.002
Primary & Secondary Spray Breakup	Reitz Diwakar ($C_S = 3.8$)
Turbulence	RNG $k-\varepsilon$ ($C_{1\varepsilon} = 1.42$)
Ignition and Combustion	MCDS2 (diesel); MCBSv2 (biodiesel)
Soot Formation	Multistep

8.3 3-D Internal Combustion Simulations

Upon model validations under spray combustion phenomena, both MCDS2 diesel surrogate fuel model and MCBSv2 biodiesel surrogate fuel model are henceforth applied in this section to study the combustion and soot formation events in a light-duty, DI diesel engine. Here, the simulated results are validated against the experimental measurements obtained from diesel combustion in a light-duty diesel engine [189]. The experimental data was obtained at closed part of engine cycle which starts at IVC and ends at exhaust valve open (EVO). The SOI timing is retained at $+2^\circ$ ATDC and pilot injection is employed prior to the main fuel injection event with a split main ratio of 98/2. The interval between pilot and main fuel injections is fixed at 25° . Exhaust gas recirculation is not employed in this study. It is evident that the experiment was conducted for diesel combustion while biodiesel is also employed in this work. This is to compare the combustion and soot formation behaviours of biodiesel with that of diesel under the same operating conditions. Hence, the MCDS2 diesel surrogate model is used as a baseline for evaluation of the biodiesel fuel blend here. MCDS2 is first validated in terms of pressure and HRR. These are the key criteria to accurately predict the in-cylinder soot formation and oxidation events. This is followed by the comparison of the computed soot density produced by MCDS2 with the measurements at EVO. Upon validations of the diesel surrogate fuel model, the

same numerical settings are applied in the simulations using MCBSv2. The actual thermo-physical properties for RME are applied in this section.

8.3.1 In-Cylinder Combustion Event

The predicted pressure and HRR are compared with the experimental measurements in Figure 8-7. The simulated ID and location of peak HRR for both diesel and biodiesel cases are seen to be similar to the experimental results at PMC phase. It is observed that ID of MCBSv2 is slightly shorter than that of MCDS2. The location of peak HRR predicted by MCBSv2 is observed to be advanced by 0.5 CAD as compared to the computation of MCDS2. The deviations between the predicted and measured peak pressures for both cases are maintained to within 10 %. Despite the over-estimation in the computation of peak cylinder pressure, the simulated peak HRR for both cases are comparable to the measurement. Apart from that, it is found that the computed peak pressure and peak HRR are comparatively lower with the use of MCBSv2. The reasons are twofold. First, MCDS2 consists of toluene which is difficult to ignite. Therefore, ignition timing is retarded which increases the amount of fuel burned during PMC phase, leading to higher peak pressure and HRR. Second, ID prediction of MCBSv2 is shorter. Thus, the period of time for mixing process is shortened which eventually contributes to lower peak pressure and HRR. Here, the adequate prediction of peak HRR location henceforth permits accurate computation of soot onset.

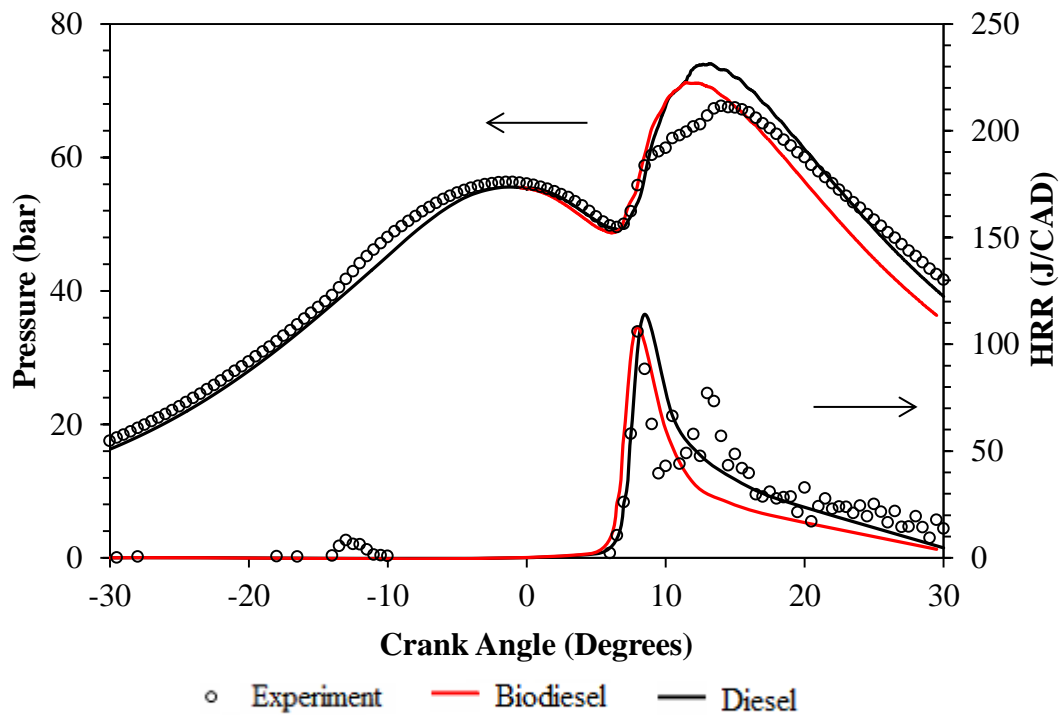


Figure 8-7: Experimental and simulated pressure and HRR curves.

8.3.2 In-Cylinder Soot Formation Event

Following that, the predicted temporal soot evolutions by the diesel and biodiesel surrogate fuel models are demonstrated in Figure 8-8. The soot density predictions at EVO for both cases are also compared against the experimental data which is measured based on the exhaust Filter Smoke Number (FSN) using an AVL 415S Variable Sampling Smoke Meter. The calculation of soot density is expressed in Equation 8-2 [190]:

$$\text{Soot density} \left[\frac{\text{g}}{\text{m}^3} \right] = \frac{K}{1000} \times \frac{4.95}{0.405} \times \text{FSN} \times e^{(0.38 \times \text{FSN})} \quad (8-2)$$

where $K = 1$ when $\text{FSN} \leq 8$ and $K = 1 + [0.5(\text{FSN} - 8)]^{10}$ when $\text{FSN} > 8$. Here, C_2H_2 is designated as the soot precursor species for the biodiesel combustion modelling studies. Meanwhile, C_6H_6 is present in the diesel surrogate fuel model and so it is selected as the soot precursor in the respective modelling work. Furthermore, C_2H_2 is applied as the soot surface growth species for both cases to compute the mass addition on soot particle surface while OH and O_2 are applied as the soot oxidant species to compute the soot mass destruction.

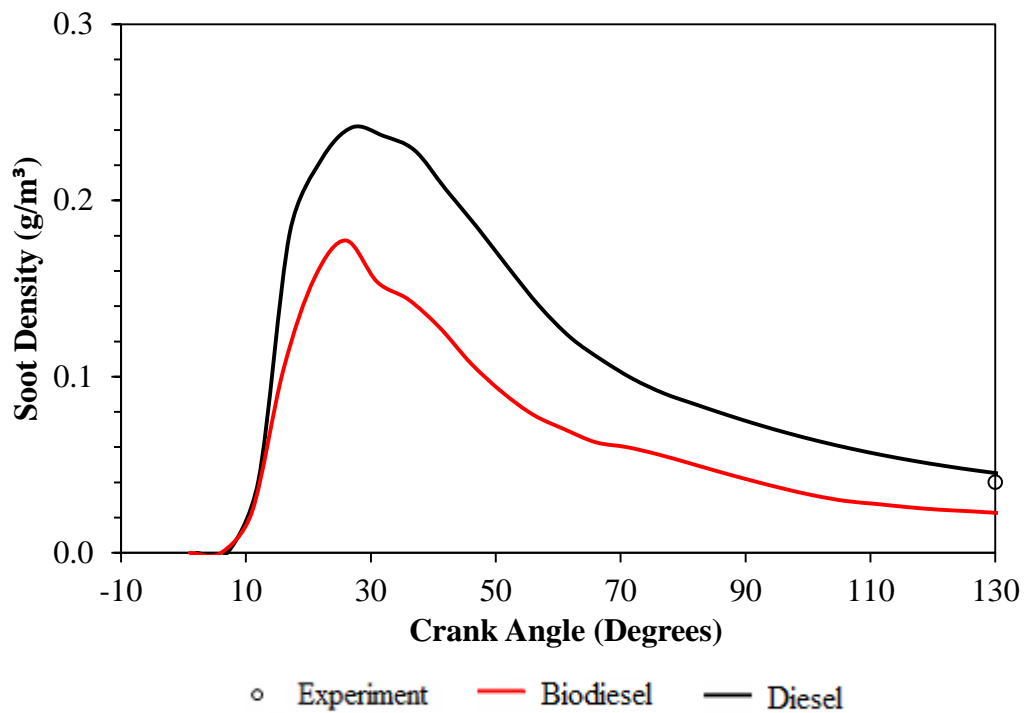


Figure 8-8: In-cylinder temporal soot evolutions for diesel and biodiesel combustions.

In Figure 8-8, it is observed that the temporal soot evolutions for both diesel and biodiesel cases are similar whereby the computed soot onsets occur when HRR peaks during PMC phase. The locations of the peak soot content for the diesel and biodiesel cases are recorded at 25 and 24 CADs ASI, respectively. The predicted soot density at EVO is approximately 11 % greater than the measurement for diesel combustion while the computation for biodiesel combustion is under-predicted by 43 %. Apart from that, the peak soot production for diesel combustion is 1.4 times greater than that for biodiesel combustion while the rates of drop of net soot production rate are comparable for both cases. Hence, a higher engine-out soot level at EVO is seen for the diesel case. The spatial soot evolutions at various CADs for both diesel and biodiesel cases are shown in Figure 8-9. It is observed that the overall soot production for diesel combustion is greater than that produced from biodiesel combustion. The soot is mostly formed near the cylinder head and the edge of the piston bowl for both cases. A significant amount of soot is formed and accumulates at the tip of fuel jet where rich mixtures are present due to continuous replenishment of injected fuel. This

corresponds well with the observations obtained from the experiment carried out by Dec and Espey [191]. Subsequently, the soot cloud moves up to the cylinder head region due to charge motion during expansion stroke [189]. Reduction in the total soot concentration is also observed after 20 CAD ASI as a result of soot oxidation process during expansion stroke.

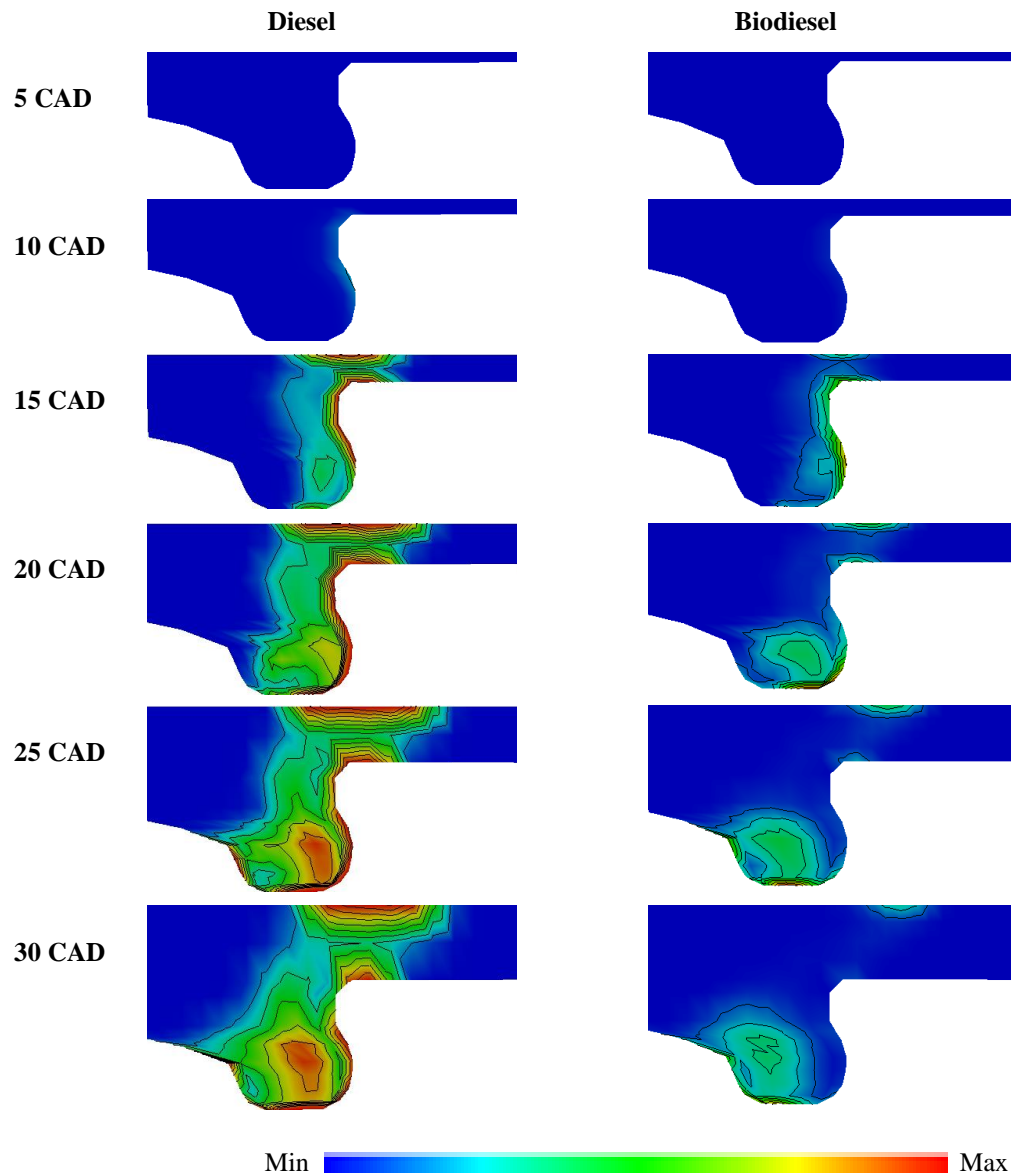


Figure 8-9: In-cylinder spatial soot evolutions for diesel and biodiesel combustions.

The temporal C_2H_2 mass fractions for both fuel combustions are illustrated in Figure 8-10. The C_2H_2 profiles for both cases correspond well with the soot

predictions in Figure 8-8 where the overall C_2H_2 mole fractions of diesel combustion are comparatively higher. However, greater amount of O_2 concentrations is obtained when the engine is fuelled with biodiesel. This can be attributed to the higher oxygen content of biodiesel. Consequently, the soot oxidation process is accelerated owing to the presence of additional oxygen atoms in biodiesel [23,169] and eventually reduces the engine-out soot level. The findings here agree with the experimental results of Nerva et al. [169] in which the fuel oxygenated effects have resulted in lower soot production for biodiesel combustion in comparison to diesel.

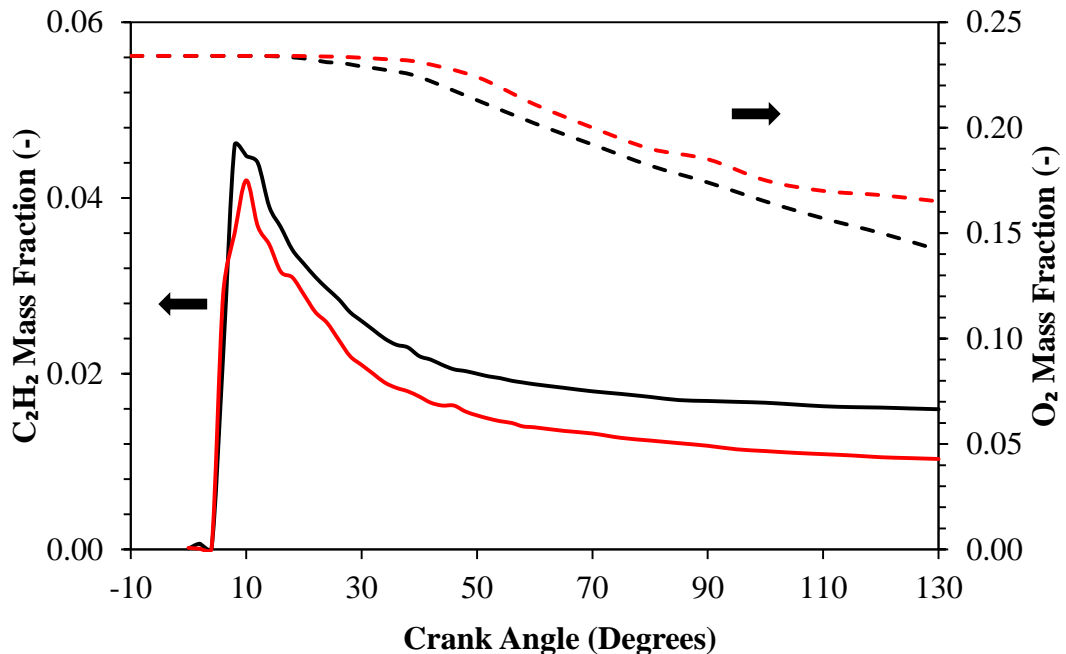


Figure 8-10: Predicted C_2H_2 (–) and O_2 (–) mass fractions for diesel (black) and biodiesel (red) fuel combustions.

8.4 Concluding Remarks

In this chapter, the fidelity of the multi-component diesel and biodiesel surrogate fuel models derived in the previous chapters are further evaluated in 3-D internal combustion engine simulations. The combustion and soot formation events in a light-duty, DI diesel engine are studied. The performance of the diesel and biodiesel surrogate fuel models is compared under the same operating conditions.

The simulated ID and HRR for both diesel and biodiesel cases agree reasonably well with those of the experimental results. However, the computed peak pressure and HRR predictions for biodiesel combustion are found to be lower than diesel due to advanced ignition timing. In addition, the overall soot production of biodiesel is 1.4 times lower than that of diesel owing to its higher oxygen content in the fuel. The numerical results obtained here offer a benchmark for diesel engine case studies in terms of ignition, combustion and soot formation events using diesel and biodiesel. The proposed integrated diesel and biodiesel surrogate fuel models have shown to be appropriate for diesel engine applications.

CHAPTER 9

CONCLUSIONS AND FUTURE WORK

9.1 Conclusions

The conclusion first deals with the appraisal of various DRG-based mechanism reduction techniques using a detailed single-component diesel surrogate fuel model (i.e. HXN), and a detailed multi-component biodiesel surrogate fuel model (i.e. MDBIO). The outcomes from the work undertaken are reported in Section 9.1.1. The second part of the conclusions deals with the development and validation of a systematic chemical kinetic mechanism reduction scheme for small- (i.e. ethylene) and large-scale (i.e. diesel, biodiesel) mechanisms. The corresponding validation results in 0-D simulations are reported in Section 9.1.2. Next, findings on the 2-D spray combustion simulations are presented in Section 9.1.3. In addition, core efforts in developing multi-component diesel surrogate fuel models and their validation results are summarised in Section 9.1.4. Apart from that, fidelity of the multi-component diesel and biodiesel surrogate fuel models derived from the mechanism reduction scheme is further assessed in terms of combustion and soot formation performances in a light-duty, DI diesel engine. The main findings obtained from the numerical simulations are highlighted in Section 9.1.5. Lastly, the suggestions for future work are addressed in Section 9.2.

9.1.1 Appraisal of Various DRG-Based Mechanism Reduction Techniques

- The performance of the DRG-based mechanism reduction techniques such as DRG, DRGEP, DRGASA and DRGEP SA are evaluated with respect to reduction scale, T_C and accuracy in ID predictions.
- A multi-stage DRG is able to provide greater reduction in N_S and T_C by 0.6 % and 1.4 %, respectively, in comparison to a two-stage DRG. Nonetheless, additional MATLAB runtime (i.e. 3 hours) is required with an additional DRG stage since the amount of sampling points for computation has increased. Therefore, it is suggested that a two-stage

DRG is appropriate for huge mechanism reduction since its accuracy in ID timing predictions is adequate and the size of the derived reduced mechanisms is only marginally larger than the reduced mechanisms generated through multi-stage DRG.

- In comparison to DRG, brute-force sensitivity analysis of DRGASA is able to further reduce the mechanism by identifying species with minor importance to the target species and global parameters. Nevertheless, the application of brute-force sensitivity analysis of DRGASA requires expensive time-cost and computational power.
- The current results show that greater reduction is achieved with the use of DRGEP as compared to DRG, while maintaining the accuracy of the model within the user-specified error limit. In DRGEP methodology, the dependence of one species on another is based on its contribution to overall production or consumption rate. Interrelated species that are situated far from each other might be more important than those directly connected to the targets. In contrast, DRG assumes that every selected species is equally significant and hence the group of strongly coupled species has to be fully retained, which may not be necessary.
- DRGEPASA offers the highest reduction scale among all the reduction methodologies. Reductions of 82.84 % and 88.63 % in terms of N_S are achieved using the detailed HXN and MDBIO mechanisms, respectively. On the other hand, the average T_C in the 0-D simulations is successfully reduced by 83.64 % and 91.67 % by applying the reduced HXN and MDBIO mechanisms generated from DRGEPASA methodology, respectively. However, the brute-force sensitivity analysis of DRGEPASA is computationally expensive and it is not favourable for application on huge mechanisms.
- Size of the reduced mechanisms generated from these DRG-based mechanism reduction techniques is not minimal yet for the multi-dimensional CFD applications.

9.1.2 Development and Validations of a Systematic Chemical Kinetic Mechanism Reduction Scheme for Small- and Large-Scale Mechanisms

- An integrated chemical kinetic mechanism reduction scheme is successfully formulated for large-scale mechanisms such as the detailed HXN and MDBIO mechanisms. The reduction scheme consists of five stages including DRGEP with Dijkstra algorithm, isomer lumping, reaction path analysis, DRG and adjustment of rate constant.
- A reduced single-component diesel surrogate fuel model (i.e. HXNv1) with 49 species and 97 elementary reactions, as well as a reduced multi-component biodiesel surrogate fuel model (i.e. MCBSv1) with 68 species and 163 elementary reactions, is successfully derived using the proposed mechanism reduction scheme. Here, only auto-ignition condition is applied as the data source for mechanism reduction. An average of 97 % reduction in mechanism size as well as T_C is attained in 0-D closed homogeneous batch reactor simulations. ID timing predictions by the reduced models are in good agreement with those predicted by the detailed models.
- However, it is found that species concentration profiles predicted by HXNv1 and MCBSv1 do not agree well with those of the detailed models. The deviations between the measurements and predictions are greater than 80 %. Hence, JSR is included as an additional criterion for the reduction work apart from the auto-ignition condition. As a result, an improved diesel surrogate fuel model (i.e. HXNv2) with 79 species and 289 elementary reactions, as well as an improved biodiesel surrogate fuel model (i.e. MCBSv2) with 80 species and 252 elementary reactions, is successfully derived. The results show that the predictions of ID timings and species concentration profiles by HXNv2 and MCBSv2 have improved as compared to those of HXNv1 and MCBSv1. The maximum deviation in ID and species concentration predictions as compared to those of the detailed mechanisms is recorded at 40 %.
- The proposed mechanism reduction scheme is also applied on an ethylene mechanism to study its applicability on small-scale mechanism reduction.

Flame temperatures under a wide range of Φ are investigated in 1-D simulations. A reduced model with 26 species is obtained. The reduced model is able to replicate the flame temperature profile with a maximum deviation of 2.8 % as compared to the detailed model. In addition, the reduced ethylene model is further validated in 0-D chemical kinetic simulations under both auto-ignition and JSR conditions. Satisfactory results are achieved in view of its simplified chemistry.

9.1.3 Validations of the Single-Component Diesel and Multi-Component Biodiesel Surrogate Fuel Models in 2-D Spray Combustion Simulations

- Fidelity of the single-component diesel (i.e. HXNv1, HXNv2) and multi-component biodiesel (i.e. MCBSv1, MCBSv2) surrogate fuel models is evaluated in 2-D spray combustion simulations. The simulation results are compared to the experimental measurements of D2 for diesel combustion and SME for biodiesel combustion.
- Simulation results show that both LPL and VPL are replicated for non-reacting diesel and biodiesel fuel spray simulations.
- For reacting diesel fuel spray, IDs predicted by both HXNv1 and HXNv2 are advanced when ambient temperatures of 900 K and 1000 K are applied. The maximum deviations between the measurements and predictions by HXNv1 and HXNv2 are 45 % and 18 %, respectively. Apart from that, LOLs predicted by HXNv2 are in closer agreements with the measurements as compared to HXNv1. This can be attributed to the improved predictions of HXNv2 in fuel and oxidiser concentrations during model formulation, in comparison with those predicted by HXNv1. In addition, it is found that the qualitative trend of SVF prediction by HXNv2 are in good agreement with those obtained from the experiment in terms of shape and soot location.
- The experimental data for reacting biodiesel fuel spray are obtained from SME combustion. However, it is noted that the compositions of the biodiesel surrogate fuel models are initially set according to those of RME which serves as the target fuel in this work. Consequently, the

compositions of the surrogate models are first adjusted according to those of SME for validation purpose, followed by the simulations using fuel compositions of RME while retaining the same numerical setups. Significant improvements in ID predictions are obtained with the use of MCBSv2 for both SME and RME cases. In contrast, the deviations between the measured and predicted LOLs by MCBSv1 and MCBSv2 are maintained to within 20 %. Following that, SVF distributions predicted by MCBSv2 agree closely with those of the experimental measurements qualitatively as compared to the predictions of MCBSv1 for both SME and RME cases. However, the predicted SVFs for SME combustion are comparatively lower as its composition of unsaturated fatty acids is lower.

9.1.4 Development and Validations of Multi-Component Diesel Surrogate Fuel Models

- Two multi-component diesel surrogate fuel models, namely MCDS1 and MCDS2 with different fuel compositions and components have been introduced. MCDS1 model consists of straight- (HXN) and branched- (HMN) alkanes while MCDS2 consists of aromatic hydrocarbon (toluene), straight- (HXN), branched- (HMN) and cyclo- (CHX) alkanes.
- Surrogate fuel models with different CN values can be produced through blending of HXN and HMN. In addition, CHX and toluene are incorporated into MCDS2 model to achieve compositional match and to improve soot formation predictions.
- Each reduced mechanism of HXN, HMN and CHX is developed using the five-stage chemical kinetic mechanism reduction scheme. Each constituent mechanism and the integrated models are validated in 0-D chemical kinetic simulations. The overall ID timings and species concentrations at the test conditions agree well with those calculated using the respective detailed mechanisms and experimental measurements.
- The fidelity of both multi-component diesel surrogate fuel models is further assessed in the 2-D spray combustion simulations. Numerical results reveal that the MCDS1 surrogate model is sensitive to the change

of CN. The predicted ID and LOL correspond well with the variation of CN. Next, ID, LOL and SVF calculated using MCDS1 and MCDS2 are validated against constant volume combustion chamber experimental data. ID and LOL predictions given by both surrogate models agree reasonably well with the D2 measurements.

- It is observed that MCDS2 surrogate model is able to provide better predictions in soot formation events than MCDS1 due to the inclusion of aromatic and cyclo-alkane components. It is revealed that $\text{ratio}_{\text{SVF}}$ of 1.6 is obtained for D2 fuel combustion when the ambient temperature increases from 900 K to 1000 K with the absence of aromatic and cyclo-alkane components. The simulated $\text{ratio}_{\text{SVF}}$ increases to 2.1 when both components are incorporated into the base mechanism as the inclusion of these two components provides alternative pathways to form rich species such as C_2H_2 and C_6H_6 .
- The effects of including aromatic and cyclo-alkane components in the surrogate model on soot formation events are highlighted. It is demonstrated that MCDS2 is a potential surrogate model for D2 fuel. Nonetheless, additional work is required to improve the coupled MCDS2-soot model in simulating the complex soot formation phenomenon.

9.1.5 Further Validations of the Multi-Component Diesel and Biodiesel Surrogate Fuel Models in 3-D Internal Combustion Engine Simulations

- The fidelity of the MCDS2 diesel surrogate fuel model and the MCBSv2 biodiesel surrogate fuel model are further evaluated in the 3-D internal combustion engine simulations. The combustion and soot formation performances of the diesel and biodiesel fuels are studied using a single main fuel injection strategy and retarded injection timing in a light-duty, DI diesel engine.
- The MCDS2 diesel surrogate fuel model is first validated against the experimental measurements in terms of pressure and HRR which are the main criteria to precisely predict the in-cylinder soot formation and oxidation events. Following that, the MCBSv2 biodiesel surrogate fuel

model is applied in the simulations using the same operating conditions as diesel combustion. It is found that the peak pressure and HRR predictions for biodiesel are lower than those of diesel due to the advanced ignition timing and the absence of aromatic compounds in the model.

- Furthermore, it is observed that the soot production of biodiesel is also lower than that of diesel. This can be attributed to its higher oxygen content found in the fuel due to the presence of additional oxygen atoms which accelerates the soot oxidation process.

9.2 Suggestions for Future Work

Five-Stage Chemical Kinetic Mechanism Reduction Scheme

An integrated chemical kinetic mechanism reduction scheme has been developed to generate compact yet comprehensive reduced models for both diesel and biodiesel fuels. The criteria for the mechanism reduction procedure have been focusing on engine-like conditions, particularly at high-pressure conditions. Hence, additional test conditions can be included to improve model predictions over a wider range of operating conditions such as low-pressure conditions.

MCDS2 Diesel Surrogate Fuel Model

It is observed that the inclusion of cyclo-alkane and aromatic compounds in the MCDS2 surrogate model improved the overall soot formation predictions in the 2-D spray combustion simulations. Higher $\text{ratio}_{\text{SVF}}$ is obtained when the ambient temperature changes from 900 K to 1000 K with the use of MCDS2. Nonetheless, the predicted $\text{ratio}_{\text{SVF}}$ is under-predicted in comparison to the experimental measurement in which $\text{ratio}_{\text{SVF}}$ of more than 3 is captured. Further improvement on the coupled MCDS2-soot model is suggested to simulate the complex soot formation phenomenon.

MCBSv2 Biodiesel Surrogate Fuel Model

Similar to the MCDS2 diesel surrogate fuel model, the computed $\text{ratio}_{\text{SVF}}$ is yet under-predicted as compared to that obtained from experiments. A coupled MCBSv2-soot model is suggested to improve the model predictions in soot formation/oxidation events.

3-D Internal Combustion Engine Simulations

The multi-component diesel and biodiesel surrogate fuel models developed here have been validated across a wide range of engine conditions in the present work. The integrated surrogate fuel models are ready to be used in future studies to parametrically investigate effects of different split-main injection ratios, SOI timings and dwell periods on the combustion and emission processes.

REFERENCES

- [1] S. Shafiee, E. Topal, When will fossil fuel reserves be diminished?, *Energy Policy*. 37 (2009) 181–189. doi:10.1016/j.enpol.2008.08.016.
- [2] N. Lior, Energy resources and use: The present situation and possible paths to the future, *Energy*. 33 (2008) 842–857. doi:10.1016/j.energy.2007.09.009.
- [3] A.S. Tomlin, T. Turányi, M.J. Pilling, Low-temperature combustion and autoignition, Vol. 35, Elsevier, 1997. doi:10.1016/S0069-8040(97)80019-2.
- [4] O. Herbinet, W.J. Pitz, C.K. Westbrook, Detailed chemical kinetic oxidation mechanism for a biodiesel surrogate, *Combust. Flame*. 154 (2008) 507–528. doi:10.1016/j.combustflame.2008.03.003.
- [5] J. Guthrie, P. Fowler, R. Sabourin, Gasoline and diesel fuel survey (2003).
- [6] N. Grumman, Diesel fuel oils, 2003 (2004).
- [7] C.K. Westbrook, W.J. Pitz, O. Herbinet, H.J. Curran, E.J. Silke, A comprehensive detailed chemical kinetic reaction mechanism for combustion of n-alkane hydrocarbons from n-octane to n-hexadecane, *Combust. Flame*. 156 (2009) 181–199. doi:10.1016/j.combustflame.2008.07.014.
- [8] H.J. Curran, P. Gaffuri, W.J. Pitz, C.K. Westbrook, A comprehensive modeling study of n-heptane oxidation, *Combust. Flame*. 114 (1998) 149–177. doi:10.1016/S0010-2180(97)00282-4.
- [9] C.V. Naik, K. Puduppakkam, E. Meeks, L. Liang, Ignition quality tester guided improvements to reaction mechanisms for n-alkanes: n-Heptane to n-hexadecane, (2012). doi:10.4271/2012-01-0149.
- [10] D.L. Siebers, Scaling liquid-phase fuel penetration in diesel sprays based on mixing-limited vaporization, *SAE Tech. Pap.* 1999-01-0528 (1999).

doi:10.4271/1999-01-0528.

- [11] D.L. Siebers, Liquid-phase fuel penetration in diesel sprays, SAE Tech. Pap. 980809 (1998).
- [12] J.T. Farrell, N.P. Cernansky, F.L. Dryer, C.K. Law, D.G. Friend, C.A. Hergart, et al., Development of an experimental database and kinetic models for surrogate diesel fuels, SAE Tech. Pap 2007-01-0201 (2007).
- [13] A. Ristori, P. Dagaut, M. Cathonnet, The oxidation of n-hexadecane: experimental and detailed kinetic modeling, Combust. Flame. 125 (2001) 1128–1137.
- [14] F.L. Dryer, Y. Ju, K. Brezinsky, R.J. Santoro, T.A. Litzinger, C.-J. Sung, Science-based design of fuel-flexible chemical propulsion/energy: Generation of comprehensive surrogate kinetic models and validation databases for simulating large molecular weight hydrocarbon fuels, AF Office of Scientific Research Final Report, Grant No. FA9550-07-1-0515, 2012.
- [15] M. Meijer, Characterization of n-heptane as a single component diesel surrogate fuel, Technical University of Eindhoven Automotive Technology, Graduation Thesis, 2010.
- [16] J. Galle, V. Sebastian, Influence of diesel surrogates on the behavior of simplified spray models, Proc. FISITA 2012 World Automot. Congr. 189 (2013) 361–374.
- [17] S. Kook, L.M. Pickett, Soot volume fraction and morphology of conventional, Fischer-Tropsch, coal-derived, and surrogate fuel at diesel conditions, SAE Int. J. Fuels Lubr. 5 (2012) 647–664. doi:10.4271/2012-01-0678.
- [18] R. Lemaire, A. Faccinetto, E. Therssen, M. Ziskind, C. Focsa, P. Desgroux, Experimental comparison of soot formation in turbulent flames of diesel and surrogate diesel fuels, Proc. Combust. Inst. 32 I (2009) 737–744. doi:10.1016/j.proci.2008.05.019.

- [19] H. Barths, H. Pitsch, N. Peters, 3D simulation of DI diesel combustion and pollutant formation using a two-component reference fuel, *Oil Gas Sci. Technol.* 54 (1999) 233–244. doi:10.2516/ogst:1999020.
- [20] P. Dagaut, M. Cathonnet, The ignition, oxidation, and combustion of kerosene: A review of experimental and kinetic modeling, *Prog. Energy Combust. Sci.* 32 (2006) 48–92. doi:10.1016/j.pecs.2005.10.003.
- [21] O. Mathieu, N. Djebaïli-Chaumeix, C.E. Paillard, F. Douce, Experimental study of soot formation from a diesel fuel surrogate in a shock tube, *Combust. Flame.* 156 (2009) 1576–1586. doi:10.1016/j.combustflame.2009.05.002.
- [22] W.J. Pitz, C.J. Mueller, Recent progress in the development of diesel surrogate fuels, *Prog. Energy Combust. Sci.* 37 (2011) 330–350. doi:10.1016/j.pecs.2010.06.004.
- [23] X. Cheng, H. Ng, S. Gan, J. Ho, Advances in computational fluid dynamics (CFD) modeling of in-cylinder biodiesel combustion, *Energy & Fuels.* 27 (2013) 4489–4506. doi:10.1021/ef4005237.
- [24] J.B. Heywood, *Internal combustion engine fundamentals*, 1988.
- [25] D.R. Tree, K.I. Svensson, Soot processes in compression ignition engines, *Prog. Energy Combust. Sci.* 33 (2007) 272–309. doi:10.1016/j.pecs.2006.03.002.
- [26] K.B. Showry, Soot processes in diesel engines - Review, *Int. J. Mech. Eng.* 3 (2015) 1–9.
- [27] G. Stiesch, *Modeling engine spray and combustion processes*, Springer Science & Business Media, 2013.
- [28] M.Y. Choi, A. Hamins, G.W. Mulholland, T. Kashiwagi, Simultaneous optical measurement of soot volume fraction and temperature in premixed flames, *Combust. Flame.* 99 (1994) 174–186.
- [29] H. Wang, M. Yao, Z. Yue, M. Jia, R.D. Reitz, A reduced toluene

- reference fuel chemical kinetic mechanism for combustion and polycyclic-aromatic hydrocarbon predictions, *Combust. Flame.* 162 (2015) 2390–2404. doi:10.1016/j.combustflame.2015.02.005.
- [30] G. Vishwanathan, R.D. Reitz, Modeling soot formation using reduced polycyclic aromatic hydrocarbon chemistry in n-heptane lifted flames with application to low temperature combustion, *J. Eng. Gas Turbines Power.* 131 (2009) 1–8. doi:10.1115/1.3043806.
- [31] C.K. Westbrook, W.J. Pitz, M. Mehl, H.J. Curran, Detailed chemical kinetic reaction mechanisms for primary reference fuels for diesel cetane number and spark-ignition octane number, *Proc. Combust. Inst.* 33 (2011) 185–192. doi:10.1016/j.proci.2010.05.087.
- [32] C.K. Westbrook, W.J. Pitz, H.J. Curran, Chemical kinetic modeling study of the effects of oxygenated hydrocarbons on soot emissions from diesel engines., *J. Phys. Chem. A.* 110 (2006) 6912–6922. doi:10.1021/jp056362g.
- [33] W. Liu, R. Sivaramakrishnan, M.J. Davis, S. Som, D.E. Longman, T.F. Lu, Development of a reduced biodiesel surrogate model for compression ignition engine modeling, *Proc. Combust. Inst.* 34 (2013) 401–409. doi:10.1016/j.proci.2012.05.090.
- [34] S. Kojima, Detailed modeling of n-butane autoignition chemistry, *Combust. Flame.* 99 (1994) 87–136. doi:10.1016/0010-2180(94)90084-1.
- [35] M.I. Strelkova, A.A. Safonov, L.P. Sukhanov, S.Y. Umanskiy, I.A. Kirillov, B.V. Potapkin, et al., Low temperature n-butane oxidation skeletal mechanism, based on multilevel approach, *Combust. Flame.* 157 (2010) 641–652. doi:10.1016/j.combustflame.2009.12.018.
- [36] Lawrence Livermore National Laboratory Physical and Life Sciences Directorate, Available from: https://www-pls.llnl.gov/?url=science_and_technology-chemistry-combustion-nc7h16.
- [37] Lawrence Livermore National Laboratory Physical and Life Sciences

- Directorate, Available from: https://www-pls.llnl.gov/?url=science_and_technology-chemistry-combustion_heptane_version_3.
- [38] P.A. Glaude, V. Conraud, R. Fournet, F. Battin-Leclerc, G.M. Côme, G. Scacchi, et al., Modeling the oxidation of mixtures of primary reference automobile fuels, *Energy & Fuels*. 16 (2002) 1186–1195. doi:10.1021/ef020025e.
- [39] F. Buda, R. Bounaceur, V. Warth, P.A. Glaude, R. Fournet, F. Battin-Leclerc, Progress toward a unified detailed kinetic model for the autoignition of alkanes from C4 to C10 between 600 and 1200 K, *Combust. Flame*. 142 (2005) 170–186. doi:10.1016/j.combustflame.2005.03.005.
- [40] K.E. Niemeyer, C.-J. Sung, M.P. Raju, Skeletal mechanism generation for surrogate fuels using directed relation graph with error propagation and sensitivity analysis, *Combust. Flame*. 157 (2010) 1760–1770. doi:10.1016/j.combustflame.2009.12.022.
- [41] T. Lu, C.K. Law, Linear time reduction of large kinetic mechanisms with directed relation graph: n-Heptane and iso-octane, *Combust. Flame*. 144 (2006) 24–36. doi:10.1016/j.combustflame.2005.02.015.
- [42] R. Seiser, H. Pitsch, K. Seshadri, W.J. Pitz, H.J. Curran, Extinction and autoignition of n-heptane in counterflow configuration, *Proc. Combust. Inst.* 28 (2000) 2029–2037. doi:10.1016/S0082-0784(00)80610-4.
- [43] T. Lu, C.K. Law, Strategies for mechanism reduction for large hydrocarbons: n-heptane, *Combust. Flame*. 154 (2008) 153–163. doi:10.1016/j.combustflame.2007.11.013.
- [44] K.M. Pang, H.K. Ng, S. Gan, Development of an integrated reduced fuel oxidation and soot precursor formation mechanism for CFD simulations of diesel combustion, *Fuel*. 90 (2011) 2902–2914. doi:10.1016/j.fuel.2011.04.027.
- [45] U.C. Müller, N. Peters, A. Liñán, Global kinetics for n-heptane ignition at high pressures, *Symp. Combust.* 24 (1992) 777–784.

doi:10.1016/S0082-0784(06)80095-0.

- [46] T. Lu, C.K. Law, Toward accommodating realistic fuel chemistry in large-scale computations, *Prog. Energy Combust. Sci.* 35 (2009) 192–215. doi:10.1016/j.pecs.2008.10.002.
- [47] E.M. Fisher, W.J. Pitz, H.J. Curran, C.K. Westbrook, Detailed chemical kinetic mechanisms for combustion of oxygenated fuels, *Proc. Combust. Inst.* 28 (2000) 1579–1586. doi:10.1016/S0082-0784(00)80555-X.
- [48] V. Shankar, B. Shankar, K. Al-qurashi, A. Ahmed, N. Atef, S.H. Chung, et al., Oxidation of alkane rich gasoline fuels and their surrogates in a motored engine, *Proc. Eur. Combust. Meet.* (2015) 1–6.
- [49] G. Moréac, E. Blurock, F. Mauss, Automatic generation of a detailed mechanism for the oxidation of n-decane, *Combust. Sci. Technol.* (2006) 8–11.
- [50] S.P. Zeppieri, S.D. Klotz, F.L. Dryer, Modeling concepts for larger carbon number alkanes: A partially reduced skeletal mechanism for n-decane oxidation and pyrolysis, *Proc. Combust. Inst.* 28 (2000) 1587–1595. doi:10.1016/S0082-0784(00)80556-1.
- [51] Y. Chang, M. Jia, Y. Liu, Y. Li, M. Xie, Development of a new skeletal mechanism for n-decane oxidation under engine-relevant conditions based on a decoupling methodology, *Combust. Flame.* 160 (2013) 1315–1332. doi:10.1016/j.combustflame.2013.02.017.
- [52] N.S. Titova, S.A. Torokhov, A.M. Starik, On kinetic mechanisms of n-decane oxidation, *Combust. Explos. Shock Waves.* 47 (2011) 129–146. doi:10.1134/S0010508211020018.
- [53] G. Bikas, N. Peters, Kinetic modelling of n-decane combustion and autoignition, *Combust. Flame.* 126 (2001) 1456–1475. doi:10.1016/S0010-2180(01)00254-1.
- [54] Z. Luo, S. Som, S.M. Sarathy, M. Plomer, W.J. Pitz, D.E. Longman, et al., Development and validation of an n-dodecane skeletal mechanism

- for spray combustion applications, *Combust. Theory Model.* 18 (2014) 187–203. doi:10.1080/13647830.2013.872807.
- [55] S. Som, D.E. Longman, Z. Luo, M. Plomer, T. Lu, Three dimensional simulations of diesel sprays using n-dodecane as a surrogate, in: *Fall Tech. Meet. of the Eastern States Sect. of the Combust. Inst.*, University of Connecticut, Storrs, CT, 2011.
- [56] I.E. Mersin, E.S. Blurock, H. Soyhan, A.A. Konnov, Automatic mechanism generation using pathways: Comparison with hand-generated tetradecane mechanism, 156 (2010).
- [57] Lawrence Livermore National Laboratory Physical and Life Sciences Directorate, Available from: https://www-pls.llnl.gov/?url=science_and_technology-chemistry-combustion-c8c16_n_alkanes.
- [58] R. Fournet, F. Battin-Leclerc, P.A. Glaude, B. Judenherc, V. Warth, G.M. Come, et al., The gas-phase oxidation of n-hexadecane, *Int. J. Chem. Kinet.* 33 (2001) 574–586.
- [59] M. Chaos, A. Kazakov, F.L. Dryer, Z. Zhao, S.P. Zeppieri, High temperature compact mechanism development for large alkanes: n-hexadecane, in: *6th Int. Conf. Chem. Kinet.*, 2005.
- [60] M. Meijer, J. Galle, L.M.T. Somers, J.G.. Griensven, S. Verhelst, High-speed characterization of ECN Spray A using various diagnostic techniques, 6 (2013) 1238–1248. doi:10.4271/2013-01-1616.
- [61] K. Schindler, Integrated Diesel European Action (IDEA): Study of diesel combustion, *SAE Tech. Pap.* 920591 (1992). doi:10.4271/920591.
- [62] W. Hentschel, K. Schindler, O. Haahtela, European diesel research IDEA-Experimental results from DI diesel engine investigations, *SAE Tech. Pap.* 941954 (1994). doi:10.4271/941954.
- [63] C. Hergart, H. Barths, N. Peters, Modeling the combustion in a small-bore diesel engine using a method based on representative interactive

- flamelets, SAE Tech. Pap. 1999-01-3550 (1999).
- [64] H. Curran, W. Pitz, C. Westbrook, C. V Callahan, F.L. Dryer, Oxidation of automotive primary reference fuels at elevated pressures, Proc. Combust. Inst. 27 (1998) 379–387.
- [65] P. Kirchen, M. Shahbakhti, C.R. Koch, A skeletal kinetic mechanism for PRF combustion in HCCI engines, Combust. Sci. Technol. 179 (2007) 1059–1083. doi:10.1080/00102200600910874.
- [66] H. Wang, M. Yao, R.D. Reitz, Development of a reduced primary reference fuel mechanism for internal combustion engine combustion simulations, Energy & Fuels. 27 (2013) 7843–7853. doi:10.1021/ef401992e.
- [67] Lawrence Livermore National Laboratory Physical and Life Sciences Directorate, Available from: https://www-pls.llnl.gov/?url=science_and_technology-chemistry-combustion-prf.
- [68] V.I. Golovitchev, M. Bergman, L. Montorsi, CFD modeling of diesel oil and DME performance in a two-stroke free piston engine, Combust. Sci. Technol. 179 (2007) 417–436. doi:10.1080/00102200600837242.
- [69] M. Chaos, Z. Zhao, A. Kazakov, P. Gokulakrishnan, M. Angioletti, F.L. Dryer, A PRF + toluene surrogate fuel model for simulating gasoline kinetics, in: 5th US Combust. Meet., 2007: pp. 1–19.
- [70] H. Wang, Q. Jiao, M. Yao, B. Yang, L. Qiu, R.D. Reitz, Development of an n-heptane/toluene/polyaromatic hydrocarbon mechanism and its application for combustion and soot prediction, Int. J. Engine Res. 14 (2013) 434–451. doi:10.1177/1468087412471056.
- [71] L.M. Pickett, D.L. Siebers, Fuel effects on soot processes of fuel jets at DI diesel conditions, SAE Tech. Pap. 2003-01-3080 (2003). doi:10.4271/2003-01-3080.
- [72] E. Ranzi, A. Frassoldati, A. Stagni, M. Pelucchi, A. Cuoci, T. Faravelli, Reduced kinetic schemes of complex reaction systems: Fossil and

- biomass-derived transportation fuels, *Int. J. Chem. Kinet.* 46 (2014) 512–542. doi:10.1002/kin.20867.
- [73] H. Wang, S.J. Warner, M.A. Oehlschlaeger, R. Bounaceur, J. Biet, P.A. Glaude, et al., An experimental and kinetic modeling study of the autoignition of α -methyl-naphthalene/air and α -methyl-naphthalene/n-decane/air mixtures at elevated pressures, *Combust. Flame.* 157 (2010) 1976–1988. doi:10.1016/j.combustflame.2010.04.007.
- [74] H.J. Curran, P. Gaffuri, W.J. Pitz, C.K. Westbrook, A comprehensive modeling study of iso-octane oxidation, *Combust. Flame.* 129 (2002) 253–280. doi:10.1016/S0010-2180(01)00373-X.
- [75] G. Côme, V. Warth, P.A. Glaude, Computer-aided design of gas-phase oxidation mechanisms- Application to the modeling of n-heptane and iso-octane oxidation, in: *Twenty-Sixth Symp. Combust.*, 1996: pp. 755–762.
- [76] Lawrence Livermore National Laboratory Physical and Life Sciences Directorate, Available from: https://www-pls.llnl.gov/?url=science_and_technology-chemistry-combustion-iso_octane_version_3.
- [77] Lawrence Livermore National Laboratory Physical and Life Sciences Directorate, Available from: https://www-pls.llnl.gov/?url=science_and_technology-chemistry-combustion-heptamethylnonane.
- [78] Lawrence Livermore National Laboratory Physical and Life Sciences Directorate, Available from: https://www-pls.llnl.gov/?url=science_and_technology-chemistry-combustion-cyclohexane.
- [79] A. El Bakali, M. Braun-Unkhoff, P. Dagaut, P. Frank, M. Cathonnet, Detailed kinetic reaction mechanism for cyclohexane oxidation at pressure up to ten atmospheres, *Proc. Combust. Inst.* 28 (2000) 1631–1638. doi:10.1016/S0082-0784(00)80561-5.
- [80] D. Bittker, Detailed mechanism of toluene oxidation and comparison

with benzene (1988).

- [81] P. Dagaut, G. Pengloan, A. Ristori, Oxidation, ignition and combustion of toluene: Experimental and detailed chemical kinetic modeling, *Phys. Chem. Chem. Phys.* 4 (2002) 1846–1854. doi:10.1039/b110282f.
- [82] W.J. Pitz, R. Seiser, J. W. Bozzelli, K. Seshadri, C.J. Chen, I.D. Costa, et al., Chemical kinetic study of toluene oxidation under premixed and nonpremixed conditions, Lawrence Livermore Natl. Lab. (2003) 1–20.
- [83] K. Nakakita, K. Akihama, W. Weissman, J.T. Farrell, Effect of the hydrocarbon molecular structure in diesel fuel on the in-cylinder soot formation and exhaust emissions, *Int. J. Engine Res.* 6 (2005) 187–205. doi:10.1243/146808705X7400.
- [84] S. Gail, M.J. Thomson, S.M. Sarathy, S.A. Syed, P. Dagaut, P. Diévert, et al., A wide-ranging kinetic modeling study of methyl butanoate combustion, *Proc. Combust. Inst.* 31 (2007) 305–311. doi:10.1016/j.proci.2006.08.051.
- [85] J.L. Brakora, Y. Ra, R.D. Reitz, J. McFarlane, C.S. Daw, Development and validation of a reduced reaction mechanism for biodiesel-fueled engine simulations, *SAE Int. J. Fuels Lubr.* 1 (2008) 675–702. doi:10.4271/2008-01-1378.
- [86] V.I. Golovitchev, J. Yang, Construction of combustion models for rapeseed methyl ester bio-diesel fuel for internal combustion engine applications., *Biotechnol. Adv.* 27 (2009) 641–55. doi:10.1016/j.biotechadv.2009.04.024.
- [87] S. Gail, S.M. Sarathy, M.J. Thomson, P. Diévert, P. Dagaut, Experimental and chemical kinetic modeling study of small methyl esters oxidation: Methyl (E)-2-butenate and methyl butanoate, *Combust. Flame.* 155 (2008) 635–650. doi:10.1016/j.combustflame.2008.04.007.
- [88] W.K. Metcalfe, S. Dooley, H.J. Curran, J.M. Simmie, A.M. El-Nahas, M. V Navarro, Experimental and modeling study of C₅H₁₀O₂ ethyl and methyl esters, *J. Phys. Chem. A.* 111 (2007) 4001–4014.

doi:10.1021/jp067582c.

- [89] H. Mohamed Ismail, H.K. Ng, S. Gan, T. Lucchini, A. Onorati, Development of a reduced biodiesel combustion kinetics mechanism for CFD modelling of a light-duty diesel engine, *Fuel*. 106 (2013) 388–400. doi:10.1016/j.fuel.2012.10.015.
- [90] G. Dayma, S. Gail, P. Dagaut, Experimental and kinetic modeling study of the oxidation of methyl hexanoate, *Energy & Fuels*. (2008) 1469–1479.
- [91] P. Glaude, O. Herbinet, S. Bax, J. Biet, Modeling of the oxidation of methyl esters—Validation for methyl hexanoate, methyl heptanoate, and methyl decanoate in a jet-stirred reactor, *Combust. Flame*. 157 (2010) 2035–2050. doi:10.1016/j.combustflame.2010.03.012.Modeling.
- [92] G. Dayma, C. Togbé, P. Dagaut, Detailed kinetic mechanism for the oxidation of vegetable oil methyl esters: new evidence from methyl heptanoate, *Energy & Fuels*. 23 (2009) 4254–4268. doi:10.1021/ef900184y.
- [93] G. Dayma, S.M. Sarathy, C. Togbé, C. Yeung, M.J. Thomson, P. Dagaut, Experimental and kinetic modeling of methyl octanoate oxidation in an opposed-flow diffusion flame and a jet-stirred reactor, *Proc. Combust. Inst.* 33 (2011) 1037–1043. doi:10.1016/j.proci.2010.05.024.
- [94] S.M. Sarathy, M.J. Thomson, W.J. Pitz, T. Lu, An experimental and kinetic modeling study of methyl decanoate combustion, *Proc. Combust. Inst.* 33 (2011) 399–405. doi:10.1016/j.proci.2010.06.058.
- [95] K. Seshadri, T. Lu, O. Herbinet, S. Humer, U. Niemann, W.J. Pitz, et al., Experimental and kinetic modeling study of extinction and ignition of methyl decanoate in laminar non-premixed flows, *Proc. Combust. Inst.* 32 (2009) 1067–1074. doi:10.1016/j.proci.2008.06.215.
- [96] Y. Shi, H.-W. Ge, J.L. Brakora, R.D. Reitz, Automatic chemistry mechanism reduction of hydrocarbon fuels for HCCI engines based on DRGEP and PCA Methods with Error Control, *Energy & Fuels*. 24

- (2010) 1646–1654. doi:10.1021/ef901469p.
- [97] P. Diévert, S.H. Won, S. Dooley, F.L. Dryer, Y. Ju, A kinetic model for methyl decanoate combustion, *Combust. Flame*. 159 (2012) 1793–1805. doi:10.1016/j.combustflame.2012.01.002.
- [98] O. Herbinet, J. Biet, M.H. Hakka, V. Warth, P.A. Glaude, A. Nicolle, et al., Modeling study of the low-temperature oxidation of large methyl esters from C11 to C19., *Proc. Combust. Inst.* 33 (2011) 391–398. doi:10.1016/j.proci.2010.07.060.
- [99] O. Herbinet, W.J. Pitz, C.K. Westbrook, Detailed chemical kinetic mechanism for the oxidation of biodiesel fuels blend surrogate, *Combust. Flame*. 157 (2010) 893–908. doi:10.1016/j.combustflame.2009.10.013.
- [100] K. HadjAli, M. Crochet, G. Vanhove, M. Ribaucour, R. Minetti, A study of the low temperature autoignition of methyl esters, *Proc. Combust. Inst.* 32 (2009) 239–246. doi:10.1016/j.proci.2008.09.002.
- [101] S.M. Walton, M.S. Wooldridge, C.K. Westbrook, An experimental investigation of structural effects on the auto-ignition properties of two C5 esters, *Proc. Combust. Inst.* 32 (2009) 255–262. doi:10.1016/j.proci.2008.06.208.
- [102] Lawrence Livermore National Laboratory Physical and Life Sciences Directorate, Available from: https://www-pls.llnl.gov/?url=science_and_technology-chemistry-combustion-md.
- [103] Lawrence Livermore National Laboratory Physical and Life Sciences Directorate, Available from: https://www-pls.llnl.gov/?url=science_and_technology-chemistry-combustion-biodiesel.
- [104] Z. Luo, M. Plomer, T. Lu, S. Som, D.E. Longman, A reduced mechanism for biodiesel surrogates with low-temperature chemistry, in: 7Th US Natl. Combust. Meet., 2011: pp. 1–10.
- [105] Z. Luo, T. Lu, M.J. Maciaszek, S. Som, D.E. Longman, A reduced

- mechanism for high-temperature oxidation of biodiesel surrogates, *Energy & Fuels*. 24 (2010) 6283–6293. doi:10.1021/ef1012227.
- [106] J.L. Brakora, Y. Ra, R.D. Reitz, Combustion model for biodiesel-fueled engine simulations using realistic chemistry and physical properties, *SAE Int. J. Engines*. 4 (2011) 931–947. doi:10.4271/2011-01-0831.
- [107] M. O’Conaire, H.J. Curran, J.M. Simmie, W.J. Pitz, C.K. Westbrook, A comprehensive modeling study of hydrogen oxidation, *Int. J. Chem. Kinet.* 36 (2004) 603–622. doi:10.1002/kin.20036.
- [108] E.L. Petersen, D.M. Kalitan, S. Simmons, G. Bourque, H.J. Curran, J.M. Simmie, Methane/propane oxidation at high pressures: Experimental and detailed chemical kinetic modeling, *Proc. Combust. Inst.* 31 (2007) 447–454. doi:10.1016/j.proci.2006.08.034.
- [109] P. Dagaut, S. Garil, M. Sahasrabudhe, Rapeseed oil methyl ester oxidation over extended ranges of pressure, temperature, and equivalence ratio: Experimental and modeling kinetic study, *Proc. Combust. Inst.* 31 (2007) 2955–2961. doi:10.1016/j.proci.2006.07.142.
- [110] H. Rabitz, M. Kramer, D. Dacol, Sensitivity analysis in chemical kinetics, *Annu. Rev. Phys. Chem.* (1983).
- [111] T. Turanyi, Reduction of large reaction mechanisms, *New J. Chem.* 14 (1990) 795–803.
- [112] A.S. Tomlin, M.J. Pilling, T. Turányi, J.H. Merkin, J. Brindley, Mechanism reduction for the oscillatory oxidation of hydrogen: Sensitivity and quasi-steady-state analyses, *Combust. Flame*. 91 (1992) 107–130. doi:10.1016/0010-2180(92)90094-6.
- [113] A.S. Tomlin, T. Turányi, M.J. Pilling, Mathematical tools for the construction, investigation and reduction of combustion mechanisms, *Compr. Chem. Kinet.* (1997) 293–437.
- [114] T. Lu, C.K. Law, A directed relation graph method for mechanism reduction, *Proc. Combust. Inst.* 30 (2005) 1333–1341.

doi:10.1016/j.proci.2004.08.145.

- [115] R. Sankaran, E.R. Hawkes, J.H. Chen, T. Lu, C.K. Law, Structure of a spatially developing turbulent lean methane–air bunsen flame, *Proc. Combust. Inst.* 31 (2007) 1291–1298. doi:10.1016/j.proci.2006.08.025.
- [116] K. Niemeyer, C. Sung, DRGEP-based mechanism reduction strategies: Graph search algorithms and skeletal primary reference fuel mechanisms, in: 49th AIAA Aerosp. Sci. Meet. Incl. New Horizons Forum Aerosp. Expo., 2011.
- [117] T. Turányi, Sensitivity analysis of complex kinetic systems. Tools and applications, *J. Math. Chem.* 5 (1990) 203–248. doi:10.1007/BF01166355.
- [118] X.L. Zheng, T.F. Lu, C.K. Law, Experimental counterflow ignition temperatures and reaction mechanisms of 1,3-butadiene, *Proc. Combust. Inst.* 31 (2007) 367–375. doi:10.1016/j.proci.2006.07.182.
- [119] T. Turányi, T. Bérces, S. Vajda, Reaction rate analysis of complex kinetic systems, *Int. J. Chem. Kinet.* 21 (1989) 83–99. doi:10.1002/kin.550210203.
- [120] A. Massias, D. Diamantis, An algorithm for the construction of global reduced mechanisms with CSP data, *Combust. Flame.* 117 (1999) 685–708. doi:10.1016/S0010-2180(98)00132-1.
- [121] M. Valorani, F. Creta, D. Goussis, J. Lee, H. Najm, An automatic procedure for the simplification of chemical kinetic mechanisms based on CSP, *Combust. Flame.* 146 (2006) 29–51. doi:10.1016/j.combustflame.2006.03.011.
- [122] U. Maas, S.B. Pope, Simplifying chemical kinetics: Intrinsic low-dimensional manifolds in composition space, *Combust. Flame.* 88 (1992) 239–264. doi:10.1016/0010-2180(92)90034-M.
- [123] C. Correa, H. Niemann, B. Schramm, J. Warnatz, Reaction mechanism reduction for higher hydrocarbons by the ILDM method, *Proc. Combust.*

- Inst. 28 (2000) 1607–1614. doi:10.1016/S0082-0784(00)80558-5.
- [124] H. Bongers, J.A. Van Oijen, L.P.H. De Goeij, Intrinsic low-dimensional manifold method extended with diffusion, *Proc. Combust. Inst.* 29 (2002) 1371–1378. doi:10.1016/S1540-7489(02)80168-7.
- [125] T. Lu, Y. Ju, C.K. Law, Complex CSP for chemistry reduction and analysis, *Combust. Flame.* 126 (2001) 1445–1455. doi:10.1016/S0010-2180(01)00252-8.
- [126] S.H. Lam, D.A. Goussis, The CSP method for simplifying kinetics, *Int. J. Chem. Kinet.* 26 (1994) 461–486. doi:10.1002/kin.550260408.
- [127] A. Zagaris, H.G. Kaper, T.J. Kaper, Analysis of the computational singular perturbation reduction method for chemical kinetics, *J. Nonlinear Sci.* 14 (2004) 59–91. doi:10.1007/s00332-003-0582-9.
- [128] M. Valorani, D.A. Goussis, Explicit time-scale splitting algorithm for stiff problems: Auto-ignition of gaseous mixtures behind a steady shock, *J. Comput. Phys.* 169 (2001) 44–79. doi:10.1006/jcph.2001.6709.
- [129] S. Vajda, P. Valko, T. Turányi, Principal component analysis of kinetic models, *Int. J. Chem. Kinet.* 17 (1985) 55–81. doi:10.1002/kin.550170107.
- [130] N.J. Brown, G. Li, M.L. Koszykowski, Mechanism reduction via principal component analysis, *Int. J. Chem. Kinet.* 29 (1997) 393–414. doi:10.1002/(SICI)1097-4601(1997)29:6<393::AID-KIN1>3.0.CO;2-P.
- [131] S. Wold, K. Esbensen, P. Geladi, Principal component analysis, *Chemom. Intell. Lab. Syst.* 2 (1987) 37–52. doi:10.1016/0169-7439(87)80084-9.
- [132] P. Pepiot, H. Pitsch, Systematic reduction of large chemical mechanisms, in: 4th Jt. Meet. U.S. Sect. Combust. Inst., 2005: pp. 1–6.
- [133] L. Liang, J.G. Stevens, S. Raman, J.T. Farrell, The use of dynamic adaptive chemistry in combustion simulation of gasoline surrogate fuels,

- Combust. Flame. 156 (2009) 1493–1502.
doi:10.1016/j.combustflame.2009.02.008.
- [134] D.A. Schwer, P. Lu, W.H. Green, An adaptive chemistry approach to modeling complex kinetics in reacting flows, *Combust. Flame.* 133 (2003) 451–465. doi:10.1016/S0010-2180(03)00045-2.
- [135] T. Løvås, P. Amnéus, F. Mauss, E. Mastorakos, Comparison of automatic reduction procedures for ignition chemistry, *Proc. Combust. Inst.* 29 (2002) 1387–1393. doi:10.1016/S1540-7489(02)80170-5.
- [136] I. Banerjee, M. Ierapetritou, An adaptive reduction scheme to model reactive flow, *Combust. Flame.* 144 (2006) 619–633. doi:10.1016/j.combustflame.2005.10.001.
- [137] T. Nagy, T. Turanyi, Reduction of very large reaction mechanisms using methods based on simulation error minimization, *Combust. Flame.* 156 (2009) 417–428. doi:10.1016/j.combustflame.2008.11.001.
- [138] H. Selim, A.K. Gupta, M. Sassi, Novel error propagation approach for reducing H₂S/O₂ reaction mechanism, *Appl. Energy.* 93 (2012) 116–124. doi:10.1016/j.apenergy.2011.01.047.
- [139] M. Davis, R. Davis, *Fundamentals of chemical reaction engineering*, 2012.
- [140] CHEMKIN-PRO 15112, 2011.
- [141] R.D. Reitz, R. Diwakar, Effect of drop breakup on fuel sprays, *SAE Tech. Pap.* 860469 (1986). doi:10.4271/860469.
- [142] R.D. Reitz, R. Diwakar, Structure of high-pressure fuel sprays, *SAE Tech. Pap.* 870598 (1987). doi:10.4271/870598.
- [143] J. Nicholls, Stream and droplet breakup by shock waves, *NASA SP-194* (1972) 126–128.
- [144] B.E. Launder, *Lectures in mathematical models of turbulence* [by] B. E.

- Launder and D. B. Spalding, Academic Press, London, New York, 1972.
- [145] V. Yakhot, S. Orszag, Renormalization group analysis of turbulence. I. Basic theory, *J. Sci. Comput.* 1 (1986) 3–51. doi:10.1007/BF01061452.
- [146] Z. Han, R.D. Reitz, Turbulence modeling of internal combustion engines using RNG κ - ϵ models, *Combust. Sci. Technol.* 106 (1995) 267–295.
- [147] R.D. Reitz, C.J. Rutland, Development and testing of diesel engine CFD models, *Prog. Energy Combust. Sci.* 21 (1995) 173–196. doi:10.1016/0360-1285(95)00003-Z.
- [148] K.M. Leung, R.P. Lindstedt, W.P. Jones, A simplified reaction mechanism for soot formation in nonpremixed flames, *Combust. Flame.* 87 (1991) 289–305. doi:10.1016/0010-2180(91)90114-Q.
- [149] G. Vishwanathan, R.D. Reitz, Development of a practical soot modeling approach and its application to low-temperature diesel combustion, *Combust. Sci. Technol.* 182 (2010) 1050–1082. doi:10.1080/00102200903548124.
- [150] J. Dec, A conceptual model of diesel combustion based on laser-sheet imaging*, *SAE Tech. Pap.* 970873 (1997).
- [151] K.B. Lee, M.W. Thring, J.M. Beér, On the rate of combustion of soot in a laminar soot flame, *Combust. Flame.* 6 (1962) 137–145. doi:10.1016/0010-2180(62)90082-2.
- [152] M.P. Raju, C.-J. Sung, K. Kundu, Integrating sensitivity analysis into directed relation graph with error propagation for effective chemical mechanism reduction, 2007.
- [153] I.G. Zsély, T. Nagy, J.M. Simmie, H.J. Curran, Reduction of a detailed kinetic model for the ignition of methane/propane mixtures at gas turbine conditions, in: *4th Eur. Combust. Meet., Vienna, Austria, 2009.* doi:10.1016/j.combustflame.2010.12.011.
- [154] L. Liang, J.G. Stevens, J.T. Farrell, A dynamic adaptive chemistry

- scheme for reactive flow computations, *Proc. Combust. Inst.* 32 I (2009) 527–534. doi:10.1016/j.proci.2008.05.073.
- [155] Y. Shi, L. Liang, H.-W. Ge, R.D. Reitz, Acceleration of the chemistry solver for modeling DI engine combustion using dynamic adaptive chemistry (DAC) schemes, *Combust. Theory Model.* 14 (2010) 69–89. doi:10.1080/13647830903548834.
- [156] E.W. Dijkstra, A note on two problems in connexion with graphs, *Numer. Math.* (1959) 269–271.
- [157] T.H. Cormen, C.E. Leiserson, R.L. Rivest, C. Stein, *Introduction to algorithms*, 2nd Ed., MIT Press, Cambridge, MA, 2001. doi:10.1080/10911359.2014.897096.
- [158] J. Yang, M. Johansson, C. Naik, K. Puduppakkam, V. Golovitchev, E. Meeks, 3D CFD modeling of a biodiesel-fueled diesel engine based on a detailed chemical mechanism, *SAE Tech. Pap.* 2012-01-0151 (2012). doi:10.4271/2012-01-0151.
- [159] Z. Luo, M. Plomer, T. Lu, S. Som, D.E. Longman, S.M. Sarathy, et al., A reduced mechanism for biodiesel surrogates for compression ignition engine applications, *Fuel.* 99 (2012) 143–153. doi:10.1016/j.fuel.2012.04.028.
- [160] F. Perini, D. Sahoo, P. Miles, R. Reitz, Modeling the ignitability of a pilot injection for a diesel primary reference fuel: Impact of injection pressure, ambient temperature and injected mass, *SAE Int. J. Fuels Lubr.* (2014) 48–64. doi:10.4271/2014-01-1258.
- [161] P. Pepiot, H. Pitsch, An automatic chemical lumping method for the reduction of large chemical kinetic mechanisms, *Combust. Theory Model.* 12 (2008) 1089–1108. doi:10.1080/13647830802245177.
- [162] M.K. Le, S. Kook, Injection pressure effects on the flame development in a light-duty optical diesel engine, *SAE Int. J. Engines.* 8 (2015) 609–624. doi:10.4271/2015-01-0791.

- [163] X. Cheng, H.K. Ng, S. Gan, J.H. Ho, K.M. Pang, Development and validation of a generic reduced chemical kinetic mechanism for CFD spray combustion modelling of biodiesel fuels, *Combust. Flame*. 162 (2015) 2354–2370. doi:10.1016/j.combustflame.2015.02.003.
- [164] H. Wang, X. You, A.V. Joshi, S.G. Davis, A. Laskin, F. Egolfopoulos, et al., USC Mech Version II. High-temperature combustion reaction model of H₂/CO/C₁-C₄ compounds (2007).
- [165] A. Ivarsson, Modeling of heat release and emissions from droplet combustion of multi component fuels in compression ignition engines, Technical University of Denmark, Graduation Thesis, 2009.
- [166] P. Dagaut, M. Cathonnet, J. Boettner, F. Gaillard, Kinetic modeling of ethylene oxidation, *Combust. Flame*. 312 (1988) 295–312.
- [167] Engine Combustion Network Experimental Data Archive, Available from: <http://www.sandia.gov/ecn/>.
- [168] S. Kook, L.M. Pickett, Liquid length and vapor penetration of conventional, Fischer–Tropsch, coal-derived, and surrogate fuel sprays at high-temperature and high-pressure ambient conditions, *Fuel*. 93 (2012) 539–548. doi:10.1016/j.fuel.2011.10.004.
- [169] J. Nerva, C.L. Genzale, S. Kook, J.M. Garcia-Oliver, L.M. Pickett, Fundamental spray and combustion measurements of soy methyl-ester biodiesel, *Int. J. Engine Res.* (2012). doi:10.1177/1468087412456688.
- [170] H. Mondal, S. Roy, Numerical analysis of droplet combustion in a cylindrical furnace, *J. Chem. Eng. C* (2010) 14–18.
- [171] C. Westbrook, C. Naik, O. Herbinet, W.J. Pitz, M. Mehl, S.M. Sarathy, et al., Detailed chemical kinetic reaction mechanisms for soy and rapeseed biodiesel fuels, *Combust. Flame*. 158 (2011) 742–755.
- [172] R.D. Morrison, B.L. Murphy, *Environmental forensics: Contaminant specific guide*, Elsevier, 2005. doi:10.1016/B978-012507751-4/50021-5.

- [173] J.D. Roberts, M.C. Caserio, Basic principles of organic chemistry, WA Benjamin, Inc., 1977.
- [174] D. Ebbing, S.D. Gammon, General chemistry, Cengage Learning, 2010.
- [175] B. Challen, R. Baranescu, Diesel engine reference book, 2nd Ed., Butterworth-Heinemann Ltd, 1999.
- [176] M.A. Oehlschlaeger, J. Steinberg, C.K. Westbrook, W.J. Pitz, The autoignition of iso-cetane at high to moderate temperatures and elevated pressures: Shock tube experiments and kinetic modeling, *Combust. Flame.* 156 (2009) 2165–2172. doi:10.1016/j.combustflame.2009.05.007.
- [177] E.J. Silke, W.J. Pitz, C.K. Westbrook, M. Ribaucour, Detailed chemical kinetic modeling of cyclohexane oxidation, *J. Phys. Chem. A.* 111 (2007) 3761–3775. doi:10.1021/jp067592d.
- [178] C.L. Yaws, Thermophysical properties of chemicals and hydrocarbons, Elsevier, 2009. doi:10.1016/B978-081551596-8.50001-8.
- [179] P. Dagaut, K. Hadj-Ali, Chemical kinetic study of the oxidation of isocetane (2, 2, 4, 4, 6, 8, 8-heptamethylnonane) in a jet-stirred reactor: experimental and modeling, *Energy & Fuels.* 19 (2009) 2389–2395.
- [180] D. Voisin, A. Marchal, M. Reuillon, J.C. Boettner, M. Cathonnet, Experimental and kinetic modeling study of cyclohexane oxidation in a JSR at high pressure, *Combust. Sci. Technol.* 138 (1998) 137–158. doi:10.1080/00102209808952066.
- [181] N. Slavinskaya, A. Zizin, U. Riedel, Towards kerosene reaction model development: propylcyclohexane, cyC₉H₁₈, n-dodecane, C₁₂H₂₆, and hexadecane C₁₆H₃₄ combustion, *AIAA.* (2010) 1–13.
- [182] D. Sahoo, B. Petersen, P. Miles, Measurement of equivalence ratio in a light-duty low temperature combustion diesel engine by planar laser induced fluorescence of a fuel tracer, *SAE Int. J. Engines.* 4 (2011) 2312–2325. doi:10.4271/2011-24-0064.

- [183] B. Petersen, P.C. Miles, D. Sahoo, Equivalence ratio distributions in a light-duty diesel engine operating under partially premixed conditions, *SAE Int. J. Engines*. 5 (2012) 526–537. doi:10.4271/2012-01-0692.
- [184] K.M. Pang, M. Jangi, X. Bai, J. Schramm, Investigation of chemical kinetics on soot formation event of n-heptane spray combustion, *SAE 2014 World Congr. Exhib.* 1 (2014). doi:10.4271/2014-01-1254.
- [185] K.M. Pang, M. Jangi, X.-S. Bai, J. Schramm, Evaluation and optimisation of phenomenological multi-step soot model for spray combustion under diesel engine-like operating conditions, *Combust. Theory Model.* (2015) 1–30. doi:10.1080/13647830.2015.1019929.
- [186] M. Bolla, Y.M. Wright, K. Boulouchos, G. Borghesi, E. Mastorakos, Soot formation modeling of n-heptane sprays under diesel engine conditions using the conditional moment closure approach, *Combust. Sci. Technol.* 185 (2013) 766–793. doi:10.1080/00102202.2012.752362.
- [187] M. Jangi, T. Lucchini, G. D’Errico, X.S. Bai, Effects of EGR on the structure and emissions of diesel combustion, *Proc. Combust. Inst.* 34 (2013) 3091–3098. doi:10.1016/j.proci.2012.06.093.
- [188] S.-C. Kong, Y. Sun, R.D. Rietz, Modeling diesel spray flame liftoff, sooting tendency, and NO_x emissions using detailed chemistry with phenomenological soot model, *J. Eng. Gas Turbines Power.* 129 (2007) 245–251. doi:10.1115/1.2181596.
- [189] K.M. Pang, H.K. Ng, S. Gan, Simulation of temporal and spatial soot evolution in an automotive diesel engine using the Moss–Brookes soot model, *Energy Convers. Manag.* 58 (2012) 171–184. doi:10.1016/j.enconman.2012.01.015.
- [190] R. Christian, F. Knopf, A. Jasmek, W. Schindler, A new method for the filter smoke number measurement with improved sensitivity, *MTZ.* 54 (1993) 16–22.
- [191] J. Dec, C. Espey, Ignition and early soot formation in a DI diesel engine

using multiple 2-D imaging diagnostics, SAE Tech. Pap. 950456 (1995).
doi:10.4271/950456.

APPENDICES

A. MATLAB CODES FOR DRG MECHANISM REDUCTION TECHNIQUE

```
number_of_species = 3299;
number_of_reactions = 10806;
max_number_of_species_in_reactions = 6;
fid1=fopen('reaction.txt');
coupling_transpose = fscanf(fid1, '%d', [max_number_of_species_in_reactions inf]);
coupling = coupling_transpose';
fclose(fid1);

species_matrix = zeros(number_of_species);
[ row col ] = size(species_matrix);
[ A B ] = size(coupling);

for f=1:A
    species_matrix(coupling(f,:),coupling(f,:))=1;
end

for r=1:row
    for c=1:col
        if(r==c)
            species_matrix(r,c) = 0;
        end
    end
end

species_matrix=species_matrix(1:number_of_species,1:number_of_species);

fid2=fopen('coef.txt');
coefficient_transpose = fscanf(fid2, '%d', [max_number_of_species_in_reactions inf]);
coupling = coupling_transpose';
fclose(fid2);

coefficient = coefficient_transpose';
v_ji = zeros(number_of_species,number_of_reactions);

[ J K ] = size(v_ji);

for a=1:A
    for b=1:B
        if (coupling(a,b) == number_of_species+1 || coupling(a,b)==number_of_species+2)
            continue;
        else
            if v_ji(coupling(a,b),a)==0
                v_ji(coupling(a,b),a)=coefficient(a,b);
            elseif v_ji(coupling(a,b),a)~=0
                v_ji(coupling(a,b),a)=coefficient(a,b)+v_ji(coupling(a,b),a);
            end
        end
    end
end
```

```

v_ji_1 = zeros(number_of_species,number_of_reactions);
v_ji_1 = v_ji;
for j=1:J
    for k=1:K
        if v_ji_1(j,k)>1
            v_ji_1(j,k)=1;
        end
    end
    delta = v_ji_1;
end

fid3=fopen('net_reaction_rate.txt');
wi = fscanf(fid3, '%e', [3 number_of_reactions]);
fclose(fid3);

important_species = zeros(number_of_species,1);
wi_prime=wi';
[S T] = size(wi_prime);

for t=1:T
    species_keep(t).keep = zeros(number_of_species,1);
    species2_keep(t).keep = zeros(number_of_species,1);
end

for t=1:T
    wi_var = wi_prime(:,t);
    species_net_production_rate = wi_var' * v_ji';
    repmat_wi = (repmat(wi_var,1,number_of_species));
    vw_1 = v_ji' .* repmat_wi;
    abs_vw_1 = abs((vw_1));
    numerator1 = 0;
    denominator1 = 0;
    r_coupling1 = 0;
    species_matrix1 = zeros(number_of_species);
    [P Q] = size(species_matrix1);

    for p=1:P
        for q=1:Q
            if species_matrix(p,q)==1
                % i row in matrix delta and abs_vw
                numerator1=0;
                denominator1=0;
                for i=1:number_of_reactions
                    numerator1=numerator1+delta(q,i)*abs_vw_1(p,i);
                    denominator1=denominator1+abs_vw_1(p,i);
                end
                r_coupling1=numerator1/denominator1;
                species_matrix1(p,q)=r_coupling1;
            end
        end
    end

    sparse_matrix1 = sparse(species_matrix1);
    [i,j,k]=find(sparse_matrix1);
    sparsed1=[i j k];
    sparsed1_sort=sortrows(sparsed1,-3);
    [row1 col] = size(sparsed1_sort);
    counter01=[fuel_species_number_1;species_number_2];

```

```

loop = zeros(row1,1);
mark = zeros(number_of_species,1);
[s3 s4] = size(mark);
[counter_row counter_col] = size(counter01);

for c_r = 1:counter_row
    species_counter(c_r).counter = zeros(number_of_species);
end

for c_r = 1:counter_row
    counter1 = counter01(c_r);
    mark(counter1) = 1;
    for i = 1:row1
        if (loop(i) == 0)
            if (mark(sparsed1_sort(i,1)) == 0 && mark(sparsed1_sort(i,2)) == 0)
                loop(i) = 1;
            elseif (mark(sparsed1_sort(i,1)) == 0 && mark(sparsed1_sort(i,2)) ~= 0)
                continue;
            elseif (mark(sparsed1_sort(i,1)) ~= 0 && mark(sparsed1_sort(i,2)) == 0)
                mark(sparsed1_sort(i,2)) = sparsed1_sort(i,3);
                loop(i) = 2;
                value = sparsed1_sort(i,3);
                for k = 1:row1
                    for k = 1:row1
                        if (loop(k) == 1)
                            if (mark(sparsed1_sort(k,1)) ~= 0 && mark(sparsed1_sort(k,2)) == 0)
                                loop(k) = 2;
                                mark(sparsed1_sort(k,2)) = value;
                            end
                        end
                    end
                end
            end
        end
        species_counter(c_r).counter = mark;
        mark = zeros(number_of_species,1);
        loop = zeros(row1,1);
    end

    mark1 = species_counter(1).counter;
    mark2 = species_counter(2).counter;
    species_keep(t).keep = mark1;
    species2_keep(t).keep = mark2;

    rdfs_60bar_ER1_650K_1a = species_keep(1).keep;
    rdfs_60bar_ER1_650K_1b = species2_keep(1).keep;
    rdfs_60bar_ER1_650K_2a = species_keep(2).keep;
    rdfs_60bar_ER1_650K_2b = species2_keep(2).keep;
    rdfs_60bar_ER1_650K_3a = species_keep(3).keep;
    rdfs_60bar_ER1_650K_3b = species2_keep(3).keep;
end

limit=0.1;
[row2 col2] = size(rdfs_60bar_ER1_650K_1a);
important_species=zeros(number_of_species,1);
[row4 col4] = size(important_species);

```

```
for rw2=1:row2
    if rdfs_60bar_ER1_650K_1a(rw2)<limit
        rdfs_60bar_ER1_650K_1a(rw2)=0;
    end
    if rdfs_60bar_ER1_650K_1a(rw2)~=0
        important_species(rw2)=1;
    end
end
```

```
for rw2=1:row2
    if rdfs_60bar_ER1_650K_1b(rw2)<limit
        rdfs_60bar_ER1_650K_1b(rw2)=0;
    end
    if rdfs_60bar_ER1_650K_1b(rw2)~=0
        important_species(rw2)=1;
    end
end
```

```
for rw2=1:row2
    if rdfs_60bar_ER1_650K_2a(rw2)<limit
        rdfs_60bar_ER1_650K_2a(rw2)=0;
    end
    if rdfs_60bar_ER1_650K_2a(rw2)~=0
        important_species(rw2)=1;
    end
end
```

```
for rw2=1:row2
    if rdfs_60bar_ER1_650K_2b(rw2)<limit
        rdfs_60bar_ER1_650K_2b(rw2)=0;
    end
    if rdfs_60bar_ER1_650K_2b(rw2)~=0
        important_species(rw2)=1;
    end
end
```

```
for rw2=1:row2
    if rdfs_60bar_ER1_650K_3a(rw2)<limit
        rdfs_60bar_ER1_650K_3a(rw2)=0;
    end
    if rdfs_60bar_ER1_650K_3a(rw2)~=0
        important_species(rw2)=1;
    end
end
```

```
for rw2=1:row2
    if rdfs_60bar_ER1_650K_3b(rw2)<limit
        rdfs_60bar_ER1_650K_3b(rw2)=0;
    end
    if rdfs_60bar_ER1_650K_3b(rw2)~=0
        important_species(rw2)=1;
    end
end
```

B. MATLAB CODES FOR DRGEP MECHANISM REDUCTION TECHNIQUE

```
number_of_species = 3299;
number_of_reactions = 10806;
max_number_of_species_in_reactions = 6;
fid1=fopen('reaction.txt');
coupling_transpose = fscanf(fid1, '%d', [max_number_of_species_in_reactions inf]);
coupling = coupling_transpose';
fclose(fid1);

species_matrix = zeros(number_of_species);
[ row col ] = size(species_matrix);
[ A B ] = size(coupling);

for f=1:A
    species_matrix(coupling(f,:),coupling(f,:))=1;
end

for r=1:row
    for c=1:col
        if(r==c)
            species_matrix(r,c) = 0;
        end
    end
end

species_matrix=species_matrix(1:number_of_species,1:number_of_species);

fid2=fopen('coef.txt');
coefficient_transpose = fscanf(fid2, '%d', [max_number_of_species_in_reactions inf]);
coupling = coupling_transpose';
fclose(fid2);

coefficient = coefficient_transpose';
v_ji = zeros(number_of_species,number_of_reactions);

[ J K ] = size(v_ji);

for a=1:A
    for b=1:B
        if (coupling(a,b) == number_of_species+1 || coupling(a,b)==number_of_species+2)
            continue;
        else
            if v_ji(coupling(a,b),a)==0
                v_ji(coupling(a,b),a)=coefficient(a,b);
            elseif v_ji(coupling(a,b),a)~=0
                v_ji(coupling(a,b),a)=coefficient(a,b)+v_ji(coupling(a,b),a);
            end
        end
    end
end
```

```

v_ji_1 = zeros(number_of_species,number_of_reactions);
v_ji_1 = v_ji;
for j=1:J
    for k=1:K
        if v_ji_1(j,k)>1
            v_ji_1(j,k)=1;
        end
    end
    delta = v_ji_1;
end

species_1 = 1;
species_2 = 2;
threshold = 0.5;

fid3=fopen('net_reaction_rate.txt');
wi = fscanf(fid3, '%e', [3 number_of_reactions]);
fclose(fid3);

important_species = zeros(number_of_species,1);
wi_prime=wi';
[S T] = size(wi_prime);

for t=1:T
    species_keep(t).keep = zeros(number_of_species,1);
end

for t=1:T
    wi_var = wi_prime(:,t);
    wi_var_prime = wi_var';
    numerator1=0;
    denominator1a=0;
    denominator1b=0;
    r_coupling1 = 0;
    species_matrix1 = zeros(number_of_species);
    [P Q] = size(species_matrix1);

    for p=1:P
        for q=1:Q
            if (p == q)
                species_matrix(p,q) = 0;
            end
        end
    end

    for p=1:P
        for q=1:Q
            if species_matrix(p,q)==1
                % i row in matrix delta and abs_vw
                numerator1=0;
                denominator1a=0;
                denominator1b=0;
                for i=1:number_of_reactions
                    numerator1=numerator1+(delta(q,i)*v_ji(p,i)*wi_var_prime(1,i));
                end
                for i=1:number_of_reactions
                    if (wi_var_prime(1,i))>0
                        denominator1a=denominator1a+v_ji(p,i)*wi_var_prime(1,i);
                    end
                end
            end
        end
    end
end

```

```

elseif (wi_var_prime(1,i))<0
    denominator1b=denominator1b+v_ji(p,i)*wi_var_prime(1,i);
end
end
if (denominator1a >= abs(denominator1b) && denominator1a ~= 0)
    r_coupling1=abs(numerator1)/denominator1a;
elseif (abs(denominator1b)> denominator1a && denominator1b ~= 0)
    r_coupling1=abs(numerator1)/abs(denominator1b);
end
species_matrix1(p,q)=r_coupling1;
end
end
end

sparse_matrix1 = sparse(species_matrix1);
[i,j,k]=find(sparse_matrix1);
sparsed1=[i j k];
sparsed1_sort=sortrows(sparsed1,-3);
[row1 col] = size(sparsed1_sort);
mark_final = zeros(number_of_species,1);
mark = zeros(number_of_species,1);
target = [species_1;species_2];
[s3 s4] = size(mark);
[S5 S6] = size(target);

for s5 = 1:S5
    mark (target(s5)) = 1;
    value = 1;
    while (value ~= 0)
        [value, location] = max(mark(:));
        mark_final(location) = value;
        mark(location) = 0;
        for h = 1:row1
            multiplication = 0;
            if(sparsed1_sort(h,1) == location && mark_final(sparsed1_sort(h,2)) == 0)
                multiplication = sparsed1_sort(h,3) * value;
                if(multiplication > mark(sparsed1_sort(h,2)) && multiplication >= threshold)
                    mark(sparsed1_sort(h,2)) = multiplication;
                end
            end
        end
    end
end
important_species(1) = 1;
for S3 = 1:s3
    if (mark_final(S3) ~= 0)
        important_species(S3) = 1;
    end
end
mark = zeros(number_of_species,1);
mark_final = zeros(number_of_species,1);
end
rdfs_60bar_ER1_650K_1 = species_keep(1).keep;
rdfs_60bar_ER1_650K_2 = species_keep(2).keep;
rdfs_60bar_ER1_650K_3 = species_keep(3).keep;
end

```

C. CHEMICAL KINETIC MECHANISMS

Table C-1: The HXNv2 diesel surrogate fuel model. Units are in mole, cm, s, K and cal.

Reaction Number	Reaction Considered	A	b	E
1	CH ₃ +H(+M)=CH ₄ (+M)	2.14E+15	-0.4	0
	H ₂	Enhanced	by	2.00E+00
	H ₂ O	Enhanced	by	5.00E+00
	CO	Enhanced	by	2.00E+00
	CO ₂	Enhanced	by	3.00E+00
2	CH ₄ +H=CH ₃ +H ₂	1.73E+04	3	8.22E+03
3	CH ₄ +OH=CH ₃ +H ₂ O	1.93E+05	2.4	2.11E+03
4	CH ₄ +O=CH ₃ +OH	3.15E+12	0.5	10290
5	C ₂ H ₆ +CH ₃ =C ₂ H ₅ +CH ₄	1.51E-07	6	6047
6	HCO+OH=CO+H ₂ O	1.02E+14	0	0
7	CO+OH=CO ₂ +H	1.40E+05	1.9	-1347
8	H+O ₂ =O+OH	1.97E+14	0	16540
9	O+H ₂ =H+OH	5.08E+04	2.7	6292
10	O+H ₂ O=OH+OH	2.97E+06	2	13400
11	OH+H ₂ =H+H ₂ O	2.16E+08	1.5	3430
12	HCO+M=H+CO+M	1.86E+17	-1	17000
	H ₂	Enhanced	by	2.50E+00
	H ₂ O	Enhanced	by	1.20E+01
	CO	Enhanced	by	1.90E+00
	CO ₂	Enhanced	by	3.80E+00
13	C ₂ H ₄ +O=CH ₃ +HCO	1.02E+07	1.9	1.79E+02
14	H+C ₂ H ₄ (+M)=C ₂ H ₅ (+M)	1.08E+12	0.5	1.82E+03
	H ₂	Enhanced	by	2.00E+00
	H ₂ O	Enhanced	by	5.00E+00
	CO	Enhanced	by	2.00E+00
	CO ₂	Enhanced	by	3.00E+00
15	C ₂ H ₆ +H=C ₂ H ₅ +H ₂	5.54E+02	3.5	5.17E+03
16	C ₂ H ₅ +O ₂ =C ₂ H ₄ +HO ₂	1.22E+30	-5.8	1.01E+04
17	C ₂ H ₆ +OH=C ₂ H ₅ +H ₂ O	5.80E+07	1.7	1160
18	C ₂ H ₆ +O=C ₂ H ₅ +OH	1.30E+07	2.1	5190
19	CH ₃ +HO ₂ =CH ₃ O+OH	1.10E+13	0	0
20	CO+HO ₂ =CO ₂ +OH	3.01E+13	0	23000
21	CH ₃ +CH ₃ (+M)=C ₂ H ₆ (+M)	9.21E+16	-1.2	635.8
	H ₂	Enhanced	by	2.00E+00
	H ₂ O	Enhanced	by	5.00E+00
	CO	Enhanced	by	2.00E+00
	CO ₂	Enhanced	by	3.00E+00
22	H ₂ O+M=H+OH+M	1.84E+27	-3	1.23E+05
	H ₂	Enhanced	by	2.50E+00
	H ₂ O	Enhanced	by	1.20E+01
	CO	Enhanced	by	1.90E+00
	CO ₂	Enhanced	by	3.80E+00
23	H+O ₂ (+M)=HO ₂ (+M)	1.48E+12	0.6	0.00E+00
	H ₂	Enhanced	by	2.50E+00
	H ₂ O	Enhanced	by	1.20E+01
	CO	Enhanced	by	1.90E+00
	CO ₂	Enhanced	by	3.80E+00
24	CO+O(+M)=CO ₂ (+M)	1.80E+10	0	2.38E+03
	H ₂	Enhanced	by	2.50E+00
	H ₂ O	Enhanced	by	1.20E+01
	CO	Enhanced	by	1.90E+00
	CO ₂	Enhanced	by	3.80E+00
25	CO+O ₂ =CO ₂ +O	1.62E+13	0	4.77E+04
26	HCO+H=CO+H ₂	7.34E+13	0	0.00E+00
27	HCO+O=CO+OH	3.02E+13	0	0
28	CH ₂ O+M=HCO+H+M	6.28E+29	-3.6	93200
29	CH ₂ O+OH=HCO+H ₂ O	3.43E+09	1.2	-447
30	CH ₂ O+H=HCO+H ₂	9.33E+08	1.5	2976
31	CH ₂ O+O=HCO+OH	4.16E+11	0.6	2762
32	CH ₃ +OH=CH ₂ O+H ₂	2.25E+13	0	4300
33	CH ₃ +O=CH ₂ O+H	8.00E+13	0	0
34	CH ₃ +O ₂ =CH ₃ O+O	2.00E+18	-1.6	29210
35	CH ₂ O+CH ₃ =HCO+CH ₄	3.64E-06	5.4	998

36	HCO+CH3=CH4+CO	1.21E+14	0	0
37	CH3O(+M)=CH2O+H(+M)	5.45E+13	0	13500
38	C2H4(+M)=C2H2+H2(+M)	1.80E+13	0	76000
39	HO2+O=OH+O2	3.25E+13	0	0
40	HCO+HO2=CH2O+O2	2.97E+10	0.3	-3861
41	CH3O+O2=CH2O+HO2	5.50E+10	0	2424
42	CH3+HO2=CH4+O2	3.60E+12	0	0
43	HCO+O2=CO+HO2	7.58E+12	0	410
44	HO2+H=OH+OH	7.08E+13	0	300
45	HO2+H=H2+O2	1.66E+13	0	820
46	HO2+OH=H2O+O2	2.89E+13	0	-500
47	OH+OH(+M)=H2O2(+M)	1.24E+14	-0.4	0
	H2	Enhanced	by	2.50E+00
	H2O	Enhanced	by	1.20E+01
	CO	Enhanced	by	1.90E+00
	CO2	Enhanced	by	3.80E+00
48	H2O2+H=H2O+OH	2.41E+13	0	3.97E+03
49	CH4+HO2=CH3+H2O2	3.42E+11	0	1.93E+04
50	CH2O+HO2=HCO+H2O2	5.82E-03	4.5	6557
51	OH+M=O+H+M	3.91E+22	-2	105300
	H2	Enhanced	by	2.50E+00
	H2O	Enhanced	by	1.20E+01
	CO	Enhanced	by	1.90E+00
	CO2	Enhanced	by	3.80E+00
52	O2+M=O+O+M	6.47E+20	-1.5	1.22E+05
	H2	Enhanced	by	2.50E+00
	H2O	Enhanced	by	1.20E+01
	CO	Enhanced	by	1.90E+00
	CO2	Enhanced	by	3.80E+00
53	H2+M=H+H+M	4.57E+19	-1.4	1.04E+05
	H2	Enhanced	by	2.50E+00
	H2O	Enhanced	by	1.20E+01
	CO	Enhanced	by	1.90E+00
	CO2	Enhanced	by	3.80E+00
54	C2H3+H(+M)=C2H4(+M)	6.10E+12	0.3	2.80E+02
55	C2H5+C2H3=C2H4+C2H4	5.76E+14	-0.6	2.49E+03
56	C2H2+H(+M)=C2H3(+M)	3.11E+11	0.6	2589
	H2	Enhanced	by	2.00E+00
	H2O	Enhanced	by	5.00E+00
	CO	Enhanced	by	2.00E+00
	CO2	Enhanced	by	3.00E+00
57	C2H4+H=C2H3+H2	8.42E-03	4.6	2.58E+03
58	C2H4+OH=C2H3+H2O	2.05E+13	0	5.95E+03
59	C2H2+O2=HCCO+OH	2.00E+08	1.5	30100
60	CH2+O2=CO+H2O	7.28E+19	-2.5	1809
61	C2H2+O=CH2+CO	6.12E+06	2	1900
62	CH2+O2=HCO+OH	1.29E+20	-3.3	284
63	CH2+O=CO+H+H	5.00E+13	0	0
64	CH2+O2=CO2+H+H	3.29E+21	-3.3	2868
65	C2H3+O2=C2H2+HO2	2.12E-06	6	9484
66	H2O2+O=OH+HO2	9.55E+06	2	3970
67	C2H2+O=HCCO+H	1.43E+07	2	1900
68	C2H2+OH=CH2CO+H	2.19E-04	4.5	-1000
69	CH2CO+H=CH3+CO	1.10E+13	0	3400
70	CH2CO+O=CH2+CO2	1.75E+12	0	1350
71	CH2+O2=CH2O+O	3.29E+21	-3.3	2868
72	CH2CO(+M)=CH2+CO(+M)	3.00E+14	0	70980
73	CH2CO+O=HCCO+OH	1.00E+13	0	8000
74	CH2CO+OH=HCCO+H2O	1.00E+13	0	2000
75	CH2CO+H=HCCO+H2	2.00E+14	0	8000
76	HCCO+OH=HCO+HCO	1.00E+13	0	0
77	HCCO+O=H+CO+CO	8.00E+13	0	0
78	C2H6+O2=C2H5+HO2	6.03E+13	0	51870
79	C2H6+HO2=C2H5+H2O2	1.32E+13	0	20470
80	CH2+O2=CO2+H2	1.01E+21	-3.3	1508
81	CH3+C2H3=CH4+C2H2	3.92E+11	0	0
82	CH3+C2H5=CH4+C2H4	1.95E+13	-0.5	0
83	C2H3+H=C2H2+H2	2.00E+13	0	2500
84	C2H5+H=CH3+CH3	3.61E+13	0	0
85	C2H3+O2=CH2O+HCO	1.70E+29	-5.3	6500
86	C2H6=C2H5+H	2.78E+21	-1.6	103800
87	PC2H4OH=C2H4+OH	1.29E+12	-0.4	26850
88	C2H4+CH3=C2H3+CH4	6.62E+00	3.7	9500

89	C3H5-A=C2H2+CH3	2.40E+48	-9.9	82080
90	C3H6=C2H3+CH3	2.73E+62	-13.3	123200
91	C3H6=C3H5-A+H	2.01E+61	-13.3	118500
92	C3H6+O=CH2CO+CH3+H	2.50E+07	1.8	76
93	C3H6+O=C2H5+HCO	1.58E+07	1.8	-1216
94	C3H6+HO2=C3H5-A+H2O2	1.50E+11	0	14190
95	C3H6+OH=C3H5-A+H2O	3.12E+06	2	-298
96	C2H4+O2=C2H3+HO2	4.00E+13	0	58200
97	CH2O+M=CO+H2+M	1.83E+32	-4.4	87120
98	NC3H7=CH3+C2H4	2.28E+14	-0.6	28400
99	NC3H7=H+C3H6	2.67E+15	-0.6	36820
100	NC3H7+O2=C3H6+HO2	3.00E+11	0	3000
101	C3H6+O=C3H5-A+OH	5.24E+11	0.7	5884
102	C3H6+H=C3H5-A+H2	1.73E+05	2.5	2492
103	C3H6+H=C2H4+CH3	4.83E+33	-5.8	18500
104	PC4H9=C2H5+C2H4	7.50E+17	-1.4	29580
105	H2O2+H=H2+HO2	4.82E+13	0	7950
106	HCO+O=CO2+H	3.00E+13	0	0
107	CH3+M=CH2+H+M	1.97E+16	0	92520
108	CH3+H=CH2+H2	9.00E+13	0	15100
109	CH3+OH=CH2+H2O	3.00E+06	2	2500
110	C2H4+O=CH2CHO+H	3.39E+06	1.9	179
111	C5H11-1=C2H4+NC3H7	7.97E+17	-1.4	29790
112	C2H5O+M=CH3+CH2O+M	1.35E+38	-7	23800
113	H2O2+O2=HO2+HO2	1.84E+14	-0.7	39540
114	H2O2+O2=HO2+HO2	5.94E+17	-0.7	53150
115	C2H3+O2=CH2CHO+O	3.50E+14	-0.6	5260
116	C2H5+HO2=C2H5O+OH	3.20E+13	0	0
117	H2O2+OH=H2O+HO2	1.00E+12	0	0
118	H2O2+OH=H2O+HO2	5.80E+14	0	9560
119	O2C2H4OH=PC2H4OH+O2	3.90E+16	-1	30000
120	O2C2H4OH=OH+CH2O+CH2O	1.25E+10	0	18900
121	C3H5O=C2H3+CH2O	2.03E+12	0.1	23560
122	C3H5-A+HO2=C3H5O+OH	7.00E+12	0	-1000
123	NC3H7O=C2H5+CH2O	1.39E+16	-0.9	19770
124	NC3H7O2H=NC3H7O+OH	1.50E+16	0	42500
125	NC3H7O2+CH2O=NC3H7O2H+HCO	5.60E+12	0	13600
126	NC3H7O2+HO2=NC3H7O2H+O2	1.75E+10	0	-3275
127	C2H4+NC3H7O2=C2H3+NC3H7O2H	1.13E+13	0	30430
128	CH4+NC3H7O2=CH3+NC3H7O2H	1.12E+13	0	24640
129	H2+NC3H7O2=H+NC3H7O2H	3.01E+13	0	26030
130	NC3H7O2+C2H6=NC3H7O2H+C2H5	1.70E+13	0	20460
131	NC3H7O2+NC3H7O2=O2+NC3H7O+NC3H7O	1.40E+16	-1.6	1860
132	NC3H7O2+CH3=NC3H7O+CH3O	7.00E+12	0	-1000
133	NC3H7O2+C2H5=NC3H7O+C2H5O	7.00E+12	0	-1000
134	NC3H7O2+NC3H7=NC3H7O+NC3H7O	7.00E+12	0	-1000
135	NC3H7O2+PC4H9=NC3H7O+PC4H9O	7.00E+12	0	-1000
136	NC3H7O2+C3H5-A=NC3H7O+C3H5O	7.00E+12	0	-1000
137	C3H6+NC3H7O2=C3H5-A+NC3H7O2H	3.24E+11	0	14900
138	NC3H7O2=NC3H7+O2	3.36E+19	-1.3	35760
139	NC3H7+HO2=NC3H7O+OH	7.00E+12	0	-1000
140	PC4H9O=NC3H7+CH2O	5.81E+16	-1	20260
141	PC4H9O2H=PC4H9O+OH	1.50E+16	0	42500
142	PC4H9O2+CH2O=PC4H9O2H+HCO	5.60E+12	0	13600
143	PC4H9O2+HO2=PC4H9O2H+O2	1.75E+10	0	-3275
144	C3H6+PC4H9O2=C3H5-A+PC4H9O2H	3.24E+11	0	14900
145	C2H4+PC4H9O2=C2H3+PC4H9O2H	1.13E+13	0	30430
146	CH4+PC4H9O2=CH3+PC4H9O2H	1.12E+13	0	24640
147	H2O2+PC4H9O2=HO2+PC4H9O2H	2.40E+12	0	10000
148	PC4H9O2+PC4H9O2=O2+PC4H9O+PC4H9O	1.40E+16	-1.6	1860
149	PC4H9O2+NC3H7O2=PC4H9O+NC3H7O+O2	1.40E+16	-1.6	1860
150	PC4H9O2+HO2=PC4H9O+OH+O2	1.40E-14	-1.6	1860
151	H2+PC4H9O2=H+PC4H9O2H	3.01E+13	0	26030
152	C2H6+PC4H9O2=C2H5+PC4H9O2H	1.70E+13	0	20460
153	PC4H9O2+CH3=PC4H9O+CH3O	7.00E+12	0	-1000
154	PC4H9O2+C2H5=PC4H9O+C2H5O	7.00E+12	0	-1000
155	PC4H9O2+NC3H7=PC4H9O+NC3H7O	7.00E+12	0	-1000
156	PC4H9O2+PC4H9=PC4H9O+PC4H9O	7.00E+12	0	-1000
157	PC4H9O2+C3H5-A=PC4H9O+C3H5O	7.00E+12	0	-1000
158	C3H6+O2=C3H5-A+HO2	4.00E+12	0	39900
159	C3H6+CH3=C3H5-A+CH4	2.21E+00	3.5	5675
160	C3H6+C2H5=C3H5-A+C2H6	1.00E+11	0	9800
161	C3H5-A+HO2=C2H3+CH2O+OH	1.00E-18	0	0

162	C3H5-A+C2H5=C2H4+C3H6	4.00E+11	0	0
163	PC4H9O2=PC4H9+O2	6.16E+19	-1.4	35510
164	PC4H9+HO2=PC4H9O+OH	7.00E+12	0	-1000
165	CH2CHO=CH2CO+H	3.09E+15	-0.3	50820
166	CH2CHO+O2=CH2O+CO+OH	2.00E+13	0	4200
167	C3H5-A+O2=CH2CHO+CH2O	7.14E+15	-1.2	21050
168	C3H5-A+O2=C2H2+CH2O+OH	9.72E+29	-5.7	21450
169	HCCO+O2=CO2+HCO	2.40E+11	0	-854
170	CH3+O2=CH2O+OH	7.47E+11	0	14250
171	C2H4+H2=CH3+CH3	3.77E+12	0.8	84710
172	NC4H9CHO+O2=NC4H9CO+HO2	2.00E+13	0.5	42200
173	NC4H9CHO+OH=NC4H9CO+H2O	2.69E+10	0.8	-340
174	NC4H9CHO+H=NC4H9CO+H2	4.00E+13	0	4200
175	NC4H9CHO+O=NC4H9CO+OH	5.00E+12	0	1790
176	NC4H9CHO+HO2=NC4H9CO+H2O2	2.80E+12	0	13600
177	NC4H9CHO+CH3=NC4H9CO+CH4	1.70E+12	0	8440
178	NC4H9CO=PC4H9+CO	1.00E+11	0	9600
179	HOCH2O=CH2O+OH	1.64E+14	-0.1	21890
180	HOCH2O=HOCHO+H	1.00E+14	0	14900
181	HOCHO+M=CO+H2O+M	2.30E+13	0	50000
182	HOCHO+M=CO2+H2+M	1.50E+16	0	57000
183	HOCHO=HCO+OH	4.59E+18	-0.5	108300
184	HOCHO+OH=H2O+CO2+H	2.62E+06	2.1	916
185	HOCHO+OH=H2O+CO+OH	1.85E+07	1.5	-962
186	HOCHO+H=H2+CO2+H	4.24E+06	2.1	4868
187	HOCHO+H=H2+CO+OH	6.03E+13	-0.3	2988
188	HOCHO+CH3=CH4+CO+OH	3.90E-07	5.8	2200
189	HOCHO+HO2=H2O2+CO+OH	1.00E+12	0	11920
190	HOCHO+O=CO+OH+OH	1.77E+18	-1.9	2975
191	C6H13-1+O2=C6H12-1+HO2	3.00E-19	0	3000
192	C6H13-1=C2H4+PC4H9	5.45E+17	-1.3	29580
193	C6H13-1=C6H12-1+H	2.09E+16	-0.9	37940
194	C6H12-1+OH=C5H11-1+CH2O	1.00E+11	0	-4000
195	C6H12-1+O=C5H11-1+HCO	1.00E+11	0	-1050
196	C6H12-1=NC3H7+C3H5-A	1.00E+16	0	71000
197	C6H13O2-1=C6H13-1+O2	5.15E+20	-1.7	35780
198	C6H13-1+C6H13O2-1=C6H13O-1+C6H13O-1	7.00E+12	0	-1000
199	C6H13O2-1+C6H13O2-1=O2+C6H13O-1+C6H13O-1	1.40E+16	-1.6	1860
200	C6H13O-1=C5H11-1+CH2O	1.81E+17	-1.1	20300
201	C6H13-1+HO2=C6H13O-1+OH	7.00E+12	0	-1000
202	C7H15-1=C5H11-1+C2H4	8.16E+17	-1.4	30840
203	C7H15O2-1=C7H15-1+O2	2.66E+20	-1.7	35400
204	C7H15-1+C7H15O2-1=C7H15O-1+C7H15O-1	7.00E+12	0	-1000
205	C7H15O2-1+C7H15O2-1=O2+C7H15O-1+C7H15O-1	1.40E+16	-1.6	1860
206	C7H15O-1=CH2O+C6H13-1	4.68E+17	-1.3	20260
207	NC4H9COCH2=PC4H9+CH2CO	1.55E+18	-1.4	43140
208	C7H15-1+HO2=C7H15O-1+OH	7.00E+12	0	-1000
209	C16H33-5+H=NC16H34	1.00E+14	0	0
210	C10H21-1+C6H13-1=NC16H34	8.00E+12	0	0
211	NC16H34+H=C16H33-5+H2	2.60E+06	2.4	4471
212	NC16H34+OH=C16H33-5+H2O	6.40E+08	1.6	-35
213	NC16H34+O=C16H33-5+OH	9.54E+04	2.7	2106
214	NC16H34+HO2=C16H33-5+H2O2	5.12E+14	0	17690
215	NC16H34+CH3=C16H33-5+CH4	5.41E+04	2.3	7287
216	NC16H34+O2=C16H33-5+HO2	4.00E+13	0	50150
217	NC16H34+C2H3=C16H33-5+C2H4	8.00E+11	0	16800
218	NC16H34+C2H5=C16H33-5+C2H6	1.00E+11	0	10400
219	NC16H34+C16H33O2-5=C16H33-5+C16H33O2H-5	1.00E+11	0	10400
220	C6H12-1+C10H21-1=C16H33-5	1.00E+12	0	8200
221	C2H4+C9H19-1=C11H23-1	1.00E+11	0	8200
222	C2H4+C8H17-1=C10H21-1	1.00E+11	0	8200
223	C2H4+C7H15-1=C9H19-1	1.00E+11	0	8200
224	C2H4+C6H13-1=C8H17-1	1.00E+11	0	8200
225	C16H33O2-5=C16H33-5+O2	1.36E+23	-2.4	37670
226	C11H23O2-1=C11H23-1+O2	2.66E+20	-1.7	35400
227	C10H21O2-1=C10H21-1+O2	2.66E+20	-1.7	35400
228	C9H19O2-1=C9H19-1+O2	2.66E+20	-1.7	35400
229	C8H17O2-1=C8H17-1+O2	2.66E+20	-1.7	35400
230	C16H33-5+C16H33O2-5=C16H33O-5+C16H33O-5	7.00E+12	0	-1000
231	C11H23-1+C11H23O2-1=C11H23O-1+C11H23O-1	7.00E+12	0	-1000
232	C10H21-1+C10H21O2-1=C10H21O-1+C10H21O-1	7.00E+12	0	-1000
233	C9H19-1+C9H19O2-1=C9H19O-1+C9H19O-1	7.00E+12	0	-1000
234	C8H17-1+C8H17O2-1=C8H17O-1+C8H17O-1	7.00E+12	0	-1000

235	C16H33-5+HO2=C16H33O-5+OH	7.00E+12	0	-1000
236	C11H23-1+HO2=C11H23O-1+OH	7.00E+12	0	-1000
237	C10H21-1+HO2=C10H21O-1+OH	7.00E+12	0	-1000
238	C9H19-1+HO2=C9H19O-1+OH	7.00E+12	0	-1000
239	C8H17-1+HO2=C8H17O-1+OH	7.00E+12	0	-1000
240	C16H33O2-5=C16OOH5-7	2.50E+10	0	20850
241	C9H19O2-1=C9OOH1-3	2.50E+10	0	20850
242	C16H33O2-5+HO2=C16H33O2H-5+O2	1.75E+10	0	-3275
243	C16H33O2-5+H2O2=C16H33O2H-5+HO2	2.40E+12	0	10000
244	C16H33O2H-5=C16H33O-5+OH	1.25E+16	0	41600
245	NC4H9CHO+C11H23-1=C16H33O-5	1.00E+11	0	12900
246	CH2O+C10H21-1=C11H23O-1	1.00E+11	0	11900
247	CH2O+C9H19-1=C10H21O-1	1.00E+11	0	11900
248	CH2O+C8H17-1=C9H19O-1	1.00E+11	0	11900
249	CH2O+C7H15-1=C8H17O-1	1.00E+11	0	11900
250	C16OOH5-7O2=C16OOH5-7+O2	1.37E+23	-2.4	37640
251	C9OOH1-3O2=C9OOH1-3+O2	1.37E+23	-2.4	37640
252	C16OOH5-7O2=C16KET5-7+OH	1.25E+10	0	17850
253	C9OOH1-3O2=C9KET1-3+OH	2.50E+10	0	21400
254	C16KET5-7=OH+NC4H9COCH2+NC9H19CHO	4.05E+16	0	41600
255	C9KET1-3=OH+CH2CHO+NC6H13CHO	1.05E+16	0	41600
256	NC9H19CHO+O2=NC9H19CO+HO2	2.00E+13	0.5	42200
257	NC9H19CHO+OH=NC9H19CO+H2O	2.69E+10	0.8	-340
258	NC9H19CHO+H=NC9H19CO+H2	4.00E+13	0	4200
259	NC9H19CHO+O=NC9H19CO+OH	5.00E+12	0	1790
260	NC9H19CHO+HO2=NC9H19CO+H2O2	2.80E+12	0	13600
261	NC9H19CHO+CH3=NC9H19CO+CH4	1.70E+12	0	8440
262	NC9H19CO=C9H19-1+CO	1.00E+11	0	9600
263	NC6H13CHO+O2=NC6H13CO+HO2	2.00E+13	0.5	42200
264	NC6H13CHO+OH=NC6H13CO+H2O	2.69E+10	0.8	-340
265	NC6H13CHO+H=NC6H13CO+H2	4.00E+13	0	4200
266	NC6H13CHO+O=NC6H13CO+OH	5.00E+12	0	1790
267	NC6H13CHO+HO2=NC6H13CO+H2O2	2.80E+12	0	13600
268	NC6H13CHO+CH3=NC6H13CO+CH4	1.70E+12	0	8440
269	NC6H13CO=C6H13-1+CO	1.00E+11	0	9600

Table C-2: The MCBSv2 biodiesel surrogate fuel model. Units are in mole, cm, s, K and cal.

Reaction Number	Reaction Considered	A	b	E
1	HOCH2O<=>CH2O+OH	2.06E+21	-2.3	25730
2	HOCH2O<=>HOCHO+H	1.00E+14	0	14900
3	CH2OH+HO2<=>HOCH2O+OH	1.00E+13	0	0
4	CH2O+H(+M)<=>CH2OH(+M)	5.40E+11	0.5	3600
	H2	Enhanced	by	2.00E+00
	H2O	Enhanced	by	6.00E+00
	CO	Enhanced	by	1.50E+00
	CO2	Enhanced	by	2.00E+00
	CH4	Enhanced	by	2.00E+00
	C2H6	Enhanced	by	3.00E+00
5	CH2OH+O2<=>CH2O+HO2	1.51E+15	-1	0
6	CH2OH+O2<=>CH2O+HO2	2.41E+14	0	5017
7	CH2OH+H<=>CH2O+H2	6.00E+12	0	0
8	CH2OH+HO2<=>CH2O+H2O2	1.20E+13	0	0
9	CH2OH+HCO<=>CH2O+CH2O	1.80E+14	0	0
10	OH+CH2OH<=>H2O+CH2O	2.40E+13	0	0
11	O+CH2OH<=>OH+CH2O	4.20E+13	0	0
12	CH3+OH<=>CH2OH+H	1.20E+10	0	13890
13	CH2CO+OH<=>CH2OH+CO	2.00E+12	0	-1010
14	CH2CO+H<=>HCCO+H2	2.00E+14	0	8000
15	CH2CO+O<=>HCCO+OH	1.00E+13	0	8000
16	CH2CO+OH<=>HCCO+H2O	1.00E+13	0	2000
17	HCCO+OH<=>H2+CO+CO	1.00E+14	0	0
18	HCCO+O<=>H+CO+CO	8.00E+13	0	0
19	HCCO+O2<=>OH+CO+CO	4.20E+10	0	850
20	C2H2+O2<=>HCCO+OH	2.00E+08	1.5	30100
21	C2H2+O<=>HCCO+H	1.35E+07	2	1900
22	H+O2<=>O+OH	3.55E+15	-0.4	16600
23	O+H2<=>H+OH	5.08E+04	2.7	6292
24	OH+H2<=>H+H2O	2.16E+08	1.5	3430
25	O+H2O<=>OH+OH	2.97E+06	2	13400
26	H2+M<=>H+H+M	4.58E+19	-1.4	104400
	H2	Enhanced	by	2.50E+00
	H2O	Enhanced	by	1.20E+01
	CO	Enhanced	by	1.90E+00
	CO2	Enhanced	by	3.80E+00
27	O2+M<=>O+O+M	4.52E+17	-0.6	118900
	H2	Enhanced	by	2.50E+00
	H2O	Enhanced	by	1.20E+01
	CO	Enhanced	by	1.90E+00
	CO2	Enhanced	by	3.80E+00
	CH4	Enhanced	by	2.00E+00
	C2H6	Enhanced	by	3.00E+00
28	OH+M<=>O+H+M	9.88E+17	-0.7	102100
	H2	Enhanced	by	2.50E+00
	H2O	Enhanced	by	1.20E+01
	CO	Enhanced	by	1.50E+00
	CO2	Enhanced	by	2.00E+00
	CH4	Enhanced	by	2.00E+00
	C2H6	Enhanced	by	3.00E+00
29	H2O+M<=>H+OH+M	1.91E+23	-1.8	118500
	H2	Enhanced	by	7.30E-01
	H2O	Enhanced	by	1.20E+01
	CH4	Enhanced	by	2.00E+00
	C2H6	Enhanced	by	3.00E+00
30	H+O2(+M)<=>HO2(+M)	1.48E+12	0.6	0
	H2	Enhanced	by	1.30E+00
	H2O	Enhanced	by	1.40E+01
	CO	Enhanced	by	1.90E+00
	CO2	Enhanced	by	3.80E+00
	CH4	Enhanced	by	2.00E+00
	C2H6	Enhanced	by	3.00E+00
31	HO2+H<=>H2+O2	1.66E+13	0	823
32	HO2+H<=>OH+OH	7.08E+13	0	295
33	HO2+O<=>OH+O2	3.25E+13	0	0
34	HO2+OH<=>H2O+O2	2.89E+13	0	-497

35	H2O2+O2<=>HO2+HO2	4.63E+16	-0.3	50670
36	H2O2+O2<=>HO2+HO2	1.43E+13	-0.3	37060
37	H2O2(+M)<=>OH+OH(+M)	2.95E+14	0	48430
	H2	Enhanced	by	2.50E+00
	H2O	Enhanced	by	1.20E+01
	CO	Enhanced	by	1.90E+00
	CO2	Enhanced	by	3.80E+00
	CH4	Enhanced	by	2.00E+00
	C2H6	Enhanced	by	3.00E+00
38	H2O2+H<=>H2O+OH	2.41E+13	0	3970
39	H2O2+H<=>H2+HO2	6.02E+13	0	7950
40	H2O2+O<=>OH+HO2	9.55E+06	2	3970
41	H2O2+OH<=>H2O+HO2	1.00E+12	0	0
42	H2O2+OH<=>H2O+HO2	5.80E+14	0	9557
43	CO+O(+M)<=>CO2(+M)	1.80E+10	0	2384
	H2	Enhanced	by	2.00E+00
	O2	Enhanced	by	6.00E+00
	H2O	Enhanced	by	6.00E+00
	CO	Enhanced	by	1.50E+00
	CO2	Enhanced	by	3.50E+00
	CH4	Enhanced	by	2.00E+00
	C2H6	Enhanced	by	3.00E+00
44	CO+O2<=>CO2+O	1.05E+12	0	42540
45	CO+OH<=>CO2+H	1.75E+05	1.9	-434.8
46	CO+HO2<=>CO2+OH	1.57E+05	2.2	17940
47	HCO+M<=>H+CO+M	1.86E+17	-1	17000
48	HCO+O2<=>CO+HO2	2.71E+10	0.7	-469
49	HCO+H<=>CO+H2	7.34E+13	0	0
50	HCO+O<=>CO+OH	3.02E+13	0	0
51	HCO+O<=>CO2+H	3.00E+13	0	0
52	HCO+OH<=>CO+H2O	1.02E+14	0	0
53	HCO+HO2<=>CH2O+O2	2.50E+14	-0.1	13920
54	HCO+HO2<=>CO2+H+OH	3.00E+13	0	0
55	CH2O+CO<=>HCO+HCO	9.19E+13	0.4	73040
56	HCO+HCO<=>H2+CO+CO	3.00E+12	0	0
57	HCO+H(+M)<=>CH2O(+M)	1.09E+12	0.5	-260
	H2	Enhanced	by	2.00E+00
	H2O	Enhanced	by	6.00E+00
	CO	Enhanced	by	1.50E+00
	CO2	Enhanced	by	2.00E+00
	CH4	Enhanced	by	2.00E+00
	C2H6	Enhanced	by	3.00E+00
58	CO+H2(+M)<=>CH2O(+M)	4.30E+07	1.5	79600
	H2	Enhanced	by	2.00E+00
	H2O	Enhanced	by	6.00E+00
	CO	Enhanced	by	1.50E+00
	CO2	Enhanced	by	2.00E+00
	CH4	Enhanced	by	2.00E+00
	C2H6	Enhanced	by	3.00E+00
59	CH2O+OH<=>HCO+H2O	7.82E+07	1.6	-1055
60	CH2O+H<=>HCO+H2	5.74E+07	1.9	2740
61	CH2O+O<=>HCO+OH	6.26E+09	1.1	2260
62	CH2O+HO2<=>HCO+H2O2	7.10E-03	4.5	6580
63	HOCHO<=>CO+H2O	2.30E+13	0	50000
64	HOCHO<=>CO2+H2	1.50E+16	0	57000
65	HOCHO<=>HCO+OH	3.47E+22	-1.5	110700
66	HOCHO+OH<=>H2O+CO2+H	2.62E+06	2.1	916
67	HOCHO+OH<=>H2O+CO+OH	1.85E+07	1.5	-962
68	HOCHO+H<=>H2+CO2+H	4.24E+06	2.1	4868
69	HOCHO+H<=>H2+CO+OH	6.03E+13	-0.3	2988
70	HOCHO+HO2<=>H2O2+CO+OH	1.00E+12	0	11920
71	HOCHO+O<=>CO+OH+OH	1.77E+18	-1.9	2975
72	CH3O(+M)<=>CH2O+H(+M)	6.80E+13	0	26170
	H2	Enhanced	by	2.00E+00
	H2O	Enhanced	by	6.00E+00
	CO	Enhanced	by	1.50E+00
	CO2	Enhanced	by	2.00E+00
	CH4	Enhanced	by	2.00E+00
	C2H6	Enhanced	by	3.00E+00
73	CH3O+O2<=>CH2O+HO2	4.38E-19	9.5	-5501
74	CH3O+H<=>CH2O+H2	2.00E+13	0	0
75	CH3O+HO2<=>CH2O+H2O2	3.01E+11	0	0
76	CH3+OH<=>CH2+H2O	5.60E+07	1.6	5420

77	CH2+O2<=>CO2+H+H	2.27E+12	0	1000
78	CH2+O<=>CO+H+H	5.00E+13	0	0
79	C2H2+O<=>CH2+CO	6.94E+06	2	1900
80	HCO+CH3<=>CH4+CO	2.65E+13	0	0
81	CH2O+CH3<=>HCO+CH4	3.83E+01	3.4	4312
82	CH3+H(+M)<=>CH4(+M)	2.11E+14	0	0
	H2	Enhanced	by	2.00E+00
	H2O	Enhanced	by	6.00E+00
	CO	Enhanced	by	1.50E+00
	CO2	Enhanced	by	2.00E+00
	CH4	Enhanced	by	2.00E+00
	C2H6	Enhanced	by	3.00E+00
83	CH4+OH<=>CH3+H2O	5.83E+04	2.6	2190
84	CH4+O<=>CH3+OH	4.40E+05	2.5	6577
85	CH4+HO2<=>CH3+H2O2	7.05E+04	2.5	21000
86	CH3+HO2<=>CH4+O2	1.16E+05	2.2	-3022
87	CH3+C2H5<=>CH4+C2H4	1.18E+04	2.5	-2921
88	CH3+OH<=>CH2O+H2	3.19E+09	0	5027
89	CH3+OH<=>CH3O+H	7.23E+11	0	5484
90	CH3+HO2<=>CH3O+OH	1.00E+12	0.3	-687.5
91	CH3+O<=>CH2O+H	5.54E+13	0.1	-136
92	CH3+O2<=>CH3O+O	7.55E+12	0	28320
93	CH3+O2<=>CH2O+OH	5.87E+11	0	13840
94	CH3+O2(+M)<=>CH3O2(+M)	1.01E+08	1.6	0
95	CH3O2+CH3<=>CH3O+CH3O	9.00E+12	0	-1200
96	CH3O2+CH3O2<=>O2+CH3O+CH3O	1.40E+16	-1.6	1860
97	CH3O2+H<=>CH3O+OH	9.60E+13	0	0
98	CH3O2+O<=>CH3O+O2	3.60E+13	0	0
99	C2H4+H(+M)<=>C2H5(+M)	5.40E+11	0.5	1820
	H2	Enhanced	by	2.00E+00
	H2O	Enhanced	by	6.00E+00
	CO	Enhanced	by	1.50E+00
	CO2	Enhanced	by	2.00E+00
	CH4	Enhanced	by	2.00E+00
	C2H6	Enhanced	by	3.00E+00
100	C2H6(+M)<=>CH3+CH3(+M)	1.88E+50	-9.7	107300
	H2	Enhanced	by	2.00E+00
	H2O	Enhanced	by	6.00E+00
	CO	Enhanced	by	1.50E+00
	CO2	Enhanced	by	2.00E+00
	CH4	Enhanced	by	2.00E+00
	C2H6	Enhanced	by	3.00E+00
101	C2H6+H<=>C2H5+H2	1.15E+08	1.9	7530
102	C2H6+O<=>C2H5+OH	3.55E+06	2.4	5830
103	C2H6+OH<=>C2H5+H2O	1.48E+07	1.9	950
104	C2H6+O2<=>C2H5+HO2	6.03E+13	0	51870
105	C2H5+C2H3<=>C2H4+C2H4	6.86E+11	0.1	-4300
106	C2H5+H<=>CH3+CH3	3.27E+17	-0.9	310
107	C2H5+H<=>C2H4+H2	2.00E+12	0	0
108	C2H5+O2<=>C2H4+HO2	7.56E+14	-1	4749
109	C2H5+O2<=>C2H4+O2	4.00E-01	3.9	13620
110	CH3CO(+M)<=>CH3+CO(+M)	3.00E+12	0	16720
111	CH3CO+H<=>CH2CO+H2	2.00E+13	0	0
112	CH3CO+O<=>CH2CO+OH	2.00E+13	0	0
113	CH2CHO<=>CH2CO+H	1.10E+13	0.4	50430
114	CH2CHO+O2<=>CH2O+CO+OH	2.00E+13	0	4200
115	CH2CO+H<=>CH3+CO	1.10E+13	0	3400
116	C2H3+H(+M)<=>C2H4(+M)	1.36E+14	0.2	660
	H2	Enhanced	by	2.00E+00
	H2O	Enhanced	by	6.00E+00
	CO	Enhanced	by	1.50E+00
	CO2	Enhanced	by	2.00E+00
	CH4	Enhanced	by	2.00E+00
	C2H6	Enhanced	by	3.00E+00
117	C2H4(+M)<=>C2H2+H2(+M)	8.00E+12	0.4	88770
	H2	Enhanced	by	2.00E+00
	H2O	Enhanced	by	6.00E+00
	CO	Enhanced	by	1.50E+00
	CO2	Enhanced	by	2.00E+00
	CH4	Enhanced	by	2.00E+00
	C2H6	Enhanced	by	3.00E+00
118	C2H4+H<=>C2H3+H2	5.07E+07	1.9	12950
119	C2H4+O<=>CH3+HCO	8.56E+06	1.9	183

120	$C_2H_4+O \rightleftharpoons CH_2CHO+H$	4.99E+06	1.9	183
121	$C_2H_4+OH \rightleftharpoons C_2H_3+H_2O$	2.09E+06	2	1160
122	$C_2H_4+O_2 \rightleftharpoons C_2H_3+HO_2$	4.00E+13	0	58200
123	$C_2H_2+H(+M) \rightleftharpoons C_2H_3(+M)$	5.60E+12	0	2400
	H2	Enhanced	by	2.00E+00
	H2O	Enhanced	by	6.00E+00
	CO	Enhanced	by	1.50E+00
	CO2	Enhanced	by	2.00E+00
	CH4	Enhanced	by	2.00E+00
	C2H6	Enhanced	by	3.00E+00
124	$C_2H_3+O_2 \rightleftharpoons C_2H_2+HO_2$	2.12E-06	6	9484
125	$C_2H_3+O_2 \rightleftharpoons CH_2O+HCO$	1.70E+29	-5.3	6500
126	$C_2H_3+O_2 \rightleftharpoons CH_2CHO+O$	5.50E+14	-0.6	5260
127	$C_2H_3+H \rightleftharpoons C_2H_2+H_2$	3.00E+13	0	0
128	$C_2H_3+OH \rightleftharpoons C_2H_2+H_2O$	5.00E+12	0	0
129	$C_2H_2+OH \rightleftharpoons CH_2CO+H$	3.24E+13	0	12000
130	$C_2H_2+OH \rightleftharpoons CH_3+CO$	4.83E-04	4	-2000
131	$CH_3COCH_2 \rightleftharpoons CH_2CO+CH_3$	1.00E+14	0	31000
132	$C_2H_3CHO \rightleftharpoons C_2H_3+HCO$	2.00E+24	-2.1	103400
133	$C_2H_3CHO+H \rightleftharpoons C_2H_3CO+H_2$	1.34E+13	0	3300
134	$C_2H_3CHO+O \rightleftharpoons C_2H_3CO+OH$	5.94E+12	0	1868
135	$C_2H_3CHO+OH \rightleftharpoons C_2H_3CO+H_2O$	9.24E+06	1.5	-962
136	$C_2H_3CHO+O_2 \rightleftharpoons C_2H_3CO+HO_2$	1.00E+13	0	40700
137	$C_2H_3CHO+HO_2 \rightleftharpoons C_2H_3CO+H_2O_2$	3.01E+12	0	11920
138	$C_2H_3CHO+C_2H_3 \rightleftharpoons C_2H_3CO+C_2H_4$	1.74E+12	0	8440
139	$C_2H_3CO \rightleftharpoons C_2H_3+CO$	1.37E+21	-2.2	39410
140	$C_2H_5CHO \rightleftharpoons C_2H_5+HCO$	1.50E+27	-3.2	87040
141	$C_2H_5CHO+H \rightleftharpoons C_2H_5CO+H_2$	4.00E+13	0	4200
142	$C_2H_5CHO+O \rightleftharpoons C_2H_5CO+OH$	5.00E+12	0	1790
143	$C_2H_5CHO+OH \rightleftharpoons C_2H_5CO+H_2O$	2.69E+10	0.8	-340
144	$C_2H_5CHO+HO_2 \rightleftharpoons C_2H_5CO+H_2O_2$	2.80E+12	0	13600
145	$C_2H_5CHO+O_2 \rightleftharpoons C_2H_5CO+HO_2$	1.00E+13	0	40700
146	$C_2H_5CHO+C_2H_3 \rightleftharpoons C_2H_5CO+C_2H_4$	1.70E+12	0	8440
147	$C_2H_5CO \rightleftharpoons C_2H_5+CO$	2.46E+23	-3.2	17550
148	$CH_3OCO \rightleftharpoons CH_3+CO_2$	7.98E+12	0.3	15640
149	$CH_3OCO \rightleftharpoons CH_3O+CO$	3.18E+13	0.5	23400
150	$NC_3H_7 \rightleftharpoons CH_3+C_2H_4$	9.97E+40	-8.6	41430
151	$NC_3H_7 \rightleftharpoons H+C_3H_6$	8.78E+39	-8.1	46580
152	$NC_3H_7+O_2 \rightleftharpoons C_3H_6+HO_2$	3.00E-19	0	3000
153	$C_2H_5CHO+C_3H_5-A \rightleftharpoons C_2H_5CO+C_3H_6$	1.70E+12	0	8440
154	$C_3H_6 \rightleftharpoons C_2H_3+CH_3$	2.73E+62	-13.3	123200
155	$C_3H_6 \rightleftharpoons C_3H_5-A+H$	2.01E+61	-13.3	118500
156	$C_3H_6+O \rightleftharpoons C_2H_5+HCO$	1.58E+07	1.8	-1216
157	$C_3H_6+O \rightleftharpoons CH_2CO+CH_3+H$	2.50E+07	1.8	76
158	$C_3H_6+O \rightleftharpoons C_3H_5-A+OH$	5.24E+11	0.7	5884
159	$C_3H_6+OH \rightleftharpoons C_3H_5-A+H_2O$	3.12E+06	2	-298
160	$C_3H_6+HO_2 \rightleftharpoons C_3H_5-A+H_2O_2$	9.64E+03	2.6	13910
161	$C_3H_6+H \rightleftharpoons C_3H_5-A+H_2$	1.73E+05	2.5	2492
162	$C_3H_6+H \rightleftharpoons C_2H_4+CH_3$	1.45E+34	-5.8	18500
163	$C_3H_6+O_2 \rightleftharpoons C_3H_5-A+HO_2$	4.00E+12	0	39900
164	$C_3H_5-A \rightleftharpoons C_2H_2+CH_3$	2.40E+48	-9.9	82080
165	$C_3H_5-A+HO_2 \rightleftharpoons C_3H_5O+OH$	7.00E+12	0	-1000
166	$C_3H_5-A+CH_3O_2 \rightleftharpoons C_3H_5O+CH_3O$	7.00E+12	0	-1000
167	$C_3H_5-A+C_2H_5 \rightleftharpoons C_2H_4+C_3H_6$	4.00E+11	0	0
168	$C_3H_5-A+O_2 \rightleftharpoons CH_2CHO+CH_2O$	7.14E+15	-1.2	21050
169	$C_3H_5-A+O_2 \rightleftharpoons C_2H_3CHO+OH$	2.47E+13	-0.4	23020
170	$C_3H_5-A+O_2 \rightleftharpoons C_2H_2+CH_2O+OH$	9.72E+29	-5.7	21450
171	$C_3H_5O \rightleftharpoons C_2H_3CHO+H$	1.00E+14	0	29100
172	$C_3H_5O \rightleftharpoons C_2H_3+CH_2O$	1.46E+20	-2	35090
173	$C_3H_5O+O_2 \rightleftharpoons C_2H_3CHO+HO_2$	1.00E+12	0	6000
174	$C_4H_8-1 \rightleftharpoons C_3H_5-A+CH_3$	1.50E+19	-1	73400
175	$C_4H_8-1 \rightleftharpoons C_2H_3+C_2H_5$	1.00E+19	-1	96770
176	$C_4H_6 \rightleftharpoons C_2H_3+C_2H_3$	4.03E+19	-1	98150
177	$C_4H_6+OH \rightleftharpoons C_2H_5+CH_2CO$	1.00E+12	0	0
178	$C_4H_6+OH \rightleftharpoons CH_2O+C_3H_5-A$	1.00E+12	0	0
179	$C_4H_6+O \rightleftharpoons C_2H_4+CH_2CO$	1.00E+12	0	0
180	$C_2H_3+C_2H_4 \rightleftharpoons C_4H_6+H$	5.00E+11	0	7300
181	$C_3H_7CHO+O_2 \rightleftharpoons C_3H_7CO+HO_2$	2.00E+13	0.5	42200
182	$C_3H_7CHO+OH \rightleftharpoons C_3H_7CO+H_2O$	2.69E+10	0.8	-340
183	$C_3H_7CHO+H \rightleftharpoons C_3H_7CO+H_2$	4.00E+13	0	4200
184	$C_3H_7CHO+O \rightleftharpoons C_3H_7CO+OH$	5.00E+12	0	1790
185	$C_3H_7CHO+HO_2 \rightleftharpoons C_3H_7CO+H_2O_2$	2.80E+12	0	13600
186	$C_3H_7CO \rightleftharpoons NC_3H_7+CO$	1.00E+11	0	9600

187	MD6J+H=MD	1.00E+14	0	0
188	MS7J+NC3H7=MD	8.00E+12	0	0
189	MB4J+C6H13-1=MD	8.00E+12	0	0
190	ME2J+C8H17-1=MD	8.00E+12	0	0
191	MD+H=MD6J+H2	1.30E+06	2.4	4471
192	MD+HO2=MD6J+H2O2	5.88E+04	2.5	14860
193	MD+OH=MD6J+H2O	4.67E+08	1.6	-35
194	MD+O2=MD6J+HO2	4.00E+13	0	50160
195	MD+O=MD6J+OH	5.95E+05	2.4	2846
196	MD+C2H3=MD6J+C2H4	4.00E+11	0	16800
197	NC3H7+MS6D=MD6J	8.80E+04	2.5	6130
198	C2H4+MF5J=MS7J	8.80E+03	2.5	6130
199	MS6D+H=MS7J	2.50E+11	0.5	2620
200	C2H4+MP3J=MF5J	8.80E+03	2.5	6130
201	C2H4+ME2J=MB4J	2.00E+11	0	7600
202	C2H4+CH3OCO=MP3J	1.06E+11	0	7350
203	CH2CO+CH3O=ME2J	5.00E+11	0	-1000
204	C2H4+C6H13-1=C8H17-1	8.80E+03	2.5	6130
205	CH2CO+C2H5=C3H7CO	1.00E+11	0	7600
206	CH2CO+CH3=C2H5CO	1.00E+11	0	7600
207	MS7J+O2=MS6D+HO2	1.60E+12	0	5000
208	MS6D=C3H5-A+MB4J	2.50E+16	0	71000
209	MD9D=C3H6+MS6D	3.98E+12	0	57630
210	MD6J+O2=MD6O2	7.54E+12	0	0
211	MF5J+O2=MF5O2	4.52E+12	0	0
212	MF5O2=MF5OOH3J	2.50E+10	0	20850
213	MD6O2=MD6OOH8J	2.50E+10	0	20850
214	MD6OOH8J+O2=MD6OOH8O2	7.54E+12	0	0
215	MF5OOH3J+O2=MF5OOH3O2	7.54E+12	0	0
216	MD6OOH8O2=MDKET68+OH	1.25E+10	0	17850
217	MF5OOH3O2=MFKET53+OH	2.50E+10	0	21400
218	MDKET68=C2H5CHO+MS6OXO7J+OH	1.05E+16	0	41600
219	MFKET53=OH+MFKET53O	1.05E+16	0	41600
220	CO+ME2J=MP3OXO3J	1.51E+11	0	4810
221	CH2CO+CH3OCO=MP3OXO3J	1.51E+11	0	4810
222	CH2CO+ME2J=MB3OXO4J	1.51E+11	0	4810
223	CH2CO+MF5J=MS6OXO7J	1.51E+11	0	4810
224	CH2CHO+MP3OXO=MFKET53O	3.33E+10	0	6397
225	MP3OXO+H=MP3OXO3J+H2	4.00E+13	0	4200
226	MP3OXO+OH=MP3OXO3J+H2O	2.69E+10	0.8	-340
227	MD9D=MS7J+C3H5-A	2.50E+16	0	71000
228	MD9D6J+H=MD9D	1.00E+14	0	0
229	MD9D+H=MD9D6J+H2	1.30E+06	2.4	4471
230	MD9D+HO2=MD9D6J+H2O2	5.88E+04	2.5	14860
231	MD9D+OH=MD9D6J+H2O	4.67E+08	1.6	-35
232	MD9D+O2=MD9D6J+HO2	4.00E+13	0	50160
233	MD9D+O=MD9D6J+OH	5.95E+05	2.4	2846
234	MD9D+C2H3=MD9D6J+C2H4	4.00E+11	0	16800
235	MD9D6J=C3H5-A+MS6D	1.31E+14	0	21460
236	MD9D6J+O2=MD9D6O2	7.54E+12	0	0
237	MD9D6O2=MD9D6OOH8J	1.25E+10	0	16350
238	MD9D6OOH8J+O2=MD9D6OOH8O2	7.54E+12	0	0
239	MD9D6OOH8O2=MD9DKET68+OH	1.25E+10	0	17850
240	MD9DKET68=OH+C2H3CHO+MS6OXO7J	1.05E+16	0	41600
241	NC7H16=H+C7H15-2	6.50E+87	-21	139500
242	NC7H16+H=C7H15-2+H2	2.60E+06	2.4	4471
243	NC7H16+O=C7H15-2+OH	9.54E+04	2.7	2106
244	NC7H16+OH=C7H15-2+H2O	9.40E+07	1.6	-35
245	NC7H16+HO2=C7H15-2+H2O2	1.12E+13	0	17690
246	NC7H16+O2=C7H15-2+HO2	4.00E+13	0	50150
247	C7H15-2+O2=C7H15O2-2	7.54E+12	0	0
248	C7H15O2-2=C7H14OOH2-4	2.50E+10	0	20850
249	C7H14OOH2-4+O2=C7H14OOH2-4O2	7.54E+12	0	0
250	C7H14OOH2-4O2=NC7KET24+OH	1.25E+09	0	17850
251	NC7KET24=OH+NC7KET24O	1.05E+16	0	41600
252	CH3COCH2+C3H7CHO=NC7KET24O	3.33E+10	0	6397

Table C-3: The reduced ethylene mechanism. Units are in mole, cm, s, K and cal.

Reaction Number	Reaction Considered	A	b	E
1	H+O2=O+OH	2.64E+16	-0.7	17041
2	O+H2=H+OH	4.59E+04	2.7	6260
3	OH+H2=H+H2O	1.73E+08	1.5	3430
4	OH+OH=O+H2O	3.97E+04	2.4	-2110
5	H+H+M=H2+M	1.78E+18	-1	0
	H2	Enhanced	by	0.00E+00
	H2O	Enhanced	by	0.00E+00
	CO2	Enhanced	by	0.00E+00
6	H+H+H2=H2+H2	9.00E+16	-0.6	0
7	H+H+H2O=H2+H2O	5.62E+19	-1.2	0
8	H+H+CO2=H2+CO2	5.50E+20	-2	0
9	H+OH+M=H2O+M	4.40E+22	-2	0
	H2	Enhanced	by	2.00E+00
	H2O	Enhanced	by	6.30E+00
	CO	Enhanced	by	1.75E+00
	CO2	Enhanced	by	3.60E+00
10	O+H+M=OH+M	9.43E+18	-1	0
	H2	Enhanced	by	2.00E+00
	H2O	Enhanced	by	1.20E+01
	CO	Enhanced	by	1.75E+00
	CO2	Enhanced	by	3.60E+00
11	O+O+M=O2+M	1.20E+17	-1	0
	H2	Enhanced	by	2.40E+00
	H2O	Enhanced	by	1.54E+01
	CO	Enhanced	by	1.75E+00
	CO2	Enhanced	by	3.60E+00
12	H+O2(+M)=HO2(+M)	5.12E+12	0.4	0
	O2	Enhanced	by	8.50E-01
	H2O	Enhanced	by	1.19E+01
	CO	Enhanced	by	1.09E+00
	CO2	Enhanced	by	2.18E+00
13	H2+O2=HO2+H	5.92E+05	2.4	53502
14	OH+OH(+M)=H2O2(+M)	1.11E+14	-0.4	0
	H2	Enhanced	by	2.00E+00
	H2O	Enhanced	by	6.00E+00
	CO	Enhanced	by	1.75E+00
	CO2	Enhanced	by	3.60E+00
15	HO2+H=O+H2O	3.97E+12	0	671
16	HO2+H=OH+OH	7.48E+13	0	295
17	HO2+O=OH+O2	4.00E+13	0	0
18	HO2+HO2=O2+H2O2	1.30E+11	0	-1630
19	HO2+HO2=O2+H2O2	3.66E+14	0	12000
20	OH+HO2=H2O+O2	1.41E+18	-1.8	60
21	OH+HO2=H2O+O2	1.12E+85	-22.3	26900
22	OH+HO2=H2O+O2	5.37E+70	-16.7	32900
23	OH+HO2=H2O+O2	2.51E+12	2	40000
24	OH+HO2=H2O+O2	1.00+136	-40	34800
25	H2O2+H=HO2+H2	6.05E+06	2	5200
26	H2O2+H=OH+H2O	2.41E+13	0	3970
27	H2O2+O=OH+HO2	9.63E+06	2	3970
28	H2O2+OH=HO2+H2O	2.00E+12	0	427
29	H2O2+OH=HO2+H2O	2.67E+41	-7	37600
30	CO+O(+M)=CO2(+M)	1.36E+10	0	2384
	H2	Enhanced	by	2.00E+00
	H2O	Enhanced	by	1.20E+01
	CO	Enhanced	by	1.75E+00
	CO2	Enhanced	by	3.60E+00
31	CO+OH=CO2+H	7.05E+04	2.1	-355.7
32	CO+OH=CO2+H	5.76E+12	-0.7	331.8
33	CO+O2=CO2+O	1.12E+12	0	47700
34	CO+HO2=CO2+OH	1.57E+05	2.2	17942.6
35	HCO+H=CO+H2	1.20E+14	0	0
36	HCO+O=CO+OH	3.00E+13	0	0
37	HCO+O=CO2+H	3.00E+13	0	0
38	HCO+OH=CO+H2O	3.02E+13	0	0
39	HCO+M=CO+H+M	1.87E+17	-1	17000

	H2	Enhanced	by	2.00E+00
	H2O	Enhanced	by	0.00E+00
	CO	Enhanced	by	1.75E+00
	CO2	Enhanced	by	3.60E+00
40	HCO+H2O=CO+H+H2O	2.24E+18	-1	17000
41	HCO+O2=CO+HO2	1.20E+10	0.8	-727
42	CO+H2(+M)=CH2O(+M)	4.30E+07	1.5	79600
	H2	Enhanced	by	2.00E+00
	H2O	Enhanced	by	6.00E+00
	CH4	Enhanced	by	2.00E+00
	CO	Enhanced	by	1.50E+00
	CO2	Enhanced	by	2.00E+00
	C2H6	Enhanced	by	3.00E+00
43	HCO+H(+M)=CH2O(+M)	1.09E+12	0.5	-260
	H2	Enhanced	by	2.00E+00
	H2O	Enhanced	by	6.00E+00
	CH4	Enhanced	by	2.00E+00
	CO	Enhanced	by	1.50E+00
	CO2	Enhanced	by	2.00E+00
	C2H6	Enhanced	by	3.00E+00
44	CH2+H(+M)=CH3(+M)	2.50E+16	-0.8	0
	H2	Enhanced	by	2.00E+00
	H2O	Enhanced	by	6.00E+00
	CH4	Enhanced	by	2.00E+00
	CO	Enhanced	by	1.50E+00
	CO2	Enhanced	by	2.00E+00
	C2H6	Enhanced	by	3.00E+00
45	CH2+O=HCO+H	8.00E+13	0	0
46	CH2+OH=CH2O+H	2.00E+13	0	0
47	CH2+H2=H+CH3	5.00E+05	2	7230
48	CH2+O2=HCO+OH	1.06E+13	0	1500
49	CH2+O2=CO2+H+H	2.64E+12	0	1500
50	CH2+HO2=CH2O+OH	2.00E+13	0	0
51	CH2+CO(+M)=CH2CO(+M)	8.10E+11	0.5	4510
	H2	Enhanced	by	2.00E+00
	H2O	Enhanced	by	6.00E+00
	CH4	Enhanced	by	2.00E+00
	CO	Enhanced	by	1.50E+00
	CO2	Enhanced	by	2.00E+00
	C2H6	Enhanced	by	3.00E+00
52	CH2+CH2=C2H2+H2	3.20E+13	0	0
53	CH2O+H(+M)=CH3O(+M)	5.40E+11	0.5	2600
	H2	Enhanced	by	2.00E+00
	H2O	Enhanced	by	6.00E+00
	CH4	Enhanced	by	2.00E+00
	CO	Enhanced	by	1.50E+00
	CO2	Enhanced	by	2.00E+00
	C2H6	Enhanced	by	3.00E+00
54	CH2O+H=HCO+H2	2.30E+10	1.1	3275
55	CH2O+O=HCO+OH	3.90E+13	0	3540
56	CH2O+OH=HCO+H2O	3.43E+09	1.2	-447
57	CH2O+O2=HCO+HO2	1.00E+14	0	40000
58	CH2O+HO2=HCO+H2O2	1.00E+12	0	8000
59	CH3+H(+M)=CH4(+M)	1.27E+16	-0.6	383
	H2	Enhanced	by	2.00E+00
	H2O	Enhanced	by	6.00E+00
	CH4	Enhanced	by	2.00E+00
	CO	Enhanced	by	1.50E+00
	CO2	Enhanced	by	2.00E+00
	C2H6	Enhanced	by	3.00E+00
60	CH3+O=CH2O+H	8.43E+13	0	0
61	CH3+OH=CH2+H2O	5.60E+07	1.6	5420
62	CH3+O2=O+CH3O	3.08E+13	0	28800
63	CH3+O2=OH+CH2O	3.60E+10	0	8940
64	CH3+HO2=CH4+O2	1.00E+12	0	0
65	CH3+HO2=CH3O+OH	1.34E+13	0	0
66	CH3+H2O2=CH4+HO2	2.45E+04	2.5	5180
67	CH3+HCO=CH4+CO	8.48E+12	0	0
68	CH3+CH2O=CH4+HCO	3.32E+03	2.8	5860
69	CH3+CH2=C2H4+H	4.00E+13	0	0

70	CH ₃ +CH ₃ (+M)=C ₂ H ₆ (+M)	2.12E+16	-1	620
	H ₂	Enhanced	by	2.00E+00
	H ₂ O	Enhanced	by	6.00E+00
	CH ₄	Enhanced	by	2.00E+00
	CO	Enhanced	by	1.50E+00
	CO ₂	Enhanced	by	2.00E+00
	C ₂ H ₆	Enhanced	by	3.00E+00
71	CH ₃ +CH ₃ =H+C ₂ H ₅	4.99E+12	0.1	10600
72	CH ₃ O+H=CH ₂ O+H ₂	2.00E+13	0	0
73	CH ₃ O+H=CH ₃ +OH	3.20E+13	0	0
74	CH ₃ O+O=CH ₂ O+OH	1.00E+13	0	0
75	CH ₃ O+OH=CH ₂ O+H ₂ O	5.00E+12	0	0
76	CH ₃ O+O ₂ =CH ₂ O+HO ₂	4.28E-13	7.6	-3530
77	CH ₄ +H=CH ₃ +H ₂	6.60E+08	1.6	10840
78	CH ₄ +O=CH ₃ +OH	1.02E+09	1.5	8600
79	CH ₄ +OH=CH ₃ +H ₂ O	1.00E+08	1.6	3120
80	CH ₄ +CH ₂ =CH ₃ +CH ₃	2.46E+06	2	8270
81	C ₂ H ₃ (+M)=C ₂ H ₂ +H(+M)	3.86E+08	1.6	37048.2
	H ₂	Enhanced	by	2.00E+00
	H ₂ O	Enhanced	by	6.00E+00
	CH ₄	Enhanced	by	2.00E+00
	CO	Enhanced	by	1.50E+00
	CO ₂	Enhanced	by	2.00E+00
	C ₂ H ₆	Enhanced	by	3.00E+00
	C ₂ H ₂	Enhanced	by	3.00E+00
	C ₂ H ₄	Enhanced	by	3.00E+00
82	C ₂ H ₂ +O=CH ₂ +CO	4.08E+07	2	1900
83	C ₂ H ₂ +OH=CH ₂ CO+H	2.18E-04	4.5	-1000
84	C ₂ H ₂ +OH=CH ₃ +CO	4.83E-04	4	-2000
85	C ₂ H ₂ +HCO=C ₂ H ₃ +CO	1.00E+07	2	6000
86	CH ₂ CO+H(+M)=CH ₂ CHO(+M)	3.30E+14	-0.1	8500
	H ₂	Enhanced	by	2.00E+00
	H ₂ O	Enhanced	by	6.00E+00
	CH ₄	Enhanced	by	2.00E+00
	CO	Enhanced	by	1.50E+00
	CO ₂	Enhanced	by	2.00E+00
	C ₂ H ₆	Enhanced	by	3.00E+00
	C ₂ H ₂	Enhanced	by	3.00E+00
	C ₂ H ₄	Enhanced	by	3.00E+00
87	CH ₂ CO+H=CH ₃ +CO	1.50E+09	1.4	2690
88	CH ₂ CO+O=CH ₂ +CO ₂	1.75E+12	0	1350
89	C ₂ H ₃ +H(+M)=C ₂ H ₄ (+M)	6.08E+12	0.3	280
	H ₂	Enhanced	by	2.00E+00
	H ₂ O	Enhanced	by	6.00E+00
	CH ₄	Enhanced	by	2.00E+00
	CO	Enhanced	by	1.50E+00
	CO ₂	Enhanced	by	2.00E+00
	C ₂ H ₆	Enhanced	by	3.00E+00
	C ₂ H ₂	Enhanced	by	3.00E+00
	C ₂ H ₄	Enhanced	by	3.00E+00
90	C ₂ H ₃ +H=C ₂ H ₂ +H ₂	9.00E+13	0	0
91	C ₂ H ₃ +O=CH ₂ CO+H	4.80E+13	0	0
92	C ₂ H ₃ +O=CH ₃ +CO	4.80E+13	0	0
93	C ₂ H ₃ +OH=C ₂ H ₂ +H ₂ O	3.01E+13	0	0
94	C ₂ H ₃ +O ₂ =C ₂ H ₂ +HO ₂	1.34E+06	1.6	-383.4
95	C ₂ H ₃ +O ₂ =CH ₂ CHO+O	3.00E+11	0.3	11
96	C ₂ H ₃ +O ₂ =HCO+CH ₂ O	4.60E+16	-1.4	1010
97	C ₂ H ₃ +HO ₂ =CH ₂ CHO+OH	1.00E+13	0	0
98	C ₂ H ₃ +H ₂ O ₂ =C ₂ H ₄ +HO ₂	1.21E+10	0	-596
99	C ₂ H ₃ +HCO=C ₂ H ₄ +CO	9.03E+13	0	0
100	C ₂ H ₃ +CH ₃ =C ₂ H ₂ +CH ₄	3.92E+11	0	0
101	C ₂ H ₃ +CH ₃ (+M)=C ₃ H ₆ (+M)	2.50E+13	0	0
	H ₂	Enhanced	by	2.00E+00
	H ₂ O	Enhanced	by	6.00E+00
	CH ₄	Enhanced	by	2.00E+00
	CO	Enhanced	by	1.50E+00
	CO ₂	Enhanced	by	2.00E+00
	C ₂ H ₆	Enhanced	by	3.00E+00
	C ₂ H ₂	Enhanced	by	3.00E+00
	C ₂ H ₄	Enhanced	by	3.00E+00
102	C ₂ H ₃ +C ₂ H ₃ =C ₂ H ₂ +C ₂ H ₄	9.60E+11	0	0
103	CH ₂ CHO=CH ₃ +CO	7.80E+41	-9.1	46900
104	CH ₂ CHO+H=CH ₃ +HCO	9.00E+13	0	0

105	CH ₂ CHO+H=CH ₂ CO+H ₂	2.00E+13	0	4000
106	CH ₂ CHO+O=CH ₂ CO+OH	2.00E+13	0	4000
107	CH ₂ CHO+OH=CH ₂ CO+H ₂ O	1.00E+13	0	2000
108	CH ₂ CHO+O ₂ =CH ₂ CO+HO ₂	1.40E+11	0	0
109	CH ₂ CHO+O ₂ =CH ₂ O+CO+OH	1.80E+10	0	0
110	CH ₂ OCH ₂ =CH ₃ +HCO	3.63E+13	0	57200
111	CH ₂ OCH ₂ =CH ₄ +CO	1.21E+13	0	57200
112	CH ₂ OCH ₂ +H=C ₂ H ₃ +H ₂ O	5.00E+09	0	5000
113	CH ₂ OCH ₂ +H=C ₂ H ₄ +OH	9.51E+10	0	5000
114	C ₂ H ₄ +H(+M)=C ₂ H ₅ (+M)	1.37E+09	1.5	1355
	H ₂	Enhanced	by	2.00E+00
	H ₂ O	Enhanced	by	6.00E+00
	CH ₄	Enhanced	by	2.00E+00
	CO	Enhanced	by	1.50E+00
	CO ₂	Enhanced	by	2.00E+00
	C ₂ H ₆	Enhanced	by	3.00E+00
115	C ₂ H ₄ +H=C ₂ H ₃ +H ₂	5.07E+07	1.9	12950
116	C ₂ H ₄ +O=C ₂ H ₃ +OH	1.51E+07	1.9	3740
117	C ₂ H ₄ +O=CH ₃ +HCO	1.92E+07	1.8	220
118	C ₂ H ₄ +O=CH ₂ +CH ₂ O	3.84E+05	1.8	220
119	C ₂ H ₄ +OH=C ₂ H ₃ +H ₂ O	3.60E+06	2	2500
120	C ₂ H ₄ +HCO=C ₂ H ₅ +CO	1.00E+07	2	8000
121	C ₂ H ₄ +CH ₃ =C ₂ H ₃ +CH ₄	2.27E+05	2	9200
122	C ₂ H ₄ +CH ₃ =nC ₃ H ₇	3.30E+11	0	7700
123	C ₂ H ₄ +O ₂ =C ₂ H ₃ +HO ₂	4.22E+13	0	60800
124	C ₂ H ₄ +HO ₂ =CH ₂ OCH ₂ +OH	2.82E+12	0	17100
125	C ₂ H ₅ +H(+M)=C ₂ H ₆ (+M)	5.21E+17	-1	1580
	H ₂	Enhanced	by	2.00E+00
	H ₂ O	Enhanced	by	6.00E+00
	CH ₄	Enhanced	by	2.00E+00
	CO	Enhanced	by	1.50E+00
	CO ₂	Enhanced	by	2.00E+00
	C ₂ H ₆	Enhanced	by	3.00E+00
126	C ₂ H ₅ +H=C ₂ H ₄ +H ₂	2.00E+12	0	0
127	C ₂ H ₅ +O=CH ₃ +CH ₂ O	1.60E+13	0	0
128	C ₂ H ₅ +O ₂ =C ₂ H ₄ +HO ₂	2.00E+10	0	0
129	C ₂ H ₅ +HO ₂ =C ₂ H ₆ +O ₂	3.00E+11	0	0
130	C ₂ H ₅ +HO ₂ =C ₂ H ₄ +H ₂ O ₂	3.00E+11	0	0
131	C ₂ H ₅ +HO ₂ =CH ₃ +CH ₂ O+OH	2.40E+13	0	0
132	C ₂ H ₅ +H ₂ O ₂ =C ₂ H ₆ +HO ₂	8.70E+09	0	974
133	C ₂ H ₆ +H=C ₂ H ₅ +H ₂	1.15E+08	1.9	7530
134	C ₂ H ₆ +O=C ₂ H ₅ +OH	8.98E+07	1.9	5690
135	C ₂ H ₆ +OH=C ₂ H ₅ +H ₂ O	3.54E+06	2.1	870
136	C ₂ H ₆ +CH ₃ =C ₂ H ₅ +CH ₄	6.14E+06	1.7	10450
137	C ₃ H ₆ +H(+M)=nC ₃ H ₇ (+M)	1.33E+13	0	3260.7
	H ₂	Enhanced	by	2.00E+00
	H ₂ O	Enhanced	by	6.00E+00
	CH ₄	Enhanced	by	2.00E+00
	CO	Enhanced	by	1.50E+00
	CO ₂	Enhanced	by	2.00E+00
	C ₂ H ₆	Enhanced	by	3.00E+00
138	C ₃ H ₆ +H=C ₂ H ₄ +CH ₃	8.00E+21	-2.4	11180
139	C ₃ H ₆ +O=CH ₂ CO+CH ₃ +H	8.00E+07	1.6	327
140	C ₃ H ₆ +O=C ₂ H ₅ +HCO	3.50E+07	1.6	-972
141	nC ₃ H ₇ +H=C ₂ H ₅ +CH ₃	3.70E+24	-2.9	12505
142	nC ₃ H ₇ +H=C ₃ H ₆ +H ₂	1.80E+12	0	0
143	nC ₃ H ₇ +O=C ₂ H ₅ +CH ₂ O	9.60E+13	0	0
144	nC ₃ H ₇ +OH=C ₃ H ₆ +H ₂ O	2.40E+13	0	0
145	nC ₃ H ₇ +O ₂ =C ₃ H ₆ +HO ₂	9.00E+10	0	0
146	nC ₃ H ₇ +HO ₂ =C ₂ H ₅ +OH+CH ₂ O	2.40E+13	0	0
147	nC ₃ H ₇ +CH ₃ =CH ₄ +C ₃ H ₆	1.10E+13	0	0

Table C-4: The MCDS1 multi-component diesel surrogate fuel model. Units are in mole, cm, s, K and cal.

Reaction Number	Reaction Considered	A	b	E
1	CH ₃ +H(+M)=CH ₄ (+M)	2.14E+15	-0.4	0
	H ₂	Enhanced	by	2.00E+00
	H ₂ O	Enhanced	by	5.00E+00
	CO	Enhanced	by	2.00E+00
	CO ₂	Enhanced	by	3.00E+00
2	CH ₄ +H=CH ₃ +H ₂	1.73E+04	3	8224
3	CH ₄ +OH=CH ₃ +H ₂ O	1.93E+05	2.4	2106
4	CH ₄ +O=CH ₃ +OH	3.15E+12	0.5	10290
5	C ₂ H ₆ +CH ₃ =C ₂ H ₅ +CH ₄	1.51E-07	6	6047
6	HCO+OH=CO+H ₂ O	1.02E+14	0	0
7	CO+OH=CO ₂ +H	1.40E+05	1.9	-1347
8	H+O ₂ =O+OH	1.97E+14	0	16540
9	O+H ₂ =H+OH	5.08E+04	2.7	6292
10	O+H ₂ O=OH+OH	2.97E+06	2	13400
11	OH+H ₂ =H+H ₂ O	2.16E+08	1.5	3430
12	HCO+M=H+CO+M	1.86E+17	-1	17000
	H ₂	Enhanced	by	2.50E+00
	H ₂ O	Enhanced	by	1.20E+01
	CO	Enhanced	by	1.90E+00
	CO ₂	Enhanced	by	3.80E+00
13	H ₂ O ₂ +OH=H ₂ O+HO ₂	1.00E+12	0	0
14	C ₂ H ₄ +O=CH ₃ +HCO	1.02E+07	1.9	179
15	H+C ₂ H ₄ (+M)=C ₂ H ₅ (+M)	1.08E+12	0.5	1822
	H ₂	Enhanced	by	2.00E+00
	H ₂ O	Enhanced	by	5.00E+00
	CO	Enhanced	by	2.00E+00
	CO ₂	Enhanced	by	3.00E+00
16	C ₂ H ₆ +H=C ₂ H ₅ +H ₂	5.54E+02	3.5	5167
17	C ₂ H ₅ +O ₂ =C ₂ H ₄ +HO ₂	1.22E+30	-5.8	10100
18	C ₂ H ₆ +OH=C ₂ H ₅ +H ₂ O	5.80E+07	1.7	1160
19	C ₂ H ₆ +O=C ₂ H ₅ +OH	1.30E+07	2.1	5190
20	CH ₃ +HO ₂ =CH ₃ O+OH	1.10E+13	0	0
21	CO+HO ₂ =CO ₂ +OH	3.01E+13	0	23000
22	CH ₃ +CH ₃ (+M)=C ₂ H ₆ (+M)	9.21E+16	-1.2	635.8
	H ₂	Enhanced	by	2.00E+00
	H ₂ O	Enhanced	by	5.00E+00
	CO	Enhanced	by	2.00E+00
	CO ₂	Enhanced	by	3.00E+00
23	H ₂ O+M=H+OH+M	1.84E+27	-3	122600
	H ₂	Enhanced	by	2.50E+00
	H ₂ O	Enhanced	by	1.20E+01
	CO	Enhanced	by	1.90E+00
	CO ₂	Enhanced	by	3.80E+00
24	H+O ₂ (+M)=HO ₂ (+M)	1.48E+12	0.6	0
	H ₂	Enhanced	by	2.50E+00
	H ₂ O	Enhanced	by	1.20E+01
	CO	Enhanced	by	1.90E+00
	CO ₂	Enhanced	by	3.80E+00
25	CO+O(+M)=CO ₂ (+M)	1.80E+10	0	2384
	H ₂	Enhanced	by	2.50E+00
	H ₂ O	Enhanced	by	1.20E+01
	CO	Enhanced	by	1.90E+00
	CO ₂	Enhanced	by	3.80E+00
26	CO+O ₂ =CO ₂ +O	1.62E+13	0	47700
27	HCO+H=CO+H ₂	7.34E+13	0	0
28	HCO+O=CO+OH	3.02E+13	0	0
29	CH ₂ O+M=HCO+H+M	6.28E+29	-3.6	93200
30	CH ₂ O+OH=HCO+H ₂ O	3.43E+09	1.2	-447
31	CH ₂ O+H=HCO+H ₂	9.33E+08	1.5	2976
32	CH ₂ O+O=HCO+OH	4.16E+11	0.6	2762
33	CH ₃ +OH=CH ₂ O+H ₂	2.25E+13	0	4300
34	CH ₃ +O=CH ₂ O+H	8.00E+13	0	0
35	CH ₃ +O ₂ =CH ₃ O+O	2.00E+18	-1.6	29210
36	CH ₂ O+CH ₃ =HCO+CH ₄	3.64E-06	5.4	998
37	HCO+CH ₃ =CH ₄ +CO	1.21E+14	0	0
38	CH ₃ O(+M)=CH ₂ O+H(+M)	5.45E+13	0	13500

39	$C2H4(+M)=C2H2+H2(+M)$	1.80E+13	0	76000
40	$HO2+O=OH+O2$	3.25E+13	0	0
41	$HCO+HO2=CH2O+O2$	2.97E+10	0.3	-3861
42	$CH3O+O2=CH2O+HO2$	5.50E+10	0	2424
43	$CH3+HO2=CH4+O2$	3.60E+12	0	0
44	$HCO+O2=CO+HO2$	7.58E+12	0	410
45	$HO2+H=OH+OH$	7.08E+13	0	300
46	$HO2+H=H2+O2$	1.66E+13	0	820
47	$HO2+OH=H2O+O2$	2.89E+13	0	-500
48	$H2O2+O2=HO2+HO2$	5.94E+17	-0.7	53150
49	$OH+OH(+M)=H2O2(+M)$	5.24E+13	-0.4	0
	H2	Enhanced	by	2.50E+00
	H2O	Enhanced	by	1.20E+01
	CO	Enhanced	by	1.90E+00
	CO2	Enhanced	by	3.80E+00
50	$H2O2+H=H2O+OH$	2.41E+13	0	3970
51	$CH4+HO2=CH3+H2O2$	3.42E+11	0	19290
52	$CH2O+HO2=HCO+H2O2$	5.82E-03	4.5	6557
53	$OH+M=O+H+M$	3.91E+22	-2	105300
	H2	Enhanced	by	2.50E+00
	H2O	Enhanced	by	1.20E+01
	CO	Enhanced	by	1.90E+00
	CO2	Enhanced	by	3.80E+00
54	$O2+M=O+O+M$	6.47E+20	-1.5	121500
	H2	Enhanced	by	2.50E+00
	H2O	Enhanced	by	1.20E+01
	CO	Enhanced	by	1.90E+00
	CO2	Enhanced	by	3.80E+00
55	$H2+M=H+H+M$	4.57E+19	-1.4	104400
	H2	Enhanced	by	2.50E+00
	H2O	Enhanced	by	1.20E+01
	CO	Enhanced	by	1.90E+00
	CO2	Enhanced	by	3.80E+00
56	$C2H3+H(+M)=C2H4(+M)$	6.10E+12	0.3	280
57	$C2H5+C2H3=C2H4+C2H4$	5.76E+14	-0.6	2490
58	$C2H2+H(+M)=C2H3(+M)$	3.11E+11	0.6	2589
	H2	Enhanced	by	2.00E+00
	H2O	Enhanced	by	5.00E+00
	CO	Enhanced	by	2.00E+00
	CO2	Enhanced	by	3.00E+00
59	$C2H4+H=C2H3+H2$	8.42E-03	4.6	2583
60	$C2H4+OH=C2H3+H2O$	2.05E+13	0	5950
61	$C2H2+O2=HCCO+OH$	2.00E+08	1.5	30100
62	$CH2+O2=CO+H2O$	7.28E+19	-2.5	1809
63	$C2H2+O=CH2+CO$	6.12E+06	2	1900
64	$CH2+O2=HCO+OH$	1.29E+20	-3.3	284
65	$CH2+O=CO+H+H$	5.00E+13	0	0
66	$CH2+O2=CO2+H+H$	3.29E+21	-3.3	2868
67	$C2H3+O2=C2H2+HO2$	2.12E-06	6	9484
68	$H2O2+O=OH+HO2$	9.55E+06	2	3970
69	$C2H2+O=HCCO+H$	1.43E+07	2	1900
70	$C2H2+OH=CH2CO+H$	2.19E-04	4.5	-1000
71	$CH2CO+H=CH3+CO$	1.10E+13	0	3400
72	$CH2CO+O=CH2+CO2$	1.75E+12	0	1350
73	$CH2+O2=CH2O+O$	3.29E+21	-3.3	2868
74	$CH2CO(+M)=CH2+CO(+M)$	3.00E+14	0	70980
75	$CH2CO+O=HCCO+OH$	1.00E+13	0	8000
76	$CH2CO+OH=HCCO+H2O$	1.00E+13	0	2000
77	$CH2CO+H=HCCO+H2$	2.00E+14	0	8000
78	$HCCO+OH=HCO+HCO$	1.00E+13	0	0
79	$HCCO+O=H+CO+CO$	8.00E+13	0	0
80	$C2H6+O2=C2H5+HO2$	6.03E+13	0	51870
81	$C2H6+HO2=C2H5+H2O2$	1.32E+13	0	20470
82	$CH2+O2=CO2+H2$	1.01E+21	-3.3	1508
83	$CH3+C2H3=CH4+C2H2$	3.92E+11	0	0
84	$CH3+C2H5=CH4+C2H4$	1.95E+13	-0.5	0
85	$C2H3+H=C2H2+H2$	2.00E+13	0	2500
86	$C2H5+H=CH3+CH3$	3.61E+13	0	0
87	$C2H3+O2=CH2O+HCO$	1.70E+29	-5.3	6500
88	$C2H6=C2H5+H$	2.78E+21	-1.6	103800
89	$C2H4+CH3=C2H3+CH4$	6.62E+00	3.7	9500
90	$CH3CO(+M)=CH3+CO(+M)$	3.00E+12	0	16720
91	$C3H5-A=C2H2+CH3$	2.40E+48	-9.9	82080

92	C3H6=C2H3+CH3	2.73E+62	-13.3	123200
93	C2H2+CH3=C3H4-A+H	6.74E+19	-2.1	31590
94	C3H6=C3H5-A+H	2.01E+61	-13.3	118500
95	C3H6+O=CH2CO+CH3+H	2.50E+07	1.8	76
96	C3H6+O=C2H5+HCO	1.58E+07	1.8	-1216
97	C3H6+HO2=C3H5-A+H2O2	1.50E+11	0	14190
98	C3H6+OH=C3H5-A+H2O	3.12E+06	2	-298
99	C2H4+O2=C2H3+HO2	4.00E+13	0	58200
100	CH2O+M=CO+H2+M	1.83E+32	-4.4	87120
101	NC3H7=CH3+C2H4	2.28E+14	-0.6	28400
102	NC3H7=H+C3H6	2.67E+15	-0.6	36820
103	NC3H7+O2=C3H6+HO2	3.00E+11	0	3000
104	C3H6+O=C3H5-A+OH	5.24E+11	0.7	5884
105	C3H6+H=C3H5-A+H2	1.73E+05	2.5	2492
106	C3H6+H=C2H4+CH3	4.83E+33	-5.8	18500
107	PC4H9=C2H5+C2H4	7.50E+17	-1.4	29580
108	H2O2+H=H2+HO2	4.82E+13	0	7950
109	HCO+O=CO2+H	3.00E+13	0	0
110	CH3+M=CH2+H+M	1.97E+16	0	92520
111	CH3+H=CH2+H2	9.00E+13	0	15100
112	CH3+OH=CH2+H2O	3.00E+06	2	2500
113	CH3CO+H=CH2CO+H2	2.00E+13	0	0
114	CH3CO+O=CH2CO+OH	2.00E+13	0	0
115	CH3CO+CH3=CH2CO+CH4	5.00E+13	0	0
116	C2H4+O=C2H3+H	3.39E+06	1.9	179
117	C5H11-1=C2H4+NC3H7	7.97E+17	-1.4	29790
118	H2O2+O2=HO2+HO2	1.84E+14	-0.7	39540
119	C2H3+O2=CH2CHO+O	3.50E+14	-0.6	5260
120	CH3O2+M=CH3+O2+M	4.34E+27	-3.4	30470
121	CH3O2+CH3=CH3O+CH3O	7.00E+12	0	-1000
122	H2O2+OH=H2O+HO2	5.80E+14	0	9560
123	CH3O2+CH3O2=O2+CH3O+CH3O	1.40E+16	-1.6	1860
124	C3H5O=C2H3+CH2O	2.03E+12	0.1	23560
125	C3H5-A+HO2=C3H5O+OH	7.00E+12	0	-1000
126	C3H5-A+CH3O2=C3H5O+CH3O	7.00E+12	0	-1000
127	C3H4-A+HO2=C2H4+CO+OH	1.00E+12	0	14000
128	C3H6+O2=C3H5-A+HO2	4.00E+12	0	39900
129	C3H6+CH3=C3H5-A+CH4	2.21E+00	3.5	5675
130	C3H6+C2H5=C3H5-A+C2H6	1.00E+11	0	9800
131	C3H5-A+HO2=C2H3+CH2O+OH	1.00E-18	0	0
132	C3H5-A+H=C3H4-A+H2	1.81E+13	0	0
133	C3H5-A+CH3=C3H4-A+CH4	1.00E+11	0	0
134	C3H5-A+C2H5=C2H6+C3H4-A	4.00E+11	0	0
135	C3H5-A+C2H5=C2H4+C3H6	4.00E+11	0	0
136	C3H5-A+C2H3=C2H4+C3H4-A	1.00E+12	0	0
137	C3H4-A+C3H6=C3H5-A+C3H5-A	8.39E+17	-1.3	33690
138	C3H4-A+HO2=CH2CO+CH2+OH	4.00E+12	0	19000
139	C3H4-A+O=C2H4+CO	7.80E+12	0	1600
140	C3H5-A=C3H4-A+H	6.66E+15	-0.4	63220
141	CH2CHO=CH2CO+H	3.09E+15	-0.3	50820
142	CH2CHO+O2=CH2O+CO+OH	2.00E+13	0	4200
143	C3H5-A+O2=C3H4-A+HO2	2.18E+21	-2.9	30760
144	C3H5-A+O2=CH2CHO+CH2O	7.14E+15	-1.2	21050
145	C3H5-A+O2=C2H2+CH2O+OH	9.72E+29	-5.7	21450
146	HCCO+O2=CO2+HCO	2.40E+11	0	-854
147	CH3+O2=CH2O+OH	7.47E+11	0	14250
148	C2H4+H2=CH3+CH3	3.77E+12	0.8	84710
149	NC4H9CHO+O2=NC4H9CO+HO2	2.00E+13	0.5	42200
150	NC4H9CHO+OH=NC4H9CO+H2O	2.69E+10	0.8	-340
151	NC4H9CHO+H=NC4H9CO+H2	4.00E+13	0	4200
152	NC4H9CHO+O=NC4H9CO+OH	5.00E+12	0	1790
153	NC4H9CHO+HO2=NC4H9CO+H2O2	2.80E+12	0	13600
154	NC4H9CHO+CH3=NC4H9CO+CH4	1.70E+12	0	8440
155	NC4H9CO=PC4H9+CO	1.00E+11	0	9600
156	HOCHO+M=CO+H2O+M	2.30E+13	0	50000
157	HOCHO+M=CO2+H2+M	1.50E+16	0	57000
158	HOCHO=HCO+OH	4.59E+18	-0.5	108300
159	HOCHO+OH=H2O+CO2+H	2.62E+06	2.1	916
160	HOCHO+OH=H2O+CO+OH	1.85E+07	1.5	-962
161	HOCHO+H=H2+CO2+H	4.24E+06	2.1	4868
162	HOCHO+H=H2+CO+OH	6.03E+13	-0.3	2988
163	HOCHO+CH3=CH4+CO+OH	3.90E-07	5.8	2200
164	HOCHO+HO2=H2O2+CO+OH	1.00E+12	0	11920

165	HOCHO+O=CO+OH+OH	1.77E+18	-1.9	2975
166	C6H13-1+O2=C6H12-1+HO2	3.00E-19	0	3000
167	C6H13-1=C2H4+PC4H9	5.45E+17	-1.3	29580
168	C6H13-1=C6H12-1+H	2.09E+16	-0.9	37940
169	C6H12-1+OH=C5H11-1+CH2O	1.00E+11	0	-4000
170	C6H12-1+O=C5H11-1+HCO	1.00E+11	0	-1050
171	C6H12-1=NC3H7+C3H5-A	1.00E+16	0	71000
172	C7H15-1=C5H11-1+C2H4	8.16E+17	-1.4	30840
173	C16H33-5+H=C16H34	1.00E+14	0	0
174	C11H23-1+C5H11-1=C16H34	8.00E+12	0	0
175	C10H21-1+C6H13-1=C16H34	8.00E+12	0	0
176	C9H19-1+C7H15-1=C16H34	8.00E+12	0	0
177	C8H17-1+C8H17-1=C16H34	8.00E+12	0	0
178	C16H34+H=C16H33-5+H2	2.60E+06	2.4	4471
179	C16H34+OH=C16H33-5+H2O	2.40E+08	1.6	-35
180	C16H34+O=C16H33-5+OH	9.54E+04	2.7	2106
181	C16H34+HO2=C16H33-5+H2O2	1.60E+14	0	17690
182	C16H34+CH3=C16H33-5+CH4	5.41E+04	2.3	7287
183	C16H34+O2=C16H33-5+HO2	4.00E+13	0	50150
184	C16H34+C2H3=C16H33-5+C2H4	8.00E+11	0	16800
185	C16H34+C2H5=C16H33-5+C2H6	1.00E+11	0	10400
186	C6H12-1+C10H21-1=C16H33-5	1.00E+11	0	8200
187	C2H4+C9H19-1=C11H23-1	1.00E+11	0	8200
188	C2H4+C8H17-1=C10H21-1	1.00E+11	0	8200
189	C2H4+C7H15-1=C9H19-1	1.00E+11	0	8200
190	C2H4+C6H13-1=C8H17-1	1.00E+11	0	8200
191	C16H33O2-5=C16H33-5+O2	1.36E+23	-2.4	37670
192	C9H19O2-1=C9H19-1+O2	2.66E+20	-1.7	35400
193	C16H33-5+HO2=C16H33O-5+OH	7.00E+12	0	-1000
194	C16H33O2-5=C16OOH5-7	3.50E+10	0	20850
195	C9H19O2-1=C9OOH1-3	2.50E+10	0	20850
196	NC4H9CHO+C11H23-1=C16H33O-5	1.00E+11	0	12900
197	C9OOH1-3O2=C9OOH1-3+O2	1.37E+23	-2.4	37640
198	C9OOH1-3O2=C9KET1-3+OH	2.50E+10	0	21400
199	C9KET1-3=OH+CH2CHO+NC6H13CHO	1.05E+16	0	41600
200	NC9H19CHO+O2=NC9H19CO+HO2	2.00E+13	0.5	42200
201	NC9H19CHO+OH=NC9H19CO+H2O	2.69E+10	0.8	-340
202	NC9H19CHO+H=NC9H19CO+H2	4.00E+13	0	4200
203	NC9H19CHO+O=NC9H19CO+OH	5.00E+12	0	1790
204	NC9H19CHO+HO2=NC9H19CO+H2O2	2.80E+12	0	13600
205	NC9H19CHO+CH3=NC9H19CO+CH4	1.70E+12	0	8440
206	NC9H19CO=C9H19-1+CO	1.00E+11	0	9600
207	NC6H13CHO+O2=NC6H13CO+HO2	2.00E+13	0.5	42200
208	NC6H13CHO+OH=NC6H13CO+H2O	2.69E+10	0.8	-340
209	NC6H13CHO+H=NC6H13CO+H2	4.00E+13	0	4200
210	NC6H13CHO+O=NC6H13CO+OH	5.00E+12	0	1790
211	NC6H13CHO+HO2=NC6H13CO+H2O2	2.80E+12	0	13600
212	NC6H13CHO+CH3=NC6H13CO+CH4	1.70E+12	0	8440
213	NC6H13CO=C6H13-1+CO	1.00E+11	0	9600
214	NC4H9COCH2=PC4H9+CH2CO	1.55E+18	-1.4	43140
215	C16KET5-7=OH+NC4H9COCH2+NC9H19CHO	4.05E+16	0	41600
216	C16OOH5-7O2=C16OOH5-7+O2	1.37E+23	-2.4	37640
217	C16OOH5-7O2=C16KET5-7+OH	1.25E+10	0	17850
218	HMN-R1+H=HMN	1.00E+14	0	0
219	HMN-R8+H=HMN	1.00E+14	0	0
220	TC4H9+FC12H25=HMN	4.00E+12	0	0
221	HMN+H=HMN-R1+H2	7.34E+05	2.8	8147
222	HMN+H=HMN-R8+H2	7.34E+06	2.8	8147
223	HMN+OH=HMN-R1+H2O	2.37E+07	1.8	298.1
224	HMN+OH=HMN-R8+H2O	6.37E+07	1.8	298.1
225	HMN+O=HMN-R1+OH	8.55E+03	3	3123
226	HMN+O=HMN-R8+OH	8.55E+03	3	3123
227	HMN+CH3=HMN-R1+CH4	4.26E-14	8.1	4150
228	HMN+CH3=HMN-R8+CH4	4.26E-14	8.1	4150
229	HMN+HO2=HMN-R1+H2O2	2.52E+13	0	20440
230	HMN+HO2=HMN-R8+H2O2	2.52E+13	0	20440
231	HMN+O2=HMN-R1+HO2	3.71E+13	0	49000
232	HMN+O2=HMN-R8+HO2	3.71E+13	0	49000
233	IC4H8+AC12H25=HMN-R1	1.00E+11	0	8200
234	IC4H8+FC12H25=HMN-R8	5.00E+09	0	8200
235	HMN-R1O2=HMN-R1+O2	3.46E+20	-1.6	35720
236	HMN-R8O2=HMN-R8+O2	3.46E+20	-1.6	35720
237	HMN-R1O2=HMNOOH1-2	2.50E+10	0	20850

238	HMN-R8O2=HMNOOH8-5	1.56E+09	0	17050
239	HMNOOH1-2O2=HMNOOH1-2+O2	1.37E+23	-2.4	37640
240	HMNOOH8-5O2=HMNOOH8-5+O2	4.73E+26	-3.2	39640
241	HMNOOH1-2O2=HMNKET1-2+OH	2.50E+10	0	21400
242	HMNOOH8-5O2=HMNKET8-5+OH	2.12E+10	0	19350
243	HMNKET1-2=IC3H6CHO+AC11H23+HCO+OH	1.05E+16	0	41600
244	HMNKET8-5=CC8H17+CH3COCH2+TC4H8CHO+OH	1.05E+16	0	41600
245	AC12H25=IC4H8+DC8H17	5.00E+12	0	28000
246	FC12H25=C3H6+CC9H19	5.00E+12	0	28000
247	AC11H23=IC4H8+PC7H15	5.00E+12	0	28000
248	CC9H19=NEOC5H11+IC4H8	5.00E+12	0	28000
249	C3H6+HO2=C3H5-T+H2O2	3.00E+09	0	9930
250	C3H6+OH=C3H5-T+H2O	1.11E+06	2	1451
251	C3H6+O=C3H5-T+OH	6.03E+10	0.7	7632
252	IC4H7=C3H4-A+CH3	1.23E+47	-9.7	74260
253	IC4H8=C3H5-T+CH3	1.92E+66	-14.2	128100
254	IC4H8=IC4H7+H	3.07E+55	-11.5	114300
255	IC4H8+O=CH2CO+CH3+CH3	3.33E+07	1.8	76
256	IC4H8+H=IC4H7+H2	3.40E+05	2.5	2492
257	IC4H8+O=IC4H7+OH	1.21E+11	0.7	7633
258	IC4H8+OH=IC4H7+H2O	5.20E+06	2	-298
259	IC4H8+CH3=IC4H7+CH4	4.42E+00	3.5	5675
260	IC4H8+HO2=IC4H7+H2O2	1.93E+04	2.6	13910
261	TC4H9=H+IC4H8	4.65E+46	-9.8	55080
262	IC4H8+H=C3H6+CH3	5.68E+33	-5.7	20000
263	TC4H9+O2=IC4H8+HO2	7.50E-19	0	5020
264	CH3COCH2=CH2CO+CH3	1.00E+14	0	31000
265	C3H6+O2=C3H5-T+HO2	1.40E+12	0	60700
266	NEOC5H11=IC4H8+CH3	3.06E+17	-1.2	32290
267	CH3O2+IC4H7=CH3O+IC4H7O	7.00E+12	0	-1000
268	IC4H7+HO2=IC4H7O+OH	7.00E+12	0	-1000
269	IC4H8+HO2=IC4H8O+OH	1.29E+12	0	13340
270	IC4H8+C3H5-A=IC4H7+C3H6	7.94E+11	0	20500
271	IC4H7O=C3H5-T+CH2O	1.01E+18	-1.4	30840
272	C3H6+CH3=C3H5-T+CH4	8.40E-01	3.5	11660
273	C3H5-T=C2H2+CH3	2.16E+10	-8.3	45110
274	C3H5-T+O2=CH3COCH2+O	3.81E+17	-1.4	5580
275	IC4H7+O2=CH3COCH2+CH2O	7.14E+15	-1.2	21050
276	C3H5-T+O2=CH2O+CH3CO	3.71E+25	-4	7043
277	IC4H8+O2=IC4H7+HO2	6.00E+12	0	39900
278	C3H6+H=C3H5-T+H2	4.05E+05	2.5	9794
279	C3H6=C3H5-T+H	5.62E+71	-16.6	139300
280	TC4H8CHO=IC4H8+HCO	8.52E+12	0	20090
281	CC8H17=IC4H8+TC4H9	3.78E+22	-2.7	32360
282	IC3H6CHO=C3H6+HCO	1.03E+15	-0.6	23170
283	DC8H17=C3H6+NEOC5H11	2.62E+19	-1.8	32110
284	PC7H15=TC4H9+C3H6	3.52E+21	-2.2	28120

Table C-5: The MCDS2 multi-component diesel surrogate fuel model. Units are in mole, cm, s, K and cal.

Reaction Number	Reaction Considered	A	b	E
1	CH ₃ +H(+M)=CH ₄ (+M)	2.14E+15	-0.4	0.00E+00
	H ₂	Enhanced	by	2.00E+00
	H ₂ O	Enhanced	by	5.00E+00
	CO	Enhanced	by	2.00E+00
	CO ₂	Enhanced	by	3.00E+00
2	CH ₄ +H=CH ₃ +H ₂	1.73E+04	3	8224
3	CH ₄ +OH=CH ₃ +H ₂ O	1.93E+05	2.4	2106
4	CH ₄ +O=CH ₃ +OH	3.15E+12	0.5	10290
5	C ₂ H ₆ +CH ₃ =C ₂ H ₅ +CH ₄	1.51E-07	6	6047
6	HCO+OH=CO+H ₂ O	1.02E+14	0	0
7	CO+OH=CO ₂ +H	1.40E+05	1.9	-1347
8	H+O ₂ =O+OH	1.97E+14	0	16540
9	O+H ₂ =H+OH	5.08E+04	2.7	6292
10	O+H ₂ O=OH+OH	2.97E+06	2	13400
11	OH+H ₂ =H+H ₂ O	2.16E+08	1.5	3430
12	HCO+M=H+CO+M	1.86E+17	-1	1.70E+04
	H ₂	Enhanced	by	2.50E+00
	H ₂ O	Enhanced	by	1.20E+01
	CO	Enhanced	by	1.90E+00
	CO ₂	Enhanced	by	3.80E+00
13	H ₂ O ₂ +OH=H ₂ O+HO ₂	1.00E+12	0	0
14	C ₂ H ₄ +O=CH ₃ +HCO	1.02E+07	1.9	179
15	H+C ₂ H ₄ (+M)=C ₂ H ₅ (+M)	1.08E+12	0.5	1.82E+03
	H ₂	Enhanced	by	2.00E+00
	H ₂ O	Enhanced	by	5.00E+00
	CO	Enhanced	by	2.00E+00
	CO ₂	Enhanced	by	3.00E+00
16	C ₂ H ₆ +H=C ₂ H ₅ +H ₂	5.54E+02	3.5	5167
17	C ₂ H ₅ +O ₂ =C ₂ H ₄ +HO ₂	1.22E+30	-5.8	10100
18	C ₂ H ₆ +OH=C ₂ H ₅ +H ₂ O	5.80E+07	1.7	1160
19	C ₂ H ₆ +O=C ₂ H ₅ +OH	1.30E+07	2.1	5190
20	CH ₃ +HO ₂ =CH ₃ O+OH	1.10E+13	0	0
21	CO+HO ₂ =CO ₂ +OH	3.01E+13	0	23000
22	CH ₃ +CH ₃ (+M)=C ₂ H ₆ (+M)	9.21E+16	-1.2	6.36E+02
	H ₂	Enhanced	by	2.00E+00
	H ₂ O	Enhanced	by	5.00E+00
	CO	Enhanced	by	2.00E+00
	CO ₂	Enhanced	by	3.00E+00
23	H ₂ O+M=H+OH+M	1.84E+27	-3	1.23E+05
	H ₂	Enhanced	by	2.50E+00
	H ₂ O	Enhanced	by	1.20E+01
	CO	Enhanced	by	1.90E+00
	CO ₂	Enhanced	by	3.80E+00
24	H+O ₂ (+M)=HO ₂ (+M)	1.48E+12	0.6	0.00E+00
	H ₂	Enhanced	by	2.50E+00
	H ₂ O	Enhanced	by	1.20E+01
	CO	Enhanced	by	1.90E+00
	CO ₂	Enhanced	by	3.80E+00
25	CO+O(+M)=CO ₂ (+M)	1.80E+10	0	2.38E+03
	H ₂	Enhanced	by	2.50E+00
	H ₂ O	Enhanced	by	1.20E+01
	CO	Enhanced	by	1.90E+00
	CO ₂	Enhanced	by	3.80E+00
26	CO+O ₂ =CO ₂ +O	1.62E+13	0	47700
27	HCO+H=CO+H ₂	7.34E+13	0	0
28	HCO+O=CO+OH	3.02E+13	0	0
29	CH ₂ O+M=HCO+H+M	6.28E+29	-3.6	93200
30	CH ₂ O+OH=HCO+H ₂ O	3.43E+09	1.2	-447
31	CH ₂ O+H=HCO+H ₂	9.33E+08	1.5	2976
32	CH ₂ O+O=HCO+OH	4.16E+11	0.6	2762
33	CH ₃ +OH=CH ₂ O+H ₂	2.25E+13	0	4300
34	CH ₃ +O=CH ₂ O+H	8.00E+13	0	0
35	CH ₃ +O ₂ =CH ₃ O+O	2.00E+18	-1.6	29210
36	CH ₂ O+CH ₃ =HCO+CH ₄	3.64E-06	5.4	998
37	HCO+CH ₃ =CH ₄ +CO	1.21E+14	0	0
38	CH ₃ O(+M)=CH ₂ O+H(+M)	5.45E+13	0	13500

39	$C_2H_4(+M)=C_2H_2+H_2(+M)$	1.80E+13	0	76000
40	$HO_2+O=OH+O_2$	3.25E+13	0	0
41	$HCO+HO_2=CH_2O+O_2$	2.97E+10	0.3	-3861
42	$CH_3O+O_2=CH_2O+HO_2$	5.50E+10	0	2424
43	$CH_3+HO_2=CH_4+O_2$	3.60E+12	0	0
44	$HCO+O_2=CO+HO_2$	7.58E+12	0	410
45	$HO_2+H=OH+OH$	7.08E+13	0	300
46	$HO_2+H=H_2+O_2$	1.66E+13	0	820
47	$HO_2+OH=H_2O+O_2$	2.89E+13	0	-500
48	$H_2O_2+O_2=HO_2+HO_2$	5.94E+17	-0.7	53150
49	$OH+OH(+M)=H_2O_2(+M)$	1.24E+14	-0.4	0.00E+00
	H ₂	Enhanced	by	2.50E+00
	H ₂ O	Enhanced	by	1.20E+01
	CO	Enhanced	by	1.90E+00
	CO ₂	Enhanced	by	3.80E+00
50	$H_2O_2+H=H_2O+OH$	2.41E+13	0	3970
51	$CH_4+HO_2=CH_3+H_2O_2$	3.42E+11	0	19290
52	$CH_2O+HO_2=HCO+H_2O_2$	5.82E-03	4.5	6557
53	$OH+M=O+H+M$	3.91E+22	-2	1.05E+05
	H ₂	Enhanced	by	2.50E+00
	H ₂ O	Enhanced	by	1.20E+01
	CO	Enhanced	by	1.90E+00
	CO ₂	Enhanced	by	3.80E+00
54	$O_2+M=O+O+M$	6.47E+20	-1.5	1.22E+05
	H ₂	Enhanced	by	2.50E+00
	H ₂ O	Enhanced	by	1.20E+01
	CO	Enhanced	by	1.90E+00
	CO ₂	Enhanced	by	3.80E+00
55	$H_2+M=H+H+M$	4.57E+19	-1.4	1.04E+05
	H ₂	Enhanced	by	2.50E+00
	H ₂ O	Enhanced	by	1.20E+01
	CO	Enhanced	by	1.90E+00
	CO ₂	Enhanced	by	3.80E+00
56	$C_2H_3+H(+M)=C_2H_4(+M)$	6.10E+12	0.3	280
57	$C_2H_5+C_2H_3=C_2H_4+C_2H_4$	5.76E+14	-0.6	2490
58	$C_2H_2+H(+M)=C_2H_3(+M)$	3.11E+11	0.6	2.59E+03
	H ₂	Enhanced	by	2.00E+00
	H ₂ O	Enhanced	by	5.00E+00
	CO	Enhanced	by	2.00E+00
	CO ₂	Enhanced	by	3.00E+00
59	$C_2H_4+H=C_2H_3+H_2$	8.42E-03	4.6	2583
60	$C_2H_4+OH=C_2H_3+H_2O$	2.05E+13	0	5950
61	$C_2H_2+O_2=HCCO+OH$	2.00E+08	1.5	30100
62	$CH_2+O_2=CO+H_2O$	7.28E+19	-2.5	1809
63	$C_2H_2+O=CH_2+CO$	6.12E+06	2	1900
64	$CH_2+O_2=HCO+OH$	1.29E+20	-3.3	284
65	$CH_2+O=CO+H+H$	5.00E+13	0	0
66	$CH_2+O_2=CO_2+H+H$	3.29E+21	-3.3	2868
67	$C_2H_3+O_2=C_2H_2+HO_2$	2.12E-06	6	9484
68	$H_2O_2+O=OH+HO_2$	9.55E+06	2	3970
69	$C_2H_2+O=HCCO+H$	1.43E+07	2	1900
70	$C_2H_2+OH=CH_2CO+H$	2.19E-04	4.5	-1000
71	$CH_2CO+H=CH_3+CO$	1.10E+13	0	3400
72	$CH_2CO+O=CH_2+CO_2$	1.75E+12	0	1350
73	$CH_2+O_2=CH_2O+O$	3.29E+21	-3.3	2868
74	$CH_2CO(+M)=CH_2+CO(+M)$	3.00E+14	0	70980
75	$CH_2CO+O=HCCO+OH$	1.00E+13	0	8000
76	$CH_2CO+OH=HCCO+H_2O$	1.00E+13	0	2000
77	$CH_2CO+H=HCCO+H_2$	2.00E+14	0	8000
78	$HCCO+OH=HCO+HCO$	1.00E+13	0	0
79	$HCCO+O=H+CO+CO$	8.00E+13	0	0
80	$C_2H_6+O_2=C_2H_5+HO_2$	6.03E+13	0	51870
81	$C_2H_6+HO_2=C_2H_5+H_2O_2$	1.32E+13	0	20470
82	$CH_2+O_2=CO_2+H_2$	1.01E+21	-3.3	1508
83	$CH_3+C_2H_3=CH_4+C_2H_2$	3.92E+11	0	0
84	$CH_3+C_2H_5=CH_4+C_2H_4$	1.95E+13	-0.5	0
85	$C_2H_3+H=C_2H_2+H_2$	2.00E+13	0	2500
86	$C_2H_5+H=CH_3+CH_3$	3.61E+13	0	0
87	$C_2H_3+O_2=CH_2O+HCO$	1.70E+29	-5.3	6500
88	$C_2H_6=C_2H_5+H$	2.78E+21	-1.6	103800
89	$C_2H_4+CH_3=C_2H_3+CH_4$	6.62E+00	3.7	9500
90	$CH_3CO(+M)=CH_3+CO(+M)$	3.00E+12	0	16720
91	$C_3H_5-A=C_2H_2+CH_3$	2.40E+48	-9.9	82080

92	C3H6=C2H3+CH3	2.73E+62	-13.3	123200
93	C2H2+CH3=C3H4-A+H	6.74E+19	-2.1	31590
94	C3H6=C3H5-A+H	2.01E+61	-13.3	118500
95	C3H6+O=CH2CO+CH3+H	2.50E+07	1.8	76
96	C3H6+O=C2H5+HCO	1.58E+07	1.8	-1216
97	C3H6+HO2=C3H5-A+H2O2	1.50E+11	0	14190
98	C3H6+OH=C3H5-A+H2O	3.12E+06	2	-298
99	C2H4+O2=C2H3+HO2	4.00E+13	0	58200
100	CH2O+M=CO+H2+M	1.83E+32	-4.4	87120
101	NC3H7=CH3+C2H4	2.28E+14	-0.6	28400
102	NC3H7=H+C3H6	2.67E+15	-0.6	36820
103	NC3H7+O2=C3H6+HO2	3.00E+11	0	3000
104	C3H6+O=C3H5-A+OH	5.24E+11	0.7	5884
105	C3H6+H=C3H5-A+H2	1.73E+05	2.5	2492
106	C3H6+H=C2H4+CH3	4.83E+33	-5.8	18500
107	PC4H9=C2H5+C2H4	7.50E+17	-1.4	29580
108	H2O2+H=H2+HO2	4.82E+13	0	7950
109	HCO+O=CO2+H	3.00E+13	0	0
110	CH3+M=CH2+H+M	1.97E+16	0	92520
111	CH3+H=CH2+H2	9.00E+13	0	15100
112	CH3+OH=CH2+H2O	3.00E+06	2	2500
113	CH3CO+H=CH2CO+H2	2.00E+13	0	0
114	CH3CO+O=CH2CO+OH	2.00E+13	0	0
115	CH3CO+CH3=CH2CO+CH4	5.00E+13	0	0
116	C2H4+O=CH2CHO+H	3.39E+06	1.9	179
117	C5H11-1=C2H4+NC3H7	7.97E+17	-1.4	29790
118	H2O2+O2=HO2+HO2	1.84E+14	-0.7	39540
119	C2H3+O2=CH2CHO+O	3.50E+14	-0.6	5260
120	CH3O2+M=CH3+O2+M	4.34E+27	-3.4	30470
121	CH3O2+CH3=CH3O+CH3O	7.00E+12	0	-1000
122	H2O2+OH=H2O+HO2	5.80E+14	0	9560
123	CH3O2+CH3O2=O2+CH3O+CH3O	1.40E+16	-1.6	1860
124	C3H5O=C2H3+CH2O	2.03E+12	0.1	23560
125	C3H5-A+HO2=C3H5O+OH	7.00E+12	0	-1000
126	C3H5-A+CH3O2=C3H5O+CH3O	7.00E+12	0	-1000
127	NC3H7O=C2H5+CH2O	1.39E+16	-0.9	19770
128	NC3H7+HO2=NC3H7O+OH	7.00E+12	0	-1000
129	CH3O2+NC3H7=CH3O+NC3H7O	7.00E+12	0	-1000
130	PC4H9O=NC3H7+CH2O	5.81E+16	-1	20260
131	C3H4-A+HO2=C2H4+CO+OH	1.00E+12	0	14000
132	C3H6+O2=C3H5-A+HO2	4.00E+12	0	39900
133	C3H6+CH3=C3H5-A+CH4	2.21E+00	3.5	5675
134	C3H6+C2H5=C3H5-A+C2H6	1.00E+11	0	9800
135	C3H5-A+HO2=C2H3+CH2O+OH	1.00E-18	0	0
136	C3H5-A+H=C3H4-A+H2	1.81E+13	0	0
137	C3H5-A+CH3=C3H4-A+CH4	1.00E+11	0	0
138	C3H5-A+C2H5=C2H6+C3H4-A	4.00E+11	0	0
139	C3H5-A+C2H5=C2H4+C3H6	4.00E+11	0	0
140	C3H5-A+C2H3=C2H4+C3H4-A	1.00E+12	0	0
141	C3H4-A+C3H6=C3H5-A+C3H5-A	8.39E+17	-1.3	33690
142	C3H4-A+HO2=CH2CO+CH2+OH	4.00E+12	0	19000
143	C3H4-A+O=C2H4+CO	7.80E+12	0	1600
144	C3H5-A=C3H4-A+H	6.66E+15	-0.4	63220
145	PC4H9+HO2=PC4H9O+OH	7.00E+12	0	-1000
146	CH3O2+PC4H9=CH3O+PC4H9O	7.00E+12	0	-1000
147	CH2CHO=CH2CO+H	3.09E+15	-0.3	50820
148	CH2CHO+O2=CH2O+CO+OH	2.00E+13	0	4200
149	C3H5-A+O2=C3H4-A+HO2	2.18E+21	-2.9	30760
150	C3H5-A+O2=CH2CHO+CH2O	7.14E+15	-1.2	21050
151	C3H5-A+O2=C2H2+CH2O+OH	9.72E+29	-5.7	21450
152	HCCO+O2=CO2+HCO	2.40E+11	0	-854
153	CH3+O2=CH2O+OH	7.47E+11	0	14250
154	C2H4+H2=CH3+CH3	3.77E+12	0.8	84710
155	NC4H9CHO+O2=NC4H9CO+HO2	2.00E+13	0.5	42200
156	NC4H9CHO+OH=NC4H9CO+H2O	2.69E+10	0.8	-340
157	NC4H9CHO+H=NC4H9CO+H2	4.00E+13	0	4200
158	NC4H9CHO+O=NC4H9CO+OH	5.00E+12	0	1790
159	NC4H9CHO+HO2=NC4H9CO+H2O2	2.80E+12	0	13600
160	NC4H9CHO+CH3=NC4H9CO+CH4	1.70E+12	0	8440
161	NC4H9CO=PC4H9+CO	1.00E+11	0	9600
162	HOCH2O=CH2O+OH	1.64E+14	-0.1	21890
163	HOCH2O=HOCHO+H	1.00E+14	0	14900
164	HOCHO+M=CO+H2O+M	2.30E+13	0	50000

165	HOCHO+M=CO ₂ +H ₂ +M	1.50E+16	0	57000
166	HOCHO=HCO+OH	4.59E+18	-0.5	108300
167	HOCHO+OH=H ₂ O+CO ₂ +H	2.62E+06	2.1	916
168	HOCHO+OH=H ₂ O+CO+OH	1.85E+07	1.5	-962
169	HOCHO+H=H ₂ +CO ₂ +H	4.24E+06	2.1	4868
170	HOCHO+H=H ₂ +CO+OH	6.03E+13	-0.3	2988
171	HOCHO+CH ₃ =CH ₄ +CO+OH	3.90E-07	5.8	2200
172	HOCHO+HO ₂ =H ₂ O ₂ +CO+OH	1.00E+12	0	11920
173	HOCHO+O=CO+OH+OH	1.77E+18	-1.9	2975
174	C ₆ H ₁₃ -1+O ₂ =C ₆ H ₁₂ -1+HO ₂	3.00E-19	0	3000
175	C ₆ H ₁₃ -1=C ₂ H ₄ +PC ₄ H ₉	5.45E+17	-1.3	29580
176	C ₆ H ₁₃ -1=C ₆ H ₁₂ -1+H	2.09E+16	-0.9	37940
177	C ₆ H ₁₂ -1+OH=C ₅ H ₁₁ -1+CH ₂ O	1.00E+11	0	-4000
178	C ₆ H ₁₂ -1+O=C ₅ H ₁₁ -1+HCO	1.00E+11	0	-1050
179	C ₆ H ₁₂ -1=NC ₃ H ₇ +C ₃ H ₅ -A	1.00E+16	0	71000
180	C ₇ H ₁₅ -1=C ₅ H ₁₁ -1+C ₂ H ₄	8.16E+17	-1.4	30840
181	C ₁₆ H ₃₃ -5+H=C ₁₆ H ₃₄	1.00E+14	0	0
182	C ₁₁ H ₂₃ -1+C ₅ H ₁₁ -1=C ₁₆ H ₃₄	8.00E+12	0	0
183	C ₁₀ H ₂₁ -1+C ₆ H ₁₃ -1=C ₁₆ H ₃₄	8.00E+12	0	0
184	C ₉ H ₁₉ -1+C ₇ H ₁₅ -1=C ₁₆ H ₃₄	8.00E+12	0	0
185	C ₈ H ₁₇ -1+C ₈ H ₁₇ -1=C ₁₆ H ₃₄	8.00E+12	0	0
186	C ₁₆ H ₃₄ +H=C ₁₆ H ₃₃ -5+H ₂	2.60E+06	2.4	4471
187	C ₁₆ H ₃₄ +OH=C ₁₆ H ₃₃ -5+H ₂ O	6.40E+08	1.6	-35
188	C ₁₆ H ₃₄ +O=C ₁₆ H ₃₃ -5+OH	9.54E+04	2.7	2106
189	C ₁₆ H ₃₄ +HO ₂ =C ₁₆ H ₃₃ -5+H ₂ O ₂	5.12E+14	0	17690
190	C ₁₆ H ₃₄ +CH ₃ =C ₁₆ H ₃₃ -5+CH ₄	5.41E+04	2.3	7287
191	C ₁₆ H ₃₄ +O ₂ =C ₁₆ H ₃₃ -5+HO ₂	4.00E+13	0	50150
192	C ₁₆ H ₃₄ +C ₂ H ₃ =C ₁₆ H ₃₃ -5+C ₂ H ₄	8.00E+11	0	16800
193	C ₁₆ H ₃₄ +C ₂ H ₅ =C ₁₆ H ₃₃ -5+C ₂ H ₆	1.00E+11	0	10400
194	C ₆ H ₁₂ -1+C ₁₀ H ₂₁ -1=C ₁₆ H ₃₃ -5	1.00E+12	0	8200
195	C ₂ H ₄ +C ₉ H ₁₉ -1=C ₁₁ H ₂₃ -1	1.00E+11	0	8200
196	C ₂ H ₄ +C ₈ H ₁₇ -1=C ₁₀ H ₂₁ -1	1.00E+11	0	8200
197	C ₂ H ₄ +C ₇ H ₁₅ -1=C ₉ H ₁₉ -1	1.00E+11	0	8200
198	C ₂ H ₄ +C ₆ H ₁₃ -1=C ₈ H ₁₇ -1	1.00E+11	0	8200
199	C ₁₆ H ₃₃ O ₂ -5=C ₁₆ H ₃₃ -5+O ₂	1.36E+23	-2.4	37670
200	C ₉ H ₁₉ O ₂ -1=C ₉ H ₁₉ -1+O ₂	2.66E+20	-1.7	35400
201	C ₁₆ H ₃₃ -5+HO ₂ =C ₁₆ H ₃₃ O-5+OH	7.00E+12	0	-1000
202	C ₁₁ H ₂₃ -1+HO ₂ =C ₁₁ H ₂₃ O-1+OH	7.00E+12	0	-1000
203	C ₁₀ H ₂₁ -1+HO ₂ =C ₁₀ H ₂₁ O-1+OH	7.00E+12	0	-1000
204	C ₉ H ₁₉ -1+HO ₂ =C ₉ H ₁₉ O-1+OH	7.00E+12	0	-1000
205	C ₈ H ₁₇ -1+HO ₂ =C ₈ H ₁₇ O-1+OH	7.00E+12	0	-1000
206	C ₁₆ H ₃₃ O ₂ -5=C ₁₆ OOH ₅ -7	2.50E+10	0	20850
207	C ₉ H ₁₉ O ₂ -1=C ₉ OOH ₁ -3	2.50E+10	0	20850
208	NC ₄ H ₉ CHO+C ₁₁ H ₂₃ -1=C ₁₆ H ₃₃ O-5	1.00E+11	0	12900
209	CH ₂ O+C ₁₀ H ₂₁ -1=C ₁₁ H ₂₃ O-1	1.00E+11	0	11900
210	CH ₂ O+C ₉ H ₁₉ -1=C ₁₀ H ₂₁ O-1	1.00E+11	0	11900
211	CH ₂ O+C ₈ H ₁₇ -1=C ₉ H ₁₉ O-1	1.00E+11	0	11900
212	CH ₂ O+C ₇ H ₁₅ -1=C ₈ H ₁₇ O-1	1.00E+11	0	11900
213	C ₉ OOH ₁ -3O ₂ =C ₉ OOH ₁ -3+O ₂	1.37E+23	-2.4	37640
214	C ₉ OOH ₁ -3O ₂ =C ₉ KET ₁ -3+OH	2.50E+10	0	21400
215	C ₉ KET ₁ -3=OH+CH ₂ CHO+NC ₆ H ₁₃ CHO	1.05E+16	0	41600
216	NC ₉ H ₁₉ CHO+O ₂ =NC ₉ H ₁₉ CO+HO ₂	2.00E+13	0.5	42200
217	NC ₉ H ₁₉ CHO+OH=NC ₉ H ₁₉ CO+H ₂ O	2.69E+10	0.8	-340
218	NC ₉ H ₁₉ CHO+H=NC ₉ H ₁₉ CO+H ₂	4.00E+13	0	4200
219	NC ₉ H ₁₉ CHO+O=NC ₉ H ₁₉ CO+OH	5.00E+12	0	1790
220	NC ₉ H ₁₉ CHO+HO ₂ =NC ₉ H ₁₉ CO+H ₂ O ₂	2.80E+12	0	13600
221	NC ₉ H ₁₉ CHO+CH ₃ =NC ₉ H ₁₉ CO+CH ₄	1.70E+12	0	8440
222	NC ₉ H ₁₉ CO=C ₉ H ₁₉ -1+CO	1.00E+11	0	9600
223	NC ₆ H ₁₃ CHO+O ₂ =NC ₆ H ₁₃ CO+HO ₂	2.00E+13	0.5	42200
224	NC ₆ H ₁₃ CHO+OH=NC ₆ H ₁₃ CO+H ₂ O	2.69E+10	0.8	-340
225	NC ₆ H ₁₃ CHO+H=NC ₆ H ₁₃ CO+H ₂	4.00E+13	0	4200
226	NC ₆ H ₁₃ CHO+O=NC ₆ H ₁₃ CO+OH	5.00E+12	0	1790
227	NC ₆ H ₁₃ CHO+HO ₂ =NC ₆ H ₁₃ CO+H ₂ O ₂	2.80E+12	0	13600
228	NC ₆ H ₁₃ CHO+CH ₃ =NC ₆ H ₁₃ CO+CH ₄	1.70E+12	0	8440
229	NC ₆ H ₁₃ CO=C ₆ H ₁₃ -1+CO	1.00E+11	0	9600
230	NC ₄ H ₉ COCH ₂ =PC ₄ H ₉ +CH ₂ CO	1.55E+18	-1.4	43140
231	C ₁₆ KET ₅ -7=OH+NC ₄ H ₉ COCH ₂ +NC ₉ H ₁₉ CHO	4.05E+16	0	41600
232	C ₁₆ OOH ₅ -7O ₂ =C ₁₆ OOH ₅ -7+O ₂	1.37E+23	-2.4	37640
233	C ₁₆ OOH ₅ -7O ₂ =C ₁₆ KET ₅ -7+OH	1.25E+10	0	17850
234	HMN-R ₈ +H=HMN	1.00E+14	0	0
235	TC ₄ H ₉ +FC ₁₂ H ₂₅ =HMN	4.00E+12	0	0
236	HMN+H=HMN-R ₈ +H ₂	7.34E+06	2.8	8147
237	HMN+OH=HMN-R ₈ +H ₂ O	6.37E+07	1.8	298.1

238	HMN+O=HMN-R8+OH	8.55E+03	3	3123
239	HMN+CH3=HMN-R8+CH4	4.26E-14	8.1	4150
240	HMN+HO2=HMN-R8+H2O2	2.52E+13	0	20440
241	HMN+O2=HMN-R8+HO2	3.71E+13	0	49000
242	IC4H8+FC12H25=HMN-R8	5.00E+09	0	8200
243	HMN-R8O2=HMN-R8+O2	7.46E+19	-1.6	35720
244	HMN-R8O2=HMNOOH8-5	1.56E+09	0	17050
245	HMNOOH8-5O2=HMNOOH8-5+O2	4.73E+26	-3.2	39640
246	HMNOOH8-5O2=HMNKET8-5+OH	2.12E+10	0	19350
247	HMNKET8-5=CC8H17+CH3COCH2+TC4H8CHO+OH	1.05E+16	0	41600
248	FC12H25=C3H6+CC9H19	5.00E+12	0	28000
249	CC9H19=NEOC5H11+IC4H8	5.00E+12	0	28000
250	C3H6+HO2=C3H5-T+H2O2	3.00E+09	0	9930
251	C3H6+OH=C3H5-T+H2O	1.11E+06	2	1451
252	C3H6+O=C3H5-T+OH	6.03E+10	0.7	7632
253	IC3H7=H+C3H6	8.57E+18	-1.6	40340
254	IC3H7+H=C2H5+CH3	2.00E+13	0	0
255	IC3H7+O2=C3H6+HO2	4.50E+11	0	5020
256	IC4H7=C3H4-A+CH3	1.23E+47	-9.7	74260
257	IC4H8=C3H5-T+CH3	1.92E+66	-14.2	128100
258	IC4H8=IC4H7+H	3.07E+55	-11.5	114300
259	IC4H8+O=CH2CO+CH3+CH3	3.33E+07	1.8	76
260	IC4H8+H=IC4H7+H2	3.40E+05	2.5	2492
261	IC4H8+O=IC4H7+OH	1.21E+11	0.7	7633
262	IC4H8+OH=IC4H7+H2O	5.20E+06	2	-298
263	IC4H8+O=IC3H7+HCO	1.58E+07	1.8	-1216
264	IC4H8+CH3=IC4H7+CH4	4.42E+00	3.5	5675
265	IC4H8+HO2=IC4H7+H2O2	1.93E+04	2.6	13910
266	TC4H9=H+IC4H8	4.65E+46	-9.8	55080
267	IC4H8+H=C3H6+CH3	5.68E+33	-5.7	20000
268	TC4H9+O2=IC4H8+HO2	7.50E-19	0	5020
269	CH3COCH2=CH2CO+CH3	1.00E+14	0	31000
270	C3H6+O2=C3H5-T+HO2	1.40E+12	0	60700
271	NEOC5H11=IC4H8+CH3	3.06E+17	-1.2	32290
272	CH3O2+IC4H7=CH3O+IC4H7O	7.00E+12	0	-1000
273	IC4H7+HO2=IC4H7O+OH	7.00E+12	0	-1000
274	IC4H8+HO2=IC4H8O+OH	1.29E+12	0	13340
275	IC4H8+C3H5-A=IC4H7+C3H6	7.94E+11	0	20500
276	IC4H7O=C3H5-T+CH2O	1.01E+18	-1.4	30840
277	C3H6+CH3=C3H5-T+CH4	8.40E-01	3.5	11660
278	C3H5-T=C2H2+CH3	2.16E+10	-8.3	45110
279	C3H5-T+O2=CH3COCH2+O	3.81E+17	-1.4	5580
280	C3H4-A+M=C3H3+H+M	1.14E+17	0	70000
281	C3H4-A+O2=C3H3+HO2	4.00E+13	0	39160
282	C3H3+H=C3H2+H2	5.00E+13	0	0
283	C3H4-A+OH=C3H3+H2O	1.00E+07	2	1000
284	C3H2+OH=C2H2+HCO	5.00E+13	0	0
285	IC4H7+O2=CH3COCH2+CH2O	7.14E+15	-1.2	21050
286	C3H3+OH=C3H2+H2O	1.00E+13	0	0
287	C3H3+O2=CH2CO+HCO	3.01E+10	0	2870
288	C3H5-T+O2=CH2O+CH3CO	3.71E+25	-4	7043
289	IC4H8+O2=IC4H7+HO2	6.00E+12	0	39900
290	IC3H7+OH=C3H6+H2O	2.41E+13	0	0
291	C3H6+H=C3H5-T+H2	4.05E+05	2.5	9794
292	C3H6=C3H5-T+H	5.62E+71	-16.6	139300
293	TC4H8CHO=IC4H8+HCO	8.52E+12	0	20090
294	CC8H17=IC4H8+TC4H9	3.78E+22	-2.7	32360
295	CH3OH+OH=CH2OH+H2O	7.10E+06	1.8	-596
296	CH3OH+H=CH3O+H2	3.60E+12	0	6095
297	CH3OH+H=CH2OH+H2	1.44E+13	0	6095
298	CH3OH+CH3=CH2OH+CH4	3.19E+01	3.2	7172
299	CH3OH+O=CH2OH+OH	3.88E+05	2.5	3080
300	CH2OH+O2=CH2O+HO2	3.81E+06	2	1641
301	CH2OH(+M)=CH2O+H(+M)	2.80E+14	-0.7	32820
302	C6H5CH3=C6H5+CH3	5.06E+74	-16.6	141539
303	C6H5CH3=C6H5CH2J+H	5.84E+53	-10.9	114712
304	C6H5CH3+O2=C6H5CH2J+HO2	9.30E+09	1.3	40939
305	C6H5CH3+H=C6H6+CH3	7.57E+18	-1.7	6410
306	C6H5CH3+H=C6H5CH2J+H2	4.00E+02	3.4	3120
307	C6H5CH3+OH=C6H5CH2J+H2O	5.19E+09	1	874
308	C6H5CH3+O=C6H5CH2J+OH	6.00E+10	0.7	7632
309	C6H5CH3+HO2=C6H5CH2J+H2O2	1.02E+04	2.5	12339.3
310	C6H5CH3+CH3=C6H5CH2J+CH4	2.21E+00	3.5	5675

311	C6H5CH3+C2H3=C6H5CH2J+C2H4	2.21E+00	3.5	4680
312	C6H5CH3+C6H5OJ=C6H5CH2J+C6H5OH	2.50E+11	0	5000
313	C6H5CH3+C6H5=C6H5CH2J+C6H6	7.94E+13	0	11949
314	C6H5CH2J=>2C2H2+C3H3	2.00E+16	0	97000
315	C6H5CH2J+O2=C6H5CHO+OH	1.12E+11	-0.3	18300
316	C6H5CH2J+O2=C6H5OJ+CH2O	5.30E+13	-1.1	10840
317	C6H5CH2J+OH=PHCH2OH	2.00E+13	0	0
318	C6H5CH2J+O=C6H5CHO+H	3.30E+14	0	0
319	PHCH2OH+OH=C6H5OH+CH2OH	2.61E+14	-0.7	1710
320	C6H5CH2J+HO2=PHCH2OJ+OH	2.46E+55	-12	28920
321	PHCH2OJ=C6H5+CH2O	1.55E-09	5.3	12530
322	PHCH2OJ=C6H5CHO+H	1.61E+08	0.3	4920
323	C6H5CHO+OH=H2O+C6H5CJO	3.44E+09	1.2	-447
324	C6H5CHO+H=H2+C6H5CJO	2.28E+10	1.1	3279
325	C6H5CJO=C6H5+CO	3.00E+12	0	34860
326	C6H5OH+C6H5=C6H6+C6H5OJ	1.00E+11	0	6064
327	C6H5OH+C3H5-A=C6H5OJ+C3H6	1.44E+01	3.1	6935
328	C6H5OH+CH3=C6H5CH3+OH	5.42E+14	-0.8	12100
329	C6H5OH+CH3=CH4+C6H5OJ	1.44E+01	3.1	6935
330	C6H5OH+O2=C6H5OJ+HO2	1.00E+13	0	37900
331	C6H5OH+OH=C6H5OJ+H2O	6.00E+12	0	0
332	C6H5OH+O=C6H5OJ+OH	1.28E+13	0	2891
333	C6H5OH+H=H2+C6H5OJ	1.15E+14	0	12390
334	C6H5OH=H+C6H5OJ	1.09E+16	0	86500
335	C6H6+O2=C6H5+HO2	6.31E+13	0	67832
336	C6H6=C6H5+H	1.67E+16	0	111500
337	C6H6+OH=C6H5+H2O	1.63E+08	1.4	1451
338	C6H6+H=C6H5+H2	2.00E+13	0	18600
339	C6H6+OH=C6H5OH+H	8.21E+13	-0.1	10673
340	C6H6+O=C6H5OJ+H	2.48E+14	-0.3	4674
341	C6H6+HO2=C6H5+H2O2	7.50E+03	2.5	27619
342	C6H5+HO2=C6H5OJ+OH	3.00E+13	0	0
343	C6H5+OH=C6H5OH	3.00E+13	0	0
344	C3H3+C3H3=C6H5+H	3.67E+26	-3.9	28960
345	C3H3+C3H3=C6H6	3.89E+50	-11	20320
346	CHXRAD+O2=CHXO2J	3.00E+12	0	0
347	CHXO2J=CYCHEXENE+HO2	3.85E+12	0	29000
348	CHXO2J=CHX1Q3J	2.86E+11	0	24077
349	CHX1Q3J+O2=CHX1Q3QJ	3.00E+12	0	0
350	HX1EN6Q6J=CHX1Q3J	5.00E+07	0.9	5900
351	CHX1Q3J=CHXYO13+OH	1.40E+12	0	20000
352	HEX5ENAL+OH=HX1EN6Q6J	4.76E+07	1.5	34700
353	HEX5ENAL+OH=HX5ENAL4J+H2O	3.17E+06	2	-1434
354	HEX5ENAL+H=HX5ENAL4J+H2	5.02E+04	2.5	-1912
355	HEX5ENAL+CH3=HX5ENAL4J+CH4	1.00E-01	3.5	4046
356	HEX5ENAL+HO2=HX5ENAL4J+H2O2	6.80E+03	2.5	10113.8
357	C4H6+CH2CHO=HX5ENAL4J	3.52E+04	2.5	6130
358	CHXYO13+OH=CHX1*O3J+H2O	3.40E+06	1.9	-1451
359	CHXYO13+H=CHX1*O3J+H2	1.20E+06	2.4	2583
360	CHXYO13+CH3=CHX1*O3J+CH4	1.79E+04	2.3	6147
361	CHXYO13+HO2=CHX1*O3J+H2O2	3.00E+04	2.5	12260
362	HXEN4AL6J=CHX1*O3J	1.00E+08	0.9	5900
363	C2H4+AC3H5C*O4=HXEN4AL6J	1.32E+04	2.5	6130
364	CH2CO+C2H3=AC3H5C*O4	2.00E+11	0	2010
365	CHX1Q3QJ=CHX1Q3Q5J	9.28E+10	0	21076.6
366	HX1N4Q6AL+OH=CHX1Q3Q5J	4.76E+07	1.5	34700
367	H1N4OJ6AL+OH=HX1N4Q6AL	1.81E+13	0	0
368	AC3H5CHO+CH2CHO=H1N4OJ6AL	1.00E+11	0	3496
369	CHX=C2H4+C2H4+C2H4	4.00E+12	0	57400
370	CHX=C3H6+C3H6	4.00E+12	0	57400
371	CHXRAD+H=CHX	1.00E+14	0	0
372	CHX+O2=CHXRAD+HO2	1.68E+14	0	48210
373	CHX+H=CHXRAD+H2	6.89E+06	2.5	4124
374	CHX+CH3=CHXRAD+CH4	3.25E+05	2.3	7287
375	CHX+HO2=CHXRAD+H2O2	1.12E+05	2.5	14147.4
376	CHX+OH=CHXRAD+H2O	1.08E+07	2	-1133
377	CHX+CH3O=CHXRAD+CH3OH	1.32E+12	0	5000
378	CHX+O=CHXRAD+OH	5.72E+05	2.7	2106
379	CHX+C2H3=CHXRAD+C2H4	4.80E+12	0	16800
380	CHX+C2H5=CHXRAD+C2H6	6.00E+11	0	10400
381	CYCHEXENE+H=CHXRAD	6.25E+11	0.5	2620
382	CYCHEXENE=C4H6+C2H4	4.00E+12	0	57400
383	CYCHEXENE+H=CYHX1N3J+H2	1.00E+05	2.5	-1912

384	CYCHEXENE+CH3=CYHX1N3J+CH4	2.00E-01	3.5	4046.1
385	CYCHEXENE+O=CYHX1N3J+OH	1.59E+11	0.7	3107.1
386	CYCHEXENE+OH=CYHX1N3J+H2O	6.34E+06	2	-1434
387	CYCHEXENE+HO2=CYHX1N3J+H2O2	1.36E+04	2.5	10113.8
388	CYHX1N3J+O2=CYHX13ENE+HO2	2.10E+09	0	0
389	CYHX1N3J+HO2=CYHX1N3OJ+OH	7.00E+12	0	-1000
390	HX2ENAL6J=CYHX1N3OJ	1.00E+08	0.9	5900
391	C2H4+SC3H5CO=HX2ENAL6J	1.32E+04	2.5	6130
392	CYHX13ENE+H=CYHX1N3J	1.25E+12	0.5	1500
393	CYHX13ENE=C6H6+H2	4.00E+12	0	57400
394	CYHX13N5J+H=CYHX13ENE	1.00E+14	0	0
395	CYHX13ENE+H=CYHX13N5J+H2	1.00E+05	2.5	-1912
396	CYHX13ENE+O=CYHX13N5J+OH	1.59E+11	0.7	3107.1
397	CYHX13ENE+OH=CYHX13N5J+H2O	6.34E+06	2	-1434
398	CYHX13ENE+CH3=CYHX13N5J+CH4	2.00E-01	3.5	4046.1
399	CYHX13ENE+HO2=CYHX13N5J+H2O2	1.36E+04	2.5	10113.8
400	C6H6+H=CYHX13N5J	5.36E+11	-0.3	-6000
401	C2H3CO=C2H3+CO	3.04E+14	-0.5	30510
402	C2H3CHO+OH=C2H3CO+H2O	9.24E+06	1.5	-962
403	C2H3CHO+H=C2H3CO+H2	1.34E+13	0	3300
404	C2H3CHO+O=C2H3CO+OH	5.94E+12	0	1868
405	C2H3CHO+HO2=C2H3CO+H2O2	3.01E+12	0	11930
406	C2H3CHO+CH3=C2H3CO+CH4	2.61E+06	1.8	5911
407	C6H11-16=CHXRAD	1.00E+08	0.9	5900
408	C6H11-16=C6H11-13	3.67E+12	-0.6	15300
409	C2H4+C4H71-4=C6H11-16	1.32E+04	2.5	6130
410	C4H6+C2H5=C6H11-13	1.32E+04	2.5	6130
411	C4H71-4=C2H4+C2H3	8.77E+12	-0.2	36290